

# PHOSPHORESCENT EMITTERS FOR OLED APPLICATIONS

FROM SYNTHESIS TO PHOTODEGRADATION

## Dissertation

Zur Erlangung des Doktorgrades der Naturwissenschaften

(Dr. rer. nat.)

an der Fakultät für Chemie und Pharmazie

der Universität Regensburg



vorgelegt von

**Susanna Schmidbauer**

aus Regensburg

2013



The experimental work was carried out between November 2009 and January 2013 under the supervision of Prof. Dr. Burkhard König at the Institute for Organic Chemistry of the University of Regensburg.

Date of the Submission

14.02.2013

Date of the Colloquium

15.03.2013

Board of Examiners:

Prof. Dr. Jörg Daub

(Chairman)

Prof. Dr. Burkhard König

(1st Referee)

Prof. Dr. Kirsten Zeitler

(2nd Referee)

Prof. Dr. Frank-Michael Matysik

(Examiner)



## DANKSAGUNG

Mein Dank gebührt meinem Promotionsbetreuer Prof. Dr. Burkhard König. Er ermöglichte mir die Mitarbeit an einem interessanten Industrieprojekt und nahm sich immer Zeit, wenn ich wissenschaftlichen Rat suchte. Ich danke ihm vor Allem für sein absolutes Vertrauen, das er mir bei der Koordination und Repräsentation unseres Teilprojektes entgegenbrachte.

Prof. Dr. Kirsten Zeitler danke ich für die Übernahme des Zweitgutachtens, Herrn Prof. Frank-Michael Matysik dafür, dass er als Drittprüfer eintritt und Prof. Dr. Jörg Daub für die Übernahme des Vorsitzes während meiner Prüfung.

Dem Bundesministerium für Bildung und Forschung (BMBF) danke ich für die Finanzierung meiner Promotion. Allen Konsortiumspartnern danke ich für die interessanten und unkomplizierten Projekttreffen. Ganz besonders gedankt an dieser Stelle ist Dr. Philipp Stöbel, Dr. Dominik Joosten und Dr. Anna Hayer. Nicht nur ihre schnelle, unkomplizierte und verlässliche Unterstützung, ihre große Hilfsbereitschaft und Geduld in der Beantwortung OLED relevanter Fragen sondern auch das lustige und entspannte „social networking“ machten diese Zusammenarbeit für mich zu etwas Besonderem.

Andreas Hohenleutner danke ich für ein unbeschreibliches Jahrzehnt, das wir Seite an Seite verbracht haben: eine tolle Abiturzeit, ein anstrengendes Studium (bezogen aufs Lernen als auch aufs Feiern), einen unglaublichen Forschungsaufenthalt in Indien, eine erfolgreiche und kollegiale Zusammenarbeit im Projekt und unvergessliche Momente inner- und außerhalb des Arbeitskreises. Mal sehen, was die Zukunft für uns bereit hält...

Ich danke der Abteilung Zentrale Analytik des Fachbereichs Chemie und Pharmazie der Universität Regensburg für die schnelle und saubere Ausführung sämtlicher Aufträge.

Dr. Rudolf Vasold danke ich ganz herzlich für seine Erfahrung und große Unterstützung, ohne die die Nutzung und Instandhaltung unseres „sensiblen Ungetüms“ nicht so einfach möglich gewesen wäre. Ja, Rudi, jetzt passt alles;

Bei Britta Badziura, Simone Strauss, Ernst Lautenschlager, Dr. Petra Hilgers, Susanne Schulze und Viola Rappenberger bedanke ich mich für ihre Unterstützung in technischen und organisatorischen Angelegenheiten. Regina Hoheisel danke ich für ihre engagierte Art und schier unendlichen Geduld, sei es bei der Messung von CVs oder dem Versuch, das Café König nicht im Chaos untergehen zu lassen. Elisabeth Liebl danke ich für ihr unbeirrbares und temperamentvolles Engagement, das die ermüdete Bürokratie der Universität kurzzeitig immer wieder zu Rekordleistungsfähigkeit anspornte. Ich wünsche Ihnen einen wundervollen Ruhezustand, vollgepackt mit nahen Radausflügen und fernen Reisen.

Ich danke Christoph Stanglmair, Stefanie Jäger, Melanie Hacker und Florian Hastreiter für ihre Mitarbeit an meinem Projekt im Rahmen von Forschungspraktika.

Auf jeden Fall will ich zum Ausdruck bringen, wie dankbar ich bin, Teil eines so wunderbaren Arbeitskreises zu sein. Kulinarische Besonderheiten wie Friday Lunch, Internationale Abende oder Kino-Nächte mit Schoko-Chili, aber auch die äußerst lehrreichen Konferenz-Besuche werde ich nie vergessen.

Meinen Laborkollegen Andreas Hohenleutner, Dr. Mouchumi Bhuyan, Christoph Stanglmair und Tamal Ghosh danke für eine gutes Arbeitsklima.

Den „alten Hasen“ Dr. Harald Schmaderer, Dr. Florian Schmidt, Dr. Robert Lechner, Dr. Carolin Fischer, Dr. Daniel Vomasta, Dr. Tatiana Mitkina, Dr. Cristian Ochoa Puentes und Dr. Carolin Ruß danke ich für eine herzliche Aufnahme in den Arbeitskreis und ihre Hilfe in allen möglichen Fragen.

Der harten „Balkonfraktion“ Dr. Benjamin Gruber, Dr. Susanne Kümmel, Michael Dobmeier, Josef Hermann und Dr. Anna Gruber danke ich für Wahrung der Tradition des Feierabend-Biers. Stefan Balk, Malte Hansen, Anna Eisenhofer, Stefan Troppmann, Thea Hering und Andreas Müller danke für unbeschreibliche Augenblicke am Lehrstuhl. Den beiden Peters Raster und Schroll danke ich für ihr ständiges Interesse am Stand meiner Forschung. Manuel Bause danke ich für seine ständigen Bemühungen den Lehrstuhl technisch immer auf dem neuesten Stand zu halten.

Maria Cherevatskaya, Thomas Zanni, Durga Prasada Rao Hari, Tamal Ghosh, Qui Sun, Dr. Javier Bardagi, Michal Poznik, Dr. Supratim Banerjee, Claire de Nonancourt, I want to thank all of you so much for bringing new spirit in our group and spoiling us with delicious specialities.

Natascha Kuzmanovic danke ich für schöne Gespräche während den Kaffeepausen, ihren ewigen Enthusiasmus und ihre Fähigkeit, jeden mit ihrem Lachen mitreißen zu können.

Christian Ehrenreich danke ich für seine Hilfe in allen Bereichen ums Thema OLED, aber vor allem für seine angenehme, ruhige Art, die jeden den Stress vergessen lässt.

Allen meinen Freunden danke ich für eine unvergessliche Zeit inner- und außerhalb der Uni, inner- und außerhalb von Deutschland und Europa. Alina, Marion und Kathi, Euch danke ich für Eure jahrelange Freundschaft, und dass trotz mancher Durststrecken der Kontakt nie eingeschlafen ist. Ich hoffe, dass das noch lange so bleiben wird. Josef danke ich für viele lustige und grummelige (vor allem montags) Stunden. Tobi, mein Retter, ohne ihn hätte ich den Glauben an die „moderne Technik“ wohl schon vor dem Antritt meiner Promotion verloren! Hanni, danke für die zahlreichen verwirrenden Gesprächen (der Puzzle-Tee Abend steht auf jeden Fall auf meiner To-do-Liste für den Ruhestand;). Doris, die Zeit mit dir in Mexiko war einfach super. Sanne danke ich, dass sie sich entschlossen hat, nach Regensburg zu kommen und dass ihre wortreiche Natur Montag früh um 6 auch noch geschlummert hat. Daniel, danke für ausgefallene Erlebnisse und Genüsse überall auf der Welt. Petr, danke für lustige Abende in Deiner Wohnung - auch wenn ich Dir für den Kanister-Fusel nicht dankbar sein kann... Sabrina, danke für unsere tolle Zeit als Wohngemeinschaft; meine Selbstgespräche vor dem Fernseher waren eine interessante Erfahrung. Andi K., danke für die letzten 10 Jahre, die wir gemeinsam durchlebt und durchfeiert haben. Seppi, Hermann, Andi P., danke dass ich mit euch Berlin in allen Facetten erleben durfte. Caro, danke dass du mir so eine gute Freundin geworden ist, und dass das auch über die Weltmeere erhalten bleibt. Paul – einfach danke für alles!

Claudia, Bada, allen (ehemaligen) Mitarbeitern und meinen langjährigen Stammgästen der Oma Plüsch danke ich für ihre große Unterstützung. Ihr habt es immer geschafft, mich auf andere Gedanken zu bring. Und natürlich Tom: du warst der tollste Chef, den man sich wünschen kann.

Meiner Familie gebührt ein ganz besonderer Dank: Meinen Eltern danke ich für ihr Vertrauen, ihre Hilfe und ihre Liebe. Danke, dass Ihr mir alle Freiheiten und Möglichkeiten eröffnet habt, die für mich wichtig waren. Meiner Schwester danke ich für ihre große Unterstützung. Ich bin froh, dass ich Dich habe. Meinen Großeltern danke ich für alles, was sie für mich getan haben. Dem ganzen Rest meiner Familie danke ich für die tollen Familientreffen. (Alle Namen zu nennen würde den Rahmen der Arbeit sprengen, aber Onkel Michael, derjenige, der mir meine eigene Doktor-Weiße braut muss auf jeden Fall ein Plätzchen in diesem Absatz finden.) Eine bessere Familie wie Euch kann man sich nicht wünschen!!

Zuletzt will ich Dominik danken, für seine Unterstützung, seinen Ansporn, seine aufbauenden Worte, seine Überraschungen, sein Verständnis.  
Danke, dass Du Du bist... dass Du da bist... dass Du mein bist...



Reach for the Sky

SD, 2004





für meine Familie  
&  
Dominik



# **INTRODUCTION** **1**

---

## **CHAPTER 1** **9**

---

### ***CHEMICAL DEGRADATION IN ORGANIC LIGHT-EMITTING DEVICES: MECHANISMS AND IMPLICATIONS FOR THE DESIGN OF NEW MATERIALS***

<b>1. Introduction</b>	<b>11</b>
<b>2. Possible Reasons for Defect Formation</b>	<b>12</b>
2.1 Charge Carrier Induced Degradation	12
2.2 Exciton Induced Degradation	13
<b>3. Useful Techniques for the Elucidation of Chemical Degradation Mechanisms</b>	<b>14</b>
3.1 Chemical Analysis Techniques	15
3.2 Theoretical Calculations	15
<b>4. Chemical Degradation Mechanisms in OLEDs and Strategies for Stability Improvement</b>	<b>16</b>
4.1 Degradation of Hole Conducting Materials	16
4.2 Degradation of Electron Conducting Materials	22
4.3 Strategies for the Stability Improvement of Transport Materials	27
4.4 Degradation of Phosphorescent Emitters	29
4.5 Strategies for the Stability Improvement of Phosphorescent Dopants	34
<b>5. Conclusion</b>	<b>36</b>
<b>6. References</b>	<b>37</b>

## **CHAPTER 2** **41**

---

### ***RAPID COMBINATORIAL SYNTHESIS AND CHROMATOGRAPHY BASED SCREENING OF PHOSPHORESCENT IRIIDIUM COMPLEXES FOR SOLUTION PROCESSING***

<b>1. Introduction</b>	<b>43</b>
<b>2. Results and Discussion</b>	<b>44</b>
2.1 Synthesis	44
2.2 Screening	47
2.3 Separation and Spectroscopic Properties	48
2.4 Photodegradation Studies	51
<b>3. Conclusions</b>	<b>53</b>
<b>4. Experimental</b>	<b>54</b>
4.1 Methods and Materials	54
4.2 Photodegradation Studies	55
4.3 Syntheses	55
<b>5. References</b>	<b>58</b>

## TABLE OF CONTENTS

### CHAPTER 3 61

---

#### *NEW APPROACHES TOWARDS COMBINATORIAL DERIVATIZATION OF Ir(PPY)<sub>3</sub>*

<b>1. Introduction</b>	<b>63</b>
<b>2. Results &amp; Discussion</b>	<b>64</b>
2.1 C-O Coupling Reactions	64
2.2 C-C Coupling Reactions	68
<b>3. Conclusions</b>	<b>69</b>
<b>4. Experimental</b>	<b>70</b>
4.1 Methods and Materials	70
4.2 Syntheses	70
<b>5. References</b>	<b>72</b>

### CHAPTER 4 73

---

#### *STUDIES ON THE PHOTODEGRADATION OF RED, GREEN AND BLUE PHOSPHORESCENT OLED EMITTERS*

<b>1. Introduction</b>	<b>75</b>
<b>2. Results and Discussion</b>	<b>76</b>
2.1 General Observations	77
2.2 The Influence of Halogenated Solvents	78
2.3 The Influence of Oxygen	80
<b>3. Conclusions</b>	<b>86</b>
<b>4. Experimental Part</b>	<b>87</b>
4.1 Methods and Materials	87
4.2 Photodegradation Studies of the Liquid Samples	87
4.3 Photodegradation Studies of the PMMA Substrates	88
<b>5. References</b>	<b>88</b>

### CHAPTER 5 91

---

#### *Pt-COMPLEXES OF TETRADENTATE LIGANDS FOR OLED-APPLICATIONS*

<b>1. Introduction</b>	<b>93</b>
<b>2. Results and Discussion</b>	<b>96</b>
2.1 Synthesis	96
2.2 X-ray Crystal Structure	97
2.3 Spectroscopic Properties	98
2.4 Electrochemical Properties	100
2.5 Photodegradation	101
2.6 Device Performance	102
<b>3. Conclusions</b>	<b>104</b>

## TABLE OF CONTENTS

<b>4. Experimental</b>	<b>105</b>
4.1 Experimental Methods and Materials	105
4.2 Photodegradation Studies of the PMMA Substrates	106
4.3 SYNTHESSES	107
<b>6. References</b>	<b>115</b>

---

<b>SUMMMARY</b>	<b>117</b>
-----------------	------------

---

<b>ZUSAMMENFASSUNG</b>	<b>121</b>
------------------------	------------

---

<b>APPENDIX</b>	<b>125</b>
-----------------	------------

<b>1. Supporting Information of Chapter 2</b>	<b>126</b>
1.1 3D-Absorption- and Emission-Plots of Library 1, 3 and 4	126
1.2 Absorption and Emission Spectra	127
1.3 Photodegradation Plots	131
1.4 Picture of the Irradiation Unit	135
<b>2. Supporting Information of Chapter 3</b>	<b>136</b>
<b>3. Supporting Information of Chapter 4</b>	<b>137</b>
3.1 Reproducibility of the degradation studies in toluene under ambient conditions	137
3.2 Reproducibility of the degradation studies in a PMMA matrix under ambient conditions	137
3.3 Degradation curves of Ir(piq) <sub>3</sub> , Ir(ppy) <sub>3</sub> , Ir(Me-ppy) <sub>3</sub> and Ir(F,CN-ppy) <sub>3</sub> in CH <sub>2</sub> Cl <sub>2</sub> under ambient and inert conditions	138
3.4 Degradation curves of Ir(piq) <sub>3</sub> , Ir(ppy) <sub>3</sub> , Ir(Me-ppy) <sub>3</sub> and Ir(F,CN-ppy) <sub>3</sub> in benzene and toluene under ambient and inert conditions	138
<b>4. Supporting Information of Chapter 5</b>	<b>139</b>
4.1 Absorption Spectra of the Ligands 5a,b and 5'a-c in Comparison with the Corresponding Complex Spectra 1a,b and 1'a-c	139
4.2 <sup>1</sup> H- and <sup>13</sup> C-NMR Spectra	140
<b>5. Abbreviations</b>	<b>153</b>
<b>6. Curriculum Vitae</b>	<b>156</b>
<b>7. List of Presentations and Publications</b>	<b>157</b>



# **INTRODUCTION**

**ORGANIC LIGHT EMITTING DIODES – BASICS CONCERNING DEVICE SETUP &  
WORKING PRINCIPLE**

**OVERVIEW OF THIS THESIS**





At least since 1987 when the first operating multilayer organic light-emitting diode (OLED) was realized in the laboratories of the Eastman Kodak company,<sup>[1]</sup> this technology drew the research interest of scientists all over the world. Till now the competition on the industrial market has exacerbated more and more. Finally, in 1997, the first commercial OLED display was introduced by the Pioneer Corporation, utilized in a car radio.<sup>[2]</sup> Applications in mobile phones, digital cameras and TVs followed. In 2008, OSRAM tapped a new market for that technology – the lighting industry – by presenting the world's first OLED lamp.<sup>[3]</sup> According to the media, the field of application - and the creativity to design new gadgets - seems to be endless: luminescent wallpapers,<sup>[4]</sup> rollable notebooks<sup>[5]</sup> or MP3-bracelets,<sup>[6]</sup> just to name a few. Data-eye-glasses with bidirectional OLED microdisplays, developed at the Fraunhofer IPMS in Dresden, were awarded on the display conference of the Society for Information Display (SID) 2012.<sup>[7]</sup> Despite all the enthusiasm, having a real chance to become market-leader in any field, there are still some deficiencies that have to be overcome. One of them is the only moderate lifetime for most of the devices. To have a closer look into this special problem, first of all, general questions concerning device setup and the basic processes resulting in their entirety in light emission will be discussed briefly.<sup>[8]</sup>

### Device Setup

An OLED consists of an organic layer sandwiched between a cathode and an anode. The latter is placed on a transparent substrate like glass or foil. The organic layer comprises different materials exhibiting charge transporting and light emitting properties, respectively (Figure 1).

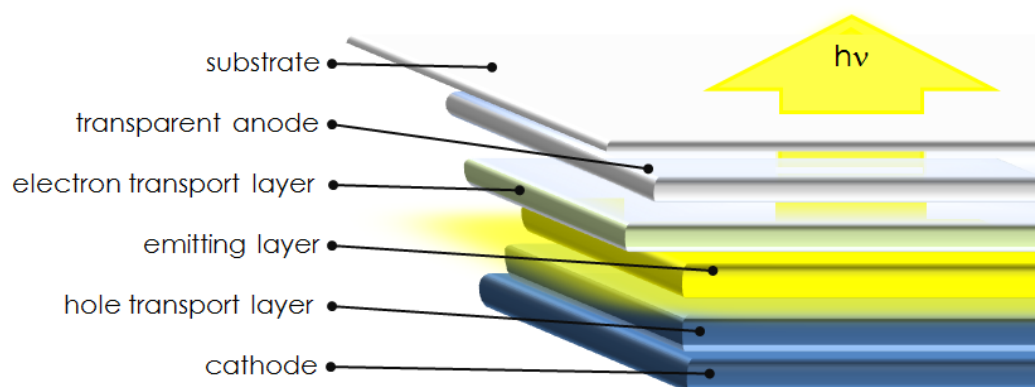


**Figure 1.** General setup of an organic light-emitting diode.

## INTRODUCTION

### Charge Injection

Applying voltage to the device, the anode injects negative charge carriers (electrons) into the electron transport layer (ETL). More detailed, electrons are transferred in the lowest unoccupied molecular orbital (LUMO) of the electron transport material, which is formally reduced to a radical anion (Figure 2a, b). Injection of positive charge carriers (holes) into the hole transport layer (HTL) via the cathode proceeds analogously: an electron is withdrawn from the highest occupied molecular orbital (HOMO) of the hole conducting material, which is therefore oxidized to a radical cation.

The energy difference between the Fermi level of the anode (cathode) and the LUMO (HOMO) of the electron (hole) transporting material results in an injection barrier  $\chi_e$  ( $\chi_h$ ). To guarantee a balanced charge carrier injection, these barriers must be comparable. Lower  $\chi_h$  and  $\chi_e$  values allow for an easier charge injection. Thus lower initial driving voltages are required, which can have beneficial effects on device lifetimes.

### Charge Transport

Charge carrier transport proceeds according to the electric field through the HTL and ETL towards the emitting layer (EML) in between. This movement is postulated as hopping process,<sup>[9]</sup> which is formally the sum of subsequent redox reactions: the reduced electron transporting molecule transfers its additional electron to the LUMO of an adjacent molecule under re-oxidation. The hole transport proceeds vice versa.

### Charge Recombination & Light Emission

When an electron and a hole get in close proximity to each other, Coulomb interactions lead to charge recombination yielding a ground state molecule and an excited, uncharged biradical molecule, the exciton (Figure 2c). Due to different spin-orientations, four configurations are possible. The antiparallel spin-orientation gives a singlet exciton, whereas diverse parallel spin-orientations yield three different triplet states. Thus, the ratio of singlet to triplet excitons is 1 to 3. According to Kasha's rule, relaxation to the ground state proceeds exclusively from the lowest excited state. If molecules reach higher energy levels, a radiationless relaxation to this state takes place (internal conversion, IC).

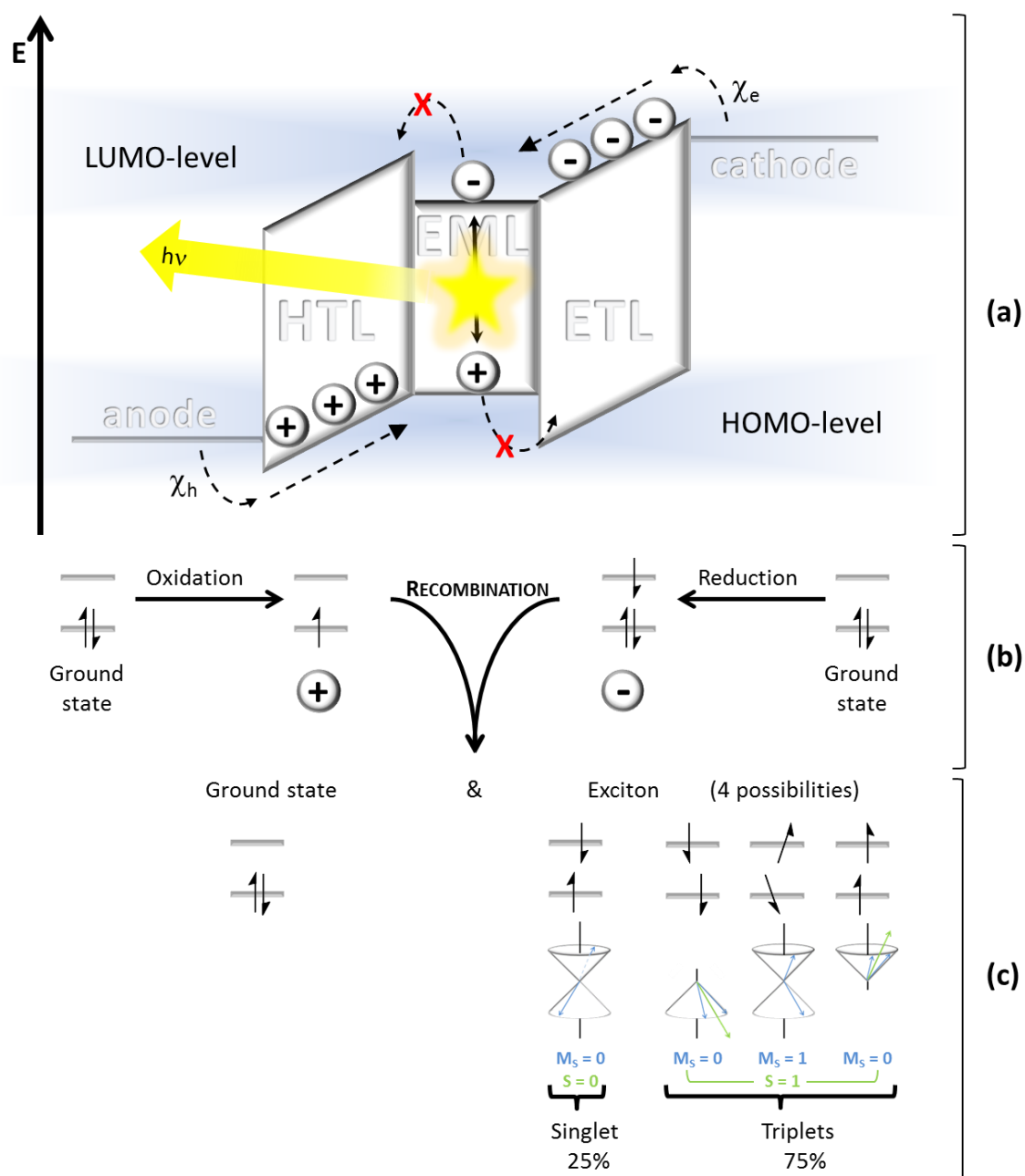


**Figure 2.** (a) Energy diagram of a multilayer OLED device under applied voltage: Anode | hole transport layer (HTL) | emission layer (EML) | electron transport layer (ETL) | cathode;  $\chi_h$ : hole injection barrier from the anode to the HOMO of the HTL;  $\chi_e$ : electron injection barrier from the cathode to the LUMO of the ETL. Charge-( $\oplus$ ,  $\ominus$ ) injection, transport and recombination, resulting in light emission, are depicted. (b) Charge transport is a formal oxidation (hole transport) or reduction (electron transport) of the appropriate conducting material. (c) Charge recombination results in the formation of a ground state molecule and an exciton with one of 4 different spin-orientations. The quantum number of the spin angular momentum ( $S$ ) and its  $z$ -component ( $M_s$ ) for the singlet and triplet states are included.

## INTRODUCTION

Pure organic compounds can only relax radiatively (fluoresce) to the ground state from the singlet excited state  $S_1$  (Figure 3). Such a process is spin forbidden for the first triplet excited state  $T_1$ . Therefore, all triplet excitons (75% of the formed excitons) decay non-radiatively. That's why organic compounds do not exceed quantum efficiencies of 0.25 in organic light-emitting devices. In order not to lose the largest amount of the available energy, transition metal complexes are used as emitters in organic light-emitting devices. Due to the strong spin-orbit coupling of the heavy atom (usually Ir, Pt) the emissive decay from the  $T_1$ -state (phosphorescence) becomes partly allowed and a fast and efficient transition from the singlet to the triplet excited state under spin conversion (intersystem crossing, ISC) takes place, the so-called triplet-harvesting effect. Using this strategy, significantly higher quantum yields can be achieved compared to fluorescent dyes.

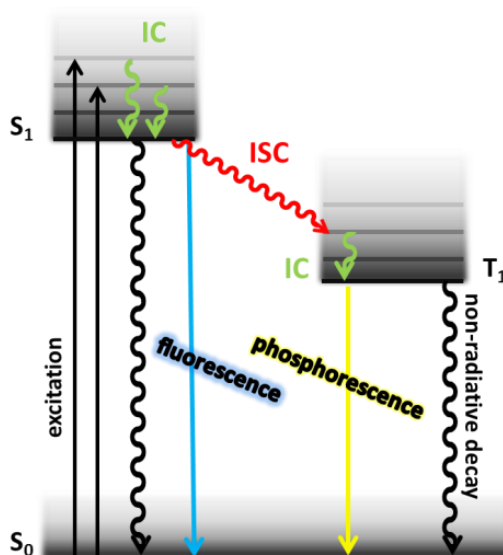


**Figure 3.** Jablonski diagram depicting the electronic transitions possible after excitation ( $S_0 \rightarrow S_1$ ): internal conversion (IC), intersystem crossing (ISC) and fluorescent ( $S_1 \rightarrow S_0$ ), phosphorescent ( $T_1 \rightarrow S_0$ ) as well as non-radiative decay.

In phosphorescent OLEDs, the emission layer usually consists of an appropriate organic matrix material (host) which is doped with organometallic emitters (guests). For an efficient phosphorescent emission, excitons formed on the matrix molecules must diffuse within the emitting layer to the dopants. This can proceed via two different energy transfer mechanisms, the Foerster or the Dexter transfer (Figure 4). The dipolar Foerster transfer proceeds between a singlet excited donor molecule (host) and an acceptor molecule (guest) in the ground state, reaching distances of several nanometers. A spectral overlap between donor-emission and acceptor-absorption is mandatory. In contrast, the Dexter transfer is an electron exchange process, only possible for neighboring molecules. In this case, an excited electron from the LUMO of a donor-molecule is transferred to the LUMO of a ground state acceptor-molecule. In exchange, an electron from the HOMO of the latter

is transferred to the HOMO of the host. This is not only possible for singlet but also for triplet excited molecules. For an efficient transfer, the exciton energy of the donor molecule should be higher than that of the acceptor molecule.

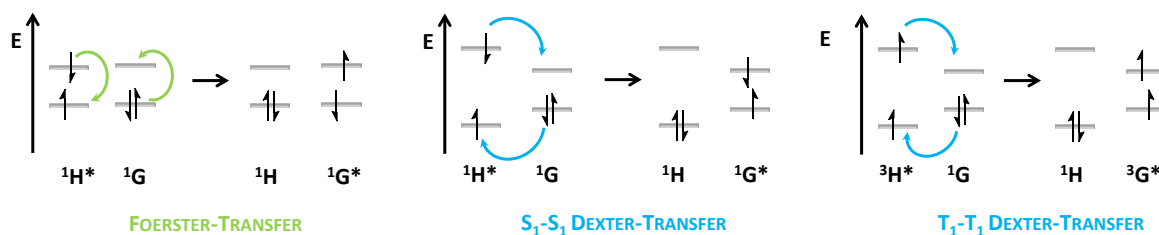


**Figure 4.** Foerster and Dexter transfer mechanisms between excited host ( $H^*$ ) and ground state guest ( $G$ ) molecules.

### Overview of this Work

Altogether, many different processes are involved in the light emission of OLEDs. Only a perfectly fine-tuned interplay of all these mechanisms results in a proper device performance which is mandatory for the successful commercial application.

Meanwhile, most of the error sources leading to device deterioration, like the formation of dark spots or the occurrence of electrical shorts are well understood and can be prevented by optimizing the device architecture and encapsulation. The intrinsic degradation, in contrast, leading to a slow but steady luminance decrease with the operation time, constitutes a more serious challenge. Chemical reactions are suspected to cause this type of degradation. Chapter 1 reviews recent advances in this research field.<sup>[10]</sup> Elucidated degradation products and mechanisms of all types of (metal)organic materials present in an OLED device are summarized, their commonalities are highlighted and resulting implications on the material design are stated. But especially for the phosphorescent emitters no reliable guidelines for the prediction of their stabilities can be provided to date. Also important spectroscopic factors like luminescence efficiencies or color purity can't be assessed theoretically yet. Thus, the discovery of new promising emitters for OLED application still follows the trial and error strategy via synthesizing and evaluating complexes individually.

In order to overcome this time-consuming approach, we developed a methodology, which combines the combinatorial derivatization of iridium complexes with a chromatography based screening setup.<sup>[11]</sup> This useful tool allowed us to characterize several complex libraries and to identify interesting photophysical and photochemical effects induced by different substitution patterns (Chapter 2). The structural diversity in the complex libraries was accomplished by combinatorial C-C and C-N coupling reactions on a bromo-functionalized  $\text{Ir}(\text{ppy})_3$ -precursor. In order to expand the pool of possible reaction

## INTRODUCTION

pathways applicable for the combinatorial approach, investigations on suitable reaction conditions for C-O couplings were studied in Chapter 3.

Interesting observations from the second chapter concerning the influence of structural changes on the degradation behavior of these complexes prompted us to study the degradation behavior of some red, green and blue emitting iridium complexes.<sup>[12]</sup> A detailed discussion on the results is given in Chapter 4.

The last chapter reports about the synthesis and photophysical characterization of a new class of cyclometalated platinum(II) complexes for the application in OLEDs.

## References

- [1] C. W. Tang, S. A. VanSlyke, *Appl. Phys. Lett.* **1987**, 51, 913-915.
- [2] <http://pioneer.jp/corp/profile-e/history/>, access date: 11/1/2013.
- [3] <http://www.oled-info.com/history-page-2>, access date: 11/1/2013.
- [4] <http://globonsomeday.blogspot.de/2010/02/oled-wallpapers-could-make-light-bulbs.html>, access date: 11/1/2013.
- [5] <http://gadget-demo.blogspot.de/2010/01/rolltop-laptop-from-future.html>, access date: 11/1/2013.
- [6] <http://pinterest.com/netizenpros/flexible-oled-gadgets/>, access date: 11/1/2013.
- [7] <http://www.printedelectronicsworld.com/articles/data-eye-glasses-based-on-bidirectional-oled-microdisplays-00004497.asp>, access date: 11/1/2013.
- [8] M. Rothmann, Ph. D. Thesis, Universität Bayreuth, GER, **2009**, <http://nbn-resolving.de/urn/resolver.pl?urn:nbn:de:bvb:703-opus-6946>.
- [9] O. Nuyken, S. Jungermann, V. Wiederhirn, E. Bacher, K. Meerholz, *Monatsh. Chem.* **2006**, 137, 811-824.
- [10] S. Schmidbauer, A. Hohenleutner, B. König, *Adv. Mater.* accepted.
- [11] A. Hohenleutner, S. Schmidbauer, R. Vasold, D. Joosten, P. Stoessel, H. Buchholz, B. König, *Adv. Funct. Mater.* **2012**, 22, 3406-3413.
- [12] S. Schmidbauer, A. Hohenleutner, B. König, submitted.

# CHAPTER 1

## **CHEMICAL DEGRADATION IN ORGANIC LIGHT-EMITTING DEVICES: MECHANISMS AND IMPLICATIONS FOR THE DESIGN OF NEW MATERIALS<sup>‡</sup>**

Degradation of the materials in organic light-emitting devices (OLEDs) is the major impediment for the development of economically feasible, highly efficient and durable devices for commercial applications. Even though this chemical degradation is complex and the least understood of the different degradation modes in OLEDs, scientists were successful in providing insight into some of the responsible processes. In this progress report we will review recent advances in the elucidation of chemical degradation mechanisms: First possible reasons for defect formation and the most common and important methods to investigate those processes are covered before discussing the reactions and their products for the different types of materials present in a device. We summarize commonalities in the occurring mechanisms, and identify structural features and moieties that can be detrimental to operational stability. Some of the resulting implications on the development of new materials are presented and backed by concrete examples from literature.

---

<sup>‡</sup> Andreas Hohenleutner and Susanna Schmidbauer were contributed equally to this work.





## 1. INTRODUCTION

From the first discovery of light emission from anthracene single crystals in 1965,<sup>[1]</sup> organic electroluminescence has developed into a field of immense research interest with hundreds of groups around the world working to improve materials and devices. While it initially did not get much scientific attention, the first heterojunction device by Tang and Van Slyke in 1987<sup>[2]</sup> sparked academic and commercial interest in the subject and the advances in the efficiency of organic light-emitting devices since then have been tremendous. In particular the discovery of the triplet harvesting effect by Baldo *et al.* was responsible for a leap in the internal quantum efficiencies of the devices, enabling the conversion of nearly 100% of the charge carriers into photons.<sup>[3]</sup> As the recombination of electrons and holes yields triplet (75%) and singlet (25%) excitons and organic materials are usually only capable of emission from singlet states (fluorescence) this used to limit the achievable internal quantum efficiency. Using phosphorescent transition metal complexes as the emitting materials could overcome this limitation. Emission of light takes place from the triplet states of these compounds and singlet excitons are rapidly converted into triplets via efficient intersystem crossing (ISC). By now, organic light-emitting devices have made their way into mass production for display applications and are also expected to find application in the commercial lighting market in the near future. Besides high efficiencies and low power consumptions, it is also important that the devices have a high operational stability. Degradation in OLEDs can be caused by the formation of dark spots, the occurrence of electrical shorts leading to a sudden decrease in luminance (catastrophic failure) or intrinsic degradation. Dark spot formation and catastrophic failure can be suppressed by carefully optimized and controlled fabrication conditions and an adequate encapsulation of the devices and thus are no longer considered an obstacle for commercial applications. Intrinsic degradation is characterized by the decrease of overall luminance over time during continuous driving. This is accompanied by a rise of the operating voltage necessary to maintain operation at a constant current. This type of degradation is believed to result mainly from the deterioration of organic (and in some cases metal-organic) molecules in the device. The location and nature of this chemical degradation is highly dependent on the employed materials as well as the device structure

## CHAPTER 1

and the occurring processes can be manifold even for a single device. It is due to this complexity that chemical degradation is still the least understood of the different modes of degradation. To enable the development of new materials with high performances and stabilities however, it is important to understand the chemical nature of defects in the organic layers and the reactions that lead to their formation.

In this progress report, we will try to shed light on the chemistry behind intrinsic degradation in OLEDs by giving an overview on recent advances in the elucidation of chemical degradation mechanisms, how they can be investigated and how the gained knowledge can impact the design of new materials. It is not our aim to present a comprehensive review about intrinsic degradation and operational lifetimes, which would include many aspects of device engineering and go beyond the scope of this manuscript, but rather to limit our discussion to the chemical aspects of device degradation. Nevertheless, to provide a basis for the understanding of the processes, we have to discuss some of the physical mechanisms responsible for the formation of defect sites in OLEDs.

## 2. POSSIBLE REASONS FOR DEFECT FORMATION

In general it is believed that intrinsic device degradation is caused by the chemical conversion of a fraction of molecules in the organic layers of the device. The degradation products can then act as non-radiative recombination centers, luminescent quenchers or deep charge traps. Luminance loss can be caused by the former two or, if the emitting dopant itself is destroyed during device operation, simply by the lack of emitting centers. Deep charge traps are sites that can “trap” an electron or hole due to suitable energy levels and thus cause a localization of charges at the defect sites. Accumulation of these immobilized charges then leads to a rise of the operating voltage. It should be noted that a single defect site is not necessarily limited to one of the mentioned roles but might in fact act as an electron- and hole-trap as well as a quenching site at the same time. The formation of these defects can be caused by different processes and proceed via a variety of possible pathways.

### 2.1 Charge Carrier Induced Degradation

Instability of the molecules corresponding radical cations or radical anions can lead to defect formation by bond rupture or via radical reactions with surrounding molecules. The degradation is in this case caused by the holes and electrons moving through the organic materials and can thus be labeled charge carrier induced degradation. In efficient, state-of-the-art OLEDs, chemical degradation in the bulk of the transport layers - that is not in the vicinity of the emitting layer - is likely to be of this origin. The formed defects can act as

traps for the charges moving through the device and should in general mainly result in a rise of the operating voltage.

## 2.2 Exciton Induced Degradation

Due to the presence of excitons, the situation is a bit more complex in the emitting layer and at its interfaces with the adjacent transport or blocking layers. Excitons can participate in defect formation either via direct degradation of molecules in the excited state or via bimolecular quenching reactions.<sup>[4]</sup> Destructive deactivation can occur via direct excitation to a repulsive potential or via thermal population of higher lying dissociative states of a molecule. These dissociation processes can produce charged fragments or radicals that can in turn react with surrounding molecules and thus lead to deterioration of the organic or metal-organic materials. Bimolecular annihilation reactions involving excitons constitute another pathway.<sup>[4-7]</sup> The annihilation of two excitons leads to the population of higher lying excited states that can undergo further reactions via two possible pathways: direct dissociative processes similar to the ones induced by normal excitonic degradation or degradation via the so called "hot molecule mechanism" (Figure 1). In this case, internal conversion from an excited singlet state gives a highly vibrationally excited electronic ground state  $S_0^{**}$ .<sup>[8]</sup> This "hot molecule" has an equivalent vibrational temperature of 2000-4000 K and can dissociate directly (path A) or via excitation by another photon (or energy transfer from another exciton, path B). The absorption bands of these hot molecules show a thermal broadening causing an enhanced absorption at lower energies.

Energy transfer from an exciton to a polaron (radical cation or anion) yields a polaron excited state (excited radical) that might decay via similar pathways.<sup>[9-10]</sup> The importance of this particular route is highlighted by the fact that exciton-polaron annihilation has even been proposed to be the dominant mechanism for different phosphorescent devices.<sup>[10]</sup>

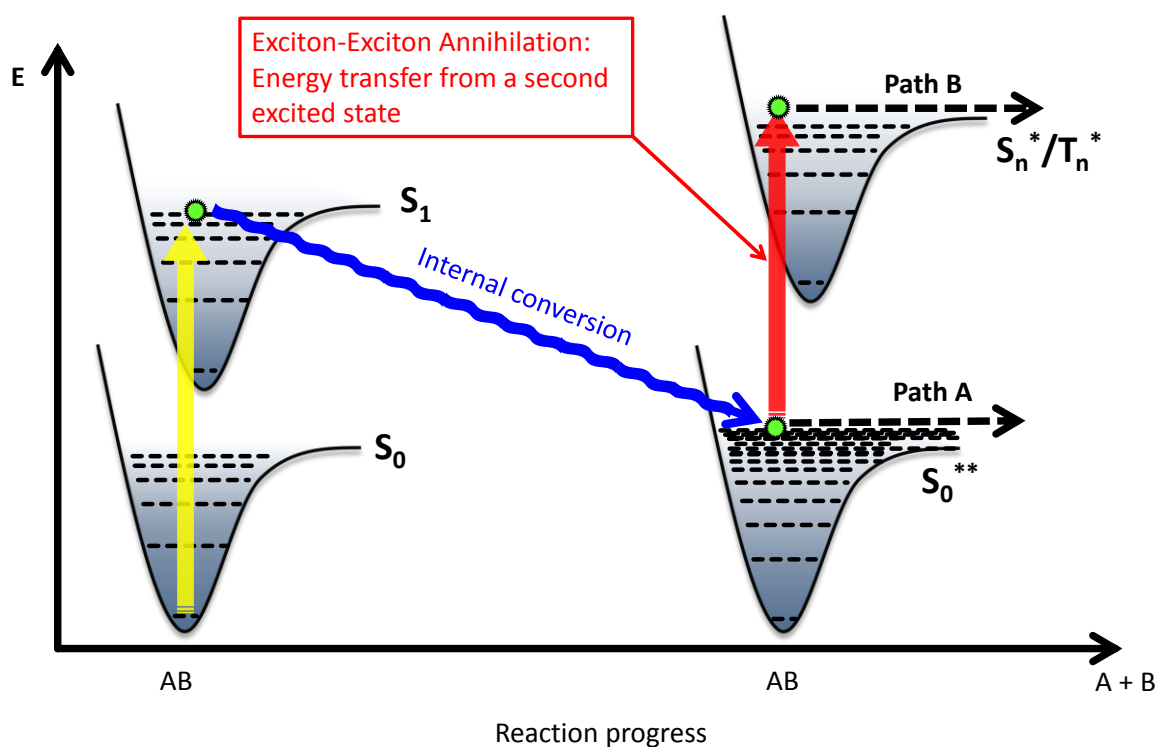


**Figure 1.** The “hot molecule” mechanism. Internal conversion from an excited singlet state gives a highly vibrationally excited electronic ground state  $S_0^{**}$ . This “hot molecule” can dissociate directly or via excitation by another photon (or energy transfer from another exciton).

### 3. USEFUL TECHNIQUES FOR THE ELUCIDATION OF CHEMICAL DEGRADATION MECHANISMS

Physical methods can provide information on the amount and location of trapped charges, luminescence quenchers and non-radiative recombination sites and often also on the electronic/(photo)-physical processes leading to their formation. However, they usually do not allow to draw conclusions regarding their chemical nature.

Since the organic layers in an OLED device are typically only several nm thick, the material available for analysis is usually very limited. The actual degradation products will only amount to a small fraction of the material even after extended operation. A defect density of 0.1% in the emission layer for example can already lead to 50% loss in luminance.<sup>[4]</sup> Considering the likely participation of different pathways and their mostly radical nature, the degradation of OLEDs is furthermore expected to lead to a multitude of deterioration products rather than to a single potentially easily identifiable one. The elucidation of chemical degradation mechanisms and products therefore presents a significant challenge.

### 3.1 Chemical Analysis Techniques

However, there are many reports on the chemical analysis of OLEDs and a number of techniques that have proven useful in gaining insight on the chemical deterioration products and pathways. Spectroscopic methods can provide information on the electronic and chemical structure of degradation products. Techniques that have been employed include UV-Vis, infrared, nuclear magnetic resonance as well as electron paramagnetic resonance spectroscopy.<sup>[11-15]</sup> Nonetheless, to gain detailed structural information from these methods, isolation of the degradation products from the bulk material is usually necessary. With the limited amount available, this represents a significant impediment. High performance liquid chromatography (HPLC) is a technique that allows the analysis and separation of complicated mixtures and the detection of very small quantities of materials. It can additionally be supplemented through above mentioned analysis methods to successfully identify degradation products.<sup>[11]</sup> HPLC and its combination with mass spectrometry (HPLC-MS) has been employed successfully to investigate degradation pathways in organic light-emitting devices for example by comparing chromatogram peaks and the corresponding ions of pristine and aged devices.<sup>[11, 16-17]</sup> While most chemical analysis techniques require dissolving the organic layers of the device before the measurements, mass spectrometry using a laser desorption/ionization (LDI) source is a powerful method for the direct analysis of organic thin films and even fully processed OLED devices. The molecules of a solid sample are ionized and accelerated via excitation with a UV-laser pulse in a strong electric field inside a vacuum chamber. This ionization mode traditionally requires preparation of the analytes within a suitable matrix material to enable excitation and ionization of the materials (MALDI: matrix-assisted laser desorption/ionization). An OLED device however presents an ideal LDI sample in itself and can thus be analyzed directly. The combination of electron accepting (electron transport layers/n-dopants) and electron donating (hole transport layers/p-dopants) properties together with the strong UV-absorption of most organic OLED materials enable an efficient excitation, desorption and ionization of the sample. The high sensitivity of the LDI method facilitates the detection and identification of degradation products even as trace impurities and has enabled the elucidation of a variety of chemical degradation pathways.

### 3.2 Theoretical Calculations

Quantum chemical calculations are a popular tool for the prediction of properties of molecules and materials in their ground and excited states, the elucidation of chemical and photochemical reaction pathways and the interpretation of experimental results. Especially density functional theory (DFT) calculations have become a standard tool in the development of new materials for organic electronics. Computational chemistry can help

## CHAPTER 1

to assess the feasibility of reaction pathways that molecules can undergo. Energies and geometries of the participating electronic states and reaction intermediates can be predicted and thus contribute to the understanding of charge and exciton induced processes in the organic materials. Calculations have for example been employed to identify "structurally weak" parts of molecules by determining bond dissociation energies or to identify deactivation routes and possible exciton induced degradation pathways for phosphorescent emitters.

### 4. CHEMICAL DEGRADATION MECHANISMS IN OLEDs AND STRATEGIES FOR STABILITY

#### IMPROVEMENT

With the different processes leading to the formation of degradation products and defect states, respectively, in combination with the variety of materials present in a typical device, it is likely that not only one pathway is responsible for the OLED instability. It is the sum of all degradation events in the different layers leading to device failure. Therefore even minor instabilities in the materials have to be elucidated and eliminated to ensure highly efficient and durable OLED devices. In the following sections we will review the degradation behavior of some materials that were investigated until now, trying to identify (re)occurring mechanisms starting with the hole conducting, followed by the electron conducting materials and ending with phosphorescent emitters. Not only the pure degradation mechanisms are summarized, but also some concluding remarks are drawn for rational changes in the molecule structures, which might lead to an improvement in device stability.

#### 4.1 Degradation of Hole Conducting Materials

Aromatic amines are widely used in organic light-emitting diodes due to their physical and electrochemical properties. They are a well investigated class of molecules for the use as hole transporting, electron blocking as well as host materials in phosphorescent devices. Much effort has been expended so far to shed light on the behavior of aromatic amines in driven OLEDs. Investigations showed that aromatic amines in the HTLs do not suffer any chemical degradation in single-carrier devices (electron- and hole-only devices, respectively). It was also observed that degradation mainly occurs in the vicinity of the HTL/EML-interface, where recombination and therefore exciton formation takes place. Both facts infer that aromatic amine degradation is mainly caused by excited states rather than charge carriers.<sup>[8, 14]</sup> Estimating the bond dissociation energies of several arylamines via DFT calculations provided some indications about the nature of the degradation pathway:<sup>[14, 18]</sup> C(sp<sup>2</sup>)-C(sp<sup>2</sup>) bonds exhibit homolytic bond dissociation energies of at least

110 kcal/mol whereas C-N bond energy-levels are at least ~30 kcal/mol lower (Figure 2) and lie therefore in the same energy range as the first singlet excited state of the arylamines. The vulnerability of arylamines might consequently lie in the high probability of C-N bond dissociation in excited molecules.

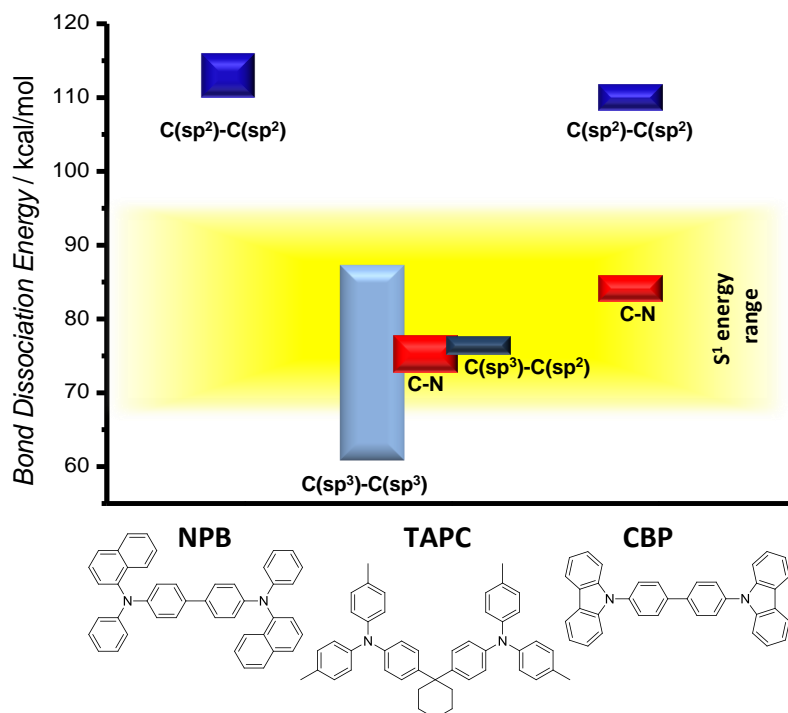
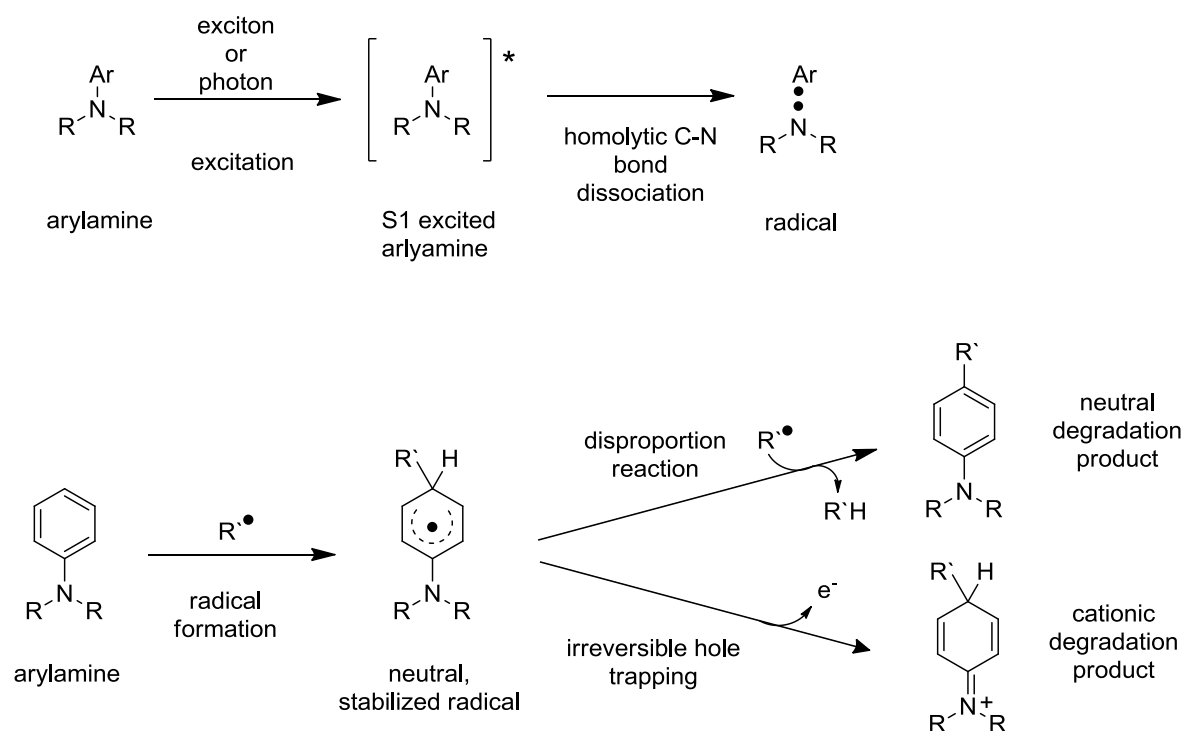


**Figure 2.** Dissociation energies of different bond types in the hole conducting materials NPB, TAPC and CBP.

Kondakov *et al.* assumed that the C-N bond cleavage is of homolytic rather than heterolytic nature due to the endothermicity of the latter.<sup>[14]</sup> The so generated reactive radical species undergo unselective subsequent reactions with adjacent neutral molecules resulting in long-lived  $\pi$ -conjugated radical species. Due to their lower lying LUMO, energy transfer from the excited matrix or dopant molecules can occur. The very low oscillator strength of the following transition leads to the non-emissive character of these excited states. Thus, the formed radicals can not only act as deep and irreversible carrier traps but also as luminescence quenchers.<sup>[11]</sup> With respect to the chemical degradation pathway, these radicals can additionally undergo hydrogen transfer, disproportion or radical addition reactions with a neighboring radical to form neutral, saturated degradation products (Scheme 1).

Several groups successfully analyzed different aged OLED devices via HPLC/MS techniques. By this means, degradation products derived from C-N bond dissociation and following reactions could be identified for a variety of arylamines, thus supporting the proposed general degradation pathway. Some of these products and more details and peculiarities of the mechanism will be discussed in the following section.

## CHAPTER 1



**Scheme 1.** General degradation pathway of aromatic amines in driven OLED devices.

The unequivocally identified degradation products of the host material CBP (4,4'-bis(carbazol-9-yl)biphenyl) are shown in Figure 3.<sup>[11, 14]</sup> Three different species (BPC, C and 3-CCBP), derived from C-N bond cleavage and subsequent reactions, could be isolated from aged OLED devices via HPLC separation. After 4000 h of operation at 40 mA/cm<sup>2</sup> (LT<sub>50</sub> = 80 h), approximately 20% of CBP had degraded. The main degradation product formed was BPC (about 1/3 of the degraded CBP molecules). The yields of the remaining two derivatives were much lower. Gel permeation chromatographic (GPC) analysis also revealed the presence of high-molecular-weight products.

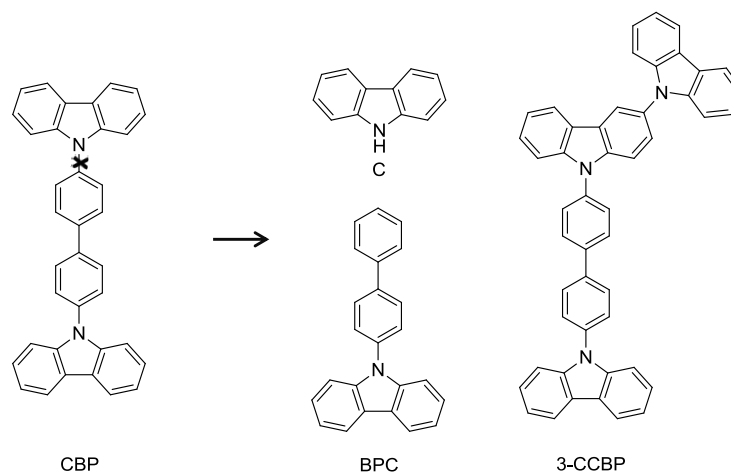


**Figure 3.** Host material CBP and degradation products C, BPC and 3-CCBP identified by Kondakov *et al.*



In the carbazole-containing matrix material TCTA (4,4',4''-tris(carbazol-9-yl)triphenylamine) bond cleavage does not affect the carbazolyl moiety, but the central triphenylamine core (Figure 4, top).<sup>[16, 19]</sup> Sivasubramaniam *et al.* could also identify [TCTA-carbazole]-fragments in MS investigations in minor amounts, but these could be attributed to degradation processes during thermal vapor deposition.<sup>[20]</sup>

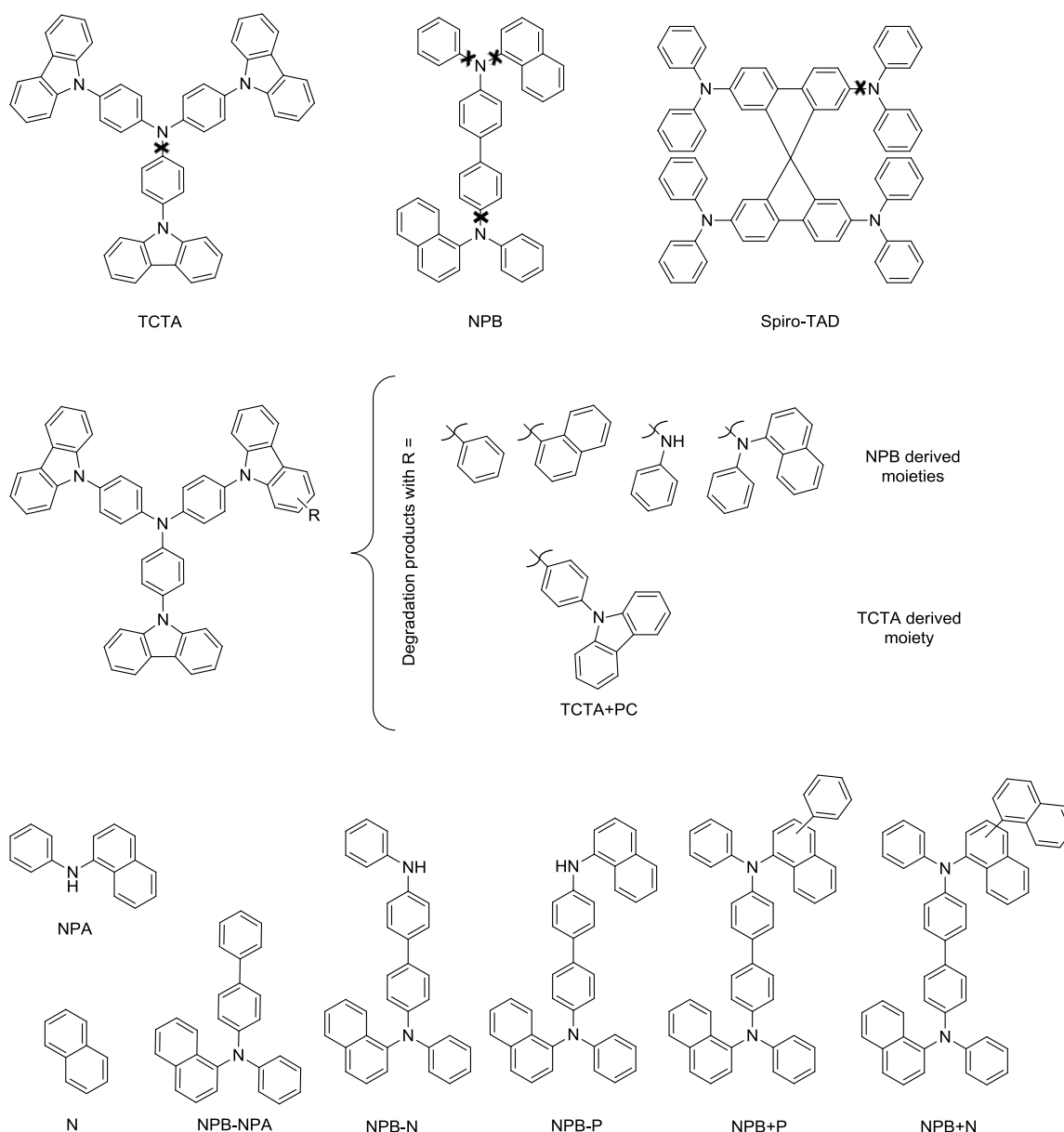


**Figure 4.** Degradation behavior of the arylamines TCTA, NPB, and spiro-TAD. Top: weak bonds of the molecules, which are responsible for degradation due to bond dissociation. Middle: identified degradation products of TCTA, resulting from substitution reactions with fragments of other TCTA molecules or of the adjacent material NPB. Bottom: identified degradation products of NPB, resulting from bond dissociation and substitution reactions of these moieties with neighboring NPB molecules.

Different mechanisms for the formation of these products have been proposed: Leo *et al.* assumed a heterolytic dissociation of the C-N bond, yielding a cationic amine species and a phenylcarbazole anion, which reacts in a nucleophilic substitution with adjacent TCTA

## CHAPTER 1

molecules to TCTA+PC. In contrast, Sivasubramaniam *et al.* postulated a radical pathway for the formation of this product.<sup>[16]</sup> Additionally, miscellaneous substitution products with moieties of the adjacent hole transport material NPB (*N,N'*-bis(naphthalen-1-yl)-*N,N'*-bis(phenyl)-benzidine, degradation behavior discussed below) could be identified (Figure 4, middle).

In mass spectrometric investigations Leo *et al.* found that the electron blocking material spiro-TAD (2,2',7,7'-tetrakis(*N,N*-diphenylamino)-9,9-spirobifluorene) undergoes an analogous dissociation between the spiro-bifluorene core and the diphenylamine (Figure 4, top).<sup>[19]</sup>

Quantum chemical calculations on the hole transport material NPB revealed that the numerous non-equivalent C-N bonds have almost identical bond dissociation energies, which explains the multitude of different degradation products that could be detected for this material. Products NPB-NPA, NPA and N (Figure 4, bottom) could be unambiguously identified.<sup>[18]</sup> Further derivatives, lacking a phenyl (NPB-P) or naphthyl (NPB-N) moiety respectively, can be assumed according to mass spectrometric analysis of the degraded device,<sup>[20-21]</sup> as well as products formed by radical attacks (NPB+N, NPB+P).<sup>[18]</sup>

Investigating the degradation behavior of the hole transport material TAPC (di-[4-(*N,N*-ditolyl-amino)-phenyl]cyclohexane), Kondakov *et al.* did not only identify the expected C-N bond dissociation and resulting substitution products of TAPC (DTA, TAPC-T and TAPC-DTA, Figure 5).<sup>[18]</sup> Species like TAPC-DTPA and DTPA could be observed, which obviously originate from C-C bond cleavage. This is also reasonable keeping in mind that the dissociation energies of bonds containing C(sp<sup>3</sup>) centers are about 30 kcal/mol lower than these of double bonds, therefore having equal energies as the first singlet excited state of TAPC (Figure 2). Another degradation route, specific for molecules incorporating saturated rings, starts with the homolytic cleavage of C(sp<sup>3</sup>)-C(sp<sup>3</sup>) bonds. Due to the ring structure not two radicals are formed, but one single biradical which can easily undergo dimerization or polymerization reactions to high-molecular-weight compounds. The enormous increase of driving voltage in aged devices containing TAPC additionally suggests the accumulation of trapped charges in the bulk of the TAPC layer. This indicates that degradation not only occurs via excitons at the vicinity of the HTL/EML interface, but is at least partly caused by charge carriers, following a still unidentified degradation pathway.

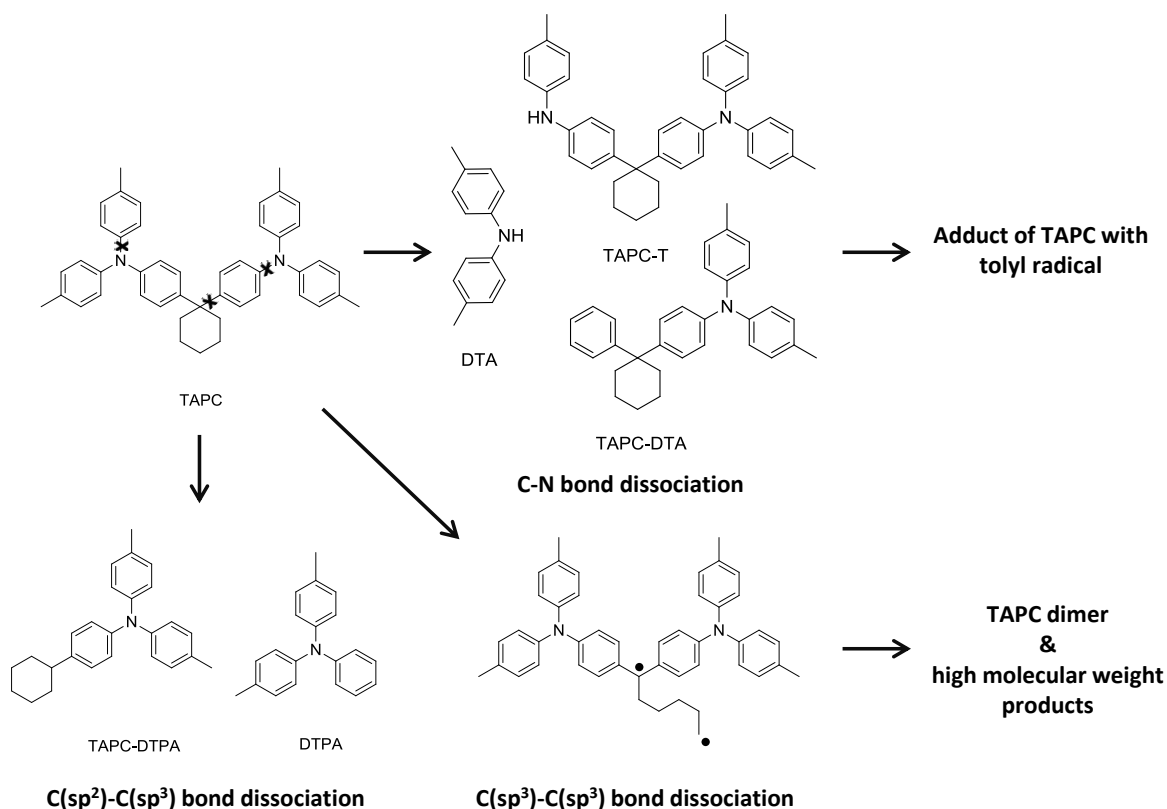


**Figure 5.** Different pathways of TAPC-degradation: low dissociation energies of C-N, C(sp<sup>3</sup>)-C(sp<sup>3</sup>)- and C(sp<sup>2</sup>)-C(sp<sup>3</sup>) bonds lead to miscellaneous degradation products.

In terms of stability, interesting effects could be observed for CBP derived materials, which are related to the planarity and  $\pi$ -conjugation of the molecules (Figure 6).<sup>[19, 22]</sup> DMFL-CBP follows a similar degradation pathway as CBP, namely C-N bond cleavage. In contrast, the 3,3'-methylated CDBP, predominantly degrades *via* C-C bond dissociation. Choi *et al.* explained this observation based on the dihedral angles of the molecules.<sup>[22]</sup> While DMFL-CBP has a planar structure, CBP and CDBP are twisted with torsion angles of 35° and 90°, respectively. In the latter configuration, having the two phenyl groups perpendicular to each other, the  $\pi$ -conjugation of this molecule is broken. This results in a decreased C-C bond dissociation energy and as a result in an increased likelihood of bond-cleavage.

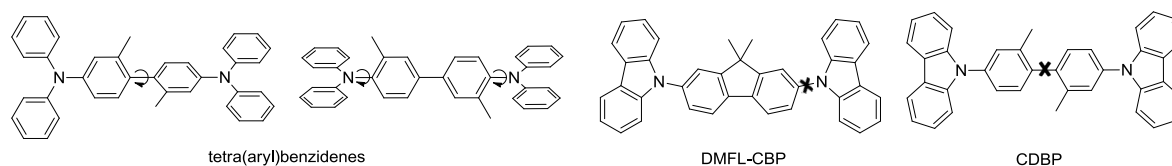


**Figure 6.** Substitution induced torsion of tetra(aryl)benzidenes and resulting changes in bond strengths for DMF-CBP and CDBP.

## CHAPTER 1

Low *et al.* showed additionally that methylation in 2,2'- or 3,3'-position of the biphenyl core in tetra(aryl)benzedenes leads to increased oxidation potentials.<sup>[23]</sup> This effect seems to result from the non-planarity of the system - and therefore the restricted conjugation between the two phenyl moieties and the lone pairs of the nitrogen - caused by the sterical hindrance of the methyl substituents (Figure 6). Rigidification of the biphenyl moiety leads to an extended  $\pi$ -conjugated system and a decreased oxidation potential. It is known that the oxidation potentials can be directly correlated to the ionization potentials of the materials. Adachi *et al.* proposed a linearity between the ionization potential and device lifetime and explain this with low initial driving voltages of devices incorporating easily ionizable hole transport materials.<sup>[24]</sup> Several groups demonstrated in experimental and theoretical investigations a linear dependence of the ionization potential and the Hammett parameter of the substituents attached to a triarylamine core structure,<sup>[25-27]</sup> giving way to a rational design of materials with appropriate ionization potentials.

### 4.2 Degradation of Electron Conducting Materials

Almost all known hole transport materials are based on aromatic amines containing either triarylamine or carbazole moieties. For electron transport materials in contrast, a much wider structural diversity of materials is available. The employed materials range from phosphinoxides over a variety of nitrogen and oxygen containing heterocycles (oxadiazoles, triazines, pyridines, phenantrolines, benzimidazoles, etc.) and metal-organic compounds to fully aromatic hydrocarbons. As a matter of course, there is not "one general" pathway explaining the chemical degradation behavior of electron conducting materials. We will start this section with a "bridge material", the ambipolar carbazole containing phosphine oxide CZPO2. This material exhibits both electron and hole conducting properties and follows, at least partly, the same exciton induced degradation pathway as the hole transporting materials. Quantum chemical calculations on CZPO2 by Chiu *et al.* revealed that the C-P bond dissociation energy is equal to that of C-N bonds, which enables the cleavage through the first singlet excited state (Figure 7).<sup>[28]</sup> This results in both, dissociation of the carbazole (discussed in the previous section) and the phosphinoyl unit from the benzene core. The main cause for a fast degradation compared to "pure" arylamines however, is the instability of the radical anion species formed through electron transport, resulting in the decrease of the C-P bond dissociation energy to almost half the original value. In contrast, the formation of the radical cation species of the carbazole unit leads to a stabilization of the C-N bond (about 10 kcal/mol). Therefore C-P bond containing materials might undergo bond cleavage not only, but also due to the presence of negative charge carriers.

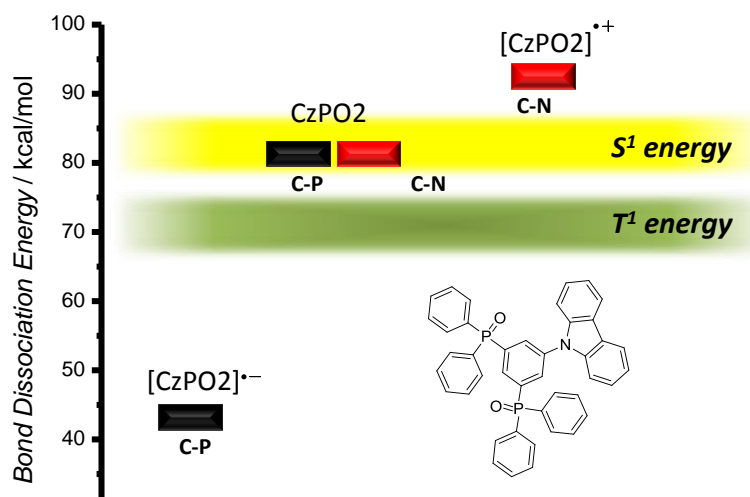
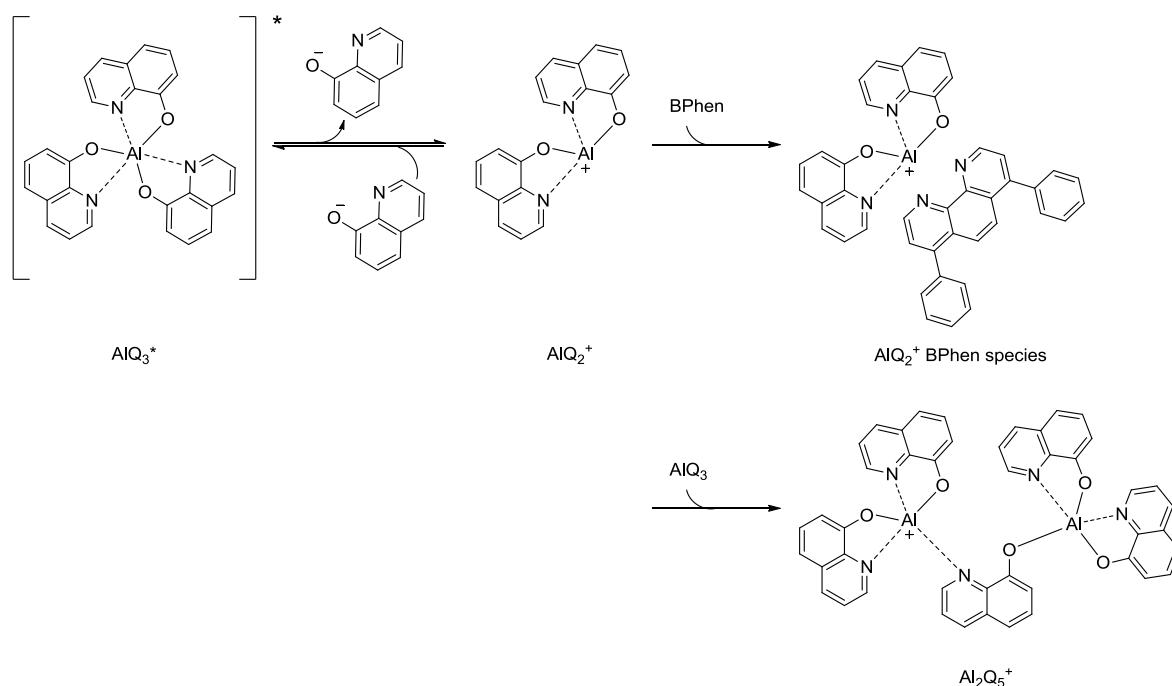


**Figure 7.** Dissociation energies of the different bond types of the bipolar conducting material CzPO2.

One important and well investigated class of fluorescent host and electron transporting materials are azaaromatic compounds, like quinolines (AlQ<sub>3</sub>, BAlQ<sub>2</sub>), phenanthrolines (BPhen) or benzimidazoles. Much effort has been spent so far on elucidating the degradation mechanisms of these materials, especially of AlQ<sub>3</sub>. Unipolar current devices of AlQ<sub>3</sub> as well as devices with tunable hole injection efficiency clearly indicated that hole injection in this material leads to device degradation.<sup>[29-31]</sup> Investigations by Papadimitrakopoulos *et al.*, showing the irreversible oxidation behavior of AlQ<sub>3</sub> in cyclic voltammetry measurements,<sup>[32]</sup> are consistent with the thesis of the hole current induced formation of unstable cationic AlQ<sub>3</sub><sup>•+</sup> species.<sup>[33-34]</sup> Scholz *et al.* assumed after LDI-TOF-MS measurements that excited AlQ<sub>3</sub> molecules undergo a reversible ligand-dissociation to AlQ<sub>2</sub><sup>+</sup> (Scheme 2).<sup>[35]</sup> While MS signals at 648 amu suggest the subsequent reaction of the cationic species with the adjacent hole blocking material BPhen (4,7-di(phenyl)-1,10-phenanthroline), no information could be obtained whether a charge transfer species [AlQ<sub>2</sub>+BPhen]<sup>+</sup> or even a coordinatively bound complex [AlQ<sub>2</sub>BPhen]<sup>+</sup> is generated.<sup>[36]</sup> Initially assumed dimerization reactions of AlQ<sub>3</sub> to the charged Al<sub>2</sub>O<sub>5</sub><sup>+</sup> species<sup>[35]</sup> turned out to occur exclusively at a very high density of excited molecules, like for example during the laser ionization process for mass spectrometric investigations and are therefore most likely no relevant degradation pathway in OLEDs.<sup>[36]</sup> The free chinoline ions, resulting from the dissociation process, can react to non-emissive, fluorescence quenching degradation products.<sup>[32, 35]</sup>



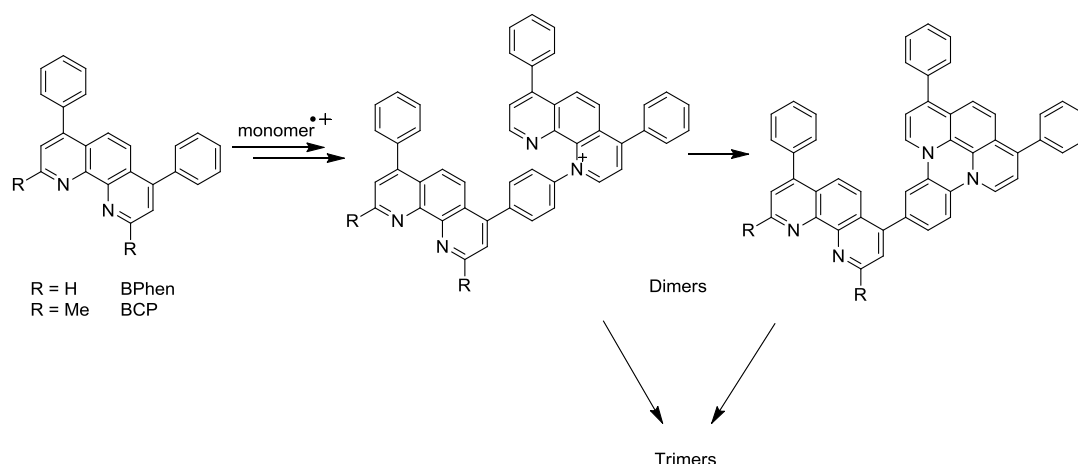
**Scheme 2.** Dissociation and degradation pathways of *tris*(8-hydroxy-quinolinato)aluminium  $\text{AlQ}_3$ .

Later on the destructive role of hole accumulation at the layer-interface was qualified, realizing that high electron density in the  $\text{AlQ}_3$  layer causes similar irreversible luminescence efficiency loss in the device. It is assumed that electron traps of still unknown nature (chemical degradation is suggested) with a luminance efficiency of  $< 1\%$  compared to  $\text{AlQ}_3$  are formed near the interface.<sup>[30, 37]</sup>

As quenching sites prevent emission from a large number of molecules surrounding them, it is obvious that even a relatively small amount of degraded  $\text{AlQ}_3$  molecules has a pronounced effect on the quantum efficiency of the whole device. Hence it is imperative to prevent accumulation of charges (both electrons and holes) in or at the interface of the  $\text{AlQ}_3$  layer. As it is known that the transit time of holes through the HTL is up to three orders of magnitude faster than for the electrons through  $\text{AlQ}_3$ ,<sup>[38-39]</sup> it is important to fine-tune the balance between electron and hole injection and mobility. Using hole transport materials with low ionization potentials is only one example, which can improve device stability. The resulting energy barrier between the HTL and the  $\text{AlQ}_3$  layer impedes the hole injection in the latter.<sup>[24, 33]</sup> This reduces hole induced  $\text{AlQ}_3$  degradation. A complementary route to enhance the device durability is to improve electron mobility. This was for example achieved by doping  $\text{AlQ}_3$  with materials like  $\text{BAIQ}_2$ <sup>[40]</sup> or BPhen.<sup>[40-41]</sup>

Investigations of the hole blocking and electron transport material BPhen showed besides faster electron transit properties compared to  $\text{AlQ}_3$  some drawbacks concerning the chemical stability in stressed devices. Dimerization as well as trimerization of BPhen molecules (Scheme 3) could be observed, leading to charge traps in the form of charged and neutral oligomers at the EML/HBL interface.<sup>[19, 35]</sup> These products can generally be ascribed to nucleophilic reactions of the lone electron pair of the  $\text{sp}^2$ -hybridized nitrogen

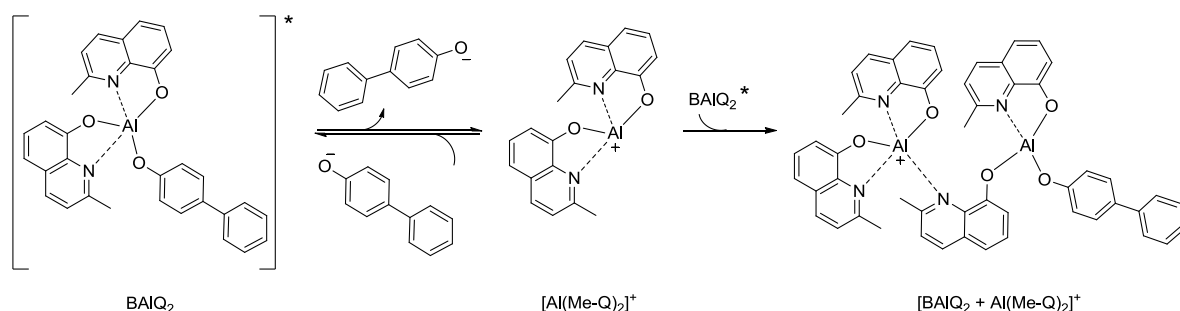
atom of an azaaromatic compound with an adjacent radical cationic species.<sup>[31]</sup> BPhen degradation seems to be dependent on the total charges passing through the device and occurs mainly at high voltages.<sup>[42]</sup> BCP generally shows a higher stability compared to BPhen, as dimer formation could only be observed to a lower extent and trimer formation not at all.<sup>[35]</sup> This can be explained by the steric hindrance of the methyl groups in the 2-positions of BCP, which leads to the conclusion that the introduction of bulkier substituents can improve the stability of phenanthroline materials by shielding the  $sp^2$ -nitrogens and impeding interactions with reactive species in the vicinity. In phosphorescent OLED devices BPhen can also form adducts with emitter fragments (see emitter section).<sup>[43-44]</sup> Both degradation pathways can result in the formation of gap states for charge carriers and excitons, causing significant luminance loss. Interestingly, complexation reactions of BPhen with the cathode materials Ag or Cs<sup>[36, 42, 45]</sup> are desired as an emerging interlayer, formed at the ETL/cathode interface during the evaporation of the cathode material, acts as a doped injection layer, enhancing electron injection into the ETL.<sup>[45]</sup>



**Scheme 3.** Oligomerization reactions of the phenanthroline based electron transporters.

With the electron transport material BAIQ<sub>2</sub> instead of BPhen, device lifetimes can be improved significantly.<sup>[46]</sup> Compared to BPhen, BAIQ<sub>2</sub> seems to exhibit better chemical stability as no coordination products with phosphorescent emitters could be identified so far. Initially, this molecule was also considered to be inert regarding self-dimerization.<sup>[35]</sup> But it turned out that it undergoes this degradation pathway as well;<sup>[42]</sup> the excited complex suffers dissociation of the phenylphenolate ligand (Scheme 4). The so formed  $[Al(Me-Q)_2]^+$  species can either undergo a subsequent back-reaction or a coordination with another excited BAIQ<sub>2</sub> to the dimer  $[BAIQ_2 + Al(Me-Q)_2]^+$ . De Moraes *et al.* found this degradation to be dependent on the current density and assumed it to be caused by bimolecular annihilation reactions (see 2nd section).<sup>[42]</sup> They also observed a direct correlation between dimer formation and device lifetime.

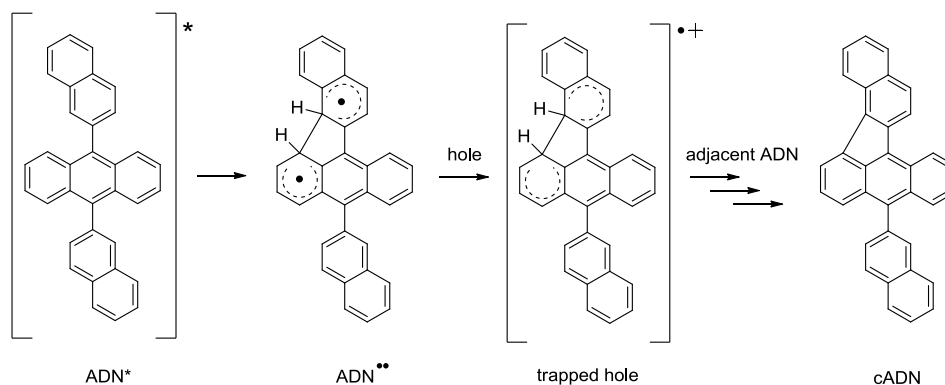
## CHAPTER 1



**Scheme 4.** Dissociation and dimerization reactions of the electron transport material BAIQ<sub>2</sub>.

Fully aromatic hydrocarbons were always considered being favorable inert host materials as they lack disadvantageous features like weak bonds (C-N, C-metal, N-metal, C-P) and highly reactive nucleophilic centers (lone pairs). Therefore homolytic bond dissociations and nucleophilic addition reactions are no critical issues for this class of host materials. But having a very closer look at devices incorporating hydrocarbons like ADN and rubrene, respectively, Kondakov *et al.* noticed a slow but steady and irreversible decrease of these molecules in chromatography based analysis of photoexcited devices.<sup>[47]</sup> Degradation mechanisms comparable to those of the arylamines can be ruled out as the weakest covalent bond in ADN has a dissociation energy of ~120 kcal/mol. The S<sub>1</sub> state energy of about 70 kcal/mol is therefore too low for exciton induced bond dissociation. Electron paramagnetic resonance (EPR) measurements nonetheless confirmed the generation of free spins during photoexcitation, formally carbon centered radicals. Oligomeric degradation products could be detected in significant amounts by gel permeation chromatography (GPC). It is assumed that the formation of these high-molecular-weight products takes place due to excited state reactions of adjacent molecules resulting in dehydrogenation reactions. Mass spectrometric investigations and additional comparison of the chromatographic retention times and absorption spectra with an authentic sample revealed the major low-molecular-mass product to be cADN (Scheme 5). The photocyclic ringclosing reaction of ADN to cADN is quite surprising as this reaction type commonly generates 6-membered-ring-derivatives. In contrast, 5-membered ring closure requires high-energy intermediates, formally biradicals. Quantum chemical calculations confirmed in case of ADN a stable biradical intermediate ADN••, which can trap both electrons and holes. Various hydrogen transfer reactions of this biradical with ion radicals or neutral adjacent molecules can occur to form neutral and charged radical species.<sup>[48]</sup> These can act as deep traps, non-radiative recombination centers and quenchers. Due to its absorption properties and the negligible fluorescent quantum yield (< 1%), the cyclization product cADN acts as an efficient fluorescence quencher.





**Scheme 5.** Radical degradation pathway of ADN.

Compared to the transformation reactions of the arylamines, the quantum yields for photochemical degradation of the hydrocarbons are extremely low: it takes up to  $1 \times 10^{11}$  excitation events to degrade one single molecule of ADN.<sup>[47]</sup> Nonetheless, this minor degradation pathway also has a non-negligible influence on device stability. Further analysis of ADN and its *t*butyl substituted analogue TBADN by Wang *et al.* revealed the appearance of an “intermolecular species” during device operation which is assumed to contribute to the loss of color purity and efficiency.<sup>[49]</sup> The mechanism of the formation and the nature of this species could not be elucidated so far, but dimerization reactions or morphological changes due to aggregation are suggested. This species shows a characteristic bathochromically shifted emission compared to the original anthracene derivatives which results in increased emission in the green part of the spectrum. Furthermore this species is capable of charge trapping and energy quenching, causing the efficiency loss of aged devices. As this degradation phenomenon occurs through aggregation processes of the anthracenes and the color shift is more pronounced in the ADN devices, the introduction of sterically demanding groups could minimize this degradation pathway. In this study it was also shown that mixing the anthracene layer with CBP also inhibits the formation of these intermolecular species.

It can be concluded that the degradation behavior of electron conducting materials can be quite different: charge as well as exciton induced degradation was found for different types of compounds. And some degradation phenomena cannot be explained to date. In the case of dimerization and accumulation processes, the introduction of bulky groups seems to be a useful tool for prevention.

### 4.3 Strategies for the Stability Improvement of Transport Materials

The degradation of transport materials can proceed via a variety of different pathways and can have different causes. Nevertheless, some common or reoccurring problems can be identified: The presence of “weak bonds” with dissociation energies close to the first excited state pose a problem concerning material stability: For many amine based hole

## CHAPTER 1

transport materials as well as phosphine oxide electron transporters, the energy of the first singlet excited state lies within the same range as the energies of C-N, C-P, C(sp<sup>2</sup>)-C(sp<sup>3</sup>) and C(sp<sup>3</sup>)-C(sp<sup>3</sup>) bonds. This can lead to exciton induced bond rupture and subsequent reactions. Consequently, the bond strengths directly affect the stability of the molecule and hence the device lifetime. Overcoming this problem, at least to some extent, can be achieved by minimizing the number of weak bonds within the molecules. Rigidifying the molecular structure, for example via bridging neighboring aryl moieties can reduce excited state initiated degradation reactions due to decreased rotational flexibility and is already considered a useful tool also to increase the thermal stability and decrease the oxidation potentials. The latter lead to a lower injection barrier at the anode/HTL interface, therefore to a reduced initial driving voltage. This principle of bridged molecules has also found entry to commercial applications (Figure 8).<sup>[50-53]</sup>

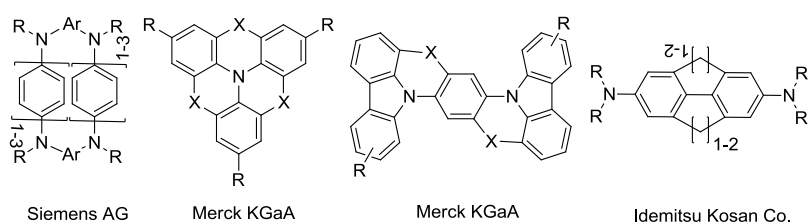


**Figure 8.** Examples for bridged aromatic amines used in commercial applications.

Another “weak link” was identified for N-heterocyclic materials. The nitrogen lone pair was found to contribute to degradation reactions resulting in oligomerization reactions with radical species or complexation with coordinatively unsaturated compounds. Shielding the sp<sup>2</sup>-N with sterically demanding groups decreases the interactions of its lone pair with reactive intermediates. Thus the possibility of undergoing degrading reactions can be reduced drastically.

A parameter which used to influence device lifetime is the thermal stability of the materials. If the device operating heat or other heat treatments exceed the specific glass transition temperature  $T_g$  of the materials, interdiffusion between the organic layers as well as crystallization of the amorphous material can occur. Therefore molecules with high  $T_g$  values are very desirable. After enormous scientific research concerning this topic it is nowadays well understood how to tune the  $T_g$  simply by influencing the molecular structure:<sup>[54-55]</sup> high glass transition temperatures can be achieved by (i) increasing the number of  $\pi$ -electrons, (ii) introducing bulky, heavy and/or rigid moieties for enlarging the molecule and decreasing the rotational freedom and (iii) incorporating an intermolecular hydrogen bonding site for the formation of super molecular structures. These guidelines were applied to already known compounds with appropriate electronic and spectroscopic properties which are suffering thermal lability (like TAD, TPD, AlQ<sub>3</sub>) for the development of high thermally stable materials (Figure 9).

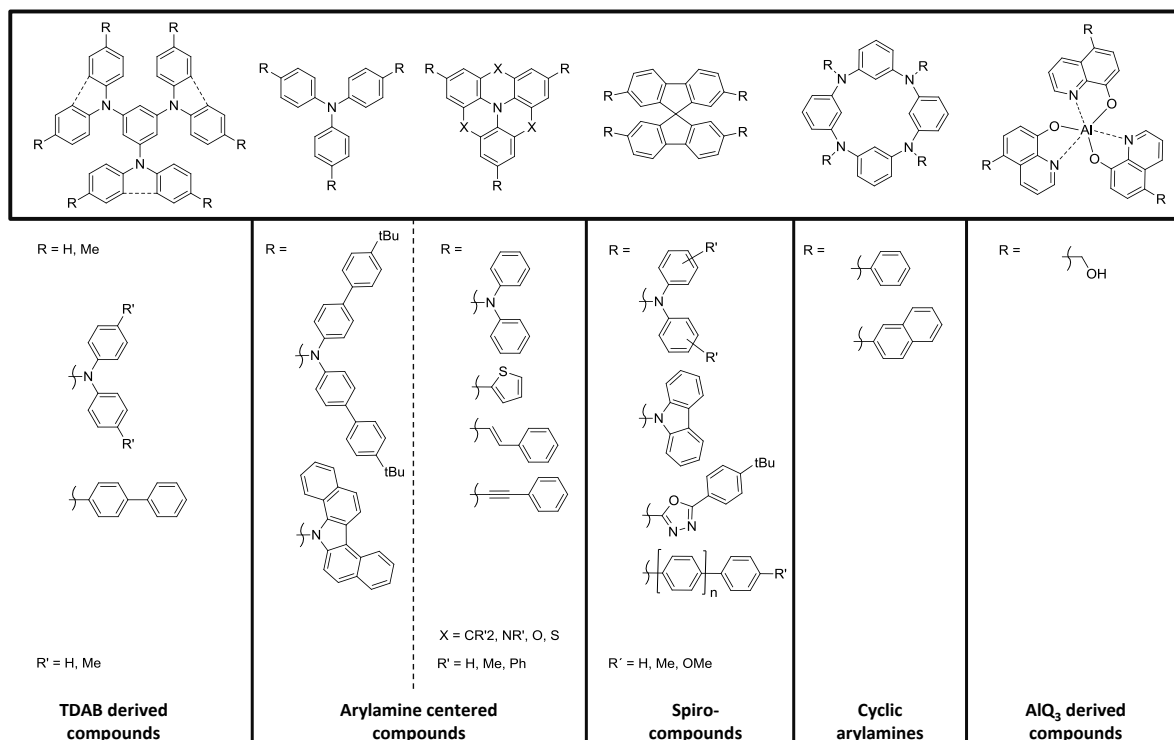


**Figure 9.** Some examples of thermally stable materials in OLED applications: TDAB derived,<sup>[56-58]</sup> arylamine centered<sup>[51, 59-60]</sup> and spiro<sup>[61]</sup> compounds as well as cyclic arylamines<sup>[50, 62]</sup> and an AlQ<sub>3</sub> derivative.<sup>[63]</sup>

#### 4.4 Degradation of Phosphorescent Emitters

Degradation products of transport and host materials can be a significant problem for the operational stability of OLEDs and the use of more robust materials can enhance the device lifetime. Nevertheless, the great impact that the type of phosphorescent dopant can often have on the device lifetimes cannot be adequately explained by a deterioration of the host and transport materials alone. In fact, while investigating the degradation of CBP in OLEDs containing Ir(ppy)<sub>3</sub> Kondakov *et al.* noticed that the phosphorescent dopant is deteriorating even faster than other materials and reasoned that it might therefore play a significant role in the degradation of the investigated devices.<sup>[11]</sup>

In phosphorescent devices, charge carrier induced degradation might play a role for host as well as guest materials in the emitting layer – depending on the contribution of the dopant to electron or hole transport. Exciton induced direct degradation and especially bimolecular annihilation reactions on the other hand are likely to be induced by guest (dopant) excitons since the excited state lifetimes of the phosphorescent metal-organic dopants are significantly longer (typically 0.5 - 5 μs)<sup>[64]</sup> than of the organic host materials. Recent investigations by Siboni and Aziz on triplet polaron annihilation furthermore indicated that positive charges (holes) located on the phosphorescent dopant are more efficient quenchers for triplet polaron annihilation than charges located on the host

## CHAPTER 1

material for the same system.<sup>[10]</sup> This indicates the importance of the stability of the phosphorescent guest for the overall operational lifetime of the devices and explains the huge efforts that are currently being expended to develop stable phosphorescent emitters. The analysis of chemical degradation mechanisms and products for these materials however proves to be significantly more difficult compared to other materials as the emitting layers typically contain only up to 15% of the phosphorescent dopants. Even though the low abundance of these species in the organic layers represents an additional challenge, there are a number of reports on the detection and structural identification of degradation products for phosphorescent emitters.

Direct LDI-MS analysis of driven devices, as developed and employed by Leo *et al.*, for example proved to be a valuable tool for the investigation of these species.<sup>[19]</sup> By comparing the mass spectra of pristine and driven phosphorescent devices they were able to demonstrate, that cyclometalated homo- and heteroleptic iridium emitters can undergo ligand dissociation reactions during device operation.<sup>[35, 65-67]</sup> A possible explanation for this degradation pathway is the thermal population of higher lying metal-centered states upon excitation. This phenomenon has been proven to be responsible for the temperature dependent emission quenching of a number of transition metal complexes at room temperature.<sup>[68-69]</sup> Spectroscopic investigations in correlation with DFT calculations for a number of green to blue emitting iridium compounds suggested that the thermal population of higher lying triplet metal-centered states (<sup>3</sup>MC, also called dd\* or ligand field states) leads to the rupture of an Ir-N bond.<sup>[70-71]</sup> The five coordinate species that is formed has been calculated to have a trigonal bipyramidal geometry with one ligand being monodentate after bond dissociation (Figure 10). This ligand showed a twisted geometry where the dihedral angle between the phenyl moiety and the heterocycle was  $> 50^\circ$ . At room temperature, these high energy states are thermally accessible only via the high excitation energies of blue emitting complexes while the activation energy is too high for green and red phosphorescent compounds. Nevertheless, it is conceivable that upon exciton-exciton or exciton-polaron annihilation (see 2nd section) these states become accessible and therefore play a role in the degradation of these materials as well.

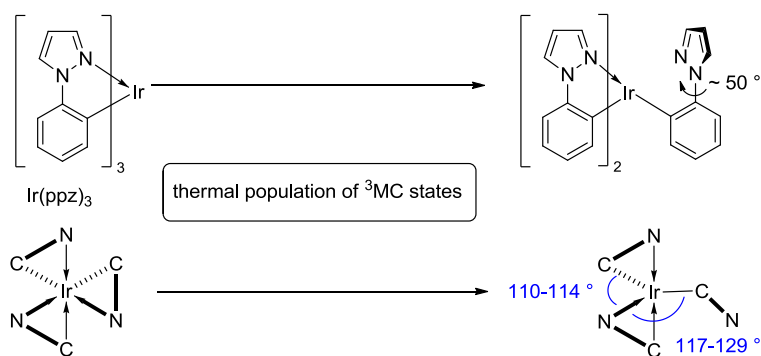
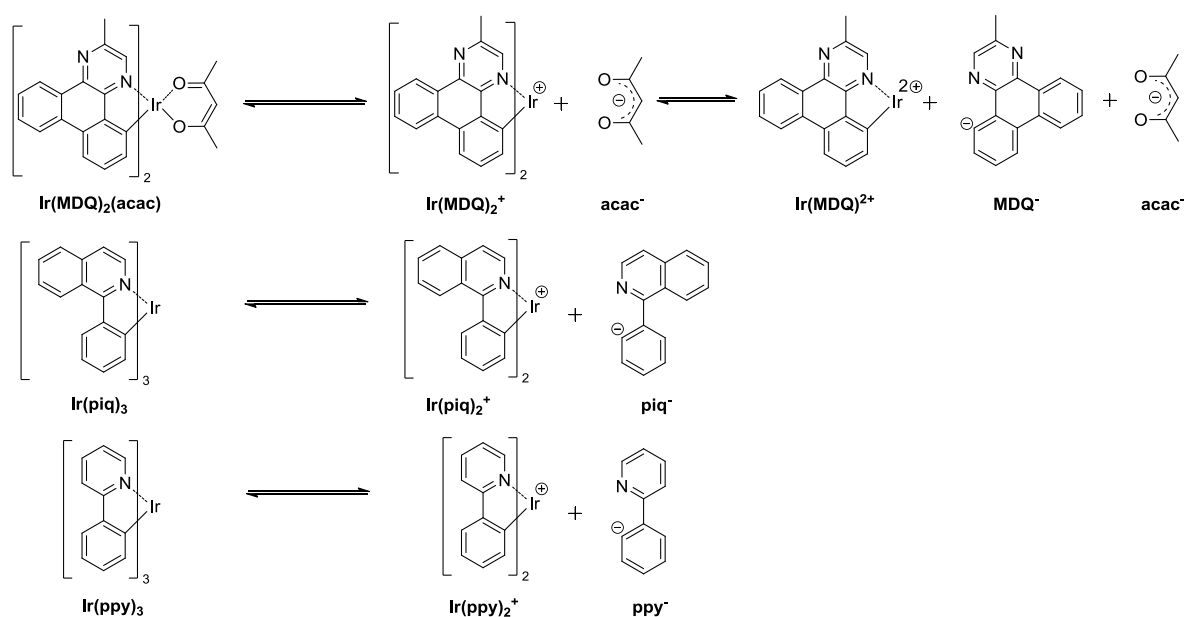


**Figure 10.** Bond rupture via the thermal population of higher lying <sup>3</sup>MC states.<sup>[70]</sup>

After excitation and thermal population of the  $^3\text{MC}$  states, the partly dissociated ligand might fully dissociate to give a fragment of type  $(\text{C}^{\wedge}\text{N})_2\text{Ir}^+$  (Scheme 6). The weaker Ir-heteroatom bonds in ancillary ligands are more prone to bond rupture and thus can explain the often observed diminished stability of heteroleptic emitters compared to homoleptic ones in OLED devices. Recently, it was shown that the cleavage of N^O and O^O ancillary ligands of iridium complexes can also be induced by the presence of protons. The authors reasoned that since protons can be present in devices, for example due to the use of PEDOT:PSS as hole injection material, acid induced degradation could also be one of the responsible mechanisms for the observed device degradation of heteroleptic emitters.<sup>[72]</sup>



**Scheme 6.** Ligand dissociation pathways for red and green phosphorescent iridium complexes.

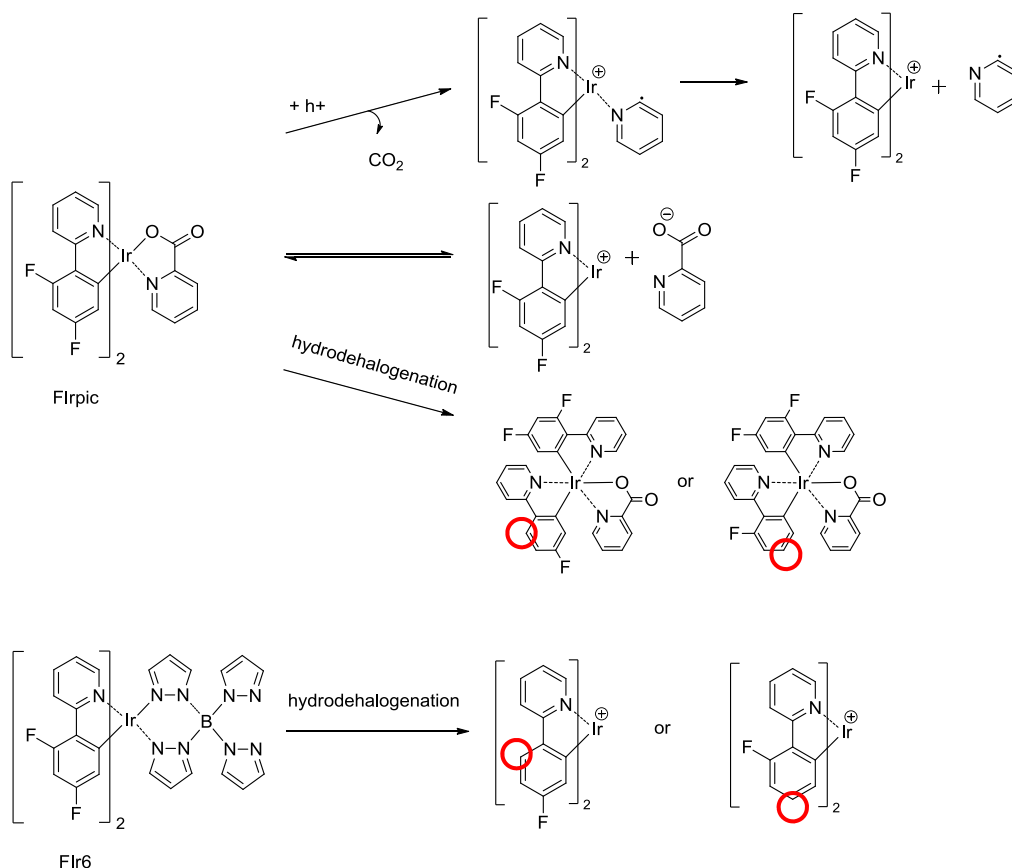
While these dissociation processes should in principle be reversible, the resulting charged, coordinatively unsaturated fragments are likely to undergo further reactions with surrounding molecules. For a variety of different homo- and heteroleptic iridium emitters such as  $\text{Ir}(\text{MDQ})_2(\text{acac})$ ,  $\text{Ir}(\text{piq})_3$ ,  $\text{Ir}(\text{ppy})_3$  and  $\text{Irpic}$ , the complex fragments were shown to undergo reactions with molecules of the adjacent transport layers. For  $\text{Ir}(\text{MDQ})_2(\text{acac})$  and  $\text{Ir}(\text{piq})_3$ -based red phosphorescent OLEDs, the interaction strength between emitter fragments and different HBL materials (BPhen, TPBi, AlQ<sub>3</sub>) correlated directly with the obtained device lifetimes.<sup>[46, 73]</sup> The stronger the interaction between the employed hole blocker and the dopant fragments, the lower was the operating stability of the corresponding devices. This emphasizes that OLED degradation and the stability of single components cannot be discussed without considering the chemical interactions between the different materials present in a device.

## CHAPTER 1

This ligand dissociation has been observed for dopants of different molecular structure and emission color in a variety of device structures and is backed by spectroscopic and quantum chemical investigations. It can therefore be considered a somewhat general pathway that might be responsible for the deterioration of phosphorescent dopants. Nevertheless, depending on the structure of the employed complexes there are multiple other possibilities for their degradation. Some groups or bonds of the dopants might be particularly prone to dissociation or bond rupture due to weaker bond strengths. However, the observed dissociation reactions cannot always be rationalized *via* bond dissociation energies.

Especially interesting is the case of the sky blue phosphorescent emitter Flrpic: While highly efficient blue OLEDs could be achieved with this emitter, its extremely low operational stability prevents its use for commercial applications. It was observed that in addition to the ligand dissociation processes known for other emitters, a loss of CO<sub>2</sub> from the picolate ligand takes place (Scheme 7). This renders the dissociation step irreversible and could thus account for its exceptionally low stability in devices.<sup>[66]</sup> Furthermore, the cleavage of fluorine substituents upon thermal vapor deposition as well as through electrical aging was detected *via* the comparison of HPLC-MS data of unprocessed materials, pristine and driven devices (Scheme 7).<sup>[17]</sup> This dissociation of fluorine atoms could recently also be shown for another blue emitter (Fir6) and might provide an explanation for the often observed detrimental effect of fluorination on device lifetimes.<sup>[74]</sup>

The exact mechanism of this fluorine cleavage nevertheless is still unknown. The C-F bond is one of the strongest single bonds known and an explanation *via* bond energies is therefore invalid in this case. It also remains unclear whether the reactions proceed *via* an ionic or a radical pathway and how the hydrodehalogenation takes place. Due to the detection of fluorinated degradation products of other materials in the examined devices, an exchange of the fluorine atoms between the emitter and neighboring molecules was suggested.



**Scheme 7.** Degradation products of blue phosphorescent emitters Irpic and Ir6 as detected via LDI-TOF MS. The exact mechanism of the fluorine cleavage remains unclear.

An interesting example for the identification of problematic structural features was presented by UDC (Universal Display Corporation) who found that N-phenyl substituted phenylimidazole (pim) based blue emitters showed significantly enhanced lifetimes compared to the corresponding N-methyl substituted ones.<sup>[75]</sup> In order to rationalize this, Treboux *et al.* performed an analysis of the triplet potential energy surface of these compounds.<sup>[76]</sup> They calculated that a homolytic dissociation of the methyl group of Ir(Me-pim)<sub>3</sub> slightly stabilizes the excited complex and therefore presents a likely pathway for its faster degradation. The authors reason that since the excited state has significant MLCT character, the additional electron, transferred to the imidazole heterocycle upon excitation, disrupts the aromaticity which can be regained by dissociation of the methyl radical. The dissociation of a phenyl radical from Ir(Ph-pim)<sub>3</sub> on the other hand would destabilize the complex and is therefore disfavored - accounting for the higher stability of this material (Figure 11).

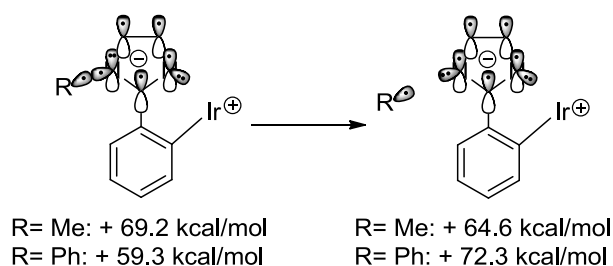


**Figure 11.** Schematic representation of the MLCT excited states before and after dissociation of  $\text{Ir}(\text{Me-pim})_3$  and  $\text{Ir}(\text{Ph-pim})_3$  and corresponding calculated energies.<sup>[76-77]</sup>

One of the major challenges in the OLED field to date is still the development of a stable phosphorescent blue. While there has been considerable progress in the lifetime of blue emitters and materials with lifetimes of up to 20,000 h are now commercially available,<sup>[78]</sup> most of the more stable materials do not exhibit a deep blue color but rather show sky- to light blue phosphorescence. Compared to lifetimes ( $\text{LT}_{50}$ ) of several hundred thousand hours for red and green phosphorescence, there is still a significant improvement in the stability required. The difficulty in their development lies in the inherent properties of blue emitting materials. Their large band gap render their reduced or oxidized form a potent reductant or oxidant, respectively, and a variety of redox processes might be induced via these species. Furthermore, the higher excited state energies often increase the accessibility of higher lying electronic states leading to dissociation and bond rupture processes as already discussed above.

## 4.5 Strategies for the Stability Improvement of Phosphorescent Dopants

When designing new materials with enhanced stabilities to reduce degradation and improve operational device stabilities, there are a few possible approaches. One way is to eliminate or reinforce parts of the structure that are known to be susceptible to degradation. Methyl groups in phenylimidazole based complexes or fluorine substituents in the case of  $\text{Flrpic}$  or  $\text{Flr6}$  are obvious examples for these approaches.

As degradation of the emitting layer often involves the participation of excitons, the exciton lifetime is likely to have a significant impact on the stability of the devices. The deactivation of excited states is always governed by a competition between the radiative decay and all non-radiative deactivation routes including possible exciton induced degradation pathways. A higher radiative rate (which at a given quantum yield corresponds to a shorter excited state lifetime) thus not only increases the external quantum efficiency of a device but also reduces the likelihood of direct degradation. Furthermore, a shorter excited state lifetime significantly reduces the exciton density in the emission layer and therefore the probability of bimolecular annihilation reactions leading to the deterioration of the materials. For an in-depth discussion on the triplet state photophysics of organo-transition metal compounds and strategies to obtain high radiative



rates, the interested reader may be referred to recent reviews on the subject by Yersin *et al.* and references therein.<sup>[64, 79]</sup>

Another promising handle to improve operational lifetimes is to reduce the probability of the ligand dissociation mechanism that has been discussed above. One strategy is to make the dissociative  $^3\text{MC}$  states less accessible. The use of strongly coordinating ligands should raise the metal-centered state energies and might thus decrease the rate of destructive deactivation. A promising approach for achieving blue phosphorescence while maintaining a sufficient energy gap between the emissive and the  $^3\text{MC}$ -states are therefore Ir-carbene complexes. Ir(pmb)<sub>3</sub> for example exhibits a significantly higher  $^3\text{MC}$  state energy (28 000 cm<sup>-1</sup>) compared to complexes with C^N ligands (21,700 to 24,000 cm<sup>-1</sup>).<sup>[70, 80]</sup>

Favoring the radiative over non-radiative decay, possibly destructive deactivation modes could also be achieved by limiting the freedom of the excited molecules to rearrange and thus preventing the dissociation of the metal-ligand bonds. Increased rigidity of the complexes can be achieved by bridging the two ring systems of the cyclometalating ligands as in Ir(bzq)<sub>3</sub> (Figure 12). Rigidified ligands are a reoccurring theme in patent literature, which shows that this approach is also being employed in industry.<sup>[81-83]</sup> Figure 12 illustrates some of the parent structures of bridged phosphorescent iridium complexes found in academic and patent literature.

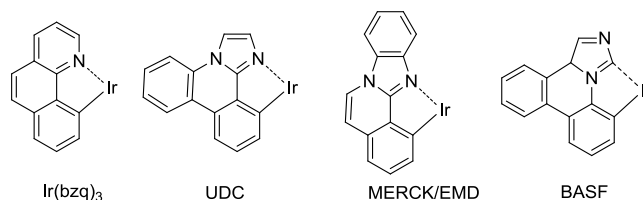


**Figure 12.** Structures of iridium complexes with rigidified ligands as found in academic and patent literature.<sup>[81-83]</sup>

Increasing the rigidity, raising the ligand field strength and thus the activation energy for quenching *via* the mentioned dd\* states can also be achieved by using higher dentate ligands. This effect has been shown to greatly enhance quantum yields in a variety of Pt-complexes when going from bidentate to tri- or even tetradentate ligands.<sup>[84-86]</sup> In fact, it was recently reported that OLEDs incorporating a red phosphorescent tetradentate Pt-complex could reach similar performance and lifetimes as ones with the iridium based emitter Ir(piq)<sub>3</sub> in comparable device setups.<sup>[87]</sup>

Optimization of the emitter environment is another interesting approach to increase stability. It was found that the population of metal-centered states can be reduced or suppressed by a rigid matrix and photoinitiated ligand dissociation reactions can be suppressed in certain cases.<sup>[64, 88]</sup> By optimizing interactions between the emitter and the host materials in order to provide a rigid Ir environment, it might be possible to significantly

## CHAPTER 1

reduce destructive deactivation of the excited states. Moreover, a careful selection of host materials might also prevent possible reactions between emitter and host molecules such as the adduct formation mentioned above. Researchers at Fujifilm utilized this strategy by screening the stability of different host:guest combinations under UV-irradiation and were thus able to significantly improve the operational stability of blue phosphorescent devices.<sup>[89]</sup>

## 5. CONCLUSION

In summary, we discussed the different chemical processes responsible for the intrinsic degradation of state-of-the-art organic light-emitting diodes. The initial step in the observed degradation reactions is often a bond dissociation process. This can be homo- or heterolytic, caused either by charge carriers, excitons or bimolecular annihilation reactions between two excitons or excitons and polarons. The resulting species are highly reactive charged or radical fragments that can undergo further reactions with surrounding molecules and thus form charge traps or luminescent quenching sites.

The observed products, in combination with the results of quantum chemical calculations, shed light on the type of bonds, structural features or electronic states that are problematic with regard to chemical stability. The insights gained via the elucidation of these reaction pathways have direct implications for the design of new materials. Some promising approaches such as rigidification, shielding of potentially reactive moieties or tuning of energy levels to limit the accessibility of certain electronic states have already been employed. The investigations also clearly show that the interactions between different materials can be of utmost importance and should be taken into consideration when trying to improve operational stabilities. An interesting example is the degradation of red phosphorescent devices containing Ir(piq)<sub>3</sub> or Ir(MDQ)<sub>2</sub>(acac) where the stability of the phosphorescent dopant seems to depend heavily on the employed hole blocking material.

Even though some of the reaction pathways could be resolved for certain materials commonly used in OLEDs, chemical degradation is a complex subject. To gain deeper insights into the processes for different types of materials, a combined effort of physicists, engineers, analytical and theoretical chemists will be required. In depth knowledge of these processes will eventually enable to overcome the shortcomings and limitations of present materials to realize highly efficient and stable organic light-emitting diodes.

## 6. REFERENCES

- [1] M. Pope, H. P. Kallmann, P. Magnante, *J. Chem. Phys.* **1963**, 38, 2042-2043.
- [2] C. W. Tang, S. A. VanSlyke, *Appl. Phys. Lett.* **1987**, 51, 913-915.
- [3] M. A. Baldo, D. F. O'Brien, Y. You, A. Shoustikov, S. Sibley, M. E. Thompson, S. R. Forrest, *Nature* **1998**, 395, 151-154.
- [4] N. C. Giebink, B. W. D'Andrade, M. S. Weaver, P. B. Mackenzie, J. J. Brown, M. E. Thompson, S. R. Forrest, *J. Appl. Phys.* **2008**, 103, 044509.
- [5] J. Kalinowski, W. Stampor, J. Mężyk, M. Cocchi, D. Virgili, V. Fattori, P. Di Marco, *Phys. Rev. B* **2002**, 66, 235321.
- [6] M. A. Baldo, S. R. Forrest, *Phys. Rev. B* **2000**, 62, 10958-10966.
- [7] M. A. Baldo, C. Adachi, S. R. Forrest, *Phys. Rev. B* **2000**, 62, 10967-10977.
- [8] N. Nakashima, K. Yoshihara, *J. Phys. Chem.* **1989**, 93, 7763-7771.
- [9] N. C. Giebink, B. W. D'Andrade, M. S. Weaver, J. J. Brown, S. R. Forrest, *J. Appl. Phys.* **2009**, 105, 124514.
- [10] H. Z. Siboni, H. Aziz, *Appl. Phys. Lett.* **2012**, 101, 063502-063504.
- [11] D. Y. Kondakov, W. C. Lenhart, W. F. Nichols, *J. Appl. Phys.* **2007**, 101, 024512-024517.
- [12] V. Jankus, C. Winscom, A. P. Monkman, *J. Chem. Phys.* **2009**, 130, 074501.
- [13] C. Y. Kwong, A. B. Djurišić, W. C. H. Choy, D. Li, M. H. Xie, W. K. Chan, K. W. Cheah, P. T. Lai, P. C. Chui, *Mater. Sci. Engin.: B* **2005**, 116, 75-81.
- [14] D. Y. Kondakov, T. D. Pawlik, W. F. Nichols, W. C. Lenhart, *J. Soc. Information Display* **2008**, 16, 37-46.
- [15] V. Jankus, C. Winscom, A. P. Monkman, *J. Chem. Phys.* **2009**, 130, 074501.
- [16] V. Sivasubramaniam, F. Brodkorb, S. Hanning, O. Buttler, H. P. Loebl, V. van Elsbergen, H. Boerner, U. Scherf, M. Kreyenschmidt, *Solid State Sci.* **2009**, 11, 1933-1940.
- [17] V. Sivasubramaniam, F. Brodkorb, S. Hanning, H. P. Loebl, V. van Elsbergen, H. Boerner, U. Scherf, M. Kreyenschmidt, *J. Fluorine Chem.* **2009**, 130, 640-649.
- [18] D. Y. Kondakov, *J. Appl. Phys.* **2008**, 104, 084520-084529.
- [19] S. Scholz, K. Walzer, K. Leo, *Adv. Funct. Mater.* **2008**, 18, 2541-2547.
- [20] V. Sivasubramaniam, Ph. D. Thesis, Bergische Universität Wuppertal, GER (urn:nbn:de:hbz:468-20110207-154757-3), **2010**.
- [21] S. Scholz, R. Meerheim, B. Lussem, K. Leo, *Appl. Phys. Lett.* **2009**, 94, 043314-043313.
- [22] A. Choi, T. Yamaguchi, C.-H. Han, *Res. Chem. Interm.* **2012**, 1-9.
- [23] P. J. Low, M. A. J. Paterson, D. S. Yufit, J. A. K. Howard, J. C. Cherryman, D. R. Tackley, R. Brook, B. Brown, *J. Mater. Chem.* **2005**, 15, 2304-2315.
- [24] C. Adachi, K. Nagai, N. Tamoto, *Appl. Phys. Lett.* **1995**, 66, 2679-2681.
- [25] S. O. Okutsu, T.; Tamano, M.; Enokida, T., *IEEE Trans. Electr. Dev.* **1997**, 44, 1302-1306.
- [26] J.-H. Pan, H.-L. Chiu, L. Chen, B.-C. Wang, *Comput. Mater. Sci.* **2006**, 38, 105-112.
- [27] J. Pan, Y. Chou, H. Chiu, B. Wang, *Aust. J. Chem.* **2009**, 62, 483-492.
- [28] N. Lin, J. Qiao, L. Duan, H. Li, L. Wang, Y. Qiu, *J. Phys. Chem. C* **2012**, 116, 19451-19457.
- [29] Z. D. Popovic, H. Aziz, N.-X. Hu, A.-M. Hor, G. Xu, *Synth. Met.* **2000**, 111-112, 229-232.

## CHAPTER 1

- [30] Y. Luo, H. Aziz, G. Xu, Z. D. Popovic, *Chem. Mater.* **2007**, *19*, 2079-2083.
- [31] V. V. Jarikov, D. Y. Kondakov, *J. Appl. Phys.* **2009**, *105*, 034905-034908.
- [32] F. Papadimitrakopoulos, X. M. Zhang, D. L. Thomsen, K. A. Higginson, *Chem. Mater.* **1996**, *8*, 1363-1365.
- [33] H. P. Aziz, Z. D.; Hu, N.-X.; Hor, A.-M.; Xu, G., *Science* **1999**, *283*, 1900-1902.
- [34] Z. D. Popovic, H. Aziz, A. Ioannidis, N.-X. Hu, P. N. M. dos Anjos, *Synth. Met.* **2001**, *123*, 179-181.
- [35] S. Scholz, C. Corten, K. Walzer, D. Kuckling, K. Leo, *Org. Electron.* **2007**, *8*, 709-717.
- [36] S. Scholz, B. Lussem, K. Leo, *Appl. Phys. Lett.* **2009**, *95*, 183309-183303.
- [37] D. Y. Kondakov, *J. Appl. Phys.* **2005**, *97*, 024503-024505.
- [38] S. C. Tse, H. H. Fong, S. K. So, *J. Appl. Phys.* **2003**, *94*, 2033-2037.
- [39] T.-Y. Chu, Y.-H. Lee, O.-K. Song, *Appl. Phys. Lett.* **2007**, *91*, 223509-223503.
- [40] R. Meerheim, S. Scholz, G. Schwartz, S. Reineke, S. Olthof, K. Walzer, K. Leo, *Proc. SPIE* **2008**, 699917-699917.
- [41] H. H. Fong, W. C. H. Choy, K. N. Hui, Y. J. Liang, *Appl. Phys. Lett.* **2006**, *88*, 113510-113513.
- [42] I. R. de Moraes, S. Scholz, B. Lüssem, K. Leo, *Org. Electron.* **2012**, *13*, 1900-1907.
- [43] S. Scholz, R. Meerheim, K. Walzer, K. Leo, *Proc. SPIE* **2008**, 69991B-69991B.
- [44] I. R. de Moraes, S. Scholz, B. Lussem, K. Leo, *Appl. Phys. Lett.* **2011**, *99*, 053302-053303.
- [45] S. Scholz, Q. Huang, M. Thomschke, S. Olthof, P. Sebastian, K. Walzer, K. Leo, S. Oswald, C. Corten, D. Kuckling, *J. Appl. Phys.* **2008**, *104*, 104502-104510.
- [46] R. Meerheim, S. Scholz, S. Olthof, G. Schwartz, S. Reineke, K. Walzer, K. Leo, *J. Appl. Phys.* **2008**, *104*, 014510-014518.
- [47] D. Y. Kondakov, C. T. Brown, T. D. Pawlik, V. V. Jarikov, *J. Appl. Phys.* **2010**, *107*, 024507-024508.
- [48] D. Y. Kondakov, C. T. Brown, T. D. Pawlik, *SID Symp. Digest Tech. Papers* **2010**, *41*, 43-46.
- [49] Q. Wang, Y. Luo, H. Aziz, *J. Appl. Phys.* **2010**, *107*, 084506-084506.
- [50] A. Kanitz, G. F. Mielke, O. Nuyken, J. Simmerer, Siemens AG, WO 01/56091 A2 , **2001**.
- [51] A. Parham, H. Vestweber, S. Heun, H. Heil, P. Stoeßel, R. Fortte, Merck Patent GmbH, DE102005043163 A1 , **2007**.
- [52] A. Parham, C. Pflumm, Merck Patent GmbH, WO 2011/128017 A1 , **2011**.
- [53] C. Hosokawa , M. Funahashi , Idemitsu Kosan Co., EP 1 219 590 A1 , **2001**.
- [54] Y. Shirota, *J. Mater. Chem.* **2000**, *10*, 1-25.
- [55] L. S. Hung, C. H. Chen, *Mater. Sci. Eng., R* **2002**, *39*, 143-222.
- [56] K. Katsuma, Y. Shirota, *Adv. Mater.* **1998**, *10*, 223-226.
- [57] W. Ishikawa, K. Noguchi, Y. Kuwabaru, Y. Shirota, *Adv. Mater.* **1993**, *5*, 559-561.
- [58] P. Kundu, K. R. Justin Thomas, J. T. Lin, Y. T. Tao, C. H. Chien, *Adv. Funct. Mater.* **2003**, *13*, 445-452.
- [59] H. Ogawa, H. Inada, Y. Shirota, *Macromol. Symp.* **1998**, *125*, 171-180.
- [60] J. P. Chen, H. Tanabe, X.-C. Li, T. Thoms, Y. Okamura, K. Ueno, *Synth. Met.* **2003**, *132*, 173-176.
- [61] J. Salbeck, N. Yu, J. Bauer, F. Weissörtel, H. Bestgen, *Synth. Met.* **1997**, *91*, 209-215.

- [62] M. Xu, C. Yi, C.-J. Yang, J.-H. Wang, Y.-Z. Liu, B. Xie, X.-C. Gao, P. Wang, D.-C. Zou, *Thin Solid Films* **2008**, 516, 7720-7726.
- [63] S. Yin, Y. Hua, X. Chen, X. Yang, Y. Hou, X. Xu, *Synth. Met.* **2000**, 111-112, 109-112.
- [64] H. Yersin, A. F. Rausch, R. Czerwieniec, T. Hofbeck, T. Fischer, *Coord. Chem. Rev.* **2011**, 255, 2622-2652.
- [65] I. R. de Moraes, S. Scholz, B. r. Lüsse, K. Leo, *Appl. Phys. Lett.* **2011**, 99, 053302.
- [66] I. R. d. Moraes, S. Scholz, B. Lüsse, K. Leo, *Org. Electron.* **2011**, 12, 341-347.
- [67] S. Scholz, R. Meerheim, B. Lussem, K. Leo, *Appl. Phys. Lett.* **2009**, 94, 043314.
- [68] F. Barigelletti, D. Sandrini, M. Maestri, V. Balzani, A. Von Zelewsky, L. Chassot, P. Joliet, U. Maeder, *Inorg. Chem.* **1988**, 27, 3644-3647.
- [69] A. Islam, N. Ikeda, K. Nozaki, Y. Okamoto, B. Gholamkhass, A. Yoshimura, T. Ohno, *Coord. Chem. Rev.* **1998**, 171, 355-363.
- [70] T. Sajoto, P. I. Djurovich, A. B. Tamayo, J. Oxgaard, W. A. Goddard, M. E. Thompson, *J. Am. Chem. Soc.* **2009**, 131, 9813-9822.
- [71] L. Yang, F. Okuda, K. Kobayashi, K. Nozaki, Y. Tanabe, Y. Ishii, M.-a. Haga, *Inorg. Chem.* **2008**, 47, 7154-7165.
- [72] E. Baranoff, B. F. E. Curchod, J. Frey, R. Scopelliti, F. Kessler, I. Tavernelli, U. Rothlisberger, M. Grätzel, M. K. Nazeeruddin, *Inorg. Chem.* **2011**, 51, 215-224.
- [73] S. Scholz, R. Meerheim, B. Lüsse, K. Leo, *SID Symp. Digest Tech. Papers* **2009**, 40, 681-684.
- [74] R. Seifert, I. R. de Moraes, S. Scholz, M. C. Gather, B. Lüsse, K. Leo, *Org. Electron.* **2013**, 14, 115-123.
- [75] C. Lin, P. B. Mackenzie, R. Walters, J.-Y. Tsai, C. S. Brown, J. Deng, Universal Display Corporation, WO 2006/121811 A1, **2006**.
- [76] G. Treboux, J. Mizukami, M. Yabe, S. Nakamura, *J. Photopolym. Sci. Technol.* **2008**, 21, 347-348.
- [77] G. Treboux, J. Mizukami, M. Yabe, S. Nakamura, *Chem. Lett.* **2007**, 36, 1344-1345.
- [78] <http://www.universaldisplay.com/default.asp?contentID=604>, access date: November 23rd **2012**.
- [79] H. Yersin, A. F. Rausch, R. Czerwieniec, in *Physics of Organic Semiconductors* (Eds.: C. Adachi, R. Holmes, W. Brütting), Wiley-VCH, **2012**, p. 371.
- [80] R. J. Holmes, S. R. Forrest, T. Sajoto, A. Tamayo, P. I. Djurovich, M. E. Thompson, J. Brooks, Y. J. Tung, B. W. D'Andrade, M. S. Weaver, R. C. Kwong, J. J. Brown, *Appl. Phys. Lett.* **2005**, 87, 243507-243503.
- [81] D. B. Knowles, C. Lin, P. B. Mackenzie, J.-Y. Tsai, R. Walters, S. A. Beers, C. S. Brown, W. H. Yeager, E. Barron, Universal Display Corporation, WO 2008/156879 A1, **2008**.
- [82] P. Stoessel, H. Heil, D. Joosten, C. Pflumm, A. Gerhard, E. Breuning, Merck Patent GmbH, WO 2010/086089 A1, **2010**.
- [83] O. Molt, C. Lennartz, E. Fuchs, K. Kahle, N. Langer, C. Schildknecht, J. Rudolph, G. Wagenblast, S. Watanabe, BASF SE, WO 2009/050281 A1, **2009**.
- [84] A. F. Rausch, L. Murphy, J. A. G. Williams, H. Yersin, *Inorg. Chem.* **2011**, 51, 312-319.
- [85] D. A. K. Vezzu, J. C. Deaton, J. S. Jones, L. Bartolotti, C. F. Harris, A. P. Marchetti, M. Kondakova, R. D. Pike, S. Huo, *Inorg. Chem.* **2010**, 49, 5107-5119.
- [86] D. Ravindranathan, D. A. K. Vezzu, L. Bartolotti, P. D. Boyle, S. Huo, *Inorg. Chem.* **2010**, 49, 8922-8928.

## CHAPTER 1

- [87] H. Fukagawa, T. Shimizu, H. Hanashima, Y. Osada, M. Suzuki, H. Fujikake, *Adv. Mater.* **2012**, 24, 5099-5103.
- [88] D. W. Thompson, C. N. Fleming, B. D. Myron, T. J. Meyer, *J. Phys. Chem. B* **2007**, 111, 6930-6941.
- [89] W. Sotoyama, T. Satoh, M. Kinoshita, M. Tobise, K. Kawato, T. Ise, H. Takizawa, S. Yamashita, *Fujifilm Research and Development* **2010**, No.055, 24-28.

# CHAPTER 2

## **RAPID COMBINATORIAL SYNTHESIS AND CHROMATOGRAPHY BASED SCREENING OF PHOSPHORESCENT IRIIDIUM COMPLEXES FOR SOLUTION PROCESSING<sup>†</sup>**

Combinatorial synthesis in combination with a chromatography based separation and characterization allows for the rapid screening of new phosphorescent iridium complexes as emitters for organic light-emitting diodes. The approach provides information on the photophysical properties, phosphorescence efficiencies and photostabilities of the new compounds and speeds up the discovery of promising new emitters for solution processing.

---

<sup>†</sup> The establishment and optimization of the screening system was done by Susanna Schmidbauer and Andreas Hohenleutner in equal contribution. Synthesis and screening of the Buchwald-Hartwig libraries were performed by A. H.; Synthesis and screening of the Suzuki-Miyaura libraries by S. S..





## 1. INTRODUCTION

Iridium complexes have been employed as dyes for biological labeling<sup>[1-3]</sup> and sensing of different analytes,<sup>[4-5]</sup> as photon upconversion agents,<sup>[6-7]</sup> dyes for dye-sensitized solar cells (DSSCs),<sup>[8]</sup> photocatalysts for CO<sub>2</sub> reduction and water splitting<sup>[9-12]</sup> and more recently as efficient catalysts in the emerging field of organo-photoredox catalysis.<sup>[13-15]</sup> While their unique properties make them promising candidates in all of the above mentioned areas, their current most important application is their use as emitters in organic light-emitting devices (OLEDs). Spurred by the discovery of the triplet harvesting effect by Forrest *et al.* in 1998,<sup>[16]</sup> enabling a theoretical internal quantum efficiency of 100%, the number of reported phosphorescent iridium complexes has grown significantly over the last decade. The preference of cyclometalated iridium complexes for OLED applications can be rationalized by their extremely high triplet quantum yields,<sup>[17-18]</sup> the predictability and tunability of their emission color over the whole visible spectrum, good thermal and photostability compared to other transition metal complexes as well as their good synthetic accessibility.<sup>[19-21]</sup> For OLEDs produced via thermal vapor deposition, the excellent performance of these devices has already allowed the technology to enter mass production. However, there are still important challenges to be met. Even though there has been substantial progress in improving the operational lifetime of phosphorescent emitters, further improvement in the stability of these materials is desirable to obtain highly efficient and long term stable devices. To realize large area display and lighting applications at a competitive price, it is furthermore of interest to develop materials with sufficient solubility in suitable solvents to enable processing from solution for example via ink jet printing.

While modern computational methods can provide reliable information on the emission energies,<sup>[22-26]</sup> the color purity and in particular the stability of the iridium complexes cannot be predicted in such a straightforward fashion. To deepen the understanding of these compounds and gain insight into structure-property relationships concerning those essential criteria, it is still necessary to synthesize and characterize a large number of compounds.

While combinatorial chemistry is a well-established tool for the rapid synthesis of potential biologically active molecules<sup>[27]</sup> or catalysts<sup>[28]</sup> there have been surprisingly few reports of combinatorial methods for the synthesis and screening of new phosphorescent emitters for OLEDs. Bernhard *et al.* reported the parallel synthesis of a number of iridium complexes and

## CHAPTER 2

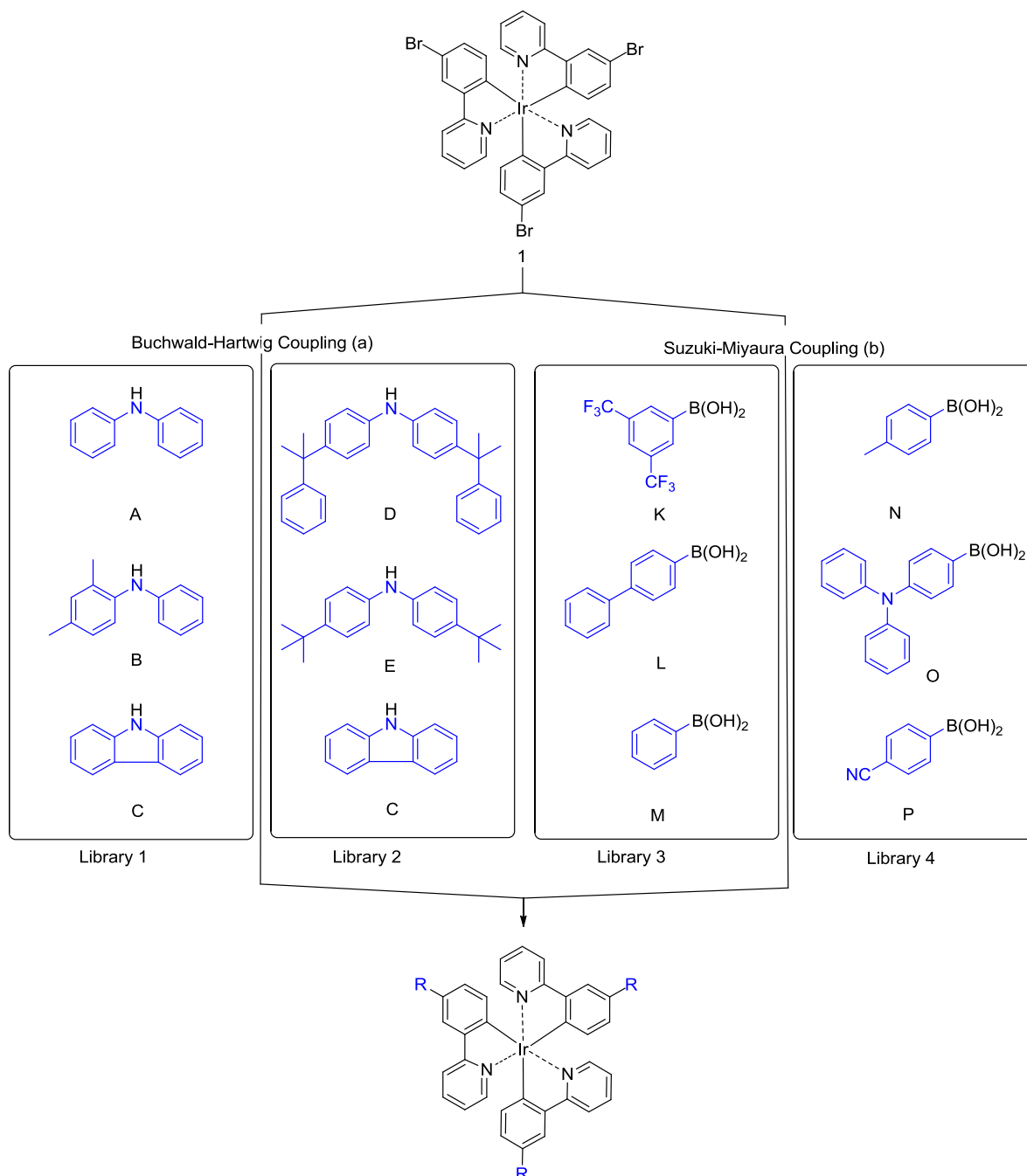
the screening of their photophysical properties directly from the reaction mixture, omitting any purification steps.<sup>[26]</sup> In 2006, Li *et al.* synthesized a library of iridium complexes by parallel solid phase synthesis and identified possible hits via their “on bead” emission.<sup>[29]</sup> Recently then, Nazeeruddin *et al.* prepared a library of 90 heteroleptic complexes via a similar approach as Bernhard's with a slightly modified procedure at room temperature.<sup>[30]</sup> However, as the purity of materials is absolutely vital for the operational device lifetime, the laborious, time consuming and therefore expensive purification of potential new emitters is still inevitable to obtain information about the stability of those compounds. Since the rapid purification of combinatorial libraries via chromatographic methods is an established technique in pharmaceutical industry,<sup>[31-33]</sup> we have developed a screening for phosphorescent iridium complexes based on this methodology. Having a small amount of the purified compounds available, we can determine the photophysical properties of the new compounds and initially assess their stability under continuous excitation.

## 2. RESULTS AND DISCUSSION

### 2.1 Synthesis

To develop the combinatorial synthesis and screening we chose to focus on structures derived from the epitomal Ir(ppy)<sub>3</sub> which despite being one of the first reported<sup>[34-35]</sup> phosphorescent emitters remains to be one of the most efficient and widely used dopants for phosphorescent OLEDs to date.<sup>[36]</sup> Incorporation of suitable dendritic structures at the periphery of an emitter is known to give special benefits to the original phosphorescent emitter: self-quenching can be suppressed via simple shielding of the emissive core by branched side chains. Following this strategy, high solid state quantum efficiencies were obtained using ethylhexyloxy chains as dendritic structures.<sup>[19]</sup> However, this benefit was limited by the fact that charge-carrier mobility and glass transition temperature  $T_g$  may be decreased. These drawbacks could be eliminated using arylated dendrons.<sup>[37-39]</sup> Another advantage using these structures is the enhanced solubility for a better compatibility regarding solution processing. Utilizing palladium mediated C-C and C-N coupling reactions (Buchwald-Hartwig and Suzuki-Miyaura respectively), arylated dendritic structures can be attached to the emitting iridium core starting from the Br-functionalized Ir(ppy)<sub>3</sub> derivative **1**<sup>[40]</sup> in order to obtain efficient and soluble phosphorescent emitters in excellent yields and purity.<sup>[41-43]</sup> The method is particularly advantageous for a combinatorial approach, as the introduction of structural diversity takes place in the last step of the synthesis. The time consuming preparation and purification of a variety of ligands can thus be avoided as boronic acids and diarylamines are widely available from commercial

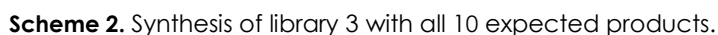
suppliers. Utilizing this post modification procedure, we synthesized 4 libraries, two of them via a Buchwald-Hartwig protocol and two via Suzuki-Miyaura reactions (Scheme 1).



**Scheme 1.** Synthesis of libraries 1-4. Reaction conditions: a)  $\text{Pd}(\text{OAc})_2$ ,  $\text{P}(\text{tBu})_3$ ,  $\text{NaOtBu}$ , toluene/dioxane, 130 °C, 4 h. b)  $\text{Pd}(\text{OAc})_2$ ,  $\text{P}(\text{o-tolyl})_3$ ,  $\text{K}_3\text{PO}_4$ , toluene/dioxane/water, 85 °C, 10 h.

For each of the libraries we combined precursor **1** with three different amines/boronic acids in a one-pot reaction, giving way to a total of 10 possible products per reaction. Scheme 2 exemplarily shows the synthesis of library 3 with all possible products. We assigned a letter to each of the coupling partners, so that all compounds prepared via the combinatorial approach can be described by a three letter code - each letter representing one introduced substituent. **MMM** for example is the compound where all three bromine

functionalities have been replaced by a phenyl group via the Suzuki coupling with phenylboronic acid **M**. This combinatorial strategy facilitates the rapid generation of a large number of structurally diverse compounds as it enables the synthesis of up to 10 products with only one reaction to be performed. As a control, we synthesized and characterized several homoleptic reference complexes *via* conventional reactions. Their absorption and emission spectra were recorded and showed excellent agreement with the ones obtained from the combinatorial synthesis and screening.



## 2.2 Screening

To enable the separation and characterization of the compounds in our libraries on a suitable timescale, a chromatography based screening was developed. Figure 2 outlines the screening setup. In a first step, the crude reaction mixture is separated via a semipreparative HPLC system. A diode array detector (DAD) and a fluorescence detector (FLD) allow a peak based automated fraction collection and the simultaneous recording of absorption and phosphorescence spectra.

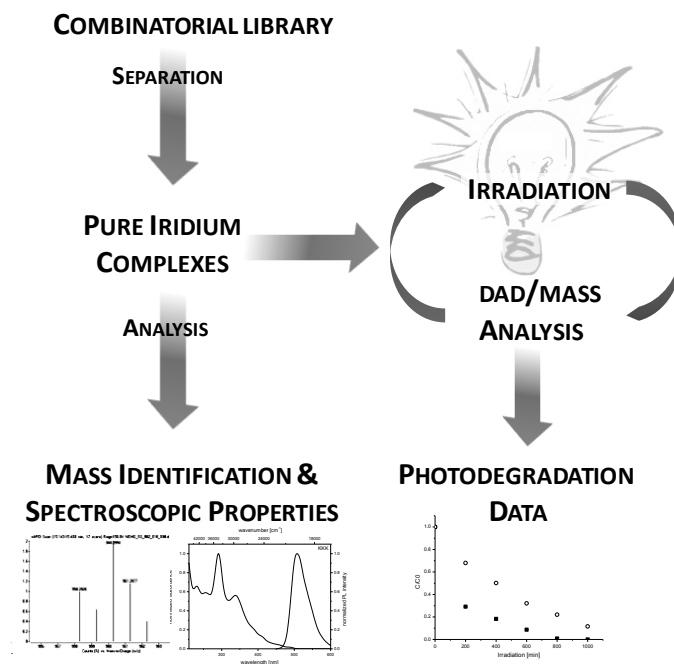


**Figure 2.** Schematic representation of the purification and screening process.

Figure 3 shows 3D-absorption- and emission-plots obtained from the separation of library 2. The eluted compounds were collected into vials, quantified and identified via LC-MS and then subjected to repeated irradiation and HPLC analysis to investigate the irradiation induced degradation of the compounds.

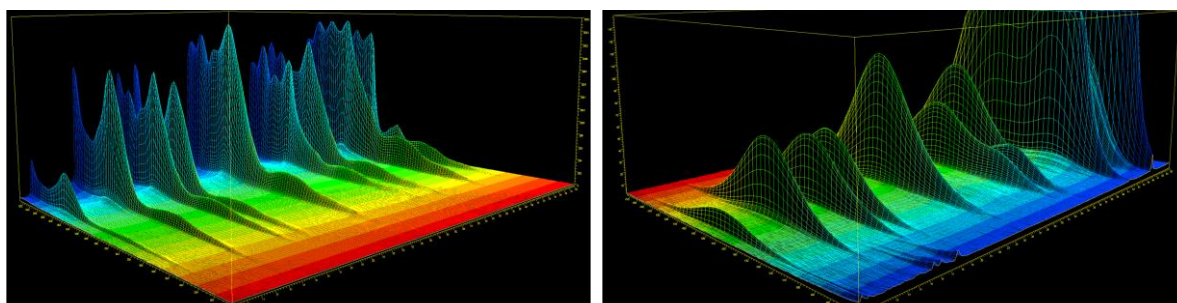


**Figure 3.** 3D-Plots from the separation of library 2. Left: Absorption intensity (z-axis) plotted against the wavelength (y-axis) and retention time (x-axis). Right: Emission intensity (z-axis) plotted against the wavelength (y-axis) and retention time (x-axis). The colors do not represent the colors as perceived by the eye.

## CHAPTER 2

### 2.3 Separation and Spectroscopic Properties

Of the 40 theoretically possible compounds, 36 could be separated and identified via LC-MS. The yields for the single compounds were estimated via the integrated area obtained from the chromatograms at 305 nm, assuming similar molar absorption coefficients for the different compounds. Apart from library 2 which showed a nearly statistical distribution of products, no clear trends in the reactivity of reactants could be elucidated. Their absorption and emission spectra (see Appendix) were recorded and the full width at half maximum (FWHM) was determined as an indicator of color purity. Table 1 gives an overview of all identified compounds, their maximum emission wavelengths and FWHM values as well as the  $m/z$  values obtained by LC-MS analysis.

While the complexes prepared via the Suzuki couplings all emit in the green region, introduction of arylamine moieties para to the metal leads to a significant bathochromic shift of the emission wavelength into the orange region. This is caused by the electron donating effect of the arylamine substituents, effectively increasing the donation to the metal via the Ir-C bond, destabilizing the metal-centered HOMO and thus reducing the HOMO-LUMO energy gap. The same trend, although not as pronounced, could also be observed depending on the substituents of the aryl or diarylamine groups. Increasing electron donating character leads to a red shifted emission while electron withdrawing substituents cause a blue shift of the emission maximum (Figure 4, left). The electronic influence of the substituents on the emission energy can be rationalized using Hammett parameters for para substitution. Plotting the emission maxima against  $\sigma_{\text{para}}$  of the substituents shows a good correlation with the notable exception of carbazole (Figure 4).

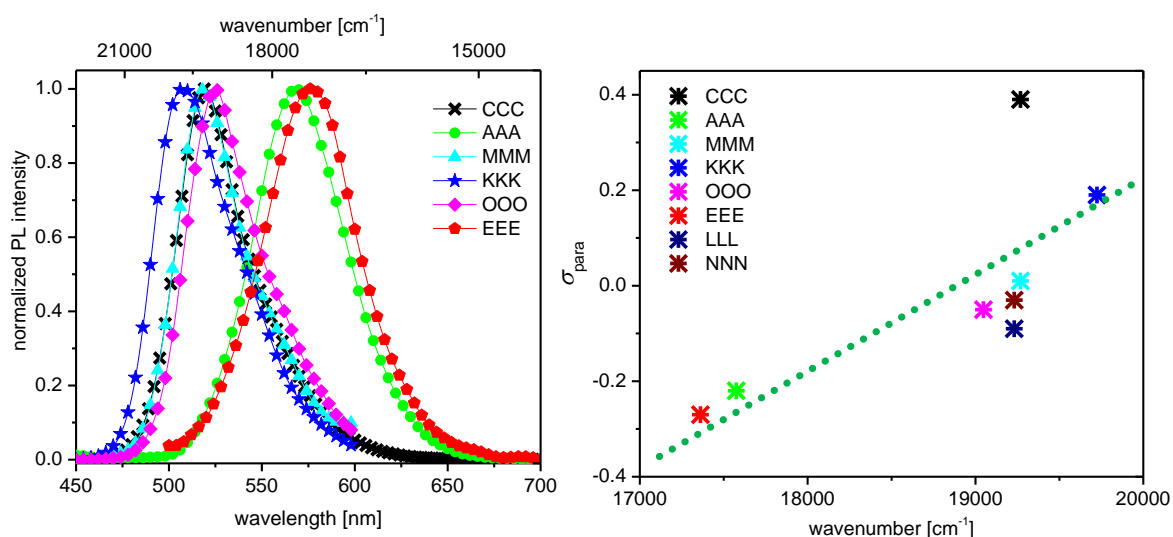


**Figure 4.** Phosphorescence spectra of selected homoleptic complexes illustrating the influence of electron donating and withdrawing groups on the emission energy (left). Hammett parameter  $\sigma_{\text{para}}$  plotted against the emission maxima (right). The dotted line is only a guide for the eye.

**Table 1.** Overview over all synthesized complexes with their yields, maximum emission wavelengths, FWHM values, PL quantum yields  $\Phi_P$  as well as the m/z (100%) values obtained via LC/MS.

	Code	Formula	m/z (100%) <sup>a)</sup>	$\lambda_{\max}$ [nm]	FWHM [nm]	$\Phi_P$ <sup>b)</sup>	Yield <sup>c)</sup>
Library 1	AAB	IrC <sub>71</sub> H <sub>55</sub> N <sub>6</sub>	1185.4227 (MH) <sup>+</sup>	571	59	0.24	6
	BBC	Ir C <sub>73</sub> H <sub>59</sub> N <sub>6</sub>	1211.4395 (MH) <sup>+</sup>	575	56	0.25	2
	AAA	IrC <sub>69</sub> H <sub>51</sub> N <sub>6</sub>	1157.3917 (MH) <sup>+</sup>	569	58	0.25	10
	ABC	IrC <sub>71</sub> H <sub>53</sub> N <sub>6</sub>	1183.4076 (MH) <sup>+</sup>	574	57	0.25	14
	AAC	IrC <sub>69</sub> H <sub>49</sub> N <sub>6</sub>	1155.3771 (MH) <sup>+</sup>	570	61	0.25	25
	BCC	IrC <sub>71</sub> H <sub>51</sub> N <sub>6</sub>	1181.3921 (MH) <sup>+</sup>	577	55	---	7
	ACC	IrC <sub>69</sub> H <sub>47</sub> N <sub>6</sub>	1153.3613 (MH) <sup>+</sup>	569	64	0.28	27
	CCC	IrC <sub>69</sub> H <sub>45</sub> N <sub>6</sub>	1151.3442 (MH) <sup>+</sup>	519	47	0.82	8
Library 2	EEE	IrC <sub>93</sub> H <sub>99</sub> N <sub>6</sub>	1493.7676 (MH) <sup>+</sup>	576	58	0.18	3
	EED	IrC <sub>103</sub> H <sub>103</sub> N <sub>6</sub>	1617.7987 (MH) <sup>+</sup>	576	60	0.16	12
	CEE	IrC <sub>85</sub> H <sub>81</sub> N <sub>6</sub>	1379.6264 (MH) <sup>+</sup>	575	61	0.19	11
	EDD	IrC <sub>113</sub> H <sub>107</sub> N <sub>6</sub>	1741.8296 (MH) <sup>+</sup>	575	59	0.19	14
	CED	IrC <sub>95</sub> H <sub>85</sub> N <sub>6</sub>	1503.6566 (MH) <sup>+</sup>	575	62	0.17	24
	CCE	IrC <sub>77</sub> H <sub>63</sub> N <sub>6</sub>	1265.4846 (MH) <sup>+</sup>	577	67	0.17	11
	CDD	IrC <sub>105</sub> H <sub>89</sub> N <sub>6</sub>	1627.6853 (MH) <sup>+</sup>	575	62	0.19	11
	CCD	IrC <sub>87</sub> H <sub>67</sub> N <sub>6</sub>	1388.5133 (MH) <sup>+</sup>	522	70	0.26	11
	CCC	IrC <sub>69</sub> H <sub>45</sub> N <sub>6</sub>	1151.3435 (MH) <sup>+</sup>	519	44	0.82	3
Library 3	KKK	IrC <sub>57</sub> H <sub>30</sub> N <sub>3</sub> F <sub>18</sub>	1292.1887 (MH) <sup>+</sup>	507	52	0.74	12
	KKM	IrC <sub>55</sub> H <sub>32</sub> N <sub>3</sub> F <sub>12</sub>	1156.2156 (MH) <sup>+</sup>	512	45	0.71	6
	KKL	IrC <sub>61</sub> H <sub>36</sub> N <sub>3</sub> F <sub>12</sub>	1232.2460 (MH) <sup>+</sup>	512	44	0.82	30
	KMM	IrC <sub>53</sub> H <sub>34</sub> N <sub>3</sub> F <sub>6</sub>	1020.2376 (MH) <sup>+</sup>	515	43	0.71	2
	KLM	IrC <sub>59</sub> H <sub>38</sub> N <sub>3</sub> F <sub>6</sub>	1096.2711 (MH) <sup>+</sup>	516	47	0.62	11
	KLL	IrC <sub>65</sub> H <sub>42</sub> N <sub>3</sub> F <sub>6</sub>	1172.2998 (MH) <sup>+</sup>	517	41	0.64	15
	MMM	IrC <sub>51</sub> H <sub>36</sub> N <sub>3</sub>	884.2608 (MH) <sup>+</sup>	519	41	0.77	1
	LMM	IrC <sub>57</sub> H <sub>40</sub> N <sub>3</sub>	960.2931 (MH) <sup>+</sup>	519	43	0.63	5
	LLM	IrC <sub>63</sub> H <sub>44</sub> N <sub>3</sub>	1036.3240 (MH) <sup>+</sup>	519	46	0.66	9
	LLL	IrC <sub>69</sub> H <sub>48</sub> N <sub>3</sub>	1112.3546 (MH) <sup>+</sup>	520	47	0.81	9
	NNN	IrC <sub>54</sub> H <sub>42</sub> N <sub>3</sub>	926.3083 (MH) <sup>+</sup>	520	46	0.85	7
Library 4	NNO	IrC <sub>65</sub> H <sub>49</sub> N <sub>4</sub>	1079.3663 (MH) <sup>+</sup>	522	45	0.77	6
	NOO	IrC <sub>76</sub> H <sub>56</sub> N <sub>5</sub>	1232.4257 (MH) <sup>+</sup>	522	49	0.77	15
	OOO	IrC <sub>87</sub> H <sub>63</sub> N <sub>6</sub>	1385.4813 (MH) <sup>+</sup>	525	45	0.71	35
	NNP	IrC <sub>54</sub> H <sub>39</sub> N <sub>4</sub>	937.2922 (MH) <sup>+</sup>	518	47	0.83	16
	NOP	IrC <sub>65</sub> H <sub>46</sub> N <sub>5</sub>	1090.3481 (MH) <sup>+</sup>	520	43	0.65	4
	OOP	IrC <sub>76</sub> H <sub>53</sub> N <sub>6</sub>	1243.4054 (MH) <sup>+</sup>	521	44	0.54	5
	NPP	IrC <sub>54</sub> H <sub>36</sub> N <sub>5</sub>	948.2694 (MH) <sup>+</sup>	515	44	0.76	11
	OPP	IrC <sub>65</sub> H <sub>43</sub> N <sub>6</sub>	1101.3259 (MH) <sup>+</sup>	517	44	---	1

a) obtained via LC/MS (+APCI). b) determined relative to the standard quinine hemisulfate monohydrate. c) estimated via the integral ratio of the products in the DAD trace.

## CHAPTER 2

To gain further insight on the photophysical properties of the compounds we also estimated the phosphorescence quantum yields  $\Phi_P$  of the complexes relative to a standard in a separate experiment. The obtained  $\Phi_P$  values vary greatly from 0.17 to 0.82. The compounds can be divided into two categories according to their quantum efficiencies: The first group exhibits good to excellent  $\Phi_P$  values of 0.62 - 0.85 and consists of the complexes obtained via the Suzuki-Miyaura reactions as well as the fully carbazole substituted **CCC**. The second group - obtained via Buchwald-Hartwig couplings - exhibits smaller  $\Phi_P$  values between 0.17 and 0.25.

It is well established that motional relaxation can be responsible for non-radiative transitions and that in return enhanced molecular rigidity and restricted intramolecular motion results in improved radiative rates.<sup>[19]</sup> Ono *et al.* examined the influence of different hole trapping moieties such as diphenylamine, carbazole and phenoxazine on Ir(ppy)<sub>3</sub> based complexes with the phenylpyridine ligands substituted at the 4-position of the phenyl ring.<sup>[45]</sup> They found significantly lower quantum yields for the conformationally free diphenylamine substituted compounds while the more rigid carbazole substituent gave an excellent  $\Phi_P$ . These observations are in good agreement with our obtained quantum yields for **CCC** ( $\Phi_P = 0.82$ ) and **AAA** ( $\Phi_P = 0.25$ ). This trend continues when looking at the different arylamine substituents in relation to each other - the higher the conformational flexibility of the arylamine substituents, the lower the  $\Phi_P$  values seem to be. Compounds containing flexible substituents such as dimethylbenzyl (**D**) or *tert*-butyl (**E**) ( $\Phi_P = 0.17 - 0.19$ ) show slightly reduced phosphorescence efficiencies compared to the methyl- or non-substituted diphenylamines **A** and **B** ( $\Phi_P \sim 0.25$ ). Interestingly, the substitution with triphenylamine (**O**) did not lead to a significant reduction of  $\Phi_P$  which indicates that the introduction of flexibility on the periphery of the molecule further away from the emitting center does not significantly reduce the quantum yields. Since the introduction of structurally flexible substituents is a common strategy for increasing solubility, this antagonistic relationship between conformational flexibility and phosphorescence efficiency should be kept in mind when designing emitters suitable for solution processing. Increasing the solubility by introducing flexibility at the periphery while preserving the rigidity near the emitting center could therefore be a promising strategy for realizing highly efficient phosphorescence from soluble molecules.

Interesting effects could be observed regarding the emission characteristics of heteroleptic compounds containing ligands of different energies: Compounds with two arylamine and one carbazole substituents show emission that seems to be dominated by the lower energy transition centered on the arylamine substituted ligand, manifesting in emission maxima around 570 - 575 nm and quantum yields between 0.17 and 0.25.

For complexes containing two carbazoles as well as one arylamine substituent dual emission effects could be observed: While compounds **CCE** (**E** = *bis*(4-*t*-butylphenyl)amine) and **CCA** (**A** = diphenylamine) exhibit an orange emission with a small shoulder in the



green region (Figure 5), complex **CCD** containing two carbazole and one 4,4'-bis( $\alpha,\alpha$ -dimethylbenzyl)diphenyl amine (**D**) substituent shows green phosphorescence with a shoulder in the orange region. To gain more information on this pronounced difference in the emission behavior of **CCD** and **CCE**, we synthesized **DDD** (which could not be obtained from the chromatographic separation of library 2) via a conventional reaction and determined its quantum yield.  $\Phi_P$  (**DDD**) was found to be 0.20, which is similar to that of **EEE** ( $\Phi_P = 0.18$ ). Since these emission efficiencies are quite similar, the reasons for the different phosphorescence characteristics must lie elsewhere.

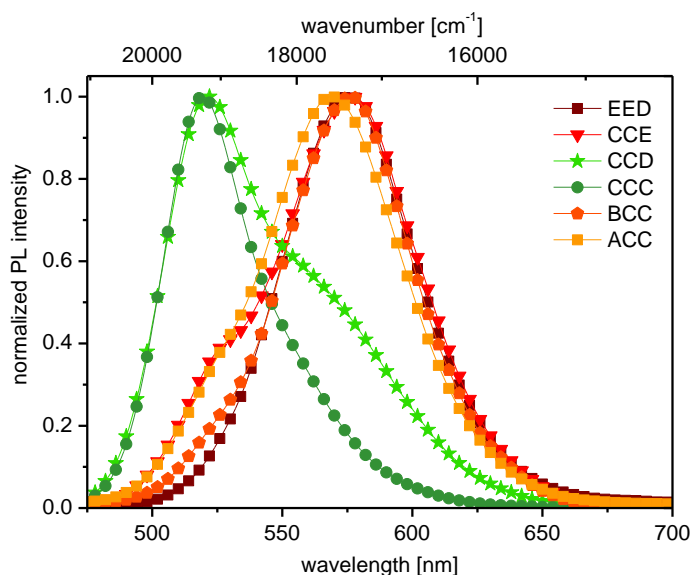


**Figure 5.** Phosphorescence spectra of compounds **EED**, **CCE**, **CCD**, **CCC**, **BCC** and **ACC**.

Detailed spectroscopic investigations might provide a deeper insight into this phenomenon in the future. Emitters with dual emission properties exhibit broad banded emission making them very promising candidates for white organic light-emitting diodes.<sup>[46]</sup> The combinatorial synthesis of focused libraries directed at the tuning of dual emission properties could be a valuable tool to facilitate the development of new emitters in this field.

## 2.4 Photodegradation Studies

While there is still not much known about the exact degradation mechanisms of emitters in PhOLEDs, most recent investigations suggest an important role of excited states.<sup>[47-49]</sup> Population of higher lying thermally accessible states for example may lead to bond rupture and possibly cause ligand dissociation.<sup>[50-51]</sup> Researchers at Fujifilm already used the analysis of irradiation induced degradation as a tool to assess the stability of new emitters. They successfully identified a new long lived phosphorescent blue emitter by spin coating layers of host material doped with a phosphorescent guest and examining the

## CHAPTER 2

photoluminescence degradation under UV irradiation.<sup>[52]</sup> To gain a first hint on the stability of our compounds under continuous excitation, we examined the irradiation induced degradation of the complexes in solution. We found LEDs with an emission maximum of 400 nm to be the ideal light source as they allow the direct excitation of the MLCT absorption band and at the same time enable the irradiation through a chromatography glass vial. Toluene was chosen as the solvent for the photodegradation studies as it is a comparably inert and non-coordinating solvent and is furthermore one of the preferred solvents for solution processing of organic light-emitting devices. The irradiation was performed once under atmospheric and once under oxygen free conditions.<sup>[44]</sup>

Ir(ppy)<sub>3</sub> and similar compounds are known to be very effective sensitizers of singlet oxygen,<sup>[53-55]</sup> so we initially expected that the presence of those highly reactive oxygen species would lead to faster degradation under atmospheric conditions. When looking at the results of the photostabilities of the complexes we were surprised to find that for most compounds, the presence of oxygen in the solution seemed to increase the photostability instead.

A possible explanation for this unexpected observation could be that singlet oxygen is deactivated relatively fast in toluene. This implies that the observed degradation in toluene occurs mainly *via* the excited molecules themselves. Oxygen efficiently quenches the <sup>3</sup>MLCT excited state at near diffusion controlled rates, leading to much shorter excited state lifetimes and may thus reduce the probability of degradation *via* those states. A comparison of the homoleptic complexes showed that the overall trends in the photostability are similar under atmospheric and inert conditions. The fastest photodegradation could be observed for compounds **AAA** and **NNN** (Figure 6). The *tris*-phenyl substituted **MMM** showed a moderate photostability whereas the fully carbazole- and 3,5-*bis*(trifluoromethyl)phenyl- substituted complexes (**CCC** and **KKK** respectively) turned out to be the most stable of all screened compounds. Figure 6 (right) illustrates the influence of the different substituents on the degradation sensitivity for library 3. The presence of trifluoromethyl groups in the substituent (**K**) seems to significantly increase the photostability of the complexes. This effect can be observed for compounds containing one to three *bis*(trifluoromethyl)phenyl groups under inert and atmospheric conditions alike. Further studies with a larger number of compounds will be necessary to establish structure-property relationships for the photostabilities in solution. More detailed investigations on the nature and products of the degradation pathways in solution as well as a comparison with device stabilities of selected emitters could shed light on the correlations and differences between the photo- and device-degradation of this class of compounds.

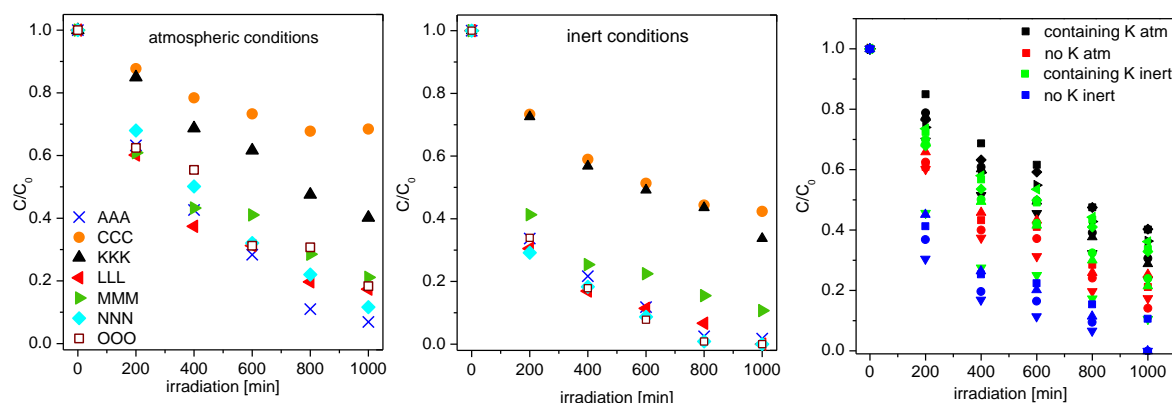


**Figure 6.** Photodegradation of the homoleptic complexes under atmospheric (left) and inert (center) conditions. Substitution effects on the photodegradation of library 3 (right).

### 3. CONCLUSIONS

In conclusion we demonstrated that the described post modification strategy combined with a chromatographic separation and screening enables the rapid synthesis and characterization of potential new OLED emitters. We examined the photophysical properties of the compounds by obtaining absorption and emission spectra directly from the chromatographic separation. Trends in the dual emission behavior of selected heteroleptic complexes were observed that upon further studies might lead to the development of promising new compounds for white light-emitting OLEDs. The determination of phosphorescence quantum yields in a separate experiment illustrated the antagonistic relationship between molecular flexibility and phosphorescence efficiency and helped to elucidate a promising new design principle for soluble and highly efficient phosphorescent emitters. By investigating the photodegradation of the libraries in solution, we found surprising trends and could identify compounds with increased stabilities compared to the rest of the libraries. Once a larger dataset will be available, a more detailed understanding of the degradation mechanisms and structure property relationships might help in the discovery of phosphorescent transition metal complexes with improved stabilities. The reported chromatography based screening of organo-transition metal complexes is not restricted to the development of new OLED emitters but may be easily applied for the accelerated discovery of materials for diverse other fields such as dyes for dye-sensitized solar cells or new photoredox catalysts.

## CHAPTER 2

### 4. EXPERIMENTAL

#### 4.1 Methods and Materials

**Semipreparative HPLC Separation & Spectra:** The semipreparative separation of the complex libraries was performed on an Agilent Technologies HPLC system consisting of a quaternary pump [G1311A], a vacuum degasser [G1322A], a thermostatted autosampler [G1329A], a thermostatted column compartment [G1316A], a diode-array detector (DAD) SL [G1315C] and a fluorescence detector (FLD) [G1321A] as well as an analytical scale fraction collector [G1364C]. The column used was a Hlbar® 250 mm x 10mm x 5µm diol column (Merck KGaA). The crude complex libraries were resolved in an appropriate volume of CH<sub>2</sub>Cl<sub>2</sub> (1-2 mL), filtered through a 2 µm PTFE syringe-filter and used for semipreparative HPLC separation using gradient elution (hexane/THF). All absorption and emission spectra were measured online via DAD and FLD detectors. The fractions were collected automatically (peak based fraction collection).

**Analytical HPLC/MS:** For the identification of the compounds, the collected samples were analyzed via LC/MS. The analysis was performed on an Agilent Technologies 1200 HPLC/MS system consisting of a binary pump SL [G1312B], a degasser [G1379B], an *Infinity* high performance micro autosampler [G1329B] with thermostat [G1330B], a thermostatted column compartment [G1316B], an *Infinity* diode-array detector (DAD) [G4212B] and an accurate Q-TOF/MS [G6530A] with an APCI (atmospheric pressure chemical ionization) source. The column used was a Hlbar® 250 mm x 4 mm x 5µm diol column (Merck KGaA).

**NMR Spectroscopy:** NMR spectra were recorded on a *Bruker Avance 400* (400.13 MHz for <sup>1</sup>H and 100.03 MHz for <sup>13</sup>C) spectrometer. Chemical shifts δ are given in [ppm], using residual solvent peaks (TCE-d<sub>2</sub>) as an internal standard. Coupling constants are reported in Hz. Characterization of the signals: s = singlet, d = doublet, dd = doublet from doublet, m = multiplet. Integration is determined as the relative number of atoms.

**Quantum Yield Estimation:** The PL quantum yields were determined relative to quinine hemisulfate monohydrate in 1 N H<sub>2</sub>SO<sub>4</sub> (Φ = 0.55). UV measurements were carried out on a *Varian Cary 50Bio* UV-Vis spectrophotometer, phosphorescence measurements on a *Varian Eclipse* Fluorescence spectrophotometer in sealable Hellma precision cells [117.100F-QS] with silicone/PTFE coated septa. The complexes were dissolved in CH<sub>2</sub>Cl<sub>2</sub> and the solutions were degassed in the cells via a vigorous argon purge through the solution prior to the measurements.

**Solvents and Reagents:** *fac*-Tris(5'-bromo-2-phenylpyridine)iridium **1** was provided by Merck KGaA.<sup>[56]</sup> All solvents and other commercially available reagents were purchased from Alfa Aesar or Sigma Aldrich and were used as received without further purification. The solvents were used in p.a. quality and degassed via purging with nitrogen over 1 h prior to use. For the chromatographic separation and analysis (sample preparation and mobile phase) we

used LiChrosolv® solvents, ( $\text{CH}_2\text{Cl}_2$ , THF and hexane) which were purchased from Merck KGaA.

## 4.2 Photodegradation Studies

The pure complexes were dissolved in varying volumes of toluene (p.a.) to give solutions of similar concentration. The volume of toluene was adjusted according to the integration area of the peaks for each complex (from the semipreparative separation). 1 mL of the resulting solutions was transferred to a headspace vial and sealed with a silicone/PTFE septum. Two samples were prepared from each complex for the testing under atmospheric and inert conditions. In case of the photodegradation studies under inert conditions, the vials were degassed *via* 4 freeze-pump thaw cycles under argon. All samples were irradiated in a custom made irradiation unit (SIM GmbH, picture see supporting information). It consists of an aluminum printed circuit board with 30 400 nm LEDs (350 mW, Edison Edixeon 3 W Emitter, [LT-1467]), connected to a cooling unit, that ensures a constant temperature of 13 °C of the board during the irradiation. Two 15 sample chromatography trays can be placed in the unit so that each of the sample vials is centered over one LED ( $d = 1 \text{ cm}$ ). The total duration of irradiation was 1000 min. After 0, 200, 400, 600, 800 and 1000 min, the samples were analyzed *via* HPLC (analytical system, see above). The percentage of remaining emitter was determined *via* integration of the DAD signal at 305 nm in relation to that of an external standard (quaterphenyl in toluene, 0.026 mM).

## 4.3 Syntheses

### General Procedure for the Combinatorial Buchwald-Hartwig Coupling

---

*Tris*(5'-bromo-2-phenylpyridine)iridium **1** (0.1 mmol), an equimolar mixture of the secondary arylamines (0.4 mmol) and NaOtBu (0.8 mmol) were placed in a headspace vial. The vial was then flushed with nitrogen and sealed with a silicone/PTFE septum. Toluene (9 mL), 1,4-dioxane (5 mL) and 1 mL of catalyst solution (containing 0.03 mmol  $\text{Pd}(\text{OAc})_2$  and 0.18 mmol  $\text{P}(\text{tBu})_3$  in degassed toluene) were added subsequently. The mixture was then stirred at 130 °C for 4 h in a custom made aluminum heating block. After the reaction mixture had cooled down to room temperature, the reaction mixture was washed with water and brine and dried over  $\text{MgSO}_4$ . The solvents were removed in vacuo to give an orange residue.

## CHAPTER 2

### General Procedure for the Combinatorial Suzuki-Miyaura Coupling

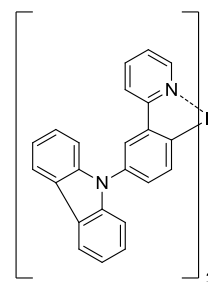
---

*Tris*(5'-bromo-2-phenylpyridine)iridium **1** (0.1 mmol), an equimolar mixture of the boronic acids (0.5 mmol) and  $K_3PO_4$  (0.8 mmol) were combined in a headspace vial. The vial was then flushed with nitrogen and sealed with a silicone/PTFE septum. Degassed toluene, dioxane and water (5 mL each) and 1 mL catalyst solution (containing 0.03 mmol  $Pd(OAc)_2$  and 0.18 mmol  $P(o\text{-tolyl})_3$  in 10 mL degassed toluene) were added. The reaction mixture was stirred at 85 °C for 10 h in a custom made aluminum heating block. The toluene phase was washed with water and brine, dried over  $MgSO_4$  and the solvent was removed in vacuo to give a yellow solid.

### Synthesis of the Homoleptic Reference Complexes

---

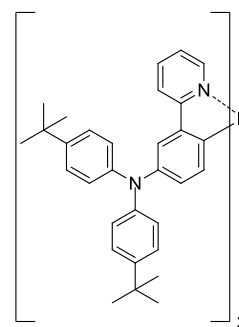
The homoleptic reference complexes were synthesized as described for the combinatorial procedures but with only one amine or boronic acid respectively. The crude products were purified by recrystallization as specified with the characterization data.



#### Complex CCC

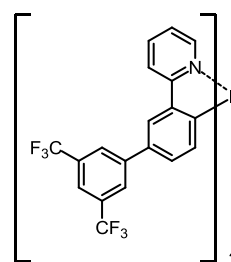
The crude product was recrystallized from THF/2-propanol to gain the title complex as a yellow solid: (90 mg, 78%).

**$^1H$ -NMR** ( $C_2Cl_4D_2$ , 400 MHz):  $\delta$  [ppm] = 8.20 – 8.09 (m, 6H), 7.80 (d,  $J$  = 1.9 Hz, 3H), 7.73 (d,  $J$  = 8.3 Hz, 3H), 7.62 (d,  $J$  = 5.3 Hz, 3H), 7.59 – 7.53 (m, 3H), 7.49 – 7.27 (m, 15H), 7.27 – 7.22 (m, 6H), 7.14 (dd,  $J$  = 8.0, 2.1 Hz, 3H), 7.04 – 6.98 (m, 3H).  **$^{13}C$ -NMR** ( $C_2Cl_4D_2$ , 101 MHz):  $\delta$  [ppm] = 166.0, 160.6, 147.6, 145.8, 141.8, 138.6, 137.2, 130.5, 129.3, 126.3, 123.4, 123.3, 123.2, 120.7, 120.0, 119.8, 110.5. **HR-MS** (+APCI):  $m/z$  ( $C_{69}H_{45}IrN_6$ ) calculated: 1151.3414 [MH] $^+$ ; found: 1151.3442.

Complex EEE

The crude product was recrystallized from THF/methanol to gain the title complex as an orange solid (97 mg, 68%).

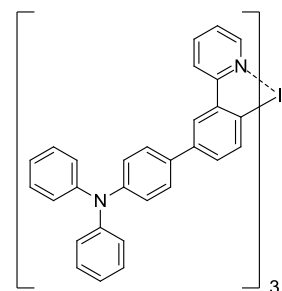
**<sup>1</sup>H-NMR** ( $C_2Cl_4D_2$ , 400 MHz):  $\delta$  [ppm] = 7.56 – 7.34 (m, 12H), 7.14 (d,  $J$  = 8.6 Hz, 12H), 6.94 (d,  $J$  = 8.6 Hz, 15H), 6.84 – 6.70 (m, 6H), 1.27 (s, 54H). **<sup>13</sup>C-NMR** ( $C_2Cl_4D_2$ , 101 MHz):  $\delta$  [ppm] = 166.3, 157.2, 147.4, 146.1, 145.4, 143.9, 140.4, 138.0, 136.6, 129.9, 126.2, 123.7, 122.7, 121.9, 119.7, 34.5, 32.0. **HR-MS** (+APCI):  $m/z$  ( $C_{87}H_{87}IrN_6$ ) calculated 1493.7643 [MH]<sup>+</sup>; found: 1493.7676.

Complex KKK

The crude product was recrystallized from toluene/ethanol to gain the title complex as a yellow solid (89 mg, 63%).

**<sup>1</sup>H-NMR** ( $C_2Cl_4D_2$ , 400 MHz):  $\delta$  [ppm] = 8.06 – 7.96 (m, 9H), 7.82 (d,  $J$ =1.6 Hz, 3H), 7.73 – 7.64 (m, 6H), 7.52 (d,  $J$ =5.0 Hz, 3H), 7.07 (dd,  $J$ =8.0, 1.8 Hz, 3H), 6.96 (dd,  $J$ =14.8, 7.2 Hz, 6H), 6.96 (dd,  $J$ =14.8 Hz, 7.2, 6H). **<sup>13</sup>C-NMR** ( $C_2Cl_4D_2$ , 101 MHz):  $\delta$  [ppm] = 166.1, 163.2, 147.6, 145.5, 144.7, 138.5, 137.2, 132.2, 130.1, 128.9, 128.06, 126.7, 125.3, 123.4, 122.6, 122.6, 119.9, 119.9. **HR-MS** (+APCI):  $m/z$  ( $C_{57}H_{30}F_{18}IrN_3$ ) calculated: 1292.1859 [MH]<sup>+</sup>; found: 1292.1890.

## CHAPTER 2



### Complex 000

The crude product was recrystallized from THF/2-propanol to gain the title complex as a yellow solid (102 mg, 67%).

**<sup>1</sup>H-NMR** ( $C_2Cl_4D_2$ , 400 MHz):  $\delta$  [ppm] = 7.97 – 7.90 (m, 3H), 7.83 (s, 3H), 7.63 – 7.56 (m, 3H), 7.51 – 7.45 (m, 9H), 7.21 – 7.14 (m, 12H), 7.10 – 7.01 (m, 21H), 6.96 – 6.86 (m, 12H). **<sup>13</sup>C-NMR** ( $C_2Cl_4D_2$ , 101 MHz):  $\delta$  [ppm] = 166.7, 160.9, 148.1, 147.5, 146.4, 145.0, 138.1, 136.8, 136.5, 131.9, 129.7, 128.4, 127.2, 125.3, 124.6, 124.4, 123.0, 122.2, 119.5. **HR-MS** (+APCI):  $m/z$  ( $C_{87}H_{63}IrN_6$ ) calculated: 1385.4825 [MH]<sup>+</sup>; found: 1385.4839.

## 5. REFERENCES

- [1] K. K.-W. Lo, C.-K. Chung, T. K.-M. Lee, L.-H. Lui, K. H.-K. Tsang, N. Zhu, *Inorg. Chem.* **2003**, 42, 6886-6897.
- [2] K. K.-W. Lo, D. C.-M. Ng, C.-K. Chung, *Organometallics* **2001**, 20, 4999-5001.
- [3] K. K.-W. Lo, K. Y. Zhang, S.-K. Leung, M.-C. Tang, *Angew. Chem. Int. Ed.* **2008**, 47, 2213-2216.
- [4] C. S. K. Mak, D. Pentlehner, M. Stich, O. S. Wolfbeis, W. K. Chan, H. Yersin, *Chem. Mater.* **2009**, 21, 2173-2175.
- [5] Y. You, S. Y. Park, *Adv. Mater.* **2008**, 20, 3820-3826.
- [6] W. Zhao, F. N. Castellano, *J. Phys. Chem. A* **2006**, 110, 11440-11445.
- [7] T. N. Singh-Rachford, F. N. Castellano, *Coord. Chem. Rev.* **2010**, 254, 2560-2573.
- [8] E. Baranoff, J.-H. Yum, M. Graetzel, M. K. Nazeeruddin, *J. Organomet. Chem.* **2009**, 694, 2661-2670.
- [9] B. F. DiSalle, S. Bernhard, *J. Am. Chem. Soc.* **2011**, 133, 11819-11821.
- [10] J. I. Goldsmith, W. R. Hudson, M. S. Lowry, T. H. Anderson, S. Bernhard, *J. Am. Chem. Soc.* **2005**, 127, 7502-7510.
- [11] N. Sutin, C. Creutz, E. Fujita, *Comments Inorg. Chem.* **1997**, 19, 67-92.
- [12] Y.-J. Yuan, Z.-T. Yu, X.-Y. Chen, J.-Y. Zhang, Z.-G. Zou, *Chem.-Eur. J.* **2011**, 17, 12891-12895.
- [13] K. Zeitler, *Angew. Chem., Int. Ed.* **2009**, 48, 9785-9789.
- [14] H.-W. Shih, M. N. Vander Wal, R. L. Grange, D. W. C. MacMillan, *J. Am. Chem. Soc.* **2010**, 132, 13600-13603.
- [15] A. G. Condie, J. C. González-Gómez, C. R. J. Stephenson, *J. Am. Chem. Soc.* **2010**, 132, 1464-1465.



- [16] M. A. Baldo, D. F. O'Brien, Y. You, A. Shoustikov, S. Sibley, M. E. Thompson, S. R. Forrest, *Nature* **1998**, 395, 151-154.
- [17] T. Hofbeck, H. Yersin, *Inorg. Chem.* **2010**, 49, 9290-9299.
- [18] H. Yersin, A. F. Rausch, R. Czerwieniec, T. Hofbeck, T. Fischer, *Coord. Chem. Rev.* **2011**, 255, 2622-2652.
- [19] Y. You, S. Y. Park, *Dalton Trans.* **2009**, 1267-1282.
- [20] Y. Chi, P.-T. Chou, *Chem. Soc. Rev.* **2010**, 39, 638-655.
- [21] P. T. Chou, Y. Chi, *Chem.-Eur. J.* **2007**, 13, 380-395.
- [22] E. Baranoff, S. Fantacci, F. De Angelis, X. Zhang, R. Scopelliti, M. Grätzel, M. K. Nazeeruddin, *Inorg. Chem.* **2010**, 50, 451-462.
- [23] F. De Angelis, S. Fantacci, N. Evans, C. Klein, S. M. Zakeeruddin, J.-E. Moser, K. Kalyanasundaram, H. J. Bolink, M. Grätzel, M. K. Nazeeruddin, *Inorg. Chem.* **2007**, 46, 5989-6001.
- [24] C. L. Ho, W. Y. Wong, Z. Q. Gao, C. H. Chen, K. W. Cheah, B. Yao, Z. Y. Xie, Q. Wang, D. G. Ma, L. X. Wang, X. M. Yu, H. S. Kwok, Z. Y. Lin, *Adv. Funct. Mater.* **2008**, 18, 319-331.
- [25] J. Li, P. I. Djurovich, B. D. Alleyne, M. Yousufuddin, N. N. Ho, J. C. Thomas, J. C. Peters, R. Bau, M. E. Thompson, *Inorg. Chem.* **2005**, 44, 1713-1727.
- [26] M. S. Lowry, W. R. Hudson, R. A. Pascal, S. Bernhard, *J. Am. Chem. Soc.* **2004**, 126, 14129-14135.
- [27] E. M. Gordon, R. W. Barrett, W. J. Dower, S. P. A. Fodor, M. A. Gallop, *J. Med. Chem.* **1994**, 37, 1385-1401.
- [28] C. Gennari, U. Piarulli, *Chem. Rev.* **2003**, 103, 3071-3100.
- [29] N.-M. Hsu, W.-R. Li, *Angew. Chem., Int. Ed.* **2006**, 45, 4138-4142.
- [30] E. Baranoff, I. Jung, R. Scopelliti, E. Solari, M. Gratzel, M. K. Nazeeruddin, *Dalton Trans.* **2011**, 40, 6860-6867.
- [31] C. E. Kibbey, *Laboratory Robotics and Automation* **1997**, 9, 309-321.
- [32] L. Zeng, L. Burton, K. Yung, B. Shushan, D. B. Kassel, *J. Chromatogr., A* **1998**, 794, 3-13.
- [33] H. N. Weller, *Mol. Diversity* **1998**, 4, 47-52.
- [34] C. Adachi, M. A. Baldo, S. R. Forrest, M. E. Thompson, *Appl. Phys. Lett.* **2000**, 77, 904-906.
- [35] Y. Kawamura, K. Goushi, J. Brooks, J. J. Brown, H. Sasabe, C. Adachi, *Appl. Phys. Lett.* **2005**, 86, 071104-071103.
- [36] D. Tanaka, H. Sasabe, Y.-J. Li, S.-J. Su, T. Takeda, J. Kido, *Jpn. J. Appl. Phys.*, 46, L10.
- [37] N. Cumpstey, R. N. Bera, P. L. Burn, I. D. W. Samuel, *Macromolecules* **2005**, 38, 9564-9570.
- [38] Y. You, C.-G. An, J.-J. Kim, S. Y. Park, *J. Org. Chem.* **2007**, 72, 6241-6246.
- [39] Y. You, C.-G. An, D.-S. Lee, J.-J. Kim, S. Y. Park, *J. Mater. Chem.* **2006**, 16, 4706-4713.
- [40] P. Stoessel, H. Spreitzer, H. Becker, WO02068435A1, Covion Organic Semiconductors, **2002**.
- [41] P. Stoessel, I. Bach, H. Spreitzer, WO2004026886A2, Covion Organic Semiconductors, **2004**.
- [42] P. Stoessel, H. Spreitzer, H. Becker, WO02081488A1, Covion Organic Semiconductors, **2002**.

## CHAPTER 2

- [43] R. M. Anemian, B. Schroeder, A. H. Parham, C. d. Nonancourt, WO2011141120A1, Merck Patent GmbH, **2011**.
- [44] The reactions were run with an excess of the respective coupling partners (1.2 eq of amines/boronic acids) to ensure complete conversion of the starting material as reactions with an equimolar ratio of starting material to coupling partners gave inseparable mixtures of products and only partially coupled starting material.
- [45] K. Ono, M. Joho, K. Saito, M. Tomura, Y. Matsushita, S. Naka, H. Okada, H. Onnagawa, *Eur. J. Inorg. Chem.* **2006**, 2006, 3676-3683.
- [46] Y. You, K. S. Kim, T. K. Ahn, D. Kim, S. Y. Park, *J. Phys. Chem. C* **2007**, 111, 4052-4060.
- [47] N. C. Giebink, B. W. D'Andrade, M. S. Weaver, J. J. Brown, S. R. Forrest, *J. Appl. Phys.* **2009**, 105, 124514-124517.
- [48] N. C. Giebink, B. W. D'Andrade, M. S. Weaver, P. B. Mackenzie, J. J. Brown, M. E. Thompson, S. R. Forrest, *J. Appl. Phys.* **2008**, 103, 044509.
- [49] R. Seifert, S. Scholz, B. Lussem, K. Leo, *Appl. Phys. Lett.* **2010**, 97, 013308-013303.
- [50] T. Sajoto, P. I. Djurovich, A. B. Tamayo, J. Oxgaard, W. A. Goddard, M. E. Thompson, *J. Am. Chem. Soc.* **2009**, 131, 9813-9822.
- [51] I. R. d. Moraes, S. Scholz, B. Lüssem, K. Leo, *Org. Electron.* **2011**, 12, 341-347.
- [52] W. Sotoyama, T. Satoh, M. Kinoshita, M. Tobise, K. Kawato, T. Ise, H. Takizawa, S. Yamashita, *Fujifilm Research and Development* **2010**, No.055, 24-28.
- [53] R. Gao, D. G. Ho, B. Hernandez, M. Selke, D. Murphy, P. I. Djurovich, M. E. Thompson, *J. Am. Chem. Soc.* **2002**, 124, 14828-14829.
- [54] S.-y. Takizawa, R. Aboshi, S. Murata, *Photochem. Photobiol. Sci.* **2011**, 10, 895-903.
- [55] P. I. Djurovich, D. Murphy, M. E. Thompson, B. Hernandez, R. Gao, P. L. Hunt, M. Selke, *Dalton Trans.* **2007**, 3763-3770.
- [56] P. Stoessel, H. Spreitzer, H. Becker, WO02060910A1, **2002**.

# CHAPTER 3

## NEW APPROACHES TOWARDS COMBINATORIAL DERIVATIZATION OF Ir(ppy)<sub>3</sub>

New approaches for the combinatorial derivatization of Ir(ppy)<sub>3</sub> are discussed in this chapter. Palladium catalyzed C-O coupling reactions are investigated towards their potential for the synthesis of arylether-coupled complex derivatives. The successful preparation of *tris*(5'-pinacolatoboron-2-phenylpyridine)iridium(III) may improve the combinatorial Suzuki-Miyaura protocol reported in Chapter 2.



## 1. INTRODUCTION

Combinatorial synthesis is a convenient method for the synthesis of huge libraries of structurally diverse molecules sharing one specific core motif. In many fields of research where even small structural changes can cause significant changes in the molecules' properties, this strategy is a welcome tool to produce an enormous amount of products for screening methodologies. Especially in pharmaceutical chemistry, one resorts to the combinatorial approach to identify new drug molecules.<sup>[1-4]</sup>

In the latter chapter, we demonstrated that this route can also be usefully applied in the field of light-emitting materials to identify structural motifs that have an influence on photophysical properties but also the ones that are beneficial or detrimental to the emitters' photostability.

We already established a versatile protocol for combinatorial C-C as well as C-N coupling reactions for the fast derivatization of one of the best known core structures of phosphorescent emitters used in organic light-emitting diodes – Ir(ppy)<sub>3</sub>. Our approach afterwards was to broaden the spectrum of possible derivatives by developing new synthetic pathways suitable for combinatorial reactions. One key requirement is the almost quantitative conversion of a substrate into the desired derivative in order to avoid a mixture of miscellaneous side products. This demand is even more essential for our precursor *tris*(5'-bromo-2-phenylpyridine)iridium(III) **1**, as three reactive sites are combined in one molecule.

We adhered to the field of palladium catalyzed cross coupling reactions and focused on the C-O bond formations. The approaches using Buchwald-Hartwig as well as Chan-Lam systems are discussed in the previous section.

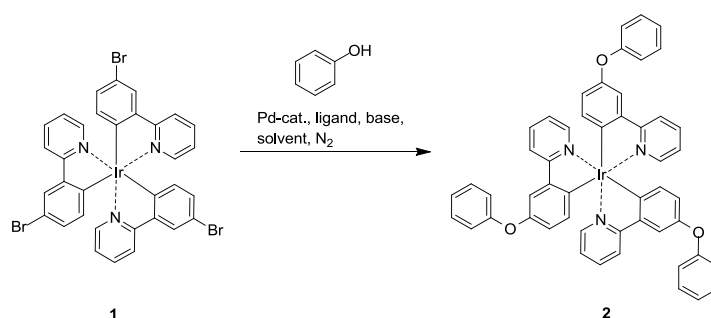
## CHAPTER 3

### 2. RESULTS & DISCUSSION

#### 2.1 C-O Coupling Reactions

##### Buchwald-Hartwig Couplings

In the field of palladium catalyzed C-heteroatom couplings, most research effort was focused on amination reactions. Buchwald and Hartwig established a synthetic protocol for these C-N bond forming reactions.<sup>[5]</sup> This approach became a reliable and versatile synthetic procedure.<sup>[6]</sup> In case of arylether synthesis, finding suitable conditions for acceptable conversion rates is more difficult. The C-O bond forming step – the reductive elimination – was found to proceed in a very slow way: Bäckvall *et al.* calculated the energy levels for the appropriate orbitals of a model complex, which are involved in this elimination step. They found that the energy gap between the HOMO and the LUMO of this complex species is significantly higher for oxygen-nucleophiles, making its nucleophile attack a disfavored pathway.<sup>[7-8]</sup> Thus, side reactions like the  $\beta$ -hydride elimination are favored, yielding bromodefuntionalized arenes. In the beginning, best results for arylether synthesis were achieved using electron deficient arylhalogenides.<sup>[9-10]</sup> Therefore, the brominated Ir(ppy)<sub>3</sub> precursor **1** was assumed to constitute a suitable starting material for the coupling with phenol, due to the electron withdrawing effects of the pyridyl substituent and the cyclometalating iridium on the brominated benzene moiety.



**Scheme 1.** C-O coupling of Ir(Br-ppy)<sub>3</sub> **1** with phenol in a Buchwald-Hartwig reaction.

Toluene was chosen as a convenient solvent for this type of reaction. The used ligands constitute representatives of different generations of C-heteroatom couplings:<sup>[11]</sup> Tri-*t*-butylphosphine **L1** was one of the first ligands successfully used therein.<sup>[12]</sup> 1,1'-Bis(diphenylphosphino)ferrocene (dppf) **L2** and 4,5-bis(diphenylphosphino)-9,9-dimethyl-xanthene (Xantphos) **L5** belong to the group of chelating bisphosphines and were tested as alternatives. Ligands (2-biphenyl)di-*t*-butylphosphine **L3** and 2-di-*t*-butylphosphino-2',4',6'-triisopropylbiphenyl **L4** (JohnPhos and *t*BuXPhos, respectively) were selected from the pool of biphenyl-based "Buchwald ligands". As catalysts Pd(OAc)<sub>2</sub>, Pd(dppf)Cl<sub>2</sub> as well as

$\text{Pd}_2(\text{dba})_3$  were used. The bases  $\text{K}_2\text{CO}_3$ ,  $\text{NaOtBu}$  and  $\text{NaH}$  were chosen as they belong to the most convenient in Buchwald coupling reactions.<sup>[11]</sup> The reaction mixtures were evaluated by LC/MS analysis (Table 1). The different bases seem to have a significant effect on the proceeding reaction pathway. The approaches using  $\text{K}_2\text{CO}_3$  did not show any conversion (Table 1, entry 1 and 2). As a reason the poor solubility of  $\text{K}_2\text{CO}_3$  in toluene can be assumed, resulting in no *in situ* deprotonation of the phenol to the phenoxide. In future approaches this base should be substituted by  $\text{Cs}_2\text{CO}_3$ , which exhibits an improved solubility in toluene. Using  $\text{NaOtBu}$ , a bromodefunctionalization takes place. Regarding the slow proceeding reductive elimination of the arylpalladium phenoxide species, bromodefunctionalized species might be formed in a proton initiated side reaction of any kind. The protons could either derive from traces of water in the reaction mixture, or from deprotonation of the phenol.

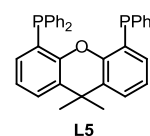
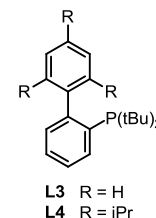
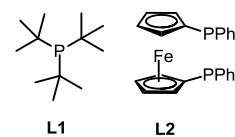
Reactions in the presence of  $\text{NaH}$  showed some potential for the C-O linkage. While in the reaction mixture using the Xantphos ligand **L5** (entry 8) only partly to completely hydrodehalogenated products could be identified, reaction mixtures with the Buchwald ligands **L3** and **L4** contained phenol coupled complexes. Best conversion was obtained for the catalytic system  $\text{Pd}_2(\text{dba})_3/\text{L4}$  (entry 10): no starting material **1** was detected in LC/MS analysis and only traces of hydrodehalogenated products were identified. The main product was the desired complex **2** with approximately 40% yield, followed by the one- and twofold coupled brominated complexes (estimated from the chromatogram of the reaction mixture). The enhancing effect of  $\text{NaH}$  on the C-O conversion rate might be ascribed to the ability of the hydride to efficiently scavenge protons, making them non-accessible for any side reaction.

To improve the yield to > 90%, making this protocol suitable for combinatorial approaches it can be considered to substitute **L4** with more sterically hindered biphenylphosphines. Bulky ligands were found to destabilize the ground state of the arylpalladium phenoxides, enforcing the reductive elimination.<sup>[13]</sup> Furthermore, a variation of the solvents can influence the reaction behavior, for example due to a better solubility of the bases.

## CHAPTER 3

**Table 1.** Conditions screening for Buchwald-Hartwig type C-O coupling reactions of Ir(Br-ppy)<sub>3</sub> **1** and phenol,<sup>a)</sup> with the used ligands depicted on the right side.

Entry	Catalyst	Ligand	Base	Proceeding reaction pathway <sup>b)</sup>
1	Pd(OAc) <sub>2</sub>	<b>L2</b>	K <sub>2</sub> CO <sub>3</sub>	No conversion
2	Pd <sub>2</sub> (dba) <sub>3</sub>	<b>L5</b>	K <sub>2</sub> CO <sub>3</sub>	No conversion
3	Pd(OAc) <sub>2</sub>	<b>L1</b>	NaOtBu	Dehalogenation
4	Pd(OAc) <sub>2</sub>	<b>L2</b>	NaOtBu	Dehalogenation <sup>c)</sup>
5	Pd <sub>2</sub> (dba) <sub>3</sub>	<b>L2</b>	NaOtBu	Dehalogenation <sup>c)</sup>
6 <sup>d)</sup>	Pd(dppf)Cl <sub>2</sub>	<b>L2</b>	NaOtBu	Dehalogenation
7	Pd(OAc) <sub>2</sub>	<b>L4</b>	NaH	C-O coupling
8	Pd(OAc) <sub>2</sub>	<b>L5</b>	NaH	Dehalogenation
9	Pd <sub>2</sub> (dba) <sub>3</sub>	<b>L3</b>	NaH	C-O coupling vs. Dehalogenation <sup>c)</sup>
10	Pd <sub>2</sub> (dba) <sub>3</sub>	<b>L4</b>	NaH	C-O coupling
11 <sup>e)</sup>	Pd <sub>2</sub> (dba) <sub>3</sub>	<b>L4</b>	NaH	C-O coupling vs. Dehalogenation



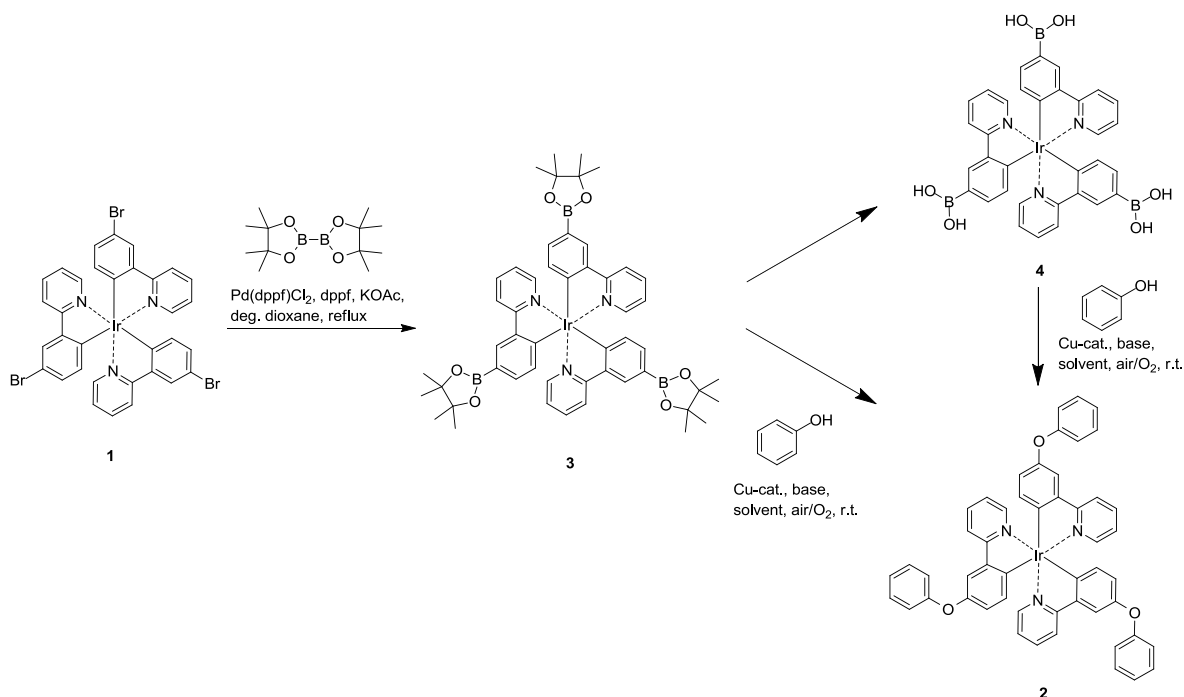
a) Ir(Br-ppy)<sub>3</sub> (1.0 eq), phenol (3.6 eq), catalyst (15 mol%), ligand (30 mol%), base (6.0 eq), deg. anhydr. toluene (5.5 mM), inert conditions (N<sub>2</sub>), reflux, 16 h. b) determined via analysis of the formed products in the reaction mixture by LC/MS. c) very poor conversion. d) Ir(Br-ppy)<sub>3</sub> **1** (1.0 eq), phenol (3.3 eq), catalyst (8 mol%), ligand (8 mol%), base (3.5 eq), deg. toluene/dioxane (1:1, 5 mM), inert conditions (N<sub>2</sub>), reflux, 18 h. e) microwave (300 W, 130 °C, 1 h).

### Chan-Lam Couplings

About 25 years ago, Chan and Lam identified boronic acids to be efficient phenylating agents in copper catalyzed reactions.<sup>[14-15]</sup> This type of reaction is outstanding for “open-flask chemistry”:<sup>[16]</sup> mild conditions like weak amine bases, ambient atmosphere and room temperature are sufficient for a proper conversion for many systems.

Starting from Ir(Br-ppy)<sub>3</sub> **1**, tris(5'-pinacolatoboron-2-phenylpyridine)iridium(III) **3** (Ir(Bpin-ppy)<sub>3</sub>) was synthesized via palladium catalyzed boronation with bis(pinacolato)-diboron (Scheme 2). Optimization experiments of the reaction conditions showed quantitative conversion in LC/MS analysis for the catalyst Pd(dppf)Cl<sub>2</sub> by adding free dppf ligand **L2**. The preparative synthesis of complex **3** caused some difficulties in the purification. Therefore, the unsatisfactory yield reported in the experimental section (10%) can most likely be significantly improved by changing the work-up procedure.





**Scheme 2.** Synthetic pathway to Ir(ppy)<sub>3</sub>-arylether derivatives **2** via Chan-Lam coupling: Synthesis of Ir(Bpin-ppy)<sub>3</sub> **3** and the C-O coupling reaction of the boronic ester or its former hydrolyzed derivative **4**.

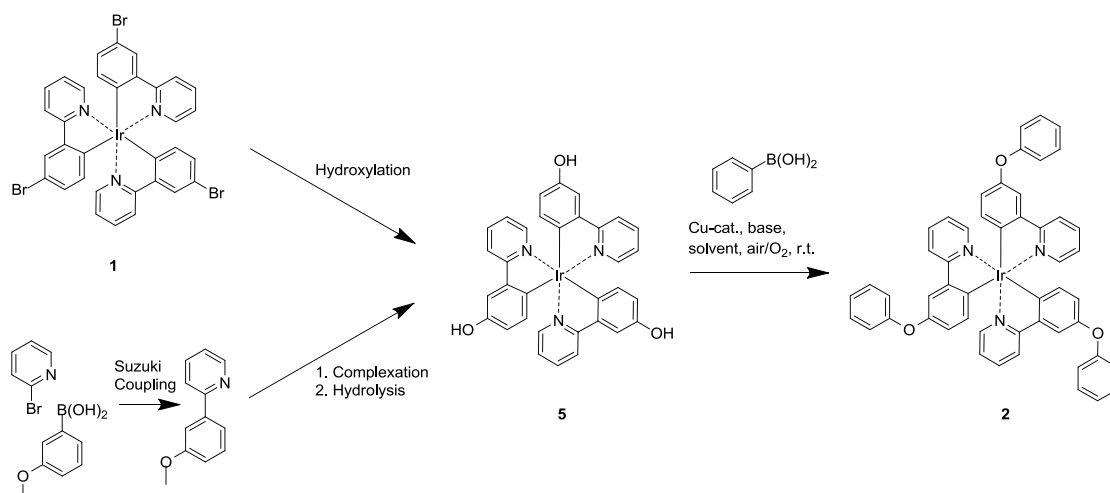
Chan-Lam couplings of boronic ester **3** with phenol were tried in different setups<sup>[17]</sup> varying the base (NEt<sub>3</sub>, pyridine), the atmosphere (ambient, oxygen saturated), the solvent (CH<sub>2</sub>Cl<sub>2</sub>, DMF) and therefore the temperature (r.t., 50 °C). But LC/MS analysis of the reaction mixtures only revealed the pure starting material.

It was observed that pinacol esters are less efficient than other boronic esters or the free boronic acids themselves.<sup>[16, 18]</sup> Thus we tried to hydrolyze complex **3** to its derivative **4**. Neither the treatment with NaIO<sub>4</sub>/HCl nor with BCl<sub>3</sub> or BBr<sub>3</sub> gave the free boronic acid **4** but complex **3** decomposed.<sup>[19]</sup>

Further approaches to get a successful protocol for Chan-Lam couplings are to synthesize more efficient, i. e. less sterically hindered,<sup>[16]</sup> boronic esters.

It is also considerable to perform the coupling in an “inverse” way, using *tris*(5'-hydroxy-2-phenylpyridine)iridium(III) **5** and aryl boronic acids, as an exchange of the reactive centers might have significant effects on the reaction out-put. Complex **5** can be synthesized by simple hydroxylation of complex **1** or in a 3-step synthesis starting from 2-bromopyridine (Scheme 3).

## CHAPTER 3

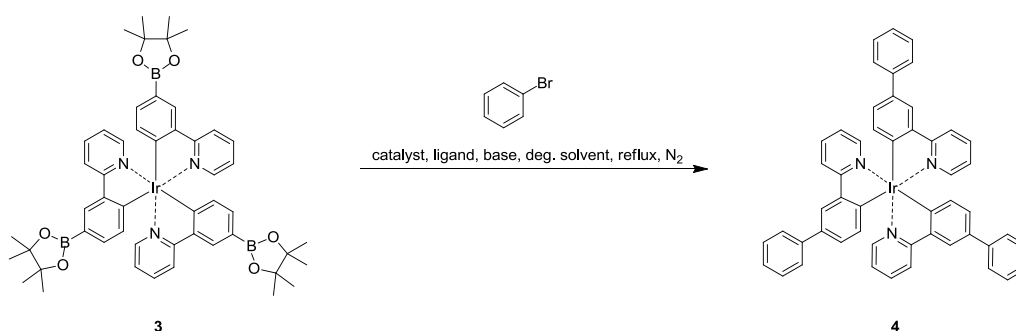


**Scheme 3.** Alternative approach towards Ir(ppy)<sub>3</sub>-arylether derivatives **2**: “inverse” Chan-Lam reaction starting from tris(5'-hydroxy-2-phenylpyridine)iridium(III) **5** and its possible synthetic accessibility.

## 2.2 C-C Coupling Reactions

### Suzuki-Miyaura Couplings

Having Ir(Bpin-ppy)<sub>3</sub> **3** available prompted us to perform Suzuki-Miyaura couplings in an inverse way compared to the procedure described in Chapter 2. If this way would be accessible for combinatorial reactions, the diversity of the synthesized libraries could easily be extended as the coupling partners, namely arylhalogenides, are much cheaper or easier to synthesize compared to their boronic acid analogues.

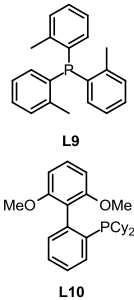


**Scheme 4.** Suzuki-Miyaura coupling of Ir(Bpin-ppy)<sub>3</sub> **3** with bromobenzene.

In a first attempt, the protocol reported in Chapter 2 was used (Table 2, entry 1). But although the combination of Pd(OAc)<sub>2</sub> and P(o-tolyl)<sub>3</sub> **19** is a versatile catalyst system for the coupling of iridium complex **1** with boronic acids, the inverse reaction suffers a hydrodehalogenation side reaction. Another well-established Suzuki protocol (see Chapter 5), using the catalyst Pd(dppf)Cl<sub>2</sub> gave the desired complex **4** in moderate yields (Entry 2, estimated by LC/MS analysis). Almost quantitative conversion was achieved with

the SPhos ligand **L10** (2-dicyclohexylphosphino-2',6'-dimethoxybiphenyl).<sup>[20]</sup> The influence of the catalyst ( $\text{Pd}(\text{OAc})_2$  and  $\text{Pd}_2(\text{dba})_3$  respectively) was negligible. These results render this approach to be a promising alternative to the former used synthetic procedure. To prove its versatility and suitability for combinatorial reactions, further experiments with a variety of different arylhalogenides have to be performed in future.

**Table 2.** Different catalytic systems for Suzuki-Miyaura coupling reactions of  $\text{Ir}(\text{Bpin-ppy})_3$  **3** and bromobenzene.<sup>a)</sup> The ligands are depicted on the right side.

Entry	Catalyst	Ligand	Base	Solvent	Proceeding reaction pathway <sup>b</sup>	
1	$\text{Pd}(\text{OAc})_2$	<b>L9</b>	$\text{K}_3\text{PO}_4$	mixture 1 <sup>c)</sup>	C-C Coupling vs. Defunctionalization	 <p><b>L9</b></p> <p><b>L10</b></p>
2	$\text{Pd}(\text{dppf})\text{Cl}_2$	--	$\text{K}_2\text{CO}_3$	mixture 1 <sup>c)</sup>	C-C Coupling <sup>e)</sup>	
3	$\text{Pd}(\text{OAc})_2$	<b>L10</b>	$\text{K}_3\text{PO}_4$	mixture 2 <sup>d)</sup>	C-C Coupling <sup>f)</sup>	
4	$\text{Pd}_2(\text{dba})_3$	<b>L10</b>	$\text{K}_3\text{PO}_4$	mixture 2 <sup>d)</sup>	C-C Coupling <sup>f)</sup>	

a)  $\text{Ir}(\text{Bpin-ppy})_3$  **3** (1.0 eq), bromobenzene (4.0 eq), catalyst (10 mol%), ligand (40 mol%), base (9.0 eq), deg. solvent mixture (2.4 mM), inert conditions ( $\text{N}_2$ ), reflux, 12 h. b) determined via analysis of the formed products in the reaction mixture by LC/MS. c) solvent mixture 1: toluene/water/dioxane (2:1:1). d) solvent mixture 2: toluene/water (3:1). e) moderate conversion. f) almost quantitative conversion.

### 3. CONCLUSIONS

In this chapter we tried to develop new protocols for the combinatorial derivatization of  $\text{Ir}(\text{Br-ppy})_3$  **1**, in order to apply them to our screening system, reported in Chapter 2. C-O coupling reactions were tried following two different strategies – the Buchwald-Hartwig and Chan-Lam approach, respectively. The former one yielded reasonable conversion using the catalytic system  $\text{Pd}_2\text{dba}_3$ /**L4**. Substitution of the catalyst with  $\text{Pd}(\text{OAc})_2$  showed no influence on the product formation. In contrast, the presence of the particular base NaH seems to be mandatory.

For the latter approach,  $\text{Ir}(\text{Bpin-ppy})_3$  **3** was successfully synthesized. Unfortunately, no conversion could be observed in the Chan-Lam experiments. This might be due to the poorer reactivity of pinacol esters compared to its alkylester derivatives.

Nevertheless, complex **3** showed great potential for the application in Suzuki-Miyaura reactions with bromobenzene. Compared to the protocol presented in Chapter 2 this “inverse” strategy, will allow for a greater variation of substituents as arylhalogenides are synthetically easier accessible and cheaper than boronic acids.

## CHAPTER 3

### 4. EXPERIMENTAL

#### 4.1 Methods and Materials

**NMR Spectroscopy:** NMR spectra were recorded on a *Bruker Avance 400* (400.13 MHz for  $^1\text{H}$  and 100.03 MHz for  $^{13}\text{C}$ ) spectrometer. Chemical shifts  $\delta$  are given in [ppm], using residual solvent (TCE- $d_2$ ) as an internal standard. Coupling constants are reported in Hz. Characterization of the signals: d = doublet, m = multiplet. Integration is determined as the relative number of atoms. (NMR spectra see supporting information)

**HPLC/MS:** The analysis of the reaction mixtures from the screening experiments were performed on an *Agilent Technologies 1200 HPLC/MS* system consisting of a binary pump SL [G1312B], a degasser [G1379B], an *Infinity* high performance micro autosampler [G1329B] with thermostat [G1330B], a thermostatted column compartment [G1316B], an *Infinity* diode-array detector (DAD) [G4212B] and an accurate mass Q-TOF/MS [G6530A] with an ESI (electrospray ionization) as well as APCI (atmospheric pressure chemical ionization) ion source. The column used was a *Hibar®* 250 mm x 4 mm x 5 $\mu\text{m}$  diol column (Merck KGaA).

**TLC Analysis and Column Chromatography:** Analytical TLC plates (silica gel 60 F<sub>254</sub>) and silica gel 60 (70-230 or 230-400 mesh) for column chromatography were purchased from Merck KGaA. Spots were visualized by UV light (254 nm).

**Solvents and Reagents:** *fac*-Tris(5'-bromo-2-phenylpyridine)iridium **1** was provided by Merck KGaA.<sup>[21]</sup> Ligand **L1** was synthesized according to a literature known procedure.<sup>[22]</sup> All solvents and other commercially available reagents were purchased from Alfa Aesar or Sigma Aldrich in p.a. quality and used as received without further purification if not stated otherwise. Degassed solvents were prepared *via* purging with nitrogen over 1 hour prior to use. Dry solvents were obtained following common procedures.<sup>[23]</sup> For the chromatographic separation and analysis (sample preparation and mobile phase) we used LiChrosolv® solvents, ( $\text{CH}_2\text{Cl}_2$ , THF and hexane) which were purchased from Merck KGaA.

#### 4.2 Syntheses

##### General Procedure for Buchwald-Hartwig Couplings

---

Tris(5'-bromo-2-phenylpyridine)iridium(III) **1** (0.022 mmol), phenol (3.6 eq) and base (6.0 eq) were placed in a headspace vial. The vial was then flushed with nitrogen and sealed with a silicone/PTFE septum. Degassed anhydrous toluene (3 mL) and 1 mL of catalyst solution (containing 15 mol% catalyst and 30 mol% ligand in degassed toluene) were added subsequently. The mixture was then stirred at 120 °C for 16 h in a custom made aluminum

heating block. After cooling down to r.t., the reaction mixture was extracted with CH<sub>2</sub>Cl<sub>2</sub>, washed with water and brine and dried over MgSO<sub>4</sub>. The resulting reaction solution was subjected to LC/MS analysis.

#### **General Procedure for the Combinatorial Suzuki-Miyaura Couplings**

---

*Tris*(5'-pinacolatoboron-2-phenylpyridine)iridium(III) **3** (4.8 μmol), bromobenzene (4.0 eq) and base (9.0 eq) were placed in a headspace vial. The vial was then flushed with nitrogen and sealed with a silicone/PTFE septum. Degassed solvent (1.5 mL) and 0.5 mL of catalyst solution (containing 10 mol% catalyst and 40 mol% ligand in degassed toluene) were added subsequently. The mixture was then stirred at 120 °C for 12 h in a custom made aluminum heating block. After cooling down to r.t., the reaction mixture was extracted with CH<sub>2</sub>Cl<sub>2</sub>, washed with water and brine and dried over MgSO<sub>4</sub>. The resulting reaction solution was subjected to LC/MS analysis.

#### **Synthesis of *tris*(5'-pinacolatoboron-2-phenylpyridine)iridium(III) **3****

---

*Tris*(5'-bromo-2-phenylpyridine)iridium(III) **1** (200 mg, 0.22 mmol), B<sub>2</sub>pin<sub>2</sub> (285 mg, 1.12 mmol), KOAc (198 mg, 2.02 mmol), Pd(dppf)Cl<sub>2</sub> (55 mg, 0.07 mmol) and dppf (37 mg, 0.07 mmol) were placed in a headspace vial. The vial was then flushed with nitrogen and sealed with a silicone/PTFE septum. Degassed dioxane (18 mL) was added subsequently. The mixture was then stirred at 110 °C for 12 h in a custom made aluminum heating block. The solvent was removed. After recrystallization from toluene and additional purification by column chromatography (THF/Hexane 30%) the title compound was obtained as a bright yellow solid (10%).

**<sup>1</sup>H-NMR** (C<sub>2</sub>Cl<sub>4</sub>D<sub>2</sub>, 400 MHz): δ [ppm] = 7.99 – 7.87 (m, 6H), 7.61 – 7.50 (m, 3H), 7.37 (d, *J* = 4.8 Hz, 3H), 7.10 (d, *J* = 7.6 Hz, 3H), 6.89 – 6.82 (m, 3H), 6.79 (d, *J* = 7.6 Hz, 3H), 1.23 (d, *J* = 3.4 Hz, 36H). **<sup>13</sup>C-NMR** (C<sub>2</sub>Cl<sub>4</sub>D<sub>2</sub>, 101 MHz): δ [ppm] = 167.7, 166.3, 147.1, 144.0, 137.1, 136.6, 136.0, 130.4, 122.7, 120.6, 119.6, 83.6, 25.4, 25.2. **HR-MS** (+APCI): *m/z* (C<sub>69</sub>H<sub>45</sub>IrN<sub>6</sub>) calculated: 1151.3414 [M+H]<sup>+</sup>; found: 1151.3442.

## CHAPTER 3

### 5. REFERENCES

- [1] V.Shankarananth, K.K.Rajasekhar, *DIT* **2010**, 2 (1), 49-52.
- [2] E. M. Gordon, R. W. Barrett, W. J. Dower, S. P. A. Fodor, M. A. Gallop, *J. Med. Chem.* **1994**, 37, 1385-1401.
- [3] H. Mario Geysen, F. Schoenen, D. Wagner, R. Wagner, *Nat. Rev. Drug. Discov.* **2003**, 2, 222-230.
- [4] R. Storer, *Drug Discov. Today* **1996**, 1, 248-254.
- [5] J. F. Hartwig, *Angew. Chem. Int. Ed.* **1998**, 37, 2046-2067.
- [6] D. S. Surry, S. L. Buchwald, *Chem. Sci.* **2011**, 2, 27-50.
- [7] J. E. Baeckvall, E. E. Bjoerkman, L. Pettersson, P. Siegbahn, *J. Am. Chem. Soc.* **1984**, 106, 4369-4373.
- [8] A. Aranyos, D. W. Old, A. Kiyomori, J. P. Wolfe, J. P. Sadighi, S. L. Buchwald, *J. Am. Chem. Soc.* **1999**, 121, 4369-4378.
- [9] G. Mann, J. F. Hartwig, *J. Am. Chem. Soc.* **1996**, 118, 13109-13110.
- [10] R. A. Widenhoefer, H. A. Zhong, S. L. Buchwald, *J. Am. Chem. Soc.* **1997**, 119, 6787-6795.
- [11] B. Schlummer, U. Scholz, *Adv. Synth. Catal.* **2004**, 346, 1599-1626.
- [12] M. Nishiyama, T. Yamamoto, Y. Koie, *Tetrahedron Lett.* **1998**, 39, 617-620.
- [13] D. Prim, J.-M. Campagne, D. Joseph, B. Andrioletti, *Tetrahedron* **2002**, 58, 2041-2075.
- [14] D. M. T. Chan, K. L. Monaco, R. Li, D. Bonne, C. G. Clark, P. Y. S. Lam, *Tetrahedron Lett.* **2003**, 44, 3863-3865.
- [15] D. M. T. Chan, K. L. Monaco, R.-P. Wang, M. P. Winters, *Tetrahedron Lett.* **1998**, 39, 2933-2936.
- [16] J. X. Qiao, P. Y. S. Lam, *Synthesis* **2011**, 2011, 829-856.
- [17] a) Ir(Bpin-ppy)<sub>3</sub> (1.0 eq), phenol (6.0 eq.), Cu(OAc)<sub>2</sub> (3.0 eq), NEt<sub>3</sub> (15.0 eq), CH<sub>2</sub>Cl<sub>2</sub> (0.02 M), 4 Å molec. sieves, r.t.; b) Ir(Bpin-ppy)<sub>3</sub> (1.0 eq), phenol (6.0 eq.), Cu(OAc)<sub>2</sub> (3.0 eq), pyridine (15.0 eq), CH<sub>2</sub>Cl<sub>2</sub> (0.02 M), 4 Å molec. sieves, r.t.; c) Ir(Bpin-ppy)<sub>3</sub> (1.0 eq), phenol (6.0 eq.), Cu(OAc)<sub>2</sub> (3.0 eq), pyridine (15.0 eq), DMF (0.02 M), O<sub>2</sub>, 4 Å molec. sieves, 50 °C.
- [18] K. Sanjeeva Rao, T.-S. Wu, *Tetrahedron* **2012**, 68, 7735-7754.
- [19] a) Ir(Bpin-ppy)<sub>3</sub> (1.0 eq), NaIO<sub>4</sub> (9.0 eq), HCl (1N), THF/water (5:1, 0.1 M), r.t.; b) Ir(Bpin-ppy)<sub>3</sub> (1.0 eq), BCl<sub>3</sub> (20.7 eq), CH<sub>2</sub>Cl<sub>2</sub> (0.5 M), -78 °C; c) Ir(Bpin-ppy)<sub>3</sub>, BBr<sub>3</sub> (6.0 eq), CH<sub>2</sub>Cl<sub>2</sub> (0.2 M), 0 °C.
- [20] C. Xia, R. Kwong, J. Brooks, B. Al-Leyne, B. Ma, E. MacKenzie, J. Fiordeliso, Universal Display Corporation, WO2008073440A2, **2008**.
- [21] P. Stoessel, H. Spreitzer, H. Becker, WO2060910A1, **2002**.
- [22] J. Modin, H. Johansson, H. Grennberg, *Org. Lett.* **2005**, 7, 3977-3979.
- [23] Team of authors, *Organikum*, 21. ed., Wiley-VCH Weinheim, **2001**.

# CHAPTER 4

## **STUDIES ON THE PHOTODEGRADATION OF RED, GREEN AND BLUE PHOSPHORESCENT OLED EMITTERS<sup>‡</sup>**

The photodegradation behavior of four well established iridium emitters is investigated in this work. Irradiation of the samples in different solvents and under atmospheric as well as inert conditions helped to identify several pathways that can contribute to the deterioration of these compounds. Degradation via singlet oxygen or the excited states of the emitters as well as the detrimental influence of halogenated solvents are discussed for the different investigated iridium complexes. Some of the resulting degradation products could be identified using LC/MS or other analytical techniques. The results show how even small structural changes can have a huge influence on rate and mechanism of the photodegradation. The observations from this study may help to better understand degradation processes occurring during the handling of the materials but also during device processing and operation.

---

<sup>‡</sup> Photodegradation studies, data evaluation and writing the manuscript was done in equal contribution by Susanna Schmidbauer and Andreas Hohenleutner.





## 1. INTRODUCTION

For applications like displays or lighting, organic light-emitting devices have to enable the efficient conversion of electrons into photons to ensure sufficient light output at low power consumptions. To achieve this, the use of organo-transition metal complexes as phosphorescent dopants has proved highly beneficial. While fluorescent dyes normally emit from their singlet excited states (at room temperature) and therefore can only utilize singlet excitons, phosphorescent organo-transition metal dopants emit from their triplet excited states and in addition are able to effectively convert singlet into triplet states via fast intersystem crossing. The recombination of electron-hole pairs generates singlet and triplet excitons in a ratio of 1:3 which means that the use of phosphorescent devices can give up to 4 times higher efficiencies than those based on fluorescent emitters – which is called the triplet harvesting effect.<sup>[1]</sup> However, while OLEDs with efficiencies comparable to fluorescent tube lamps have been realized,<sup>[2]</sup> the operational stability of the devices remains to be a challenge in this field. In particular, the chemical degradation of the materials during operation is still considered the major obstacle for the development of economically feasible devices. In many cases of highly efficient phosphorescent devices it is indeed likely that the luminance loss over time can be in part or even largely attributed to the deterioration of the phosphorescent dopants.<sup>[3-4]</sup> The development of highly stable phosphorescent dopants is therefore a topic of high interest (see chapter 1). Thus, investigating the mechanisms and pathways responsible for the degradation of these materials is of high importance as the insights from these studies can guide the development of new materials with enhanced stabilities. Most studies on the degradation mechanisms of materials in OLEDs in general and of the phosphorescent emitters in particular suggest the participation of excited states.<sup>[3, 5-13]</sup> This can proceed *via* direct instability of the excited states, or *via* higher lying unstable states that are accessible through annihilation reactions<sup>[14-15]</sup> or thermal population.<sup>[16]</sup> Investigations on the photo-degradation of these compounds could therefore potentially provide valuable information on the processes that are responsible for the limited stability of phosphorescent OLEDs. In a previous study we already used the photoinduced degradation of phosphorescent iridium complexes in solution as a fast screening tool for their degradation behavior and observed interesting differences and effects in correlation to the examined structures.<sup>[17]</sup> In

## CHAPTER 4

this context, we wanted to gain a deeper understanding of the processes at work and examine whether the photostability in solution and in a solid organic matrix would show a similar behavior. We therefore selected four well known phosphorescent emitters for a detailed investigation of their photodegradation behavior in solution and thin polymer films. To gain information on the chemical degradation mechanisms, we tried to identify formed deterioration products via liquid chromatography mass spectrometry (LC/MS) and other analytical methods where applicable.

## 2. RESULTS AND DISCUSSION

For our investigations, we chose the four iridium complexes depicted in Figure 1. The compounds exhibit emission in the red ( $\text{Ir}(\text{piq})_3$ ), green ( $\text{Ir}(\text{Me-ppy})_3$  and  $\text{Ir}(\text{ppy})_3$ ) and blue region ( $\text{Ir}(\text{F,CN-ppy})_3$ ) respectively. Especially  $\text{Ir}(\text{piq})_3$  and  $\text{Ir}(\text{ppy})_3$  are popular phosphorescent emitters and often used in devices.

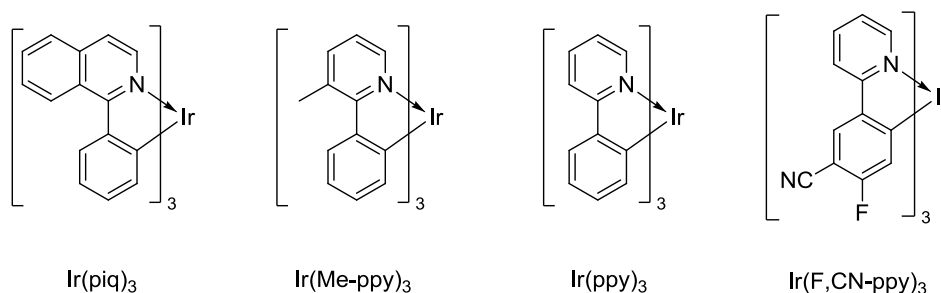


**Figure 1.** Structures of the investigated phosphorescent *tris*cyclometalated iridium complexes.

For the investigation of the behavior of these compounds under continuous excitation, the samples were irradiated with light of 400 nm high power LEDs (350 mW). This allows the excitation of the MLCT absorption band and further enables the irradiation through standard chromatography glass vials or glass substrates without having to resort to quartz cuvettes. Toluene was chosen as solvent since it is a comparably inert non-coordinating solvent that is also preferably used for the processing of OLEDs from solution. To check for the solvent influence, we also performed experiments in  $\text{CH}_2\text{Cl}_2$ . To be able to compare the behavior in solution and solid state, we further prepared thin poly(methyl metacrylate) (PMMA) films doped with the different materials via spin coating and subjected them to irradiation under the same conditions. For the degradation studies in solution, the ratio of remaining to initial complex concentration after the different irradiation times was determined via HPLC analysis, for the solid samples via measuring the luminescence intensities of the samples. The majority of the experiments was performed at least twice and was reproducible within an estimated error of < 10%. The degradation curves were generated using the average value of the obtained data (the results of the individual

experiments are provided in the Appendix). We will first discuss general trends and observations and then elaborate on the role of halogenated solvents followed by a more detailed discussion for each of the investigated compounds behavior.

## 2.1 General Observations

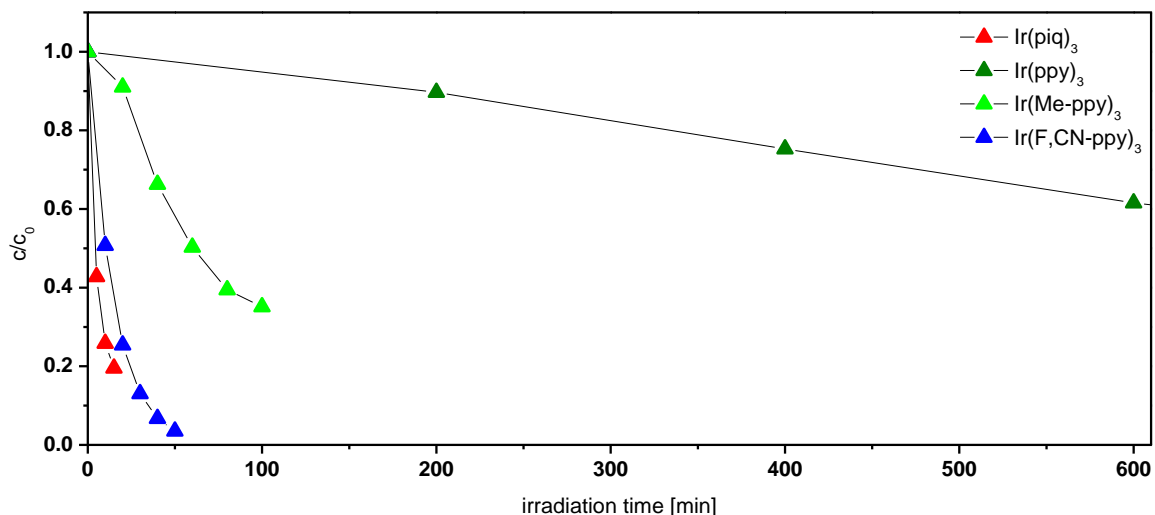


**Figure 2.** Photodegradation of different complexes in toluene in an ambient atmosphere. Plotted is the ratio between the remaining and initial concentrations for the respective compound against the irradiation time.

The rate of photodegradation shows substantial differences as can be seen in Figure 2, which compares the concentration decrease of the four substances in toluene at ambient conditions. While  $\text{Ir}(\text{ppy})_3$  is fairly stable,  $\text{Ir}(\text{Me-ppy})_3$  is degrading considerably faster and  $\text{Ir}(\text{piq})_3$  as well as  $\text{Ir}(\text{F,CN-ppy})_3$  exhibit an extremely fast deterioration in the course of only a few minutes. While this general trend for the stability of the different complexes ( $\text{Ir}(\text{ppy})_3 \gg \text{Ir}(\text{Me-ppy})_3 > \text{Ir}(\text{piq})_3/\text{Ir}(\text{F,CN-ppy})_3$ ) was found to apply to all examined conditions, the matrix can have a pronounced influence on the degradation rate. All compounds exhibit at least equal or higher stabilities in toluene compared to  $\text{CH}_2\text{Cl}_2$  (no reproducible results could be obtained for  $\text{Ir}(\text{F,CN-ppy})_3$  in  $\text{CH}_2\text{Cl}_2$ ). Interestingly, deterioration in the solid PMMA matrix also follows the overall trends as observed for the experiments in solution. This may be an indicator that the processes leading to the deterioration of these compounds might indeed at least partly be the same in solution and solid state. Figure 3 shows the degradation in different matrices at ambient conditions for all four compounds (note the different scale for the separate graphs).

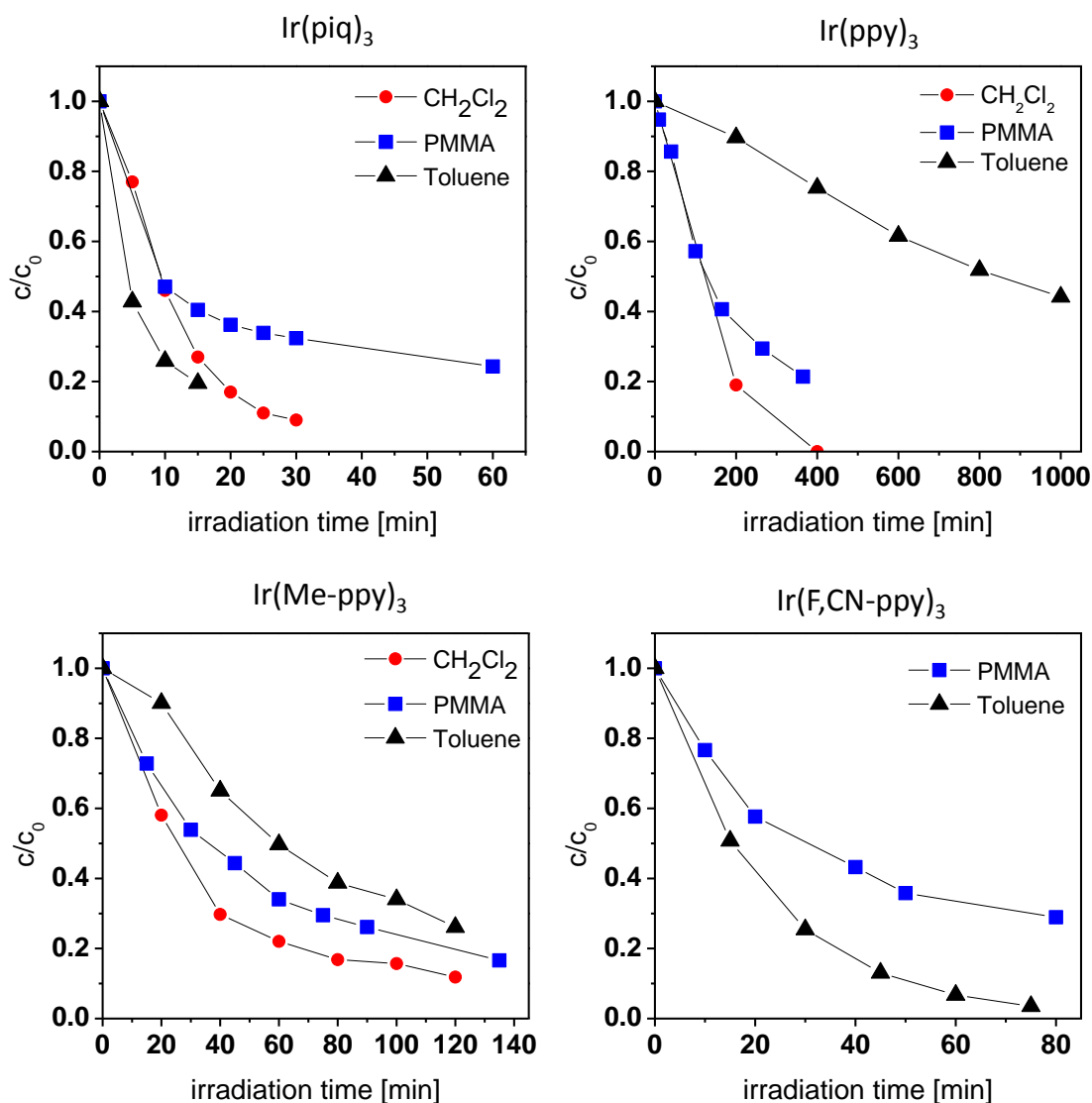


**Figure 3.** Photodegradation behavior of the iridium complexes in  $\text{CH}_2\text{Cl}_2$  and toluene solution and in a spin coated PMMA polymer film under ambient conditions. For measurements that were performed repeatedly, the depicted values represent the mean of all experiments.

## 2.2 The Influence of Halogenated Solvents

Though halogenated solvents often provide the best solubility for this class of compounds, it is generally believed that their use is detrimental to the stability of these materials. The observed higher degradation rates of the compounds in  $\text{CH}_2\text{Cl}_2$  seem to support this assumption. The higher the general stability of the investigated compounds, the stronger the detrimental effect of using  $\text{CH}_2\text{Cl}_2$  seems to be. While there is little to no solvent influence observable for  $\text{Ir}(\text{F,CN-ppy})_3$  and  $\text{Ir}(\text{piq})_3$ , it is more pronounced for  $\text{Ir}(\text{Me-ppy})_3$  and becomes particularly striking for  $\text{Ir}(\text{ppy})_3$  with the degradation being about eight times faster in  $\text{CH}_2\text{Cl}_2$  compared to toluene. A possible explanation for this observation could be that solvent independent processes are responsible for the generally very low photostabilities of the red and blue emitter and the solvent effect is therefore negligible.

With the overall higher stabilities of the green emitting compounds however, processes associated with  $\text{CH}_2\text{Cl}_2$  as the solvent become apparent. LC/MS analysis indeed revealed that the main observed degradation products of  $\text{Ir}(\text{ppy})_3$  after irradiation in  $\text{CH}_2\text{Cl}_2$  were chlorinated species, formed via the exchange of one or two hydrogen atoms for a chlorine substituent (Figure 4). This can be concluded from the  $m/z$  values as well as isotope distribution patterns. Analogous products could also be observed for  $\text{Ir}(\text{Me-ppy})_3$  though only as a side product (see below) while no indication of halogen abstraction was found for the other two complexes.

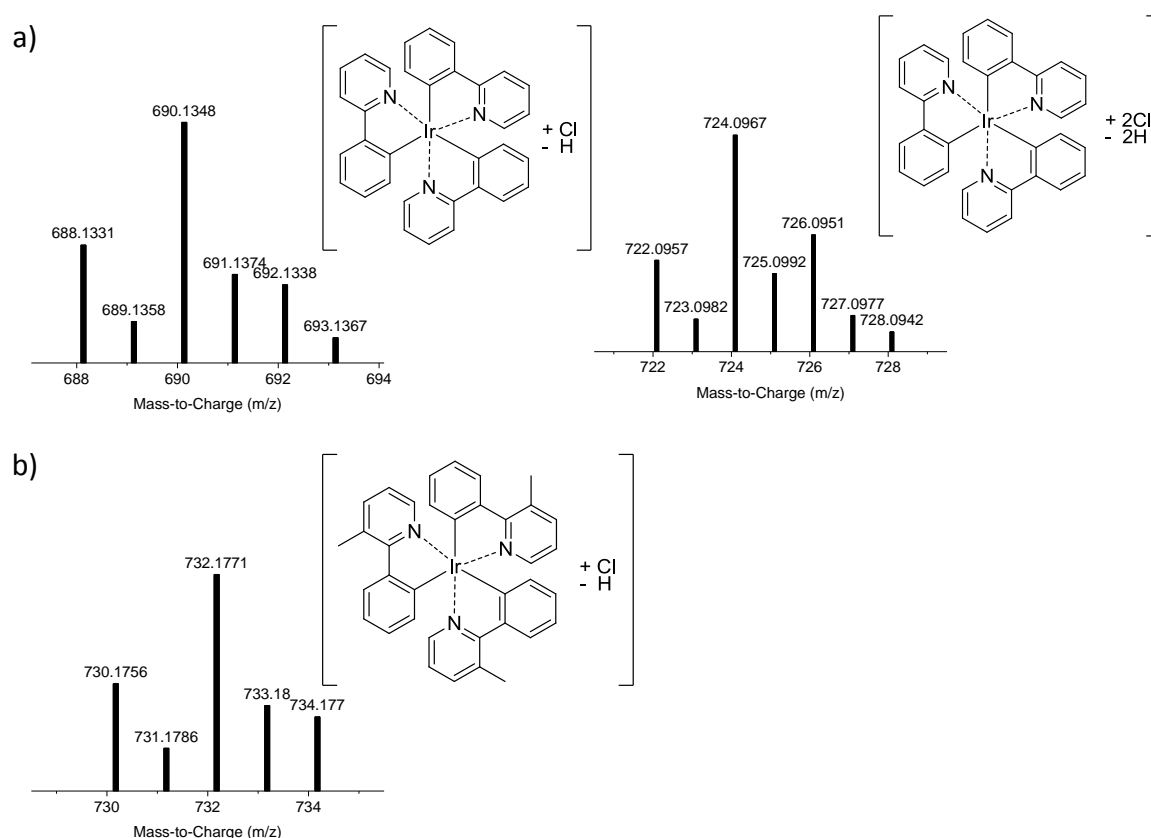


**Figure 4.** Mass spectra of the identified halogenated degradation products of a)  $\text{Ir}(\text{ppy})_3$  after 200 min of irradiation in  $\text{CH}_2\text{Cl}_2$  and b)  $\text{Ir}(\text{Me-ppy})_3$  after 120 min of irradiation in  $\text{CH}_2\text{Cl}_2$  (obtained from the LC/MS analysis of the respective samples).

## CHAPTER 4

### 2.3 The Influence of Oxygen

As cyclometalated Ir-complexes are very efficient singlet oxygen sensitizers, we wanted to investigate the influence of oxygen on the photostability of the compounds.  $^1\text{O}_2$  is known to undergo a variety of reactions with nitrogen heterocycles<sup>[18]</sup> and might thus attack the emitters, leading to the formation of a variety of deterioration products. We therefore performed the irradiation experiments in different solvents under atmospheric as well as inert conditions (freeze-pump-thaw, then argon atmosphere). All compounds were irradiated in  $\text{CH}_2\text{Cl}_2$  and toluene as mentioned above, but also in benzene and benzene- $\text{d}_6$ . Singlet oxygen has a significantly higher lifetime in deuterated solvents, resulting in an enhancement of processes induced by this highly reactive species. The comparison of degradation rates in benzene and benzene- $\text{d}_6$  should therefore help to elucidate the role singlet oxygen plays in the degradation of these materials as the degradation should be faster under atmospheric conditions than under inert atmosphere and show a further increase when performed in benzene- $\text{d}_6$ .

Other processes, possibly competing with the above singlet oxygen induced degradation route can be proposed to proceed via the excited state of the emitter molecule. This might be due to instability of the excited molecule itself, via interaction of the excited molecule with its local environment or even other excited states.<sup>[16, 19-20]</sup> Supposed the molecule is not susceptible to an attack of  $^1\text{O}_2$ , it would be expected that the presence of oxygen in this case actually increases the photostability of the material. This is due to the very fast quenching of the excited state by  $\text{O}_2$ ,<sup>[21]</sup> leading to a significantly shorter lifetime of the excited states and consequently a reduced degradation rate for processes induced via those states.

The observations from the photodegradation experiments suggest strong differences in the contribution of these two pathways for the four examined compounds. We therefore discuss the photodegradation behavior and the observed degradation products individually for each of the emitters.

The investigations in  $\text{CH}_2\text{Cl}_2$  under both ambient and inert conditions showed the same trend as those in benzene for all complexes. Within the range of measurement accuracy, no differences in the degradation behavior between experiments in toluene and benzene were observable. For clarity, only the results of the measurements in benzene and benzene- $\text{d}_6$  are therefore depicted and discussed in the following part (the Appendix provides the additional experimental degradation data).

#### **$\text{Ir}(\text{piq})_3$**

---

As mentioned above, red emitting  $\text{Ir}(\text{piq})_3$  is one of the most unstable compounds in the series of complexes investigated here. Irradiation in benzene under atmospheric conditions led to fast degradation with only about 10% of the initial concentration after 30 min of

irradiation (Figure 5). Under the exclusion of oxygen, however, the degradation is suppressed significantly. Therefore, reactive oxygen species are likely to be responsible for the decomposition of  $\text{Ir}(\text{piq})_3$ . Experiments in deuterated benzene under atmospheric conditions support this assumption showing more than 80% decrease in the complex concentration after only 5 min of irradiation. The observation that the degradation is also considerably faster in deuterated benzene under inert conditions might be attributed to the fact that a quantitative removal of oxygen is unlikely by the employed procedure. The repeated punctuation of the septa by the injector needle of the HPLC-autosampler might further allow small quantities of oxygen to enter the sample vial. This suggests that only traces of oxygen can have a pronounced effect on the durability of the complexes.

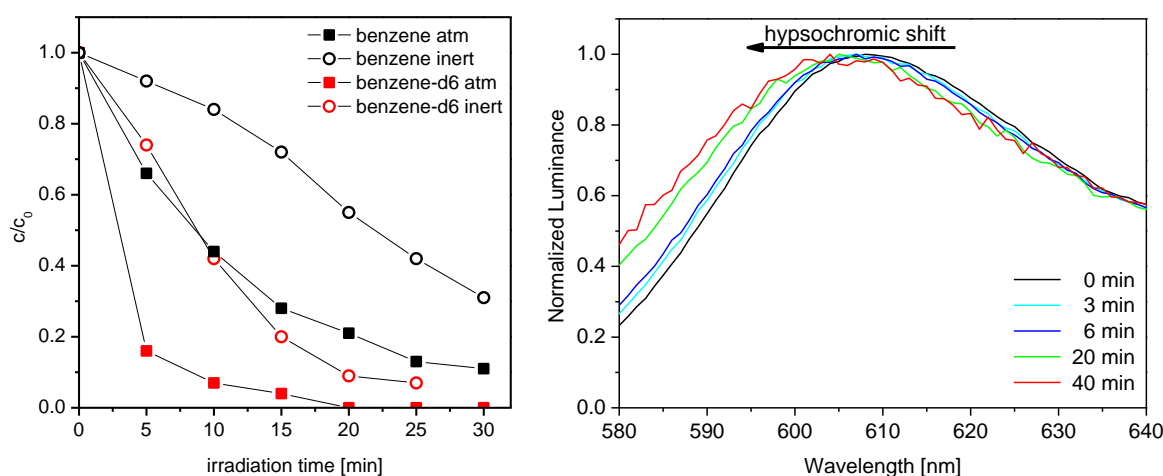


**Figure 5.** Degradation curves of  $\text{Ir}(\text{piq})_3$  in benzene and benzene- $\text{d}_6$  under ambient and inert conditions (left). Hypsochromic shift of the phosphorescence of an  $\text{Ir}(\text{piq})_3$  doped PMMA film with increased irradiation time (right).

Incorporation of the complex in a PMMA matrix leads to similar degradation rates at the beginning of the experiment (Figure 3). However, after 15-20 min of irradiation, the luminance changes decrease significantly. A possible explanation is the formation of degradation products which are still capable of phosphorescent emission, albeit at lower luminescence quantum efficiencies. This rational is supported by comparing the normalized phosphorescence spectra after consecutive irradiation periods (Figure 5). A hypsochromic shift and signal broadening with increased irradiation times is observed, indicating the presence of other species contributing to the emission.

In fact, the HPLC-DAD chromatograms of the soluble samples show that the decrease of the complex signal is accompanied by the emergence of two new peaks (Figure 6). These degradation products can be assigned to the  $m/z$  values 811 (①) and 824 (②) respectively. Despite NMR investigations of the decomposed sample, the structure of these two products could not be elucidated so far.

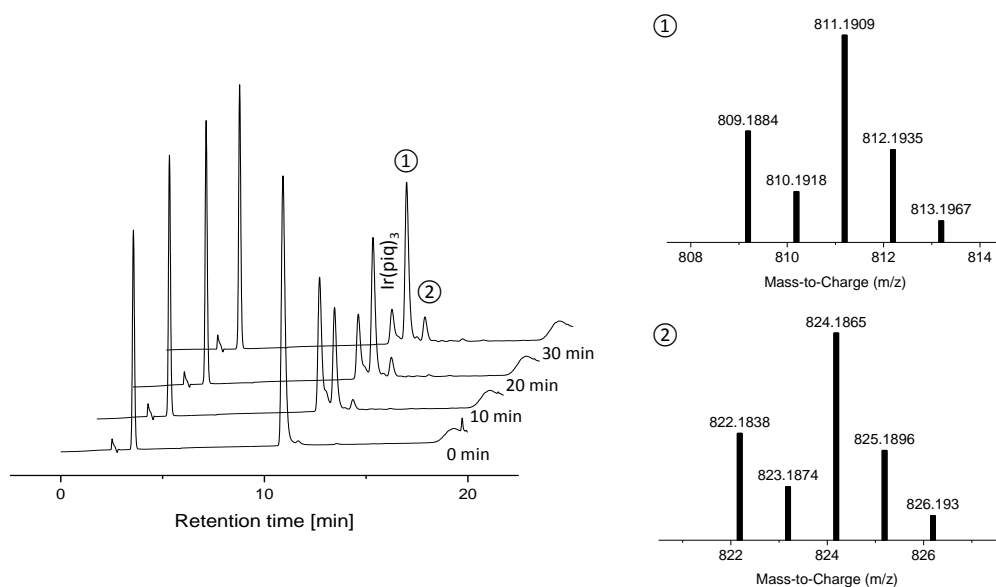


**Figure 6.** DAD chromatogram showing the formation of two main degradation products (left) and their assigned mass spectra (right).

### $\text{Ir(ppy)}_3$

In contrast, for the green emitting  $\text{Ir(ppy)}_3$  the presence of oxygen in benzene has a beneficial effect on the compounds stability. This is likely due to the ability of oxygen to quench the triplet excited state of the complex, thus preventing degradation through this state (Figure 7). Newly formed species, substantiating the contribution of the excited state on the complexes degradation, were identified via HPLC/MS analysis: the  $m/z$  value of 501 can be assigned to a species formed by the dissociation of one phenylpyridine ligand (③, Figure 8). This literature known phenomenon can be explained by the population of higher lying metal-centered states leading to bond rupture.<sup>[9-10, 22-23]</sup>

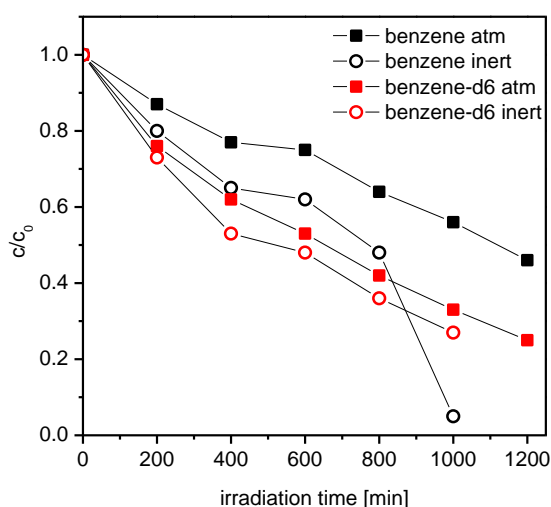


**Figure 7.** Degradation curves of  $\text{Ir(ppy)}_3$  in benzene and benzene-d6 under ambient and inert conditions.



Mass spectrometric investigations revealed the formation of three additional degradation products with the  $m/z$  values 603, 632 and 686, respectively. For the latter, an oxygenated species  $[\text{Ir}(\text{ppy})_3 + 2\text{O} - 2\text{H}]$  ④ can be assumed (Figure 8). However, the very small amounts did not allow for additional analyses by NMR to confirm the suggested structures.

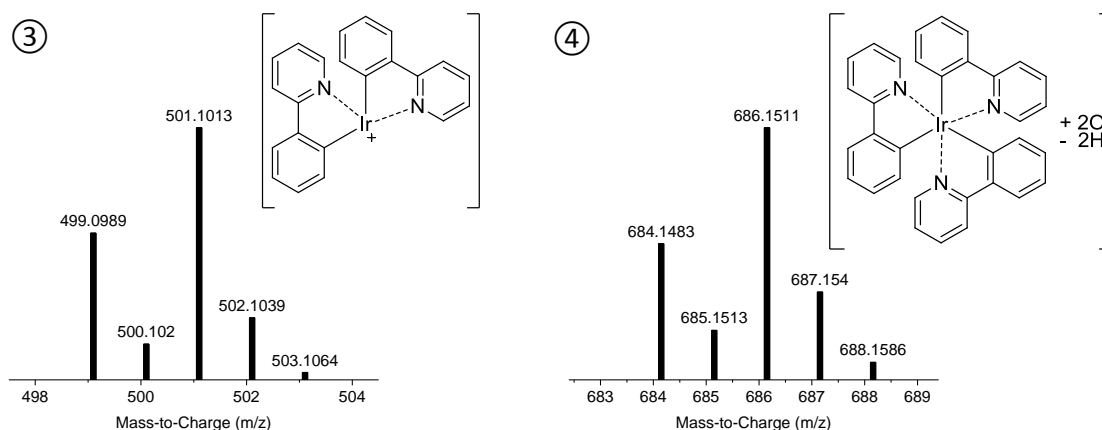


**Figure 8.** Mass spectra of two degradation products of  $\text{Ir}(\text{ppy})_3$  with the assigned structures.

### $\text{Ir}(\text{Me-ppy})_3$

As already observed for  $\text{Ir}(\text{ppy})_3$ , the methylated derivative  $\text{Ir}(\text{Me-ppy})_3$  degrades much faster under inert than under atmospheric conditions in benzene (Figure 9), which indicates the degradation *via* excited state induced processes. The same trend can be observed in benzene- $\text{d}_6$  albeit with a significantly diminished stability.

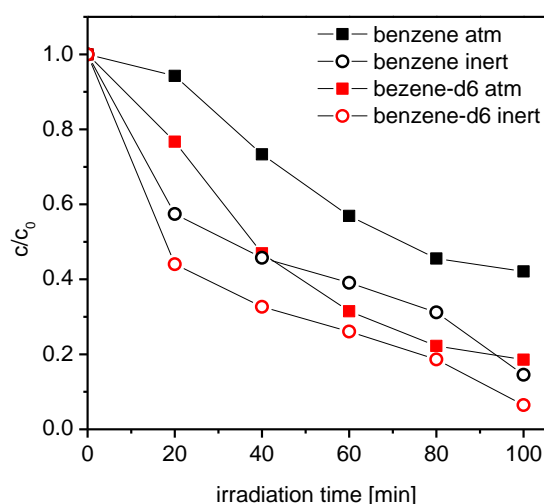


**Figure 9.** Degradation curves of  $\text{Ir}(\text{Me-ppy})_3$  in benzene and benzene- $\text{d}_6$  under ambient and inert conditions.

According to the DAD chromatogram, the decrease of the complex signal with the irradiation time was accompanied by the formation of only one visible degradation

## CHAPTER 4

product with a mass of 712 ( $MH^+ + 14$ ). This species was attributed to the aldehyde functionalized complex derivative (⑤, Figure 10), as the carbonyl functionality was confirmed by NMR spectroscopy with a signal at 10.5 ppm as well as IR spectroscopy with a typical signal at around  $1700\text{ cm}^{-1}$ . As it is known that singlet oxygen can oxidize methyl substituted aromatic systems to form aromatic aldehydes,<sup>[24]</sup> this proposed structure is in good agreement with the course of the degradation curve of the experiments in benzene- $d_6$  under ambient conditions. The increased lifetime of  $^1O_2$  in the deuterated solvent enhances the complex oxidation. Nonetheless, the observation that the degradation proceeds fastest under inert conditions in deuterated benzene cannot be explained with this deterioration model. As this behavior can also be observed for the green analogue  $Ir(ppy)_3$  (Figure 7) the contribution of another, still unidentified, deterioration pathway is most likely.

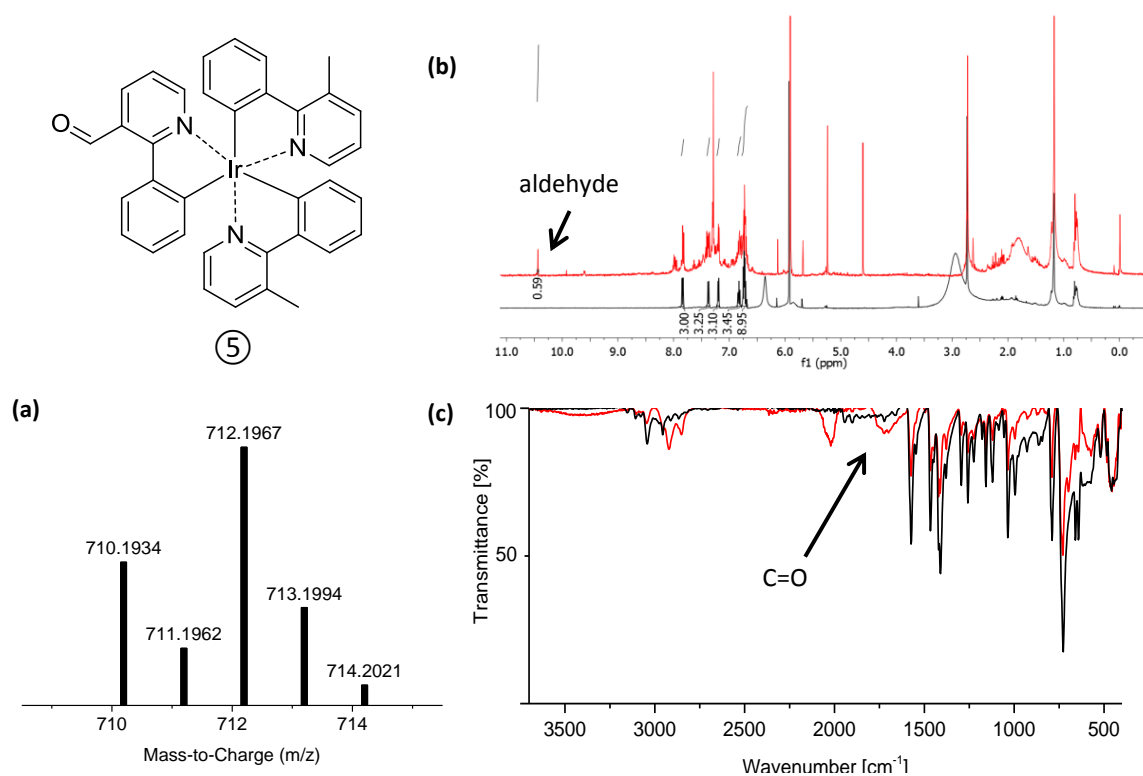


**Figure 10.** Structure of the main degradation product of  $Ir(Me-ppy)_3$  as confirmed by mass spectrometry (a), NMR (b) and IR (c) spectroscopy. (b) NMR spectra of  $Ir(Me-ppy)_3$  before (black) and after (red) irradiation, showing an arising aldehyde signal at 10.5 ppm. (c) IR spectra of  $Ir(Me-ppy)_3$  before (black) and after (red) irradiation, showing an emerging carbonyl signal at around  $1700\text{ cm}^{-1}$ .

### $Ir(F,CN-ppy)_3$

The degradation behavior of the blue emitting  $Ir(F,CN-ppy)_3$  is more complex. The solubility of this compound in all chosen solvents was poor and the complex turned out to be very

unstable in solution even without irradiation: after one day in the dark, the DAD signal of this complex decreased by half in toluene, benzene and benzene-d<sub>6</sub>. Therefore, the reproducibility of the experiments was not satisfying. Reliable results were only achieved for the measurements in toluene under atmospheric conditions, with an estimated error of ~10% (Figure 11). The experiment in benzene and benzene-d<sub>6</sub> under ambient conditions showed similar degradation behavior. Under inert conditions, no reliable dataset could be obtained.

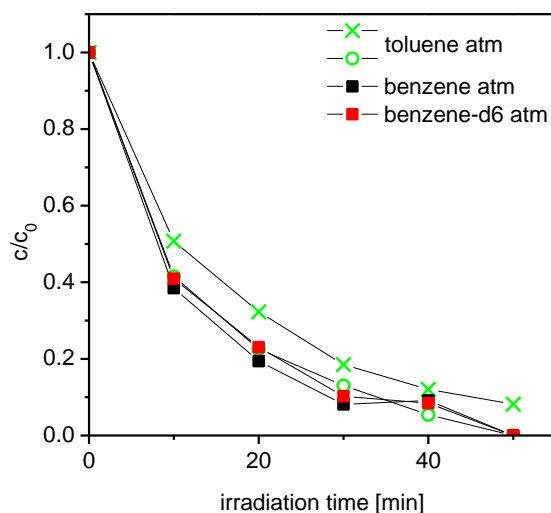


**Figure 11.** Degradation curves of Ir(F,CN-ppy)<sub>3</sub> in benzene, benzene-d<sub>6</sub> and toluene under ambient conditions.

Expected degradation products like species formed by fluorine cleavage, which were reported previously for blue emitting iridium analogues,<sup>[25-26]</sup> could not be observed. This might be due to the generally poor ionization of the complex. Only small traces of a degradation product with  $m/z = 816$  were detected (⑥, Figure 12), which may correspond to a double oxidized derivative [Ir(F,CN-ppy)<sub>3</sub> + 2O].

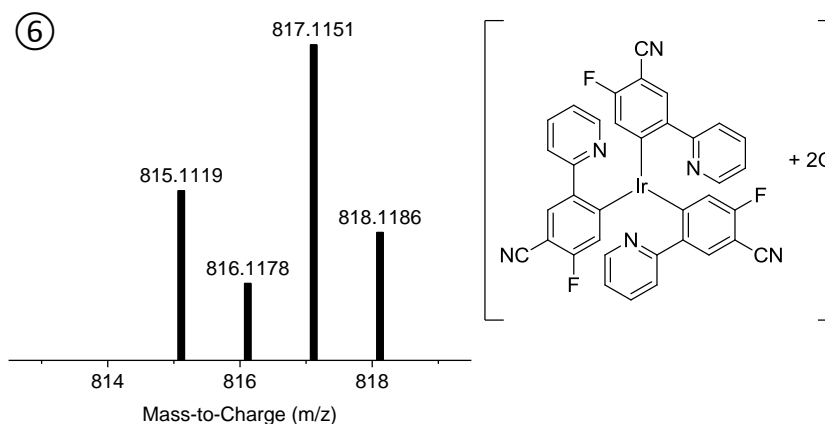


**Figure 12.** Mass spectrum of the detected degradation product of Ir(F,CN-ppy)<sub>3</sub>, which matches a twofold oxidized derivative with regard to its  $m/z$  value and the corresponding isotope pattern.

## CHAPTER 4

### 3. CONCLUSIONS

In conclusion, we have investigated the degradation behavior of four well established iridium emitters. The general stability of these complexes in solution and thin solid films follows the trend  $\text{Ir(ppy)}_3 \gg \text{Ir(Me-ppy)}_3 > \text{Ir(piq)}_3 \sim \text{Ir(F,CN-ppy)}_3$ . Irradiation of the samples in different solvents and under atmospheric as well as inert conditions allowed us to suggest several pathways that can contribute to the deterioration of these compounds.

$\text{CH}_2\text{Cl}_2$  as a representative of halogenated solvents has a detrimental influence on the stability of the compounds. The fast deterioration in this solvent and the identification of chlorinated species after the irradiation experiments for  $\text{Ir(ppy)}_3$  and  $\text{Ir(Me-ppy)}_3$  support the general notion that halogenated solvents should be avoided for these complexes when possible.

Utilizing the enhanced lifetime of  $^1\text{O}_2$  in deuterated solvents, we showed that the emitters can be very susceptible to singlet oxygen induced degradation depending on their structure. This pathway was identified as the predominant degradation mechanism for the red emitting  $\text{Ir(piq)}_3$ .  $\text{Ir(Me-ppy)}_3$  also showed sensitivity towards reactive oxygen species and an oxidized deterioration product could be identified after irradiation. The very fast degradation under the influence of oxygen and light emphasizes the necessity to process the devices and handle and store the materials under inert atmosphere and the exclusion of light whenever possible.

While the mechanisms for these reactions can be manifold and the exact structural identification of specific products is very difficult, the results suggest a strong contribution of degradation via the excited state. These processes are likely also the ones that are most relevant for the operational degradation of these compounds in OLEDs. We could for example observe the dissociation of one phenylpyridine ligand for  $\text{Ir(ppy)}_3$ , a product that has been identified in aged OLEDs as well.<sup>[7]</sup>

However, the photodegradation of these materials is complex and likely caused not only by one but many different mechanisms. Observations indicating the contribution of the excited states, singlet oxygen, and possibly other unidentified pathways to the degradation of  $\text{Ir(Me-ppy)}_3$  show that the different mechanisms are competing for this emitter.

The results from this study furthermore show how even small changes in the ligand structure can have a huge impact not only on the rate but also on the mechanisms of their degradation. The comparison between  $\text{Ir(ppy)}_3$  and  $\text{Ir(Me-ppy)}_3$  is particularly striking as they only differ in one methyl group. Knowledge on the mechanisms and products may contribute to understand degradation processes occurring during device operation but also to avoid adverse conditions such as halogenated solvents, light or oxygen during preparation, storage and handling of these materials. This can prevent the formation of degradation products that might be detrimental to the stability of organic light emitting devices.

## 4. EXPERIMENTAL PART

### 4.1 Methods and Materials

**NMR Spectroscopy:** NMR spectra were recorded on a *Bruker Avance 400* (400.13 MHz for  $^1\text{H}$  and 100.03 MHz for  $^{13}\text{C}$ ) spectrometer. Chemical shifts  $\delta$  are given in [ppm], using residual solvent (TCE- $d_2$ ) as an internal standard.

**IR Spectroscopy:** IR spectra of the solid samples were recorded on a *BIO-RAD Excalibur* IR spectrometer.

**High-Performance Liquid Chromatography/Mass Spectrometry:** The HPLC/MS analysis were performed on an *Agilent Technologies 1200 HPLC/MS* system consisting of a binary pump SL [G1312B], a degasser [G1379B], an *Infinity* high performance micro autosampler [G1329B] with thermostat [G1330B], a thermostatted column compartment [G1316B], an *Infinity* diode-array detector (DAD) [G4212B] and an accurate mass Q-TOF/MS [G6530A] with an APCI (atmospheric pressure chemical ionization) ion source. The column used was a *Hilbar®* 250 mm x 4 mm x 5  $\mu\text{m}$  diol column (Merck KGaA).

**Solvents and Reagents:** The complexes were provided by Merck KGaA. The solvents were purchased from Merck KGaA, Acros and Sigma Aldrich and were used as received without further purification. Toluene and benzene were used in p.a. quality.  $\text{CH}_2\text{Cl}_2$ , THF and hexane were LiChrosolv solvents.

### 4.2 Photodegradation Studies of the Liquid Samples

The complexes were dissolved in the appropriate solvent (50  $\mu\text{M}$ ). 1 mL of the resulting solution was transferred to a headspace vial and sealed with a silicone/PTFE septum. Two samples were prepared from each complex for the testing under atmospheric and inert conditions. In case of the photodegradation studies under inert conditions, the vials were degassed via 3 consecutive freeze-pump thaw cycles under argon. All samples were irradiated in a custom made irradiation unit (SIM GmbH). It consists of an aluminum printed circuit board with 30 400 nm LEDs (350 mW, Edison Edixeon 3 W Emitter, [LT-1467]), connected to a cooling unit, that ensures a constant temperature of 20  $^\circ\text{C}$  of the board during the irradiation. Two 15 sample chromatography trays can be placed in the unit so that each of the sample vials is centered over one LED ( $d = 1\text{ cm}$ ). The irradiation intervals were chosen individually for each complex according to the overall lifetime. After each irradiation cycle, the samples were analyzed via HPLC/MS. The remaining emitter concentration was determined via integration of the DAD signal at 305 nm in relation to that of an external standard (quaterphenyl in toluene, 0.026 mM). For each investigated compound the measurements in toluene under atmospheric conditions were performed at least twice to check for the accuracy of the measurement (< 10%, see Appendix). For NMR

## CHAPTER 4

and IR investigations, the solvent (toluene) was removed from the irradiated sample in a nitrogen stream.

### 4.3 Photodegradation Studies of the PMMA Substrates

PMMA and the complex (0.17 wt%) were dissolved in CH<sub>2</sub>Cl<sub>2</sub> and spin coated on a glass substrate. The films were irradiated as described for the liquid samples. The analysis of the PMMA substrates was performed on a *HORIBA Scientific* Fluoromax-4 spectrofluorometer using a solid sample holder, which ensures an accurate positioning of the substrate for the measurement. The  $c/c_0$ -values were determined via the ratio of the integrated phosphorescence spectra after irradiation to its initial value. All measurements were performed twice to check for the accuracy of the measurement (< 5%, see supporting information).

## 5. REFERENCES

- [1] M. A. Baldo, D. F. O'Brien, Y. You, A. Shoustikov, S. Sibley, M. E. Thompson, S. R. Forrest, *Nature* **1998**, 395, 151-154.
- [2] S. Reineke, F. Lindner, G. Schwartz, N. Seidler, K. Walzer, B. Lussem, K. Leo, *Nature* **2009**, 459, 234-238.
- [3] D. Y. Kondakov, W. C. Lenhart, W. F. Nichols, *J. Appl. Phys.* **2007**, 101, 024512-024517.
- [4] H. Z. Siboni, H. Aziz, *Appl. Phys. Lett.* **2012**, 101, 063502-063504.
- [5] D. Y. Kondakov, T. D. Pawlik, W. F. Nichols, W. C. Lenhart, *J. Soc. Inf. Display* **2008**, 16, 37-46.
- [6] I. R. de Moraes, S. Scholz, B. Lüssem, K. Leo, *Org. Electron.* **2012**, 13, 1900-1907.
- [7] I. R. de Moraes, S. Scholz, B. r. Lüssem, K. Leo, *Appl. Phys. Lett.* **2011**, 99, 053302.
- [8] R. Meerheim, S. Scholz, S. Olthof, G. Schwartz, S. Reineke, K. Walzer, K. Leo, *J. Appl. Phys.* **2008**, 104, 014510-014518.
- [9] I. R. d. Moraes, S. Scholz, B. Lüssem, K. Leo, *Org. Electron.* **2011**, 12, 341-347.
- [10] S. Scholz, C. Corten, K. Walzer, D. Kuckling, K. Leo, *Org. Electron.* **2007**, 8, 709-717.
- [11] S. Scholz, R. Meerheim, K. Walzer, K. Leo, Vol. 6999, 1 ed. (Eds.: P. L. Heremans, M. Muccini, E. A. Meulenkaamp), SPIE, Strasbourg, France, **2008**, pp. 69991B-69910.
- [12] S. Scholz, K. Walzer, K. Leo, *Adv. Funct. Mater.* **2008**, 18, 2541-2547.
- [13] S. Winter, S. Reineke, K. Walzer, K. Leo, Vol. 6999, 1 ed. (Eds.: P. L. Heremans, M. Muccini, E. A. Meulenkaamp), SPIE, Strasbourg, France, **2008**, pp. 69992N-69998.
- [14] N. C. Giebink, B. W. D'Andrade, M. S. Weaver, P. B. Mackenzie, J. J. Brown, M. E. Thompson, S. R. Forrest, *J. Appl. Phys.* **2008**, 103, 044509.
- [15] N. C. Giebink, B. W. D'Andrade, M. S. Weaver, J. J. Brown, S. R. Forrest, *J. Appl. Phys.* **2009**, 105, 124514-124517.
- [16] T. Sajoto, P. I. Djurovich, A. B. Tamayo, J. Oxgaard, W. A. Goddard, M. E. Thompson, *J. Am. Chem. Soc.* **2009**, 131, 9813-9822.

- [17] A. Hohenleutner, S. Schmidbauer, R. Vasold, D. Joosten, P. Stoessel, H. Buchholz, B. König, *Adv. Funct. Mater.* **2012**, 22, 3406-3413.
- [18] M. V. George, V. Bhat, *Chem. Rev. (Washington, DC, U. S.)* **1979**, 79, 447-478.
- [19] N. C. Giebink, B. W. D'Andrade, M. S. Weaver, P. B. Mackenzie, J. J. Brown, M. E. Thompson, S. R. Forrest, *J. Appl. Phys.* **2008**, 103, 044509.
- [20] M. A. Baldo, C. Adachi, S. R. Forrest, *Phys. Rev. B* **2000**, 62, 10967-10977.
- [21] H. Yersin, A. F. Rausch, R. Czerwieniec, T. Hofbeck, T. Fischer, *Coord. Chem. Rev.* **2011**, 255, 2622-2652.
- [22] I. R. de Moraes, S. Scholz, B. Lussem, K. Leo, *Appl. Phys. Lett.* **2011**, 99, 053302-053303.
- [23] S. Scholz, R. Meerheim, B. Lussem, K. Leo, *Appl. Phys. Lett.* **2009**, 94, 043314-043313.
- [24] A. G. Griesbeck, M. Cho, *Org. Lett.* **2007**, 9, 611-613.
- [25] V. Sivasubramaniam, F. Brodkorb, S. Hanning, H. P. Loeb, V. van Elsbergen, H. Boerner, U. Scherf, M. Kreyenschmidt, *J. Fluorine Chem.* **2009**, 130, 640-649.
- [26] R. Seifert, I. Rabelo de Moraes, S. Scholz, M. C. Gather, B. Lüssem, K. Leo, *Org. Electron.* **2013**, 14, 115-123.





# CHAPTER 5

## PT-COMPLEXES OF TETRADENTATE LIGANDS FOR OLED-APPLICATIONS†

A new class of Pt(II) cyclometalating complexes with tetradentate ligands was synthesized. Photophysical characterization in combination with degradation experiments and device studies render this class of complexes a promising representative of platinum derived OLED emitters.

---

The synthesis of the complexes was done by Susanna Schmidbauer. Quantum yields were determined by Christian Ehrenreich. Device fabrication and characterization was performed by Merck KGaA. All other experiments were also done by Susanna Schmidbauer.



## 1. INTRODUCTION

Apart from iridium complexes, platinum complexes attracted attention for their application as emitters in organic light-emitting diodes. With the synthesis of the cyclometalated platinum complex  $\text{Pt}(\text{ppy})_2$  in 1983 (Figure 1),<sup>[1]</sup> Zelewsky *et al.* paved the way for a target structure which is utilized in many complex design approaches to date. Unfortunately, this  $\text{Pt}(\text{II})$  complex, like many others, only emits in the solid state or at very low temperatures while they barely show emission in solution at ambient temperature ( $\Phi < 0.1$ ).<sup>[2-3]</sup>

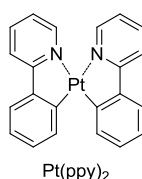


**Figure 1.** *Bis*(2-phenylpyridine)platinum(II) complex synthesized by Zelewsky *et al.*

$\text{Pt}(\text{II})$  complexes have a high affinity to square planar geometries. According to the ligand-field theory, the splitting of the orbitals results in four different energy levels ( $e_g$ ,  $a_{1g}$ ,  $b_{2g}$  and  $b_{1g}$ , Figure 2). In metal- $d(8)$  complexes the first three levels are populated with electrons, with the  $b_{2g}$  state acting as the highest occupied molecular orbital (HOMO). The  $b_{1g}$  orbitals, by contrast, exhibit a strongly antibonding character (Figure 3).

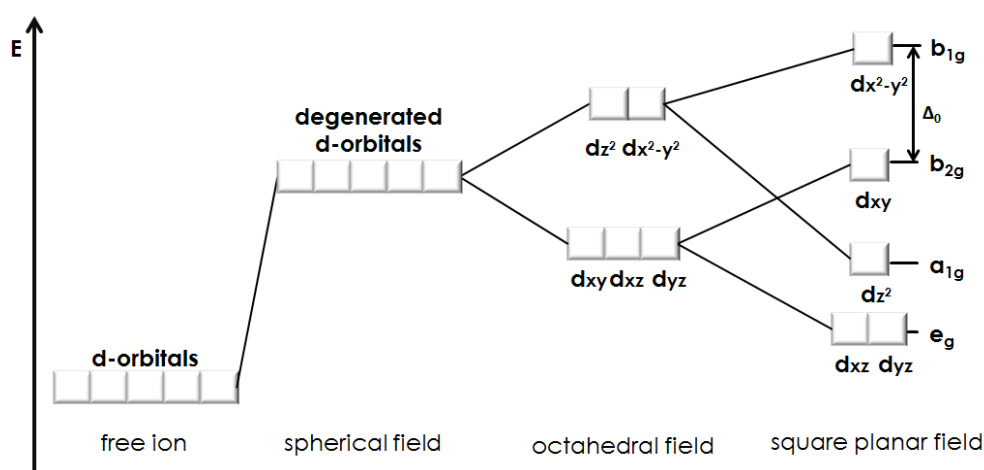


**Figure 2.** Ligand-field splitting of square planar complexes.

## CHAPTER 5

These states, the so called ligand-field states, can be populated via a metal-centered (MC) transition from the  $b_{2g}$ -level of the platinum atom. But they can also be thermally reached from ligand-centered  $\pi^*$  states, populated either via ligand-centered (LC) or metal-to-ligand charge-transfer (MLCT) transitions. The resulting excited metal-centered states are of highly distorted geometry and their relaxation to the ground state is of non-radiative nature.<sup>[4-6]</sup> To avoid radiationless decay, the accessibility of the  $b_{1g}$ -level must be prevented. Raising this state energetically to an extent that the energy gap  $\Delta E$  towards ligand-centered or charge-transfer states is increased to a greater value than  $kT$  constitutes one possible pathway (Figure 3b).

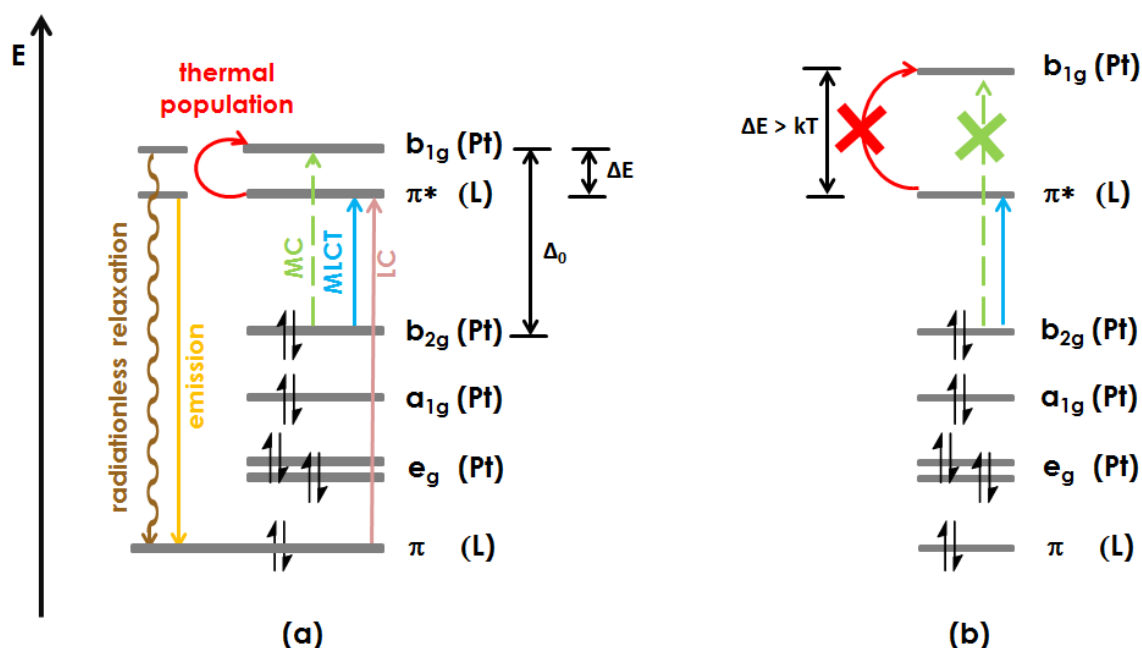


**Figure 3.** a) Simplified MO diagram of a typical square planar Pt(II)L<sub>x</sub> complex, illustrating the prevalent excitation and relaxation modes. b) The same diagram showing the effects of raising the ligand field state  $b_{1g}$ .

This can be achieved by using co-ligands with increased ligand-field strength, like cyanides or acetylides.<sup>[7]</sup> Following this strategy, cyclometalating ligands are a neat surrogate for purely coordinatively bound pyridyl ligands as the formally generated carbanion exhibits high ligand-field strength due to its strong  $\sigma$ -donation. This can be demonstrated (Figure 4) starting from the coordinative terpyridyl complex Pt(tpy)Cl<sup>+</sup> which does not show any emission in solution at room temperature.<sup>[7]</sup> Introducing one cyclometalating site in the ligand system, Pt(phbpy)Cl shows a quantum efficiency of 0.03 and Pt(dpyb)Cl of astounding 0.60.<sup>[8]</sup> The latter effect can be explained by a significantly shorter Pt–C bond of Pt(dpyb)Cl compared to the other terdentate complex resulting in a higher ligand-field strength.

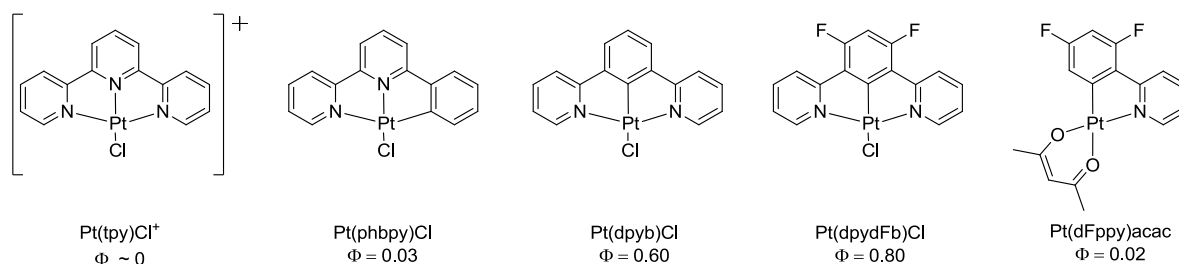


**Figure 4.** Selected Pt(II) complexes demonstrating the beneficial effects of cyclometalation and rigidity on luminescence quantum yields.<sup>[6-8]</sup>

The above mentioned lack of luminescence of  $\text{Pt}(\text{ppy})_2$ , however, shows that another parameter has to be taken into account in terms of high quantum efficiencies: the rigidity of the system. Excited complexes are prone to distortion through bond elongations as well as ligand-twisting towards a tetrahedral coordination sphere. This stabilizes the  $b_{1g}$ -states and therefore facilitates their population.<sup>[6]</sup>

To introduce more rigidity into the system, and thus limit the degree of freedom, bidentate ligands were substituted by terdentate ligands. Yersin *et al.* demonstrated the effect of enhanced quantum efficiency using this substitution approach, comparing the two blue emitters  $\text{Pt}(\text{dFppy})\text{acac}$  and  $\text{Pt}(\text{dpydFb})\text{Cl}$  (Figure 4). The terdentate coordinated complex exhibits an excellent quantum yield of 0.80 whereas the luminance of the bidentate derivative is almost negligible at ambient temperature.

Further developing this approach, a number of Pt(II) complexes with tetradentate ligand systems were synthesized. Therefore, two phenylpyridine units were linked through different moieties (Figure 5): Huo *et al.* presented arylamines as an efficient linker group. They synthesized several derivatives exhibiting quantum efficiencies up to 0.75.<sup>[9]</sup> Recently Fukagawa *et al.* reported the fabrication of highly stable OLED devices using these complexes, with efficiencies close to those of red emitting iridium complexes.<sup>[10]</sup> Weck *et al.* reported complexes of methylene bridged tetradentate ligands with quantum efficiencies around 0.50<sup>[11]</sup> and Merck KGaA started experiments with the rigid, fluorene bridged phenylpyridine complex **1a**, having an excellent quantum efficiency of 0.91.<sup>[3]</sup>

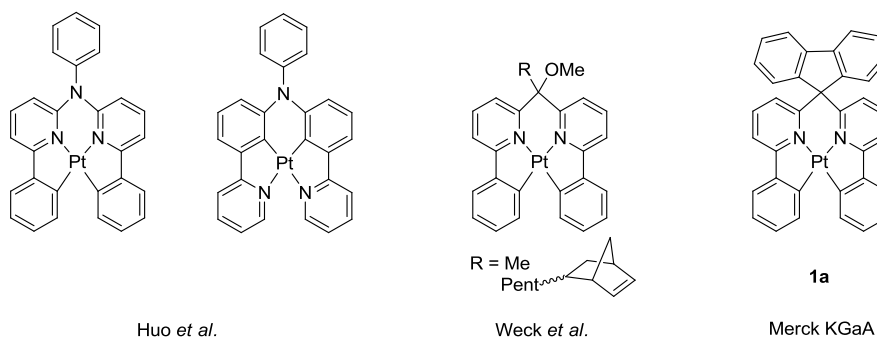


**Figure 5.** Lead structures of selected cyclometalated Pt(II) complexes with tetradentate ligands.

## CHAPTER 5

In cooperation with Merck KGaA, a new lead structure, the xanthene linked tetradentate ligand system, was developed. In this chapter, the synthesis of fluorene as well as xanthene bridged Pt(II) complexes is reported. The already known structure **1a** depicted in Figure 5 was additionally synthesized as reference complex. Photophysical and electrochemical properties are described and compared, and device data of complex **1a** are provided.

## 2. RESULTS AND DISCUSSION

### 2.1 Synthesis

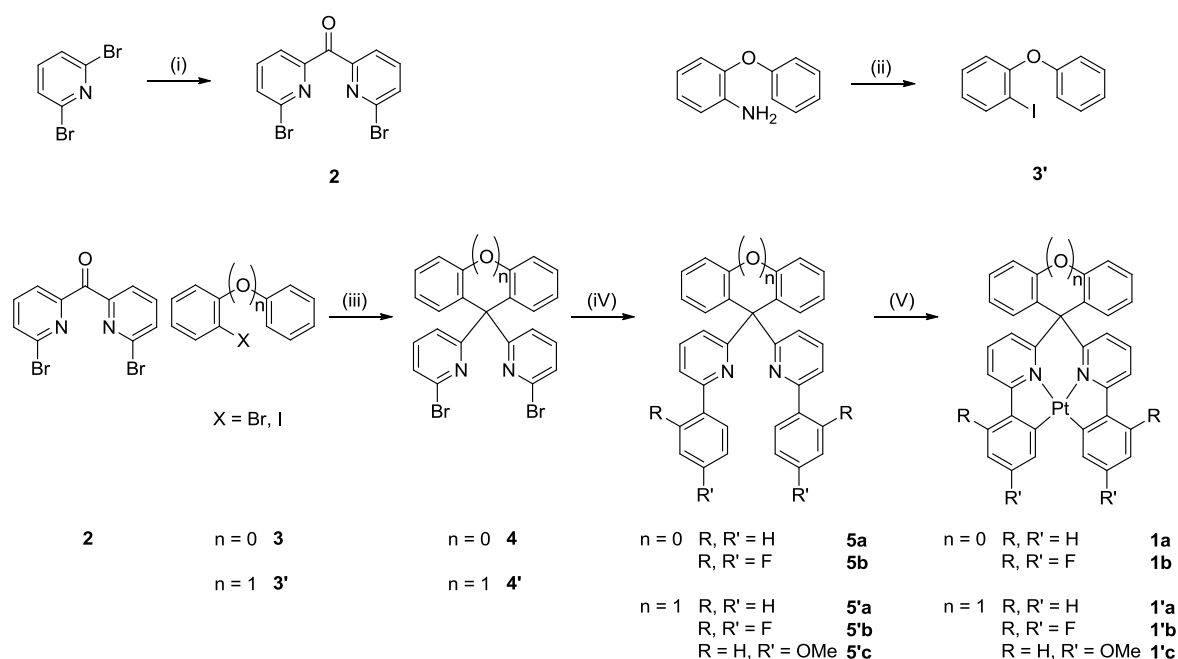


**Figure 6.** Synthetic route towards tetradentate platinum complexes: (i) 1. *n*BuLi, -80 °C, ether; 2. dimethylcarbamoyl chloride, -80 °C, ether. (ii) 1. NaNO<sub>2</sub>, 0 °C, HCl/water; 2. KI, -5 °C to 80 °C. (iii) 1. *n*BuLi, -79 °C, THF or *i*PrMgCl\*LiCl, r.t., THF; 2. acetic anhydride, conc. sulfuric acid, conc. acetic acid, 130 °C. (iv) boronic acid (**a-c**), Pd(dppf)Cl<sub>2</sub>, Na<sub>2</sub>CO<sub>3</sub>, toluene/dioxane/water, 120 °C. (v) K<sub>2</sub>PtCl<sub>4</sub>, AcOH, 130 °C.

The key molecules for the fast derivatization of fluorene and xanthene linked ligand systems are the bis(bromopyridyl) compounds **4** and **4'**, respectively. Compound **4** was synthesized performing a lithiation/transmetalation reaction of 2-bromobiphenyl **3** with bis(6-bromopyridin-2-yl)methanone **2** and a subsequent ring closing step under acidic conditions. Derivative **4'** was obtained via a Grignard reaction of ketone **2** with 1-iodo-2-phenoxybenzene **3'**, which was synthesized from the respective amine following a Sandmeyer protocol.<sup>[12]</sup> Ring closure to xanthene **4'** was achieved as for the fluorene analogue. These key structures can easily be derivatized by palladium catalyzed Suzuki-

Miyaura coupling reactions, yielding the tetradentate ligands **5** and **5'** in good to excellent yields (68-80%). Metalation with the platinum(II) precursor  $\text{K}_2\text{PtCl}_4$  gave the title complexes **1** and **1'** (Figure 7). While complex **1'a** and the fluorinated derivatives **1b** and **1'b** just precipitated from the reaction mixture in pure form (~58% yield), complexes **1b** and **1'c** had to be purified additionally by column chromatography, which led to decreased yields (12-22%). All complexes were characterized by HR-MS as well as 2D-NMR spectroscopy (NMR spectra are provided in the Appendix).

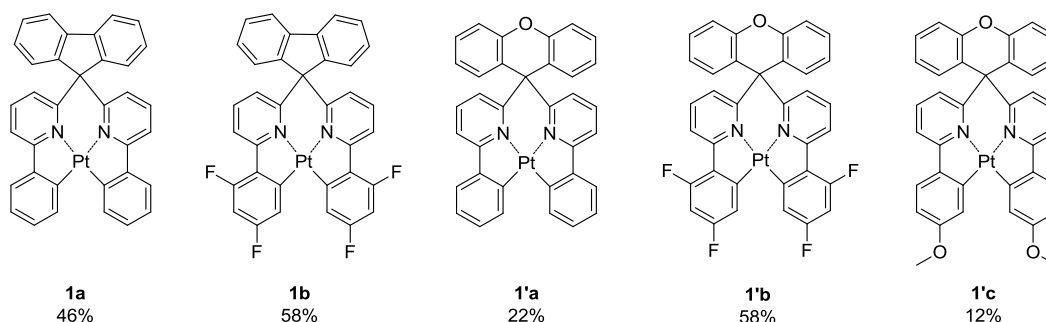


**Figure 7.** Structures and yields of the synthesized cyclometalated tetradentate Pt(II) complexes.

## 2.2 X-ray Crystal Structure

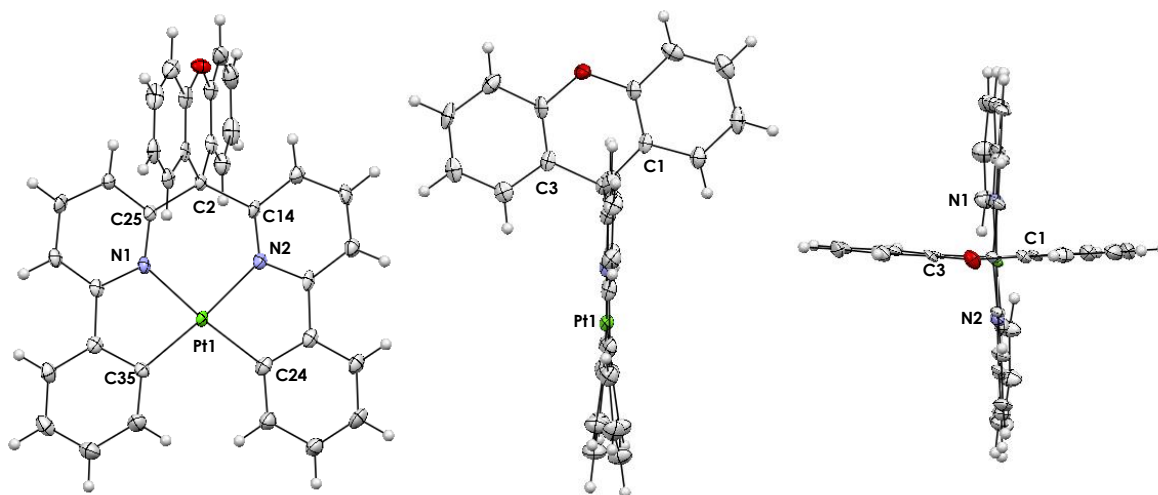


**Figure 8.** ORTEP plot (50% probability ellipsoids) of the molecular structure of complex **1'a**. Different perspectives provide an insight on the slight non-planarity of the system.

The crystal structure of complex **1'a** was determined by single crystal X-ray diffraction analysis. Selected bond lengths and angles are listed in Table 1 (all additional details are provided in the Appendix). The platinum is fully coordinated to the tetradentate ligand **5'a** in a slightly non-planar geometry (Figure 8). The phenylpyridine moieties are twisted, likely due to steric effects. In average, the Pt-N bonds are 0.060(5) Å longer than the Pt-C bonds.

## CHAPTER 5

This trend is in good agreement with the results for the arylamine bridged derivatives, investigated by Huo *et al.*<sup>[9]</sup> The xanthene does not have a planar structure but is slightly buckled. It is attached almost perpendicular to the coordination plane and tilted.

**Table 1.** Selected bond lengths and angles of complex **1'a**.

Bond length [Å]		Bond angle [deg]	
Pt(1)-N(1)	2.076(4)	N(1)-Pt(1)-N(2)	93.97(15)
Pt(1)-N(2)	2.079(4)	N(1)-Pt(1)-C(24)	174.18(17)
Pt(1)-C(24)	2.014(5)	N(1)-Pt(1)-C(35)	81.75(17)
Pt(1)-C(35)	2.020(5)	N(2)-Pt(1)-C(24)	81.52(18)
C(2)-C(1)	1.529(6)	N(2)-Pt(1)-C(35)	175.42(17)
C(2)-C(3)	1.541(6)	C(24)-Pt(1)-C(35)	102.9(2)
C(2)-C(14)	1.547(5)	C(1)-C(2)-C(14)	106.0(3)
C(2)-C(25)	1.548(6)	C(3)-C(2)-C(14)	106.6(3)
		C(1)-C(2)-C(25)	105.8(3)
		C(3)-C(2)-C(25)	104.3(3)

### 2.3 Spectroscopic Properties

The absorption and emission spectra of the complexes in CH<sub>2</sub>Cl<sub>2</sub> at ambient temperature are depicted in Figure 9 and the spectroscopic data summarized in Table 2. The bridge moiety does not show any effect on the emission properties of the complexes. All complexes have a strong absorbance below 325 nm ( $\epsilon > 2.5 \times 10^4 \text{ M}^{-1}\text{cm}^{-1}$ ) which can be assigned to ligand-centered transitions ( $\pi\text{-}\pi^*$ ). Two other absorbance peaks around 330 and 400 nm are less pronounced with absorption coefficients  $\epsilon > 1.0 \times 10^4$  and  $< 0.8 \times 10^4 \text{ M cm}^{-1}$  respectively. As these bands are absent in the absorption spectra of the free ligands **5a,b** and **5'a-c** (see Appendix), they can be assigned to metal-to-ligand charge transitions of any kind. A hypsochromic shift can be observed for the fluoro-substituted complexes **1b** and **1'b**, most pronounced in the region of the MLCT transitions. The electron-donating methoxy substituent of complex **1'c** induces a bathochromic shift.



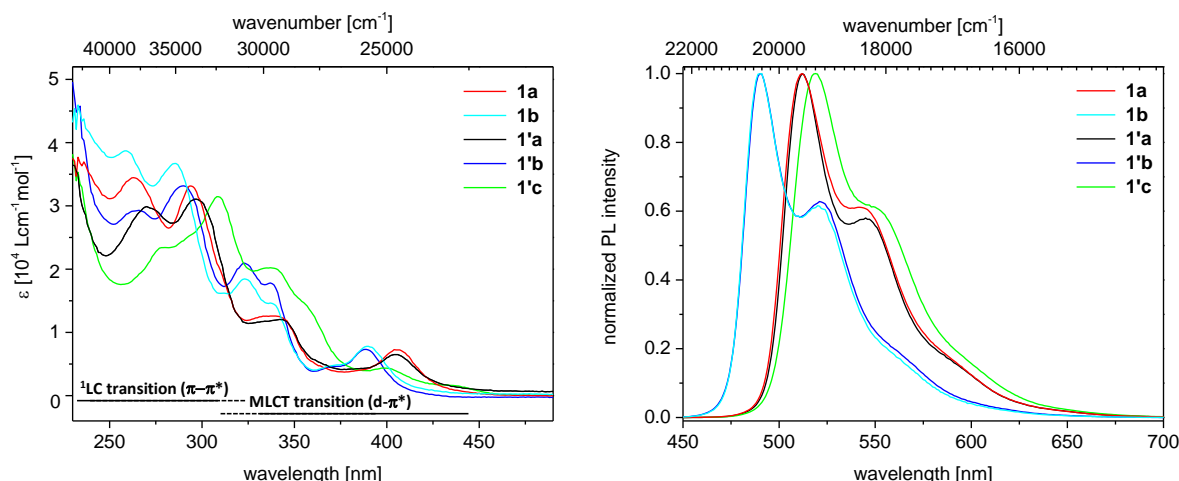


**Figure 9.** Absorption (left) and emission (right) spectra of complexes **1a-b** and **1'a-c**.

The emission properties of complex **1a** and **1'a** are comparable, with a maximum green emission at 512 nm and a vibronic sideband at 544 nm. The fluorinated analogues **1b** and **1'b** are shifted towards a turquoise emission at 490 nm (Figure 10). It can be assumed that both the benzene moiety and the metal contribute to the HOMO, as it was calculated for structurally similar phenylamine bridged complex systems.<sup>[9]</sup> Thus, the hypsochromic shift can be explained by the electron withdrawing effect of the fluorine substituents, stabilizing the HOMO. This results in an increasing HOMO-LUMO energy gap and a blue shifted emission. The electron donating methoxy substituent in complex **1'c** induces the contrary effect, a slightly red shifted emission with a maximum at 519 nm.

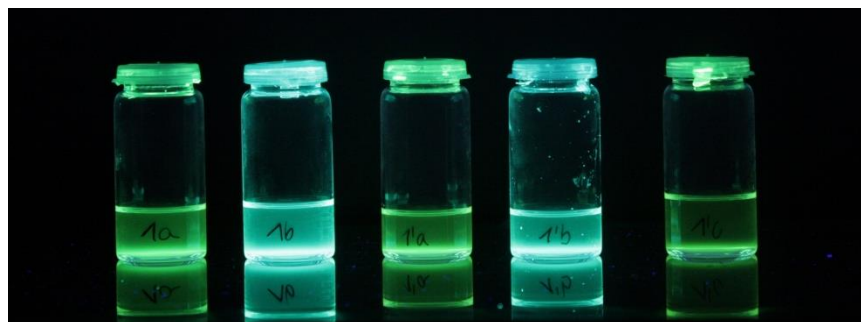


**Figure 10.** Emitting complexes **1a-b** and **1'a-c**.

The quantum yield of complex **1a** was determined to be 0.85, which is slightly lower than the literature reported value (0.91).<sup>[3]</sup> The other green emitting complexes **1'a** and **1'c** are also strongly luminescent with quantum efficiencies of 0.80 and 0.78, respectively. Interestingly, in both systems fluorination causes a significant decrease in the luminescence quantum yields (~30%). As a reason it might be carefully considered that the decrease of the metal-centered HOMO energy, due to the electron withdrawing effect of the fluorine substituents, is accompanied by a lowering of the ligand-field states making them accessible to thermal population. This would result in an activation of non-radiative decay

## CHAPTER 5

channels, and therefore diminish the quantum efficiencies. To prove this hypothesis, further experiments and computational approaches are necessary.

**Table 2.** Spectroscopic data of complexes **1a-b** and **1'a-c**.

	$\lambda_{\text{abs}} (\epsilon)^{\text{a)}}$ [nm] ([Lmol <sup>-1</sup> cm <sup>-1</sup> )]	$\lambda_{\text{em}}^{\text{b)}}$ [nm]	FWHM <sup>c)</sup> [nm]	$\Phi_{\text{P}}^{\text{c)}$
<b>1a</b>	228 (39374), 263 (34349), 294 (33046), 338 (12696), 406 (7314)	512	55	0.85
<b>1b</b>	259 (38785), 286 (36753), 324 (18559), 338 (14619), 371 (4801), 390 (7919)	491	50	0.59
<b>1'a</b>	271 (29696), 297 (30999), 344 (12107), 405 (6600)	512	53	0.80
<b>1'b</b>	230 (49441), 265 (29214), 290 (33279), 324 (20839), 337 (17845), 390 (7190)	490	51	0.55
<b>1'c</b>	278 (23460), 309 (31371), 339 (20234), 340 (4444), 438 (1807)	519	57	0.78

a) measured in CH<sub>2</sub>Cl<sub>2</sub> solution at r.t. (c = 1.5x10<sup>-5</sup> M and 7.5x10<sup>-6</sup> M. b) measured in degassed CH<sub>2</sub>Cl<sub>2</sub>,  $\lambda_{\text{exc}}$  = 400 nm. c) measured in degassed toluene solution at r.t. (c = 4x10<sup>-5</sup> M) at multiple excitation wavelengths.

### 2.4 Electrochemical Properties

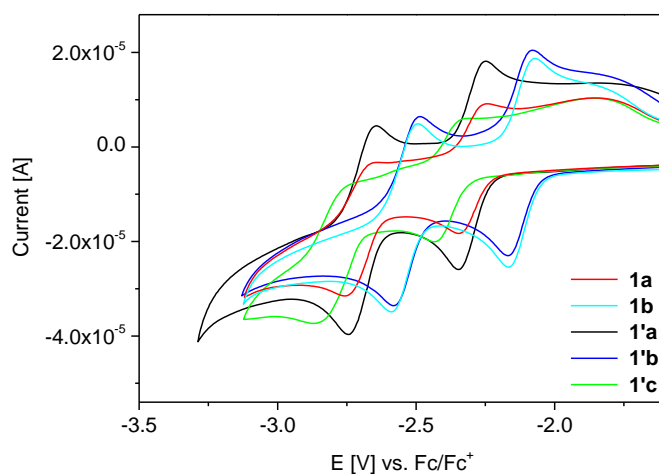


**Figure 11.** Cyclic voltammograms of complexes **1a-b** and **1'a-c** referenced to the Fc/Fc<sup>+</sup> standard.

The electrochemical properties were studied in cyclic voltammetric measurements (Figure 11). The complexes show two reversible reduction processes. The peak potentials of the first reduction lie between -2.12 and -2.38 V, those of the second one in the range of -2.53 and -2.80 V, all referenced against the Fc/Fc<sup>+</sup> standard (Table 3). The detection of oxidation peaks was not successful. The LUMO energies were calculated from the first reduction potential  $E_{1/2}^{\text{Red}}$  according to equation 1. The ferrocene standard is thereby assumed to have an energy level of 4.8 eV below the vacuum level.<sup>[13]</sup>

$$E_{LUMO}^{CV} = -E_{\frac{1}{2}}^{CV} - 4.8 \text{ eV} \quad (\text{equation 1})$$

The bridging moiety does not show any effect on the LUMO energies of the complexes. Incorporation of electron withdrawing substituents gives a decrease in the reduction potential of ~18 V, whereas an increase of 8 V can be observed for the methoxy substituted complex **1'c**. This behavior was also observed for other platinum(II) complexes.<sup>[11]</sup>

**Table 3.** Electrochemical data of complexes **1a-b** and **1'a-c**.

	1 <sup>st</sup> E <sub>1/2</sub> <sup>Red</sup> [V] <sup>a)</sup>	2 <sup>nd</sup> E <sub>1/2</sub> <sup>Red</sup> [V] <sup>a)</sup>	E <sub>LUMO</sub> <sup>CV</sup> [eV] <sup>b)</sup>
<b>1a</b>	-2.29	-2.70	-2.51
<b>1b</b>	-2.12	-2.54	-2.68
<b>1'a</b>	-2.30	-2.69	-2.50
<b>1'b</b>	-2.12	-2.53	-2.68
<b>1'c</b>	-2.38	-2.80	-2.42

a) measured in degassed DMF against the Fc/Fc<sup>+</sup> standard. E<sub>1/2</sub><sup>Red</sup> is determined as the center voltage between the peak for the reductions of the complex and the peak for the re-oxidation of the reduced species. B) calculated from the 1<sup>st</sup> E<sub>1/2</sub><sup>Red</sup> using equation 1.

## 2.5 Photodegradation

Photodegradation studies of the complexes in a polymer matrix (polymethyl(metacrylate), PMMA) were performed in the same way as reported for several iridium complexes in Chapter 4. Two substrates for each complex were irradiated with 400 nm LEDs over defined time periods and their remaining luminance intensity was subsequently analyzed by phosphorescence measurements. The average luminance values are plotted against the irradiation time (Figure 12). Complexes **1'a** and **1'c** show almost similar degradation rates, whereas emitter **1a** seems to be slightly more stable. The fluorinated derivatives **1b** and **1'b** degrade faster. Compared to the iridium emitters investigated in Chapter 4, the platinum complexes exhibit degradation rates in a comparable range as the stable green emitting standard iridium complex Ir(ppy)<sub>3</sub>.

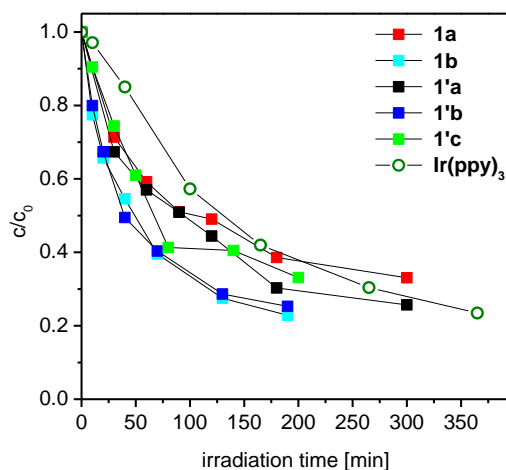


**Figure 12.** Photodegradation rates of the emitters **1a-b** and **1'a-c** and Ir(ppy)<sub>3</sub> in a PMMA matrix.

## 2.6 Device Performance

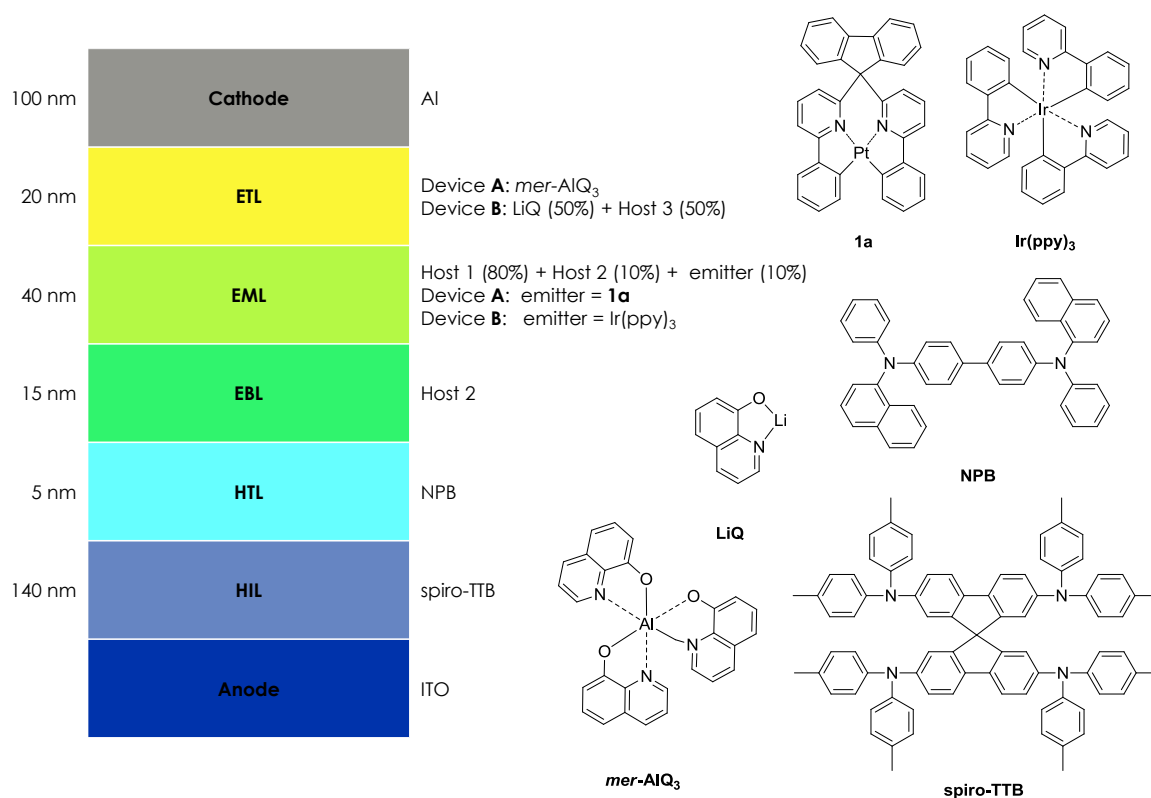


**Figure 13.** Device structure and used materials: anode: indium-tin oxide (ITO) | hole injection layer (HIL): 2,2',7,7'-tetra(*N,N*-ditolyl)amino-9,9-spiro-bifluorene (spiro-TTB) | hole transport layer (HTL): *N,N'*-bis(naphthalen-1-yl)-*N,N'*-bis(phenyl)benzidine (NPB) | Electron blocking layer (EBL): host 2 | emitting layer (EML): host 1 + host 2 + complex **1a**/tris(2-phenylpyridine)iridium(III) (Ir(ppy)<sub>3</sub>) | electron transport layer (ETL): *mer*-tris(8-hydroxy-quinolinato)aluminum (*mer*-AIQ<sub>3</sub>)/ 8-hydroxyquinolinolato-lithium (LiQ) + host 3 | cathode: aluminum. The structures of host 1-3 are subject to a non-disclosure agreement with Merck KGaA.

The performance of complex **1a** in OLED device **A** was investigated. For a better evaluation of the results, the obtained data were compared to those of another device **B** with a similar device structure using Ir(ppy)<sub>3</sub> as emitter. The results are listed in Table 4. Both devices were prepared using vapor deposition techniques. The multilayer device **A** has the following structure (Figure 13): ITO | Spiro-TTB (140 nm) | NPB (5 nm) | host 2 (15 nm) | host 1 + 10 wt% host 2 + 10 wt% **1a** (40 nm) | mer-AIQ<sub>3</sub> (20 nm) | Al (100 nm). Device **B** is constructed equally, with the exception of the electron transport layer: mer-AIQ<sub>3</sub> was substituted by host 3 + LiQ (each 50 wt%). With this change, only device parameters are affected, which are not discussed in this chapter. The combination of host 1 and host 2 in the emitting layer ensures an improved charge balance therein. Host 2 is additionally incorporated as an electron blocker at the NPB interface.

**Table 4.** Performance data of OLED devices **A** and **B**.

	Emitter	$\lambda_{\max}$ [nm]	CIE (x/y)	Efficiency [cd/A] @ 1000 cd/m <sup>2</sup>	EQE [%] @ 1000 cd/m <sup>2</sup>
Device A	<b>1a</b>	516	0.332/0.627	66.2	17.9
Device B	Ir(ppy) <sub>3</sub>	516	0.320/0.621	56.6	15.8

Both emitters have an emission maximum at 516 nm. Compared to Ir(ppy)<sub>3</sub>, the spectrum of complex **1a** is sharper and narrower. This results in a “cleaner” green emission for emitter **1a**, which is confirmed by the shift in the CIE coordinates (Figure 14).

Device **A** exhibits a good luminance efficiency of 66.1 cd/A and external quantum efficiency (EQE) of 17.9% at 1000 cd/m<sup>2</sup>, which are both slightly higher than for the Ir(ppy)<sub>3</sub> incorporated device **B**.

However, as device architecture and the choice of proper materials have a significant effect on the OLED-performance, it has to be considered that the used setup is not optimized for both emitters. Thus, a fair analogy between emitter **1a** and Ir(ppy)<sub>3</sub> would regard them anyway equal in terms of device performance.

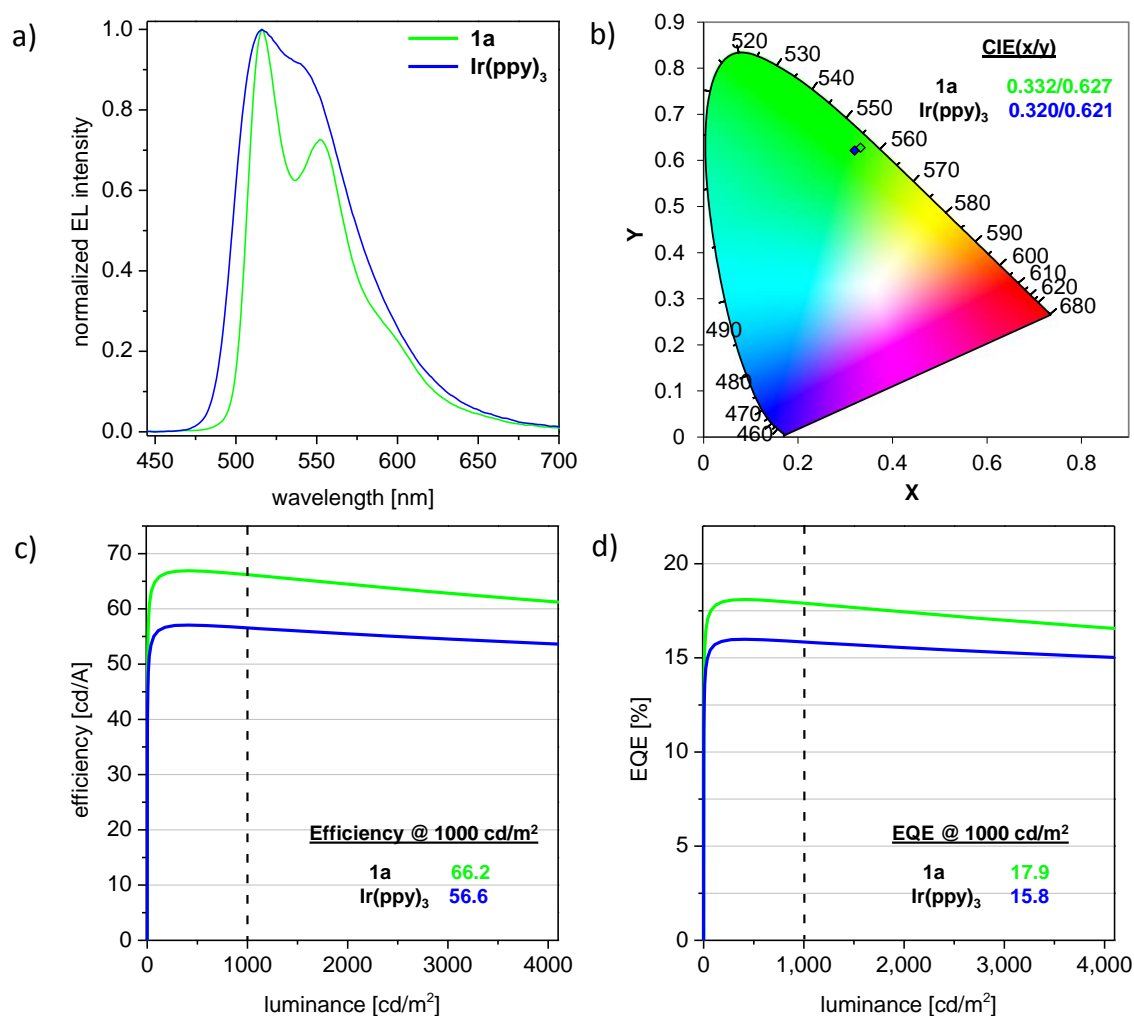


**Figure 14.** Performance characteristics of devices **A** and **B**: a) electroluminescence spectra, b) CIE coordinates, c) efficiency vs. luminance and d) external quantum efficiency (EQE) vs. luminance.

## 3. CONCLUSIONS

In summary, new lead structures for platinum(II) complexes with tetradentate ligands were investigated. Fluorene as well as xanthene bridged di(2-phenylpyridine) ligand systems and their platinum(II) complexed species were successfully synthesized. Compared to the fluorene bridged complexes **1a** and **1b**, their xanthene derived analogues **1'a-c** did not show significant differences in their photophysical and electrochemical properties. Those can, in contrast, be influenced through the substitution pattern of the phenyl moiety: electron withdrawing fluorine causes a hypsochromically shifted absorption and emission and a decrease in the reduction potential, whereas an electron donating methoxy substituent induces the converse effect. The detrimental character of fluorine substituents can be observed in the significantly decreased quantum efficiencies as well as photostabilities in solid films. Nonetheless, this new class of tetradenate platinum complexes

exhibits photostabilities comparable to the prominent stable, green emitting Ir(ppy)<sub>3</sub>. The device performance of complex **1a** is equal to Ir(ppy)<sub>3</sub>, reaching luminance efficiencies of ~60 cd/A and external quantum efficiencies of ~17% at 1000 cd/m<sup>2</sup>. Together with the enhanced color purity compared to Ir(ppy)<sub>3</sub>, complex **1a** is a promising candidate for display applications.

## 4. EXPERIMENTAL

### 4.1 Experimental Methods and Materials

**X-Ray Crystallography:** The data were acquired at an Agilent Technologies SuperNova device employing a microfocus copper source with Atlas CCD detector. An analytical absorption correction from crystal faces<sup>[14]</sup> was applied. The structures were solved by SUPERFLIP<sup>[15]</sup> and a least-square refinement on *F*<sup>2</sup> with SHELXL-97<sup>[16]</sup> was carried out.

**Absorption Spectroscopy:** Absorption Spectra were recorded on a Varian Cary Bio 50 UV/VIS spectrometer using a 1 cm quartz cuvette (Hellma) and LiChrosolv solvents (CH<sub>2</sub>Cl<sub>2</sub>) purchased by Merck KGaA. The extinction coefficients were determined according to Lambert Beers Law measuring each complex in two concentrations (1.5x10<sup>-5</sup> M, 7.5x10<sup>-6</sup> M).

**Emission Spectroscopy:** Phosphorescence spectra were recorded on a HORIBA Scientific Fluoromax-4 spectrofluorometer using sealable Hellma precision cells [117.100F-QS] (d = 1 cm) with silicone/PTFE coated septa. LiChrosolv solvents (CH<sub>2</sub>Cl<sub>2</sub>) were purchased by Merck KGaA. The dissolved samples were degassed via a purge of argon through the sealed cuvette. The excitation wavelength was 400 nm.

**NMR Spectroscopy:** NMR spectra were recorded on a Bruker Avance 300 (300.13 MHz for <sup>1</sup>H and 75.03 MHz for <sup>13</sup>C), Bruker Avance 400 (400.13 MHz for <sup>1</sup>H and 100.03 MHz for <sup>13</sup>C) and Bruker Avance 600 (Cryo) (600.1 MHz for <sup>1</sup>H and 150.1 MHz for <sup>13</sup>C) spectrometers. Chemical shifts δ are given in [ppm], using residual solvent peaks (reported for each spectrum) or tetramethylsilane as an internal standard. Coupling constants are reported in Hz. Characterization of the signals: s = singlet, d = doublet, t = triplet, q = quartet, m = multiplet, bs = broad singlet, dd = double doublet. Integration is determined as the relative number of atoms. Assignment of signals in <sup>13</sup>C-spectra was determined with DEPT-, HSQC- as well as HMBC-techniques (C<sub>q</sub> for quaternary C).

**Mass Spectrometry:** Mass spectra were recorded on a Varian CH-5 (EI), Finnigan MAT 95 (CI) and Finnigan MAT TSQ 7000 (ESI). High resolution mass spectra (HR-MS) were obtained from an Agilent 6530 accurate-Mass Q-TOF (APCI) in combination with a LC system (Hilbar® 250 mm x 4 mm x 5µm diol column).

## CHAPTER 5

**Cyclic Voltammetry:** Cyclic voltammetry measurements were carried out on an *Autolab PGSTAT 302N* setup using a conventional undivided electrochemical cell, a glassy carbon working electrode, platinum wire as the counter electrode and silver wire as a pseudo-reference electrode. Measurements were performed in DMF solution containing the complexes (2.5 mM) at 20 °C under argon atmosphere. The redox potentials were referenced against ferrocene/ferrocenium ( $\text{Fc}/\text{Fc}^+$ , 1.5 mM). In all experiments, the scan rate was  $50 \text{ mV s}^{-1}$  and  $\text{Bu}_4\text{N}^+\text{BF}_4^-$  (tetrabutylammonium tetrafluoroborate, 0.07 M) was used as the supporting electrolyte.

**Quantum Yield Estimation:** The complexes as well as toluene were deaerated in a glove box over night. The complexes were then dissolved in the toluene (0.04 mM) and the solution filled in a screw-cap cuvette. The sealed sample was removed from the glove box. The measurements were performed in an Ulbricht sphere (*Hamamatsu Photonic Multi-Channel Analyzer C10027*). The quantum yields were determined for several wavelengths (430, 420, 410, 400, 390, 370 and 350 nm) and averaged.

**TLC Analysis and Column Chromatography:** Analytical TLC plates (silica gel 60  $\text{F}_{254}$ ) and silica gel 60 (70-230 or 230-400 mesh) for column chromatography were purchased from Merck KGaA. Spots were visualized by UV light (254 nm). Gradient column chromatography was performed on a *Biotage® Isolera™* flash purification system.

**Solvents and Reagents:** All solvents and other commercially available reagents were purchased from Alfa Aesar or Sigma Aldrich and were used as received without further purification if not stated otherwise. Prior to use 2,6-dibromopyridine was dissolved in  $\text{CH}_2\text{Cl}_2$  and extracted with NaOH-solution (10 wt%) to deprotonate pyridinium adducts. The solvents were used in p.a. quality and degassed via purging with nitrogen or argon over 1 h.

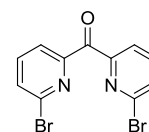
### 4.2 Photodegradation Studies of the PMMA Substrates

PMMA and the respective complex (0.17 wt%) were dissolved in  $\text{CH}_2\text{Cl}_2$  and spin coated on a glass substrate. Two samples were prepared from each complex. The substrates were irradiated in a custom made irradiation unit (SIM GmbH). It consists of an aluminum printed circuit board with 30 400 nm LEDs (350 mW, *Edison Edixeon 3 W Emitter*, [LT-1467]), connected to a cooling unit, that ensures a constant temperature of 20 °C of the board during the irradiation. Each of the samples is centered over one LED ( $d = 1 \text{ cm}$ ). The irradiation intervals were chosen individually for each complex according to the overall lifetime. After each irradiation cycle, the analysis of the PMMA substrates was performed on a *HORIBA Scientific Fluoromax-4* spectrofluorometer using a solid sample holder, which ensures an accurate positioning of the substrate for the measurement. The  $c/c_0$ -values were determined via the ratio of the integrated phosphorescence spectra after irradiation to its initial value (average of both samples).



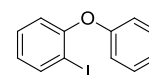
## 4.3 SYNTHESSES

## Syntheses of the Building Blocks

Bis(6-bromopyridin-2-yl)methanone 2

A solution of 2,6-dibromopyridine (10.0 g, 42.58 mmol) in dry ether (40 mL) was cooled to -80 °C under a nitrogen atmosphere. *n*BuLi (1.6 M, 26.6 mL) was dropped to the reaction mixture, which was allowed to warm to -10 °C during a 1 h periode. After cooling to -80 °C again, a 4.5 M solution of dimethylcarbamoyl chloride (5.00 mL, 19.16 mmol) in dry ether was slowly added. After stirring for additional 2.5 h, the reaction was quenched by adding conc. acetic acid (0.20 mL) in water (20 mL) via a syringe at -10 °C. After stirring at r.t. during night, the precipitate was filtered off and washed with ether, followed by ethanol. The product was obtained as a beige solid in 65% yield.

**<sup>1</sup>H-NMR** (CDCl<sub>3</sub>, 300 MHz): δ [ppm] = 8.07 (dd, *J* = 7.4, 1.1 Hz, 2H), 7.79–7.71 (m, 2H), 7.68 (dd, *J* = 8.0, 1.1 Hz, 2H). **<sup>13</sup>C-NMR** (CDCl<sub>3</sub>, 75 MHz): δ [ppm] = 189.2, 154.1, 141.6, 139.0, 131.5, 124.4.

1-Iodo-2-phenoxybenzene 3'

This compound was synthesized from 2-phenoxyaniline in a Sandmeyer reaction following a literature known procedure.<sup>[12]</sup>

**General Procedure for Suzuki-Miyaura Couplings**

A mixture of toluene (30 mL), dioxane (25 mL) and water (25 mL) were degassed in a Schlenk flask by purging with nitrogen for 1 h. The dibromide (2.00 mmol), boronic acid (3.0 eq), sodium carbonate (4.0 eq) and Pd(dppf)Cl<sub>2</sub> (0.1 eq) were added. The reaction mixture was refluxed at 110 °C for 2-4 h. After cooling to r.t. the phases were separated. The aqueous phase was extracted with CH<sub>2</sub>Cl<sub>2</sub> and the combined organic phases washed with water and brine and dried over MgSO<sub>4</sub> afterwards. The solvent was distilled off and the product was purified by column chromatography.

## CHAPTER 5

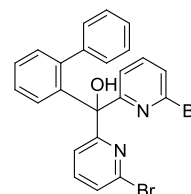
### General Procedure for Pt-Complexations

---

The ligand and  $\text{K}_2\text{PtCl}_4$  (each 1.0 eq) were placed in a headspace vial and set under an argon atmosphere. Conc. acetic acid was degassed via an argon purge and added (0.2 M). The reaction mixture was heated to 130 °C for 6-96 h. After cooling to r.t., the precipitated complex was filtered off and washed with water and hexane.

### Syntheses of the Fluorene Bridged Complexes

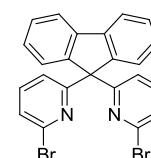
---



#### [1,1'-Biphenyl]-2-yl-bis(6-bromopyridin-2-yl)methanol

A solution of 2-bromobiphenyl (1.0 mL, 6.98 mmol) in dry THF (120 mL) was cooled to -80 °C. *n*BuLi (1.6 M, 6.98 mmol) was added dropwise and the solution was allowed to warm to -40 °C during 1 h. After cooling to -80 °C again, a solution of bis(6-bromo-pyridine-2-yl)methanone (2.39 g, 6.98 mmol) in dry THF (50 mL) was dropped to the reaction mixture and stirred at r.t. for 18 h. The reaction mixture was quenched with a saturated  $\text{NH}_4\text{Cl}$  solution and extracted in ether. Column chromatography (ethyl acetate in hexanes 10%) gave the alcohol as a pure white foam in 33% yield.

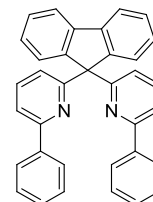
**<sup>1</sup>H-NMR** ( $\text{CDCl}_3$ , 600 MHz):  $\delta$  [ppm] = 7.71 (dd,  $J$  = 7.8, 0.7 Hz, 2H), 7.37 (t,  $J$  = 7.8 Hz, 2H), 7.32 (td,  $J$  = 7.5, 1.3 Hz, 1H), 7.25–7.20 (m, 3H), 7.14 (dd,  $J$  = 7.5, 1.4 Hz, 1H), 7.11–7.07 (m, 1H), 7.07–7.02 (m, 2H), 7.00–6.95 (m, 2H), 6.80 (dd,  $J$  = 8.0, 1.1 Hz, 1H). **<sup>13</sup>C-NMR** ( $\text{CDCl}_3$ , 75 MHz):  $\delta$  [ppm] = 163.9 (q), 143.4 (q), 143.4 (q), 142.0 (q), 139.2 (q), 138.5, 132.5, 130.2, 129.0, 127.6, 126.7, 126.6, 126.3, 126.1, 122.3, 80.5 (q). **MS** (+ES):  $m/z$  (%) = 497.0 (100) [ $\text{MH}^+$ ].



#### 6,6'-(9H-Fluorene-9,9-diyl)bis(2-bromopyridine) 4

[1,1'-Biphenyl]-2-yl-bis(6-bromopyridin-2-yl)methanol (1.10 g, 2.22 mmol) was dissolved in conc. acetic acid (11 mL). Acetic anhydride (1.3 mL, 13.97 mmol) was added and the solution heated to 80 °C. A 1:1-mixture of conc. acetic acid and conc. sulfuric acid (1.2 mL) was dropped to the reaction mixture which was refluxed for 2 h. After cooling to 0 °C a NaOH solution (1.0 g/2 mL) was added carefully and the resulting suspension extracted with  $\text{CH}_2\text{Cl}_2$ . The combined organic phases were washed with NaOH solution (10 wt%) and dried over  $\text{MgSO}_4$  before being concentrated to a small volume. The product precipitated as white crystals in 75% yield.

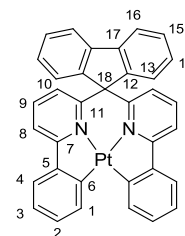
**<sup>1</sup>H-NMR** (CDCl<sub>3</sub>, 600 MHz): δ [ppm] = 7.92–7.89 (m, 2H), 7.79 – 7.76 (m, 2H), 7.43 (td, *J* = 7.4, 1.4 Hz, 2H), 7.37 (td, *J* = 7.5, 1.4 Hz, 2H), 7.28–7.24 (m, 4H), 6.97 (dd, *J* = 5.6, 3.0 Hz, 2H). **<sup>13</sup>C-NMR** (CDCl<sub>3</sub>, 75 MHz): δ [ppm] = 164.8 (q), 146.6 (q), 141.6 (q), 140.8 (q), 138.6, 128.5, 128.0, 127.6, 126.3, 120.3 119.6, 67.8 (q). **MS** (+ESI): *m/z* (%) = 479.0 (100) [MH]<sup>+</sup>. **HR-MS** (+ESI): *m/z* (C<sub>23</sub>H<sub>14</sub>Br<sub>2</sub>N<sub>2</sub>) calculated: 478.9577 [MH]<sup>+</sup>, found: 478.9579.



6,6'-(9H-Fluorene-9,9-diyl)bis(2-phenylpyridine) **5a**

The synthesis was performed using the general procedure for Suzuki-Miyaura couplings mentioned above. Column chromatography (CH<sub>2</sub>Cl<sub>2</sub> in hexane 20% - 50%) gave the desired product as a white solid in 68% yield.

**<sup>1</sup>H-NMR** (CDCl<sub>3</sub>, 600 MHz): δ [ppm] = 8.02 (d, *J* = 7.6 Hz, 2H), 7.93–7.88 (m, 4H), 7.83 (d, *J* = 7.1 Hz, 2H), 7.60–7.52 (m, 4H), 7.46–7.41 (m, 2H), 7.36 (dd, *J* = 28.7, 7.2 Hz, 8H), 7.09 (dd, *J* = 7.3, 1.1 Hz, 2H). **<sup>13</sup>C-NMR** (CDCl<sub>3</sub>, 75 MHz): 164.2 (q), 156.0 (q), 148.4 (q), 141.1 (q), 139.7 (q), 136.8, 128.7, 128.6, 127.9, 127.9, 127.6, 126.9, 120.1, 119.6, 117.7, 69.2 (q). **MS** (+ESI): *m/z* (%) = 473.2 (100) [MH]<sup>+</sup>. **HR-MS** (+ESI): *m/z* (C<sub>35</sub>H<sub>24</sub>N<sub>2</sub>) calculated: 473.2012 [MH]<sup>+</sup>, found: 473.2020.



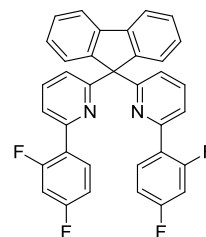
6,6'-(9H-Fluorene-9,9-diyl)bis(2-phenylpyridine)platinum(II) **1a**

The synthesis was performed following the general complexation procedure described above. Column chromatography (THF in hexane 30% - 100%) gave the title compound as yellow solid in 46% yield.

**<sup>1</sup>H-NMR** (TCE-d<sub>2</sub>, 600 MHz): δ [ppm] = 8.29 (d, *J* = 7.3 Hz, 2H, H-1), 8.07 (d, *J* = 7.6 Hz, 2H, H-13), 7.75 (d, *J* = 7.4 Hz, 2H, H-16), 7.64 (d, *J* = 7.4 Hz, 2H, H-8), 7.58 (d, *J* = 6.9 Hz, 2H, H-4), 7.44 (t, *J* = 8.1 Hz, 2H, H-9), 7.39 (td, *J* = 7.5, 1.0 Hz, 2H, H-15), 7.34 (td, *J* = 7.5, 1.2 Hz, 2H, H-2), 7.28 (td, *J* = 7.6, 1.1 Hz, 2H, H-14), 7.17 – 7.11 (m, 2H, H-3), 6.60 (dd, *J* = 8.1, 0.8 Hz, 2H, H-10). **<sup>13</sup>C-NMR** (TCE-d<sub>2</sub>, 151 MHz): δ [ppm] = 166.5 (q, C-7), 157.4 (q, C-11), 149.0 (q, C-6), 148.8 (q, C-12), 148.1 (q, C-5), 140.3 (q, C-17), 138.6 (C-9), 136.5 (C-1), 130.0 (C-2), 129.3 (C-14), 129.2 (C-15), 127.4 (C-13), 124.5 (C-4), 124.0 (C-3), 121.3 (C-10 /16), 121.2 (C-10/16), 118.2 (C-8), 73.2 (q, C-18). **HR-MS** (+APCI): *m/z* (C<sub>35</sub>H<sub>22</sub>N<sub>2</sub>Pt) calculated: 666.1507 [MH]<sup>+</sup>, found: 666.1558.

## CHAPTER 5

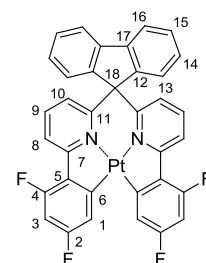
**UV** ( $\text{CH}_2\text{Cl}_2$ ):  $\lambda$  [nm] ( $\epsilon$ ) [ $\text{Lmol}^{-1}\text{cm}^{-1}$ ] = 228 (39374), 263 (34349), 294 (33046), 338 (12696), 406 (7314). **PL** (deg.  $\text{CH}_2\text{Cl}_2$ ):  $\lambda_{\text{em}}$  [nm] = 512.



6,6'-(9H-Fluorene-9,9-diyl)bis(2-(2,4-difluorophenyl)pyridine) **5b**

The synthesis was performed using the general procedure for Suzuki-Miyaura couplings mentioned above. Column chromatography ( $\text{CH}_2\text{Cl}_2$  in hexanes 20% - 60%) gave the desired product as a white solid in 77% yield.

**$^1\text{H-NMR}$**  ( $\text{CDCl}_3$ , 300 MHz):  $\delta$  [ppm] = 7.90 (d,  $J$  = 7.3 Hz, 2H), 7.86–7.73 (m, 4H), 7.63 (ddd,  $J$  = 7.9, 2.2, 0.9 Hz, 2H), 7.54 (t,  $J$  = 7.8 Hz, 2H), 7.44 (td,  $J$  = 7.5, 1.2 Hz, 2H), 7.34 (td,  $J$  = 7.5, 1.2 Hz, 2H), 7.05 (dd,  $J$  = 7.7, 0.9 Hz, 2H), 6.91–6.80 (m, 4H).  **$^{13}\text{C-NMR}$**  ( $\text{CDCl}_3$ , 75 MHz):  $\delta$  [ppm] = 164.2 (q), 163.7 (q, dd,  $J$  = 163.4, 12.0 Hz), 160.3 (q, dd,  $J$  = 165.5, 12.0 Hz), 151.3 (q, d,  $J$  = 2.9 Hz), 148.2 (q), 141.1 (q), 136.7, 132.3 (dd,  $J$  = 9.6, 4.7 Hz), 128.1, 127.7, 127.6, 124.0 (q, dd,  $J$  = 11.3, 3.8 Hz), 121.8 (d,  $J$  = 11.1 Hz), 120.3, 120.0, 111.8 (dd,  $J$  = 21.0, 3.6 Hz), 104.3 (dd,  $J$  = 27.1, 25.4 Hz), 69.1 (q). **MS** (+ESI):  $m/z$  (%) = 545.2 (100) [ $\text{MH}^+$ ]. **HR-MS** (+ESI):  $m/z$  ( $\text{C}_{35}\text{H}_{20}\text{F}_4\text{N}_2$ ) calculated: 545.1635 [ $\text{MH}^+$ ], found: 545.1647.



6,6'-(9H-Fluorene-9,9-diyl)  
bis(2-(2,4-difluorophenyl)pyridine)platinum(II) **1b**

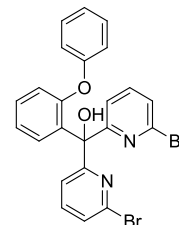
The synthesis was performed following the general complexation procedure described above. The title compound was obtained as a yellow solid in 58% yield.

**$^1\text{H-NMR}$**  ( $\text{TCE-d}_2$ , 600 MHz):  $\delta$  [ppm] = 8.01 (d,  $J$  = 9.2 Hz, 2H, H-8), 7.92 (d,  $J$  = 7.7 Hz, 2H, H-13), 7.76 (d,  $J$  = 7.6 Hz, 2H, H-16), 7.62 (dd,  $J$  = 9.2, 2.2 Hz, 2H, H-1), 7.49 (t,  $J$  = 8.1 Hz, 2H, H-9), 7.41 (t,  $J$  = 7.5 Hz, 2H, H-15), 7.28 (t,  $J$  = 7.6 Hz, 2H, H-14), 6.63–6.57 (m, 2H, H-3), 6.60 (d,  $J$  = 8.4 Hz, 2H, H-10).  **$^{13}\text{C-NMR}$**  ( $\text{TCE-d}_2$ , 151 MHz):  $\delta$  [ppm] = 164.4–62.7 (q, dd, C-2), 163.1 (q, d, C-5), 161.8–160.1 (q, dd, C-4), 157.7 (q, C-11), 154.1, (q, d, C-6), 148.8 (q, C-12), 140.4 (q, C-17), 139.5 (C-9), 131.0 (C-7), 129.5/129.4 (C-14/C-15), 127.2 (C-13), 122.1 (d, C-8), 121.5 (C-16), 121.4 (C-10), 118.3 (d, C-1), 100.3 (t, C-3), 73.6 (q, C-18). **HR-MS** (+APCI):  $m/z$  ( $\text{C}_{35}\text{H}_{18}\text{F}_4\text{N}_2\text{Pt}$ ) calculated: 738.113 [ $\text{MH}^+$ ], found: 738.1171. **UV** ( $\text{CH}_2\text{Cl}_2$ ):  $\lambda$  [nm] ( $\epsilon$ )

$[\text{Lmol}^{-1}\text{cm}^{-1}] = 259 \text{ (38785)}, 286 \text{ (36753)}, 324 \text{ (18559)}, 338 \text{ (14619)}, 371 \text{ (4801)}, 390 \text{ (7919)}.$

**PL** (deg.  $\text{CH}_2\text{Cl}_2$ ):  $\lambda_{\text{em}} [\text{nm}] = 491.$

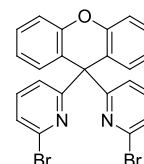
### Synthesis of the Xanthene Bridged Complexes



#### Bis(6-bromopyridin-2-yl)(2-phenoxyphenyl)methanol

1-Iodo-2-phenoxybenzene (5.00 g, 16.89 mmol) was suspended in dry THF (110 mL) under a nitrogen atmosphere.  $i\text{PrMgCl} \cdot \text{LiCl}$  (1.3 M in THF, 18.58 mmol) was added over 20 min at r.t.. After stirring for additional 15 min, bis(6-bromopyridin-2-yl)methanone (5.74 g, 16.89 mmol) in dry THF (50 mL) was added dropwise. Stirring at r.t. was continued for 19 h. The reaction mixture was quenched with a saturated  $\text{NH}_4\text{Cl}$  solution and extracted in ether. Column chromatography (ethyl acetate in hexanes 5% - 40%) gave the alcohol as white foam in 63% yield.

**$^1\text{H-NMR}$**  ( $\text{CDCl}_3$ , 600 MHz):  $\delta$  [ppm] = 7.85 (dd,  $J = 7.8, 0.8$  Hz, 2H), 7.48 (t,  $J = 7.8$  Hz, 2H), 7.29–7.26 (m, 3H), 7.20–7.16 (m, 2H), 7.06–7.02 (m, 1H), 6.99–6.94 (m, 2H), 6.90 (dd,  $J = 8.1, 1.2$  Hz, 1H), 6.70–6.63 (m, 2H).  **$^{13}\text{C-NMR}$**  ( $\text{CDCl}_3$ , 151 MHz):  $\delta$  [ppm] = 163.7 (q), 156.7 (q), 154.5 (q), 139.8 (q), 139.0, 137.0 (q), 129.9, 129.6, 129.2, 126.6, 123.3, 122.6, 121.8, 120.8, 117.6, 79.2 (q). **MS** (+ESI):  $m/z$  (%) = 513.0 (100)  $[\text{MH}]^+$ .



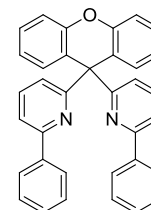
#### 6,6'-(9H-Xanthene-9,9-diyl)bis(2-bromopyridine) 4'

Bis(6-bromopyridin-2-yl)(2-phenoxyphenyl)methanol (4.92 g, 9.64 mmol) was dissolved in conc. acetic acid (50 mL) and acetic anhydride (5.6 mL, 59.76 mmol) at 80 °C. A mixture of conc. acetic acid and conc. sulfuric acid (2.5 mL:2.5 mL) was dropped to the solution and which was refluxed at 130 °C for 5 h. The reaction mixture was cooled in an ice bath and NaOH solution (10 mL, 50 wt%) was added carefully, followed by the addition of water (30 mL). After extraction with  $\text{CH}_2\text{Cl}_2$ , the combined organic phases were neutralized with NaOH solution (10 wt%), dried over  $\text{MgSO}_4$  and filtered over celite. The solvent was reduced to a minimal amount for precipitation to gain the product as a grey solid in 38% yield.

**$^1\text{H-NMR}$**  ( $\text{CDCl}_3$ , 600 MHz):  $\delta$  [ppm] = 7.40 (t,  $J = 7.8$  Hz, 2H), 7.31–7.28 (m, 4H), 7.23 (dd,  $J = 7.9, 1.5$  Hz, 2H), 7.16 (dd,  $J = 8.2, 1.1$  Hz, 2H), 7.07–7.03 (m, 2H), 6.93 (d,  $J = 7.7$  Hz, 2H).  **$^{13}\text{C-NMR}$**  ( $\text{CDCl}_3$ , 75 MHz):  $\delta$  [ppm] = 166.2 (q), 151.0 (q), 140.8 (q), 138.3, 131.2, 128.7, 125.8,

## CHAPTER 5

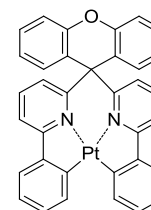
124.9 (q), 123.2, 123.1, 116.5, 56.5 (q). **MS** (+ESI):  $m/z$  [%] = 495.0 (100) [MH]<sup>+</sup>. **HR-MS** (+ESI):  $m/z$  (C<sub>23</sub>H<sub>14</sub>Br<sub>2</sub>N<sub>2</sub>O) calculated: 494.9527 [MH]<sup>+</sup>, found: 494.9533.



### 6,6'-(9H-Xanthene-9,9-diyl)bis(2-phenylpyridine) 5'a

The synthesis was performed using the general procedure for Suzuki-Miyaura couplings mentioned above. Column chromatography (CH<sub>2</sub>Cl<sub>2</sub> in hexanes 20% - 70%) gave the desired product as white foam in 77% yield.

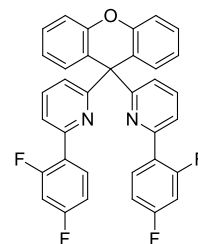
**<sup>1</sup>H-NMR** (CDCl<sub>3</sub>, 600 MHz):  $\delta$  [ppm] = 7.84 (dt,  $J$  = 8.5, 2.2 Hz, 4H), 7.63 (t,  $J$  = 7.7 Hz, 2H), 7.59 (dd,  $J$  = 7.8, 0.8 Hz, 2H), 7.37–7.27 (m, 10H), 7.20 (dd,  $J$  = 8.2, 1.1 Hz, 2H), 7.04 (td,  $J$  = 7.9, 1.1 Hz, 4H). **<sup>13</sup>C-NMR** (CDCl<sub>3</sub>, 75 MHz):  $\delta$  [ppm] = 165.1 (q), 155.2 (q), 151.5 (q), 139.5 (q), 136.7, 131.7, 128.8, 128.6, 128.2, 127.1 (q), 126.9, 123.1, 122.7, 117.2, 116.3, 57.9 (q). **MS** (+ESI):  $m/z$  (%) = 489.2 (100) [MH]<sup>+</sup>. **HR-MS** (+ESI):  $m/z$  (C<sub>35</sub>H<sub>24</sub>N<sub>2</sub>O) calculated: 489.1961 [MH]<sup>+</sup>, found: 489.1966.



### 6,6'-(9H-Xanthene-9,9-diyl)bis(2-phenylpyridine)platinum(II) 1'a

The synthesis was performed following the general complexation procedure described above. The title compound was obtained as a yellow solid in 22% yield.

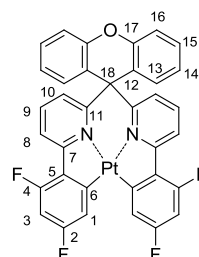
**<sup>1</sup>H-NMR** (TCE-d<sub>2</sub>, 400 MHz):  $\delta$  [ppm] = 8.21 (d,  $J$  = 7.4 Hz, 2H), 7.61–7.50 (m, 6H), 7.32 (td,  $J$  = 7.5, 1.2 Hz, 2H), 7.24–7.20 (m, 2H), 7.19–7.11 (m, 6H), 6.86–6.80 (m, 4H). **<sup>13</sup>C-NMR** (TCE-d<sub>2</sub>, 151 MHz):  $\delta$  [ppm] = 164.9 (q), 162.0 (q), 148.8 (q), 148.4 (q), 147.7 (q), 138.2, 136.6, 131.0, 130.2, 129.6, 127.5, 126.7 (q), 124.8, 124.3, 124.1, 117.7, 116.8, 62.3 (q). **HR-MS** (+APCI):  $m/z$  (C<sub>35</sub>H<sub>22</sub>N<sub>2</sub>OPt) calculated: 682.1456 [MH]<sup>+</sup>, found: 682.1502. **UV** (CH<sub>2</sub>Cl<sub>2</sub>):  $\lambda$  [nm] ( $\epsilon$ ) [Lmol<sup>-1</sup>cm<sup>-1</sup>] = 271 (29696), 297 (30999), 344 (12107), 405 (6600). **PL** (deg. CH<sub>2</sub>Cl<sub>2</sub>):  $\lambda_{em}$  [nm] = 512.



6,6'-(9H-Xanthene-9,9-diyl)bis(2-(2,4-difluorophenyl)pyridine) 5'b

The synthesis was performed using the general procedure for Suzuki-Miyaura couplings mentioned above. Column chromatography ( $\text{CH}_2\text{Cl}_2$  in hexanes 15% - 30%) gave the desired product as white solid in 80% yield.

**$^1\text{H-NMR}$**  ( $\text{CDCl}_3$ , 600 MHz):  $\delta$  [ppm] = 7.69–7.61 (m, 6H), 7.30 (ddd,  $J$  = 8.4, 7.2, 1.6 Hz, 2H), 7.22 (dd,  $J$  = 7.9, 1.5 Hz, 2H), 7.20 (dd,  $J$  = 8.2, 1.2 Hz, 2H), 7.07–7.02 (m, 4H), 6.85 (ddd,  $J$  = 11.4, 8.8, 2.5 Hz, 2H), 6.80 (td,  $J$  = 8.2, 2.3 Hz, 2H).  **$^{13}\text{C-NMR}$**  ( $\text{CDCl}_3$ , 75 MHz):  $\delta$  [ppm] = 165.0 (q), 163.7 (q, dd,  $J$  = 162.7, 12.0 Hz), 160.4 (q, dd,  $J$  = 164.5, 12.1 Hz), 151.6 (q), 150.4 (q, d,  $J$  = 2.7 Hz), 136.7, 132.5 (dd,  $J$  = 9.5, 4.6 Hz), 131.5, 128.4, 126.9 (q), 123.6 (q, dd,  $J$  = 11.2, 3.8 Hz), 123.3, 122.8, 121.4 (d,  $J$  = 11.7 Hz), 116.5, 111.8 (dd,  $J$  = 20.9, 3.5 Hz), 104.2 (dd,  $J$  = 27.2, 25.4 Hz), 57.9 (q). **MS** (+ESI):  $m/z$  (%) = 561.2 (100)  $[\text{MH}]^+$ . **HR-MS** (+ESI):  $m/z$  ( $\text{C}_{35}\text{H}_{20}\text{F}_4\text{N}_2\text{O}$ ) calculated: 562.1617  $[\text{MH}]^+$ , found: 562.1632.



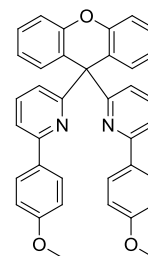
6,6'-(9H-Xanthene-9,9-diyl)

bis(2-(2,4-difluorophenyl)pyridine)platinum(II) 1'b

The synthesis was performed following the general complexation procedure described above. The title compound was obtained as a yellow greenish solid in 58% yield.

**$^1\text{H-NMR}$**  ( $\text{TCE-d}_2$ , 600 MHz):  $\delta$  [ppm] = 7.93 (d,  $J$  = 9.2 Hz, 2H, H-8), 7.60 (t,  $J$  = 8.1 Hz, 2H, H-9), 7.55 (dd,  $J$  = 9.1, 2.3 Hz, 2H, H-1), 7.24–7.17 (m, 4H, H-15/H-16), 7.14–7.10 (m, 2H, H-13), 6.90–6.82 (m, 4H, H-10/H-14), 6.65–6.58 (m, 2H, H-3).  **$^{13}\text{C-NMR}$**  ( $\text{TCE-d}_2$ , 151 MHz):  $\delta$  [ppm] = 164.5–162.8 (q, dd, C-2), 162.2 (q, C-11), 161.8–160.0 (q, dd, C-4), 161.3 (q, d, C-5), 153.7, (q, d, C-6), 148.4 (q, C-17), 139.0 (C-9), 130.8 (C-13), 130.7 (q, C-7), 129.9 (C-15), 127.4 (C-10), 126.2 (q, C-12), 124.9 (C-14), 120.8 (d, C-8), 118.2 (d, C-1), 118.0 (C-16), 100.3 (t, C-3), 62.8 (q, C-18). **HR-MS** (+APCI):  $m/z$  ( $\text{C}_{35}\text{H}_{18}\text{F}_4\text{N}_2\text{OPT}$ ) calculated: 754.1079  $[\text{MH}]^+$ ; found: 754.1128. **UV** ( $\text{CH}_2\text{Cl}_2$ ):  $\lambda$  [nm] ( $\epsilon$ ) [ $\text{Lmol}^{-1}\text{cm}^{-1}$ ] = 230 (49441), 265 (29214), 290 (33279), 324 (20839), 337 (17845), 390 (7190). **PL** (deg.  $\text{CH}_2\text{Cl}_2$ ):  $\lambda_{\text{em}}$  [nm] = 490.

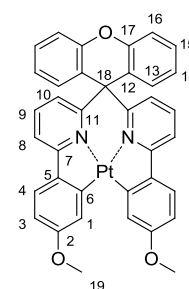
## CHAPTER 5



6,6'-(9H-Xanthene-9,9-diyl)bis(2-(4-methoxyphenyl)pyridine) 5'c

The synthesis was performed using the general procedure for Suzuki-Miyaura couplings mentioned above. Column chromatography (CH<sub>2</sub>Cl<sub>2</sub> in hexanes 50% - 70%) gave the desired product as white foam in 76% yield.

**<sup>1</sup>H-NMR** (CDCl<sub>3</sub>, 300 MHz): δ [ppm] = 7.79 (q, *J* = 5.0 Hz, 2H), 7.79 (d, *J* = 8.9 Hz, 2H), 7.58 (t, *J* = 7.7 Hz, 2H), 7.51 (dd, *J* = 7.8, 0.9 Hz, 2H), 7.32–7.24 (m, 4H), 7.18 (dd, *J* = 8.1, 1.2 Hz, 2H), 7.02 (td, *J* = 7.7, 1.4 Hz, 2H), 6.97 (dd, *J* = 7.6, 0.9 Hz, 2H), 6.86 (q, *J* = 5.0 Hz, 2H), 6.86 (d, *J* = 8.9 Hz, 2H), 3.80 (s, 6H). **<sup>13</sup>C-NMR** (CDCl<sub>3</sub>, 75 MHz): δ [ppm] = 164.94 (q), 160.3 (q), 154.9 (q), 151.6 (q), 136.6, 132.2 (q), 131.7, 128.2, 128.1, 127.3 (q), 122.7, 122.3, 116.4, 116.3, 114.0, 57.9 (q), 55.4. **MS** (+ESI): *m/z* (%) = 549.2 (100) [MH]<sup>+</sup>. **HR-MS** (+ESI): *m/z* (C<sub>37</sub>H<sub>28</sub>N<sub>2</sub>O<sub>3</sub>) calculated: 549.2173 [MH]<sup>+</sup>, found: 549.2178.



6,6'-(9H-Xanthene-9,9-diyl)

bis(2-(4-methoxyphenyl)pyridine)platinum(II) 1'c

The synthesis was performed following the general complexation procedure described above. Column chromatography (THF in hexane 30% - 100%) gave the title compound as yellow solid in 12% yield.

**<sup>1</sup>H-NMR** (TCE-d<sub>2</sub>, 400 MHz): δ [ppm] = 7.73 (d, *J* = 2.5 Hz, 2H, H-1), 7.54 (d, *J* = 8.7 Hz, 2H, H-4), 7.49 (t, *J* = 7.9 Hz, 2H, H-9), 7.46–7.41 (m, 2H, H-8), 7.23–7.17 (m, 6H, H-13/15/16), 6.87–6.81 (m, *J* = 8.2, 6.2, 2.2 Hz, 2H, H-14), 6.73 (dd, *J* = 7.9, 1.1 Hz, 2H, H-10), 6.70 (dd, *J* = 8.5, 2.4 Hz, 2H, H-3), 3.89 (s, 6H, H-19). **<sup>13</sup>C-NMR** (TCE-d<sub>2</sub>, 151 MHz): δ [ppm] = 164.7 (q, C-7), 162.0 (q, C-11), 160.8 (q, C-2), 151.5 (q, C-6), 148.4 (q, C-17), 140.5 (q, C-5), 138.2 (C-9), 131.1 (C-13), 129.5 (C-15), 126.8 (q, C-12), 126.4 (C-10), 126.0 (C-4), 124.7 (C-14), 120.5 (C-1), 117.7 (C-16), 116.1 (C-8), 110.8 (C-3), 62.1 (C-18), 55.7 (C-19). **HR-MS** (+APCI): *m/z* (C<sub>37</sub>H<sub>26</sub>N<sub>2</sub>O<sub>3</sub>Pt) calculated: 742.1667[MH]<sup>+</sup>; found: 742.1722. **UV** (CH<sub>2</sub>Cl<sub>2</sub>): λ [nm] (ε) [Lmol<sup>-1</sup>cm<sup>-1</sup>] = 278 (23460), 309 (31371), 339 (20234), 340 (4444), 438 (1807). **PL** (deg. CH<sub>2</sub>Cl<sub>2</sub>): λ<sub>em</sub> [nm] = 519.



## 6. REFERENCES

- [1] L. Chassot, A. Von Zelewsky, *Helv. Chim. Acta* **1983**, 66, 2443-2444.
- [2] M. Maestri, D. Sandrini, V. Balzani, L. Chassot, P. Jolliet, A. von Zelewsky, *Chem. Phys. Lett.* **1985**, 122, 375-379.
- [3] H. Yersin, A. F. Rausch, R. Czerwieniec, T. Hofbeck, T. Fischer, *Coord. Chem. Rev.* **2011**, 255, 2622-2652.
- [4] J. Brooks, Y. Babayan, S. Lamansky, P. I. Djurovich, I. Tsyba, R. Bau, M. E. Thompson, *Inorg. Chem.* **2002**, 41, 3055-3066.
- [5] T. K. Aldridge, E. M. Stacy, D. R. McMillin, *Inorg. Chem.* **1994**, 33, 722-727.
- [6] A. F. Rausch, L. Murphy, J. A. G. Williams, H. Yersin, *Inorg. Chem.* **2011**, 51, 312-319.
- [7] J. A. Gareth Williams, S. Develay, D. L. Rochester, L. Murphy, *Coord. Chem. Rev.* **2008**, 252, 2596-2611.
- [8] J. A. G. Williams, *Chem. Soc. Rev.* **2009**, 38, 1783-1801.
- [9] D. A. K. Vezzu, J. C. Deaton, J. S. Jones, L. Bartolotti, C. F. Harris, A. P. Marchetti, M. Kondakova, R. D. Pike, S. Huo, *Inorg. Chem.* **2010**, 49, 5107-5119.
- [10] H. Fukagawa, T. Shimizu, H. Hanashima, Y. Osada, M. Suzuki, H. Fujikake, *Adv. Mater.* **2012**, 24, 5099-5103.
- [11] K. Feng, C. Zuniga, Y.-D. Zhang, D. Kim, S. Barlow, S. R. Marder, J. L. Brédas, M. Weck, *Macromolecules* **2009**, 42, 6855-6864.
- [12] L. F. Tietze, F. Lotz, *Eur. J. Org. Chem.* **2006**, 2006, 4676-4684.
- [13] C. Uhrich, R. Schueppel, A. Petrich, M. Pfeiffer, K. Leo, E. Brier, P. Kilickiran, P. Baeuerle, *Adv. Funct. Mater.* **2007**, 17, 2991-2999.
- [14] Agilent Technologies **2006-2012**, CrysAlisPro Software system, different versions, Agilent Technologies UK Ltd, Oxford, UK.
- [15] L. Palatinus, G. Chapuis, *J. Appl. Crystallogr.* **2007**, 40, 786-790.
- [16] G. M. Sheldrick, *Acta Cryst.* **2008**, A64, 112-122.



# SUMMARY



This thesis reports the synthesis and characterization of phosphorescent emitters for the application in organic light-emitting diodes. Thereby, the focus lies on their chemical degradation behavior in order to gain a deeper knowledge of the prevalent mechanisms, responsible for materials- and therefore device-deterioration.

**Chapter 1** summarizes recent advances, but also the occurring problems in the elucidation of manifold chemical degradation pathways proceeding in a working OLED device. Starting with a short overview of the chemical mechanisms themselves and the analytical techniques used for their investigation, the gained insights are discussed for all groups of functional materials present in a device. Commonalities in their degradation behavior are highlighted. The observed products, in combination with the results of quantum chemical calculations, shed light on the type of bonds, structural features or electronic states that are unfavorable. Implications on the structural improvement of the materials are drawn and backed by literature examples.

**Chapter 2** reports the fast derivatization of the prominent emitting lead structure *tris*(2-phenylpyridine)iridium(III)  $\text{Ir}(\text{ppy})_3$  via a combinatorial approach. Post-modification of a bromo-functionalized precursor is achieved by palladium catalyzed C-C and C-N coupling reactions. Through the establishment of a chromatography based screening-setup, complex libraries of up to ten structurally diverse derivatives can be separated and the individual complexes identified, photophysically characterized and evaluated in terms of their photostability. Interesting effects of the substitution pattern on the emission properties could be observed, like the dual emission of some heteroleptic complexes. A comparison of the obtained quantum yields with those of literature known complexes revealed that the introduction of flexibility into the system must not necessarily cause a decrease in the luminescence efficiencies. The finding implies that dendritic ligand structures, which are known for their improved solubility, preserve good quantum efficiencies if the rigidity of the emitting core is retained. Photodegradation studies on the complexes showed interesting general tendencies of the degradation behavior under the influence of oxygen, and a deterioration of these complexes via their excited state can be deduced.

Adhering to palladium catalyzed cross coupling reactions, we tried to broaden the pool of combinatorial derivatization protocols by developing a suitable C-O coupling procedure.

**Chapter 3** reports the tested synthetic pathways. Performing Buchwald-Hartwig couplings, the most dominant side reaction is the hydrodehalogenation of the brominated precursor, due to the assumed very slow reductive elimination step in the catalytic cycle. Nevertheless a catalytic system could be identified, yielding moderate conversion, which acts as starting point for the further optimization of reaction conditions. With the intention to perform C-O bond formations according to a Chan-Lam protocol, *tris*(5'-pinacolatoboron-2-phenylpyridine)-iridium(III) was successfully synthesized. Although no conversion of this complex with aryl alcohols could be achieved yet, this derivative shows potential for the application in Suzuki-Miyaura reactions with arylhalogenides. Compared to the protocol

## SUMMARY

presented in Chapter 2 this "inverse" strategy, allows for a greater variation of substituents as arylhalogenides are synthetically easier accessible and cheaper than boronic acids.

Back to our efforts to gain a deeper understanding on the degradation behavior of phosphorescent emitters, **Chapter 4** provides the results of irradiation experiments on four well-known iridium complexes. The influence of different solvents as well as oxygen on the complex stability was studied by determining the degradation rates and identifying deterioration products of each compound. The detrimental effect of halogenated solvents on the complex lifetimes could be observed and degradation pathways, induced by singlet oxygen reactions or excited state mechanisms, were identified. In this chapter it is shown, that the degradation of these materials proceeds in a very complex way as several mechanism can interlock.

In **Chapter 5**, finally the focus was changed towards platinum complexes as emitters in OLED applications. New tetradentate, phenylpyridine based ligand systems were successfully synthesized. The respective complexes show emission in the green to turquoise region, depending on the electronic character of the substituents. The detrimental character of fluorine substituents could be observed in the significantly decreased quantum efficiencies as well as lower photostabilities in solid films. Nonetheless, this new class of tetradentate platinum complexes exhibits photostabilities comparable to the prominent stable, green emitting Ir(ppy)<sub>3</sub>. A device performance equal to that of Ir(ppy)<sub>3</sub> render the fluorene bridged complex 6,6'-(9H-fluorene-9,9-diyl)bis(2-phenylpyridine)-platinum(II) a promising representative of phosphorescent platinum(II) emitters for OLED-applications.

# **ZUSAMMENFASSUNG**





Im Rahmen dieser Arbeit wird die Synthese und Charakterisierung phosphoreszenter Emitter für die Anwendung in organischen Leuchtdioden (OLEDs) beschrieben. Der Schwerpunkt wird dabei auf das chemische Degradationsverhalten dieser Substanzen gelegt. Dadurch soll ein tieferes Verständnis für die vorherrschenden Mechanismen erlangt werden, die zu einer Materialveränderung und somit zu einer Verschlechterung der Bauteilleistung führen.

In **Kapitel 1** werden aktuelle Fortschritte in der Aufklärung verschiedener chemischer Degradationswege zusammengefasst, und dabei auftretende Schwierigkeiten erläutert. Zuerst wird ein kurzer Überblick über die Mechanismen an sich gegeben, und analytische Verfahren zu deren Erforschung werden präsentiert. Anschließend werden die gewonnenen Einblicke in das Degradationsverhalten der verschiedenen funktionellen Materialien einer Leuchtdiode diskutiert und Gemeinsamkeiten herausgearbeitet. Die Identifizierung von Degradationsprodukten liefert in Kombination mit theoretischen Rechnungen Hinweise auf sich nachteilig auswirkende Strukturelemente und instabile elektronische Zustände. Daraus resultierende strukturelle Verbesserungsvorschläge werden aufgezeigt und durch literaturbekannte Beispiele belegt.

**Kapitel 2** beschreibt die schnelle Derivatisierung der bekannten phosphoreszenten Leitstruktur *Tris*(2-phenylpyridin)iridium(III) Ir(ppy)<sub>3</sub> mittels kombinatorischer Ansätze. Die strukturelle Modifikation wird durch palladiumkatalysierte C-C- und C-N- Kupplungsreaktionen an einer bromierten Vorstufe erzielt. Der Aufbau eines chromatographiebasierten Screening Systems ermöglicht eine schnelle Auftrennung von Komplex-Bibliotheken mit bis zu zehn strukturell verschiedenen Derivaten, gefolgt von der Identifizierung und photophysikalischen Charakterisierung der Einzelverbindungen. Abschließend werden diese bezüglich ihrer Photostabilität bewertet. Interessante Auswirkungen des Substitutionsmusters auf die Emissionseigenschaften wurden beobachtet, wie zum Beispiel die duale Emission einiger heteroleptischer Komplexe. Ein Vergleich der gemessenen Quantenausbeuten mit denen literaturbekannter Verbindungen zeigt, dass das Einbringen erhöhter Flexibilität in das System nicht zwingend eine Verschlechterung der Leuchteffizienz zur Folge hat. Demzufolge können durch dendritische Liganden, welche sich durch eine erhöhte Löslichkeit auszeichnen, gute Quantenausbeuten erzielt werden, sofern die Starrheit der emittierenden Kernstruktur gewährleistet ist. Untersuchungen über den lichtinduzierten Abbau der Komplexe zeigen interessante Tendenzen des Degradationsverhaltens unter Einfluss von Sauerstoff auf. Demzufolge kann auf eine Zerstörung dieser Komplexe überwiegend durch ihren angeregten Zustand rückgeschlossen werden.

Festhaltend an dem Prinzip der palladiumkatalysierten Kreuzkupplungsreaktionen war es unser Ziel, die Auswahl an relevanten Syntheseprotokollen für die kombinatorische Derivatisierung der Komplexe zu vergrößern. **Kapitel 3** fasst die getesteten Syntheserouten für C-O-Bindungsknüpfungen zusammen. Reaktionen nach dem Buchwald-Hartwig Protokoll ergaben eine Hydrodehalogenierung der bromierten Emitter-Vorstufe als

## ZUSAMMENFASSUNG

dominante Nebenreaktion. Dies kann auf die langsame reduktive Eliminierung innerhalb des Katalysezyklus zurückgeführt werden. Trotzdem konnte ein katalytisches System gefunden werden, mit dem annehmbare Umsätze erzielt wurden. Dieses soll nun als Ausgangspunkt für weitere Optimierungsschritte genutzt werden. Im Hinblick auf das Knüpfen von C-O Bindungen mittels eines Chan-Lam Protokolls wurde *Tris*(5'-Pinacolato-boron-2-phenylpyridin)iridium(III) erfolgreich dargestellt. Obwohl dieses Ausgangsprodukt nicht mit aromatischen Alkoholen verknüpft werden konnte, zeigte es großes Potential für die Anwendung in Suzuki-Miyaura Reaktionen mit Arylhalogeniden. Verglichen mit dem in Kapitel 2 beschriebenen Syntheseprotokoll ermöglicht dieser „inverse“ Ansatz zukünftig eine größere Variabilität der Substituenten, da aromatische Halogenide synthetisch leichter zugänglich und billiger erhältlich sind als entsprechende Boronsäuren.

Zurückkommend auf unsere Bemühungen, ein tieferes Verständnis für das Degradationsverhalten phosphoreszenter Emitter zu erlangen, wurden Belichtungs-experimente mit vier etablierten Iridium-Komplexen durchgeführt. Die Ergebnisse sind in **Kapitel 4** zusammengefasst. Die Einflüsse verschiedener Lösemittel sowie von Sauerstoff auf die Komplexstabilität wurden durch die Bestimmung der Abbaugeschwindigkeit und etwaiger Degradationsprodukte unter variierenden Bedingungen untersucht. Der nachteilige Effekt von halogenierten Lösemitteln auf die Lebensdauern konnte aufgezeigt werden. Des Weiteren wurden Degradationswege identifiziert, die durch Singulett-Sauerstoff oder durch die angeregten Zustände der Komplexe induziert werden. Dieses Kapitel vermittelt zudem, dass die Degradation dieser Materialien durch ineinander greifende und konkurrierende Mechanismen einen sehr komplexen Vorgang darstellt.

Zuletzt ändert sich der Fokus der Arbeit in **Kapitel 5** hin zu Platin-Komplexen für die Anwendung in OLEDs. Neue vierzählige Ligandsysteme auf der Basis von Phenylpyridinen wurden erfolgreich synthetisiert. Die entsprechenden Komplexe emittieren im grünen bis in den türkisen Spektralbereich, abhängig vom elektronischen Charakter der Substituenten. Der nachteilige Einfluss von Fluor-Gruppen wird ersichtlich durch den starken Abfall der Quantenausbeuten und der verminderten Photostabilität in Polymerfilmen. Nichtsdestotrotz ist diese Klasse von Komplexen ähnlich stabil wie der robuste, grün emittierende Standardkomplex  $\text{Ir}(\text{ppy})_3$ . Zu diesem Referenzkomplex vergleichbare Leistungsdaten machen 6,6'-(9H-Fluoren-9,9-diyl)bis(2-phenylpyridine)platin(II) zu einem vielversprechenden Repräsentanten phosphoreszenter Platin(II)-Komplexe für die Anwendung in organischen Leuchtdioden.

# **APPENDIX**

## **SUPPORTING INFORMATION OF CHAPTER 2-5**

### **ABBREVIATIONS**

### **CURRICULUM VITAE**

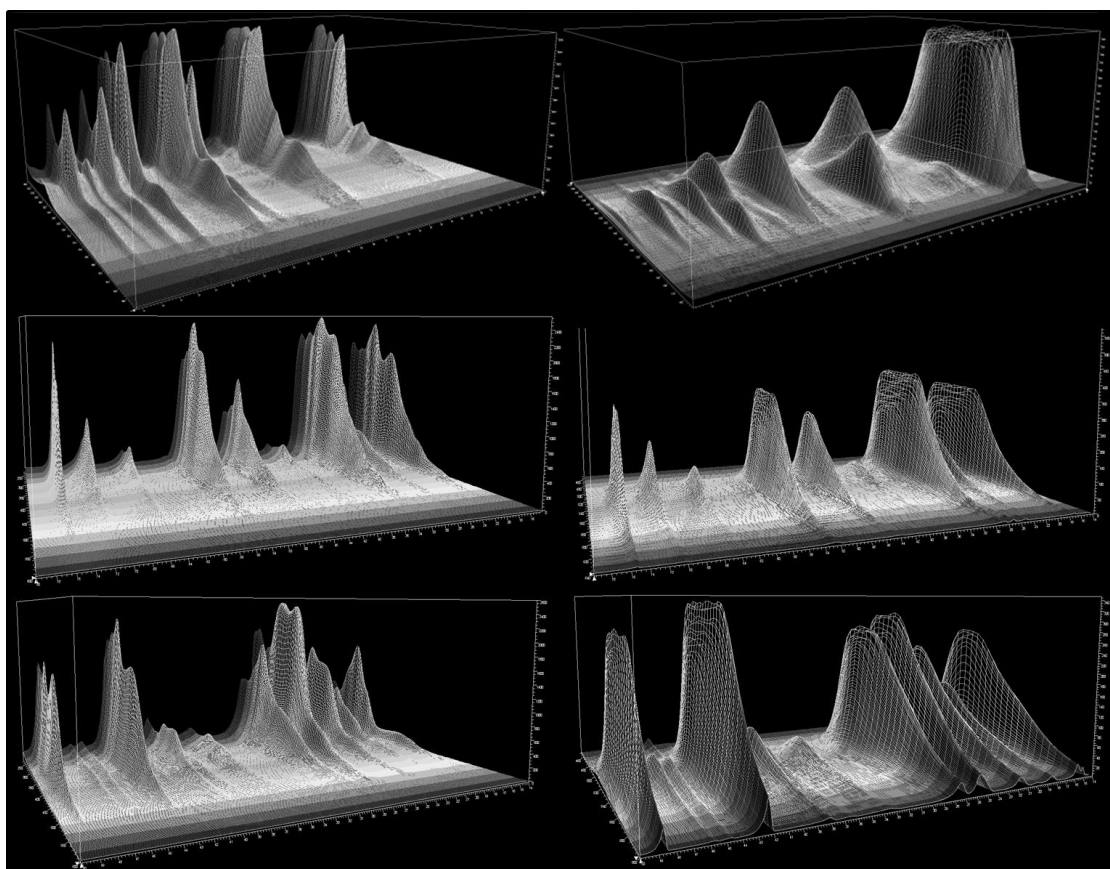
### **LIST OF PRESENTATIONS AND PUBLICATIONS**

## APPENDIX

### 1. SUPPORTING INFORMATION OF CHAPTER 2

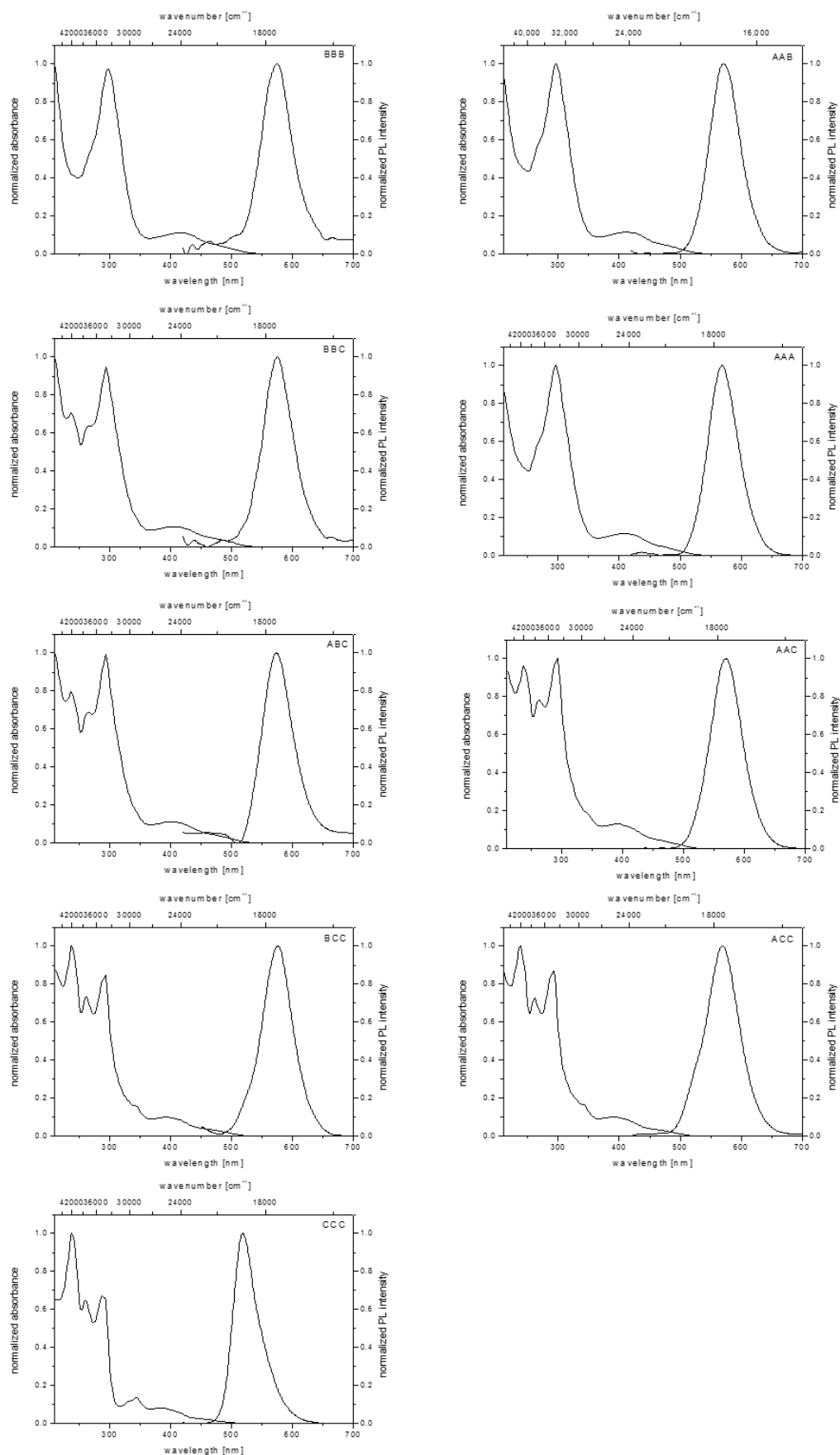
#### 1.1 3D-Absorption- and Emission-Plots of Library 1, 3 and 4

Library 1 (top), library 3 (middle) and library 4 (bottom). Left: absorbance; right: emission. X-axis: retention time [min]; y-axis: wavelength [nm]; z-axis: absorption intensity [mAU] / emission intensity [LU].



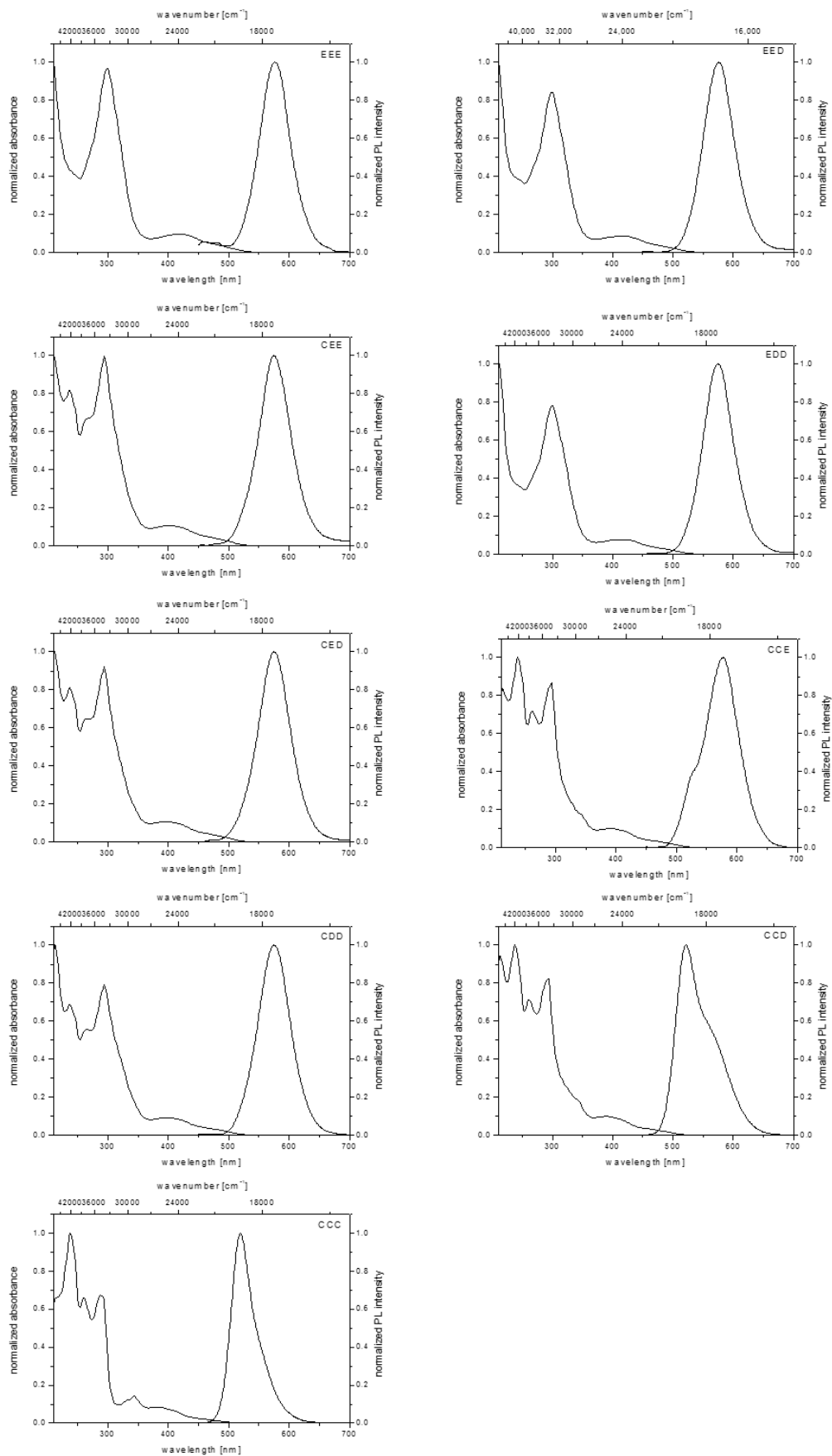
## 1.2 Absorption and Emission Spectra

## NORMALIZED ABSORPTION AND EMISSION SPECTRA OF COMPLEX LIBRARY I

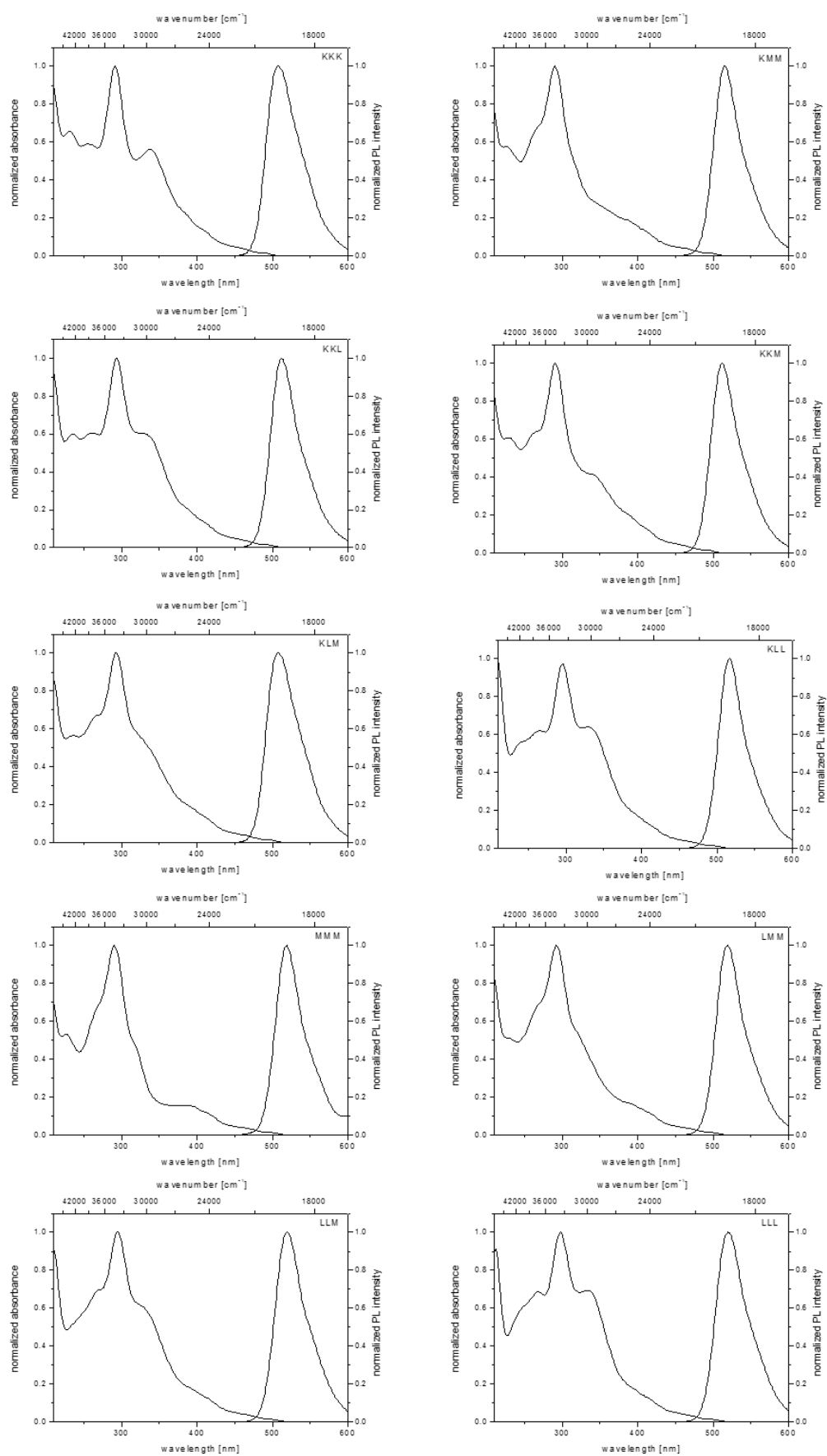


# APPENDIX

## NORMALIZED ABSORPTION AND EMISSION SPECTRA OF COMPLEX LIBRARY 2

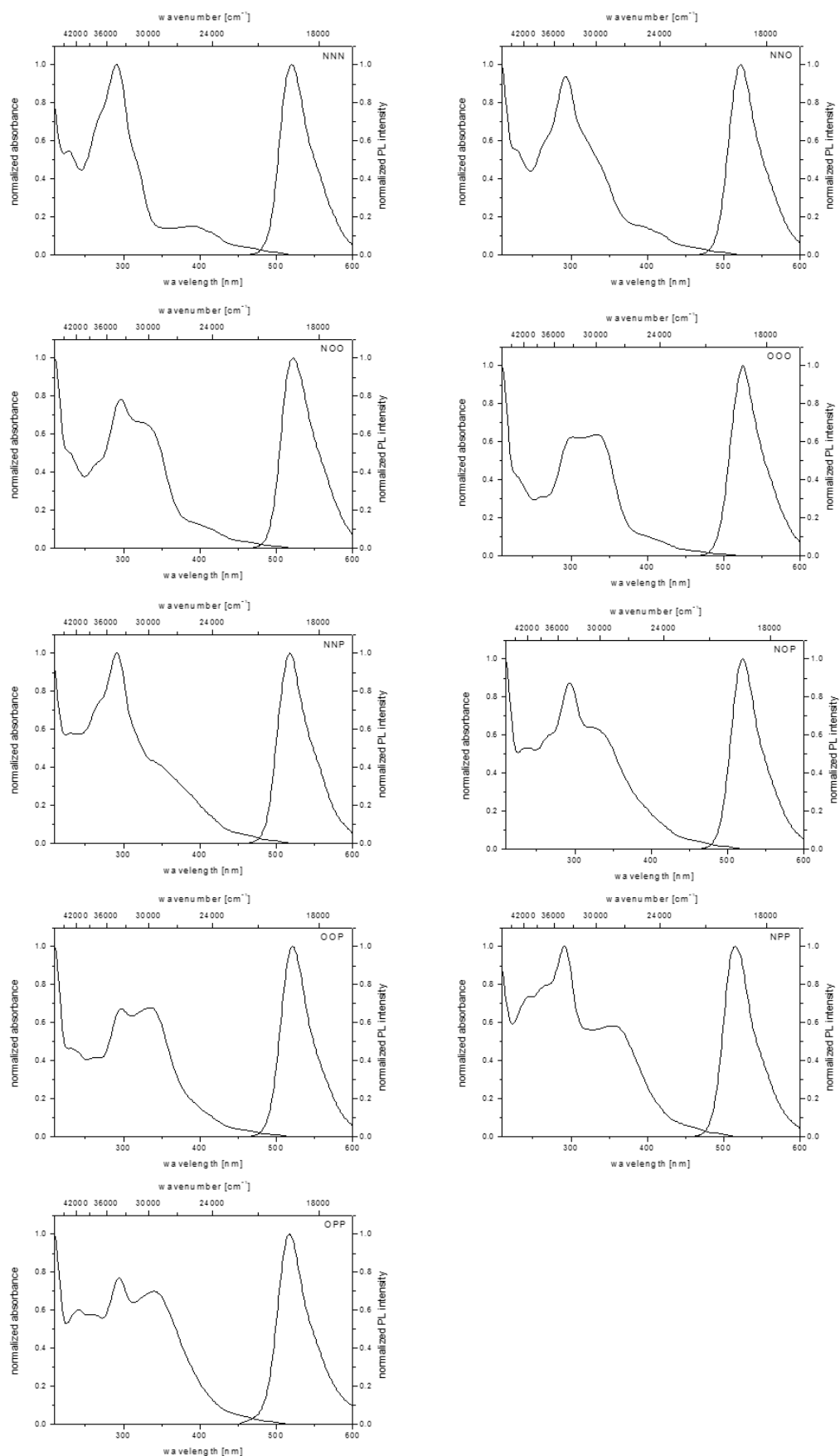


## NORMALIZED ABSORPTION AND EMISSION SPECTRA OF COMPLEX LIBRARY 3



# APPENDIX

## NORMALIZED ABSORPTION AND EMISSION SPECTRA OF COMPLEX LIBRARY 4

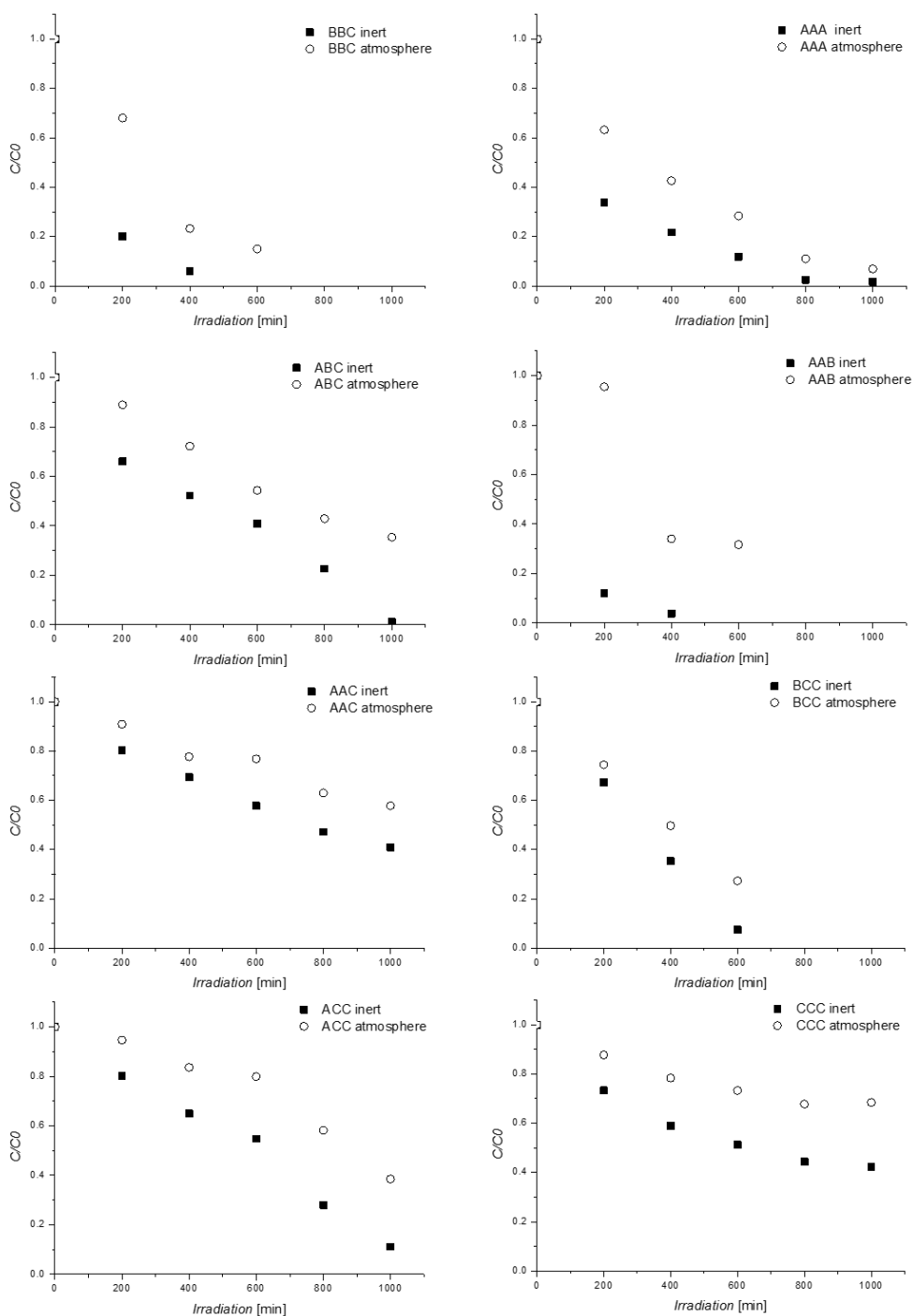




### 1.3 Photodegradation Plots

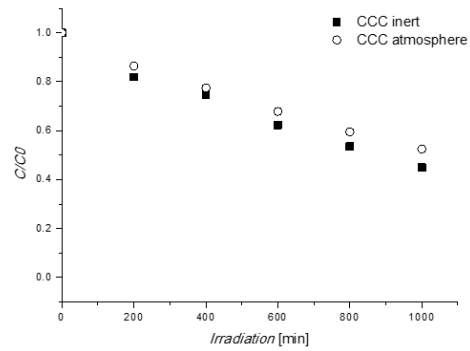
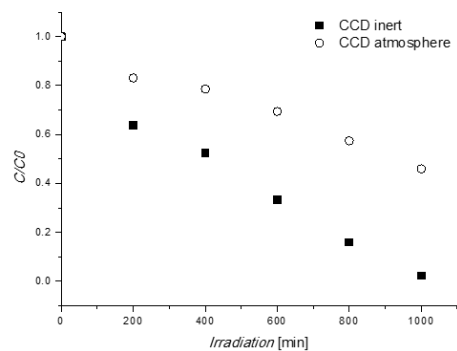
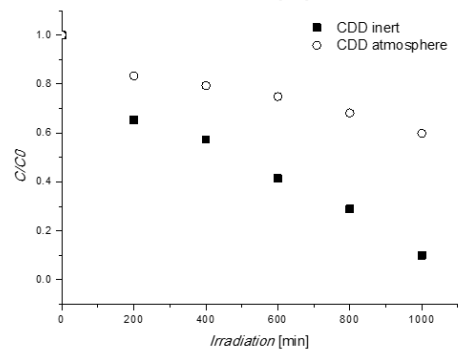
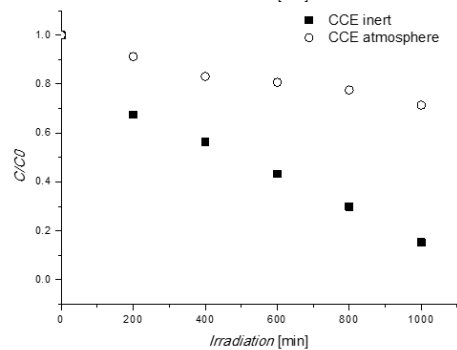
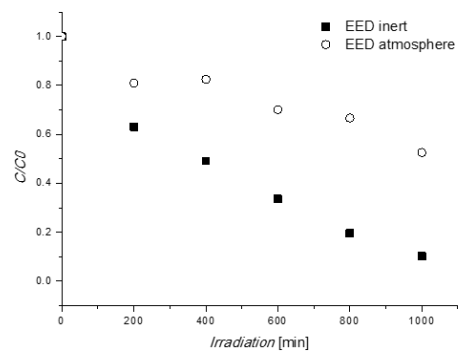
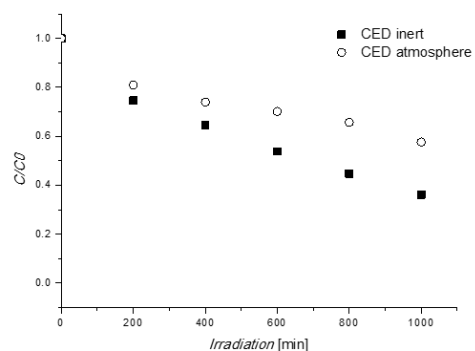
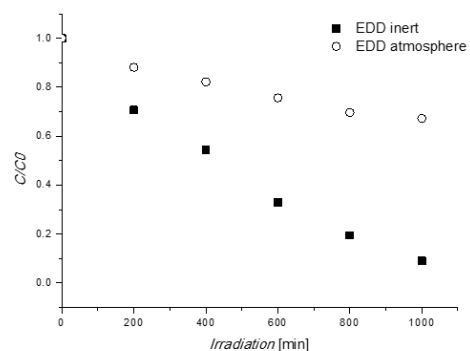
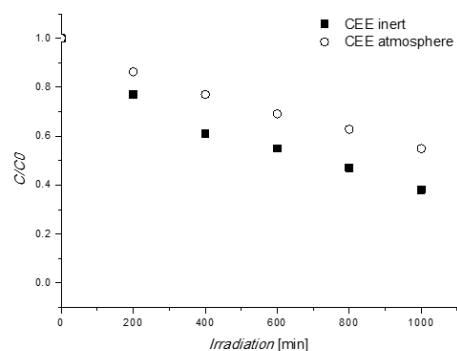
X-axis: irradiation time with 400 nm LEDs [min]; y-axis: ratio  $C/C^0$ , whereas  $C^0$  is the initial emitter-concentration and  $C$  is the emitter concentration after irradiation; estimated through the integrated DAD signals of the HPLC-setup.

#### PHOTODEGRADATION PLOTS OF COMPLEX LIBRARY 1

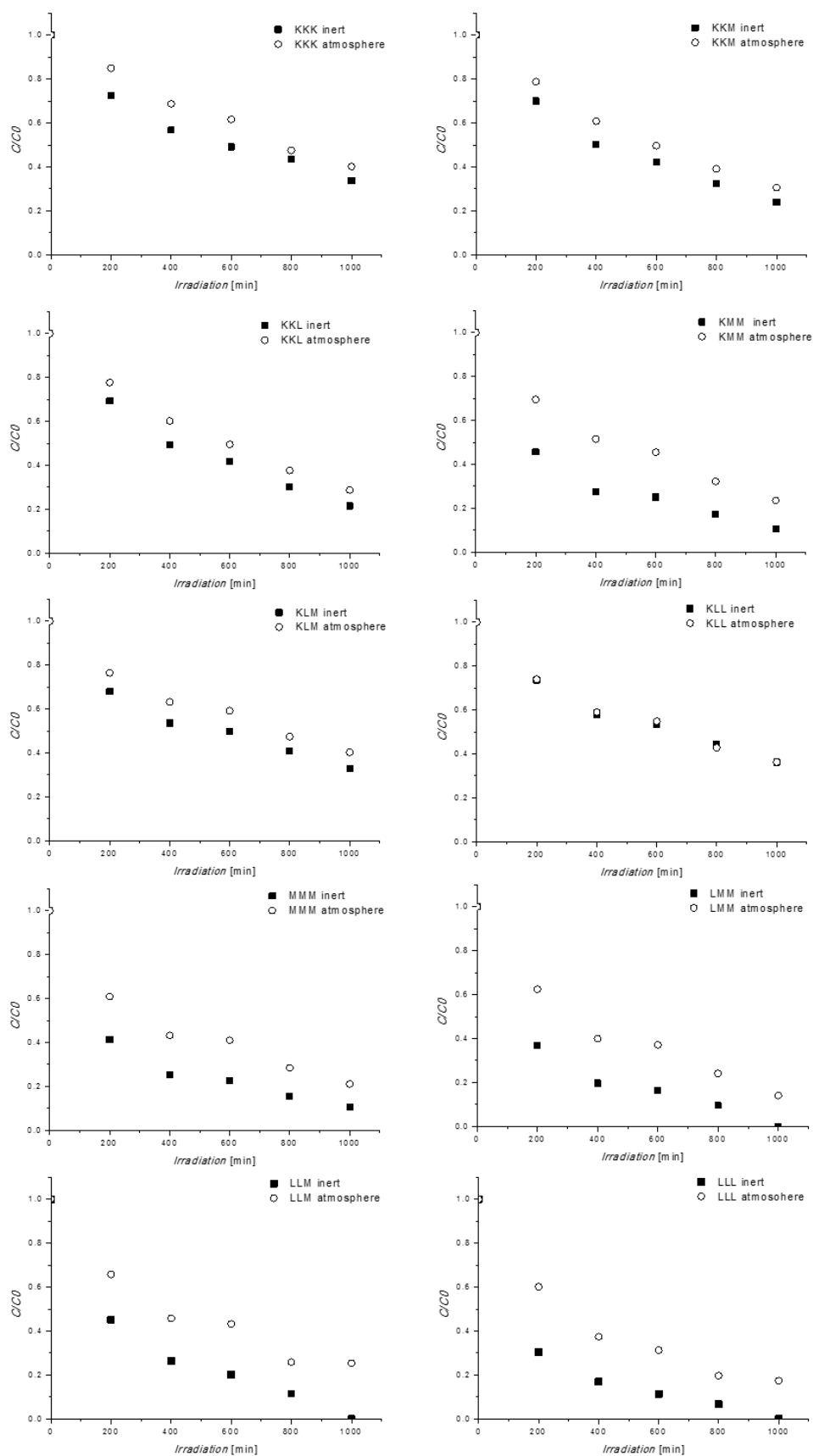


# APPENDIX

## PHOTODEGRADATION PLOTS OF COMPLEX LIBRARY 2

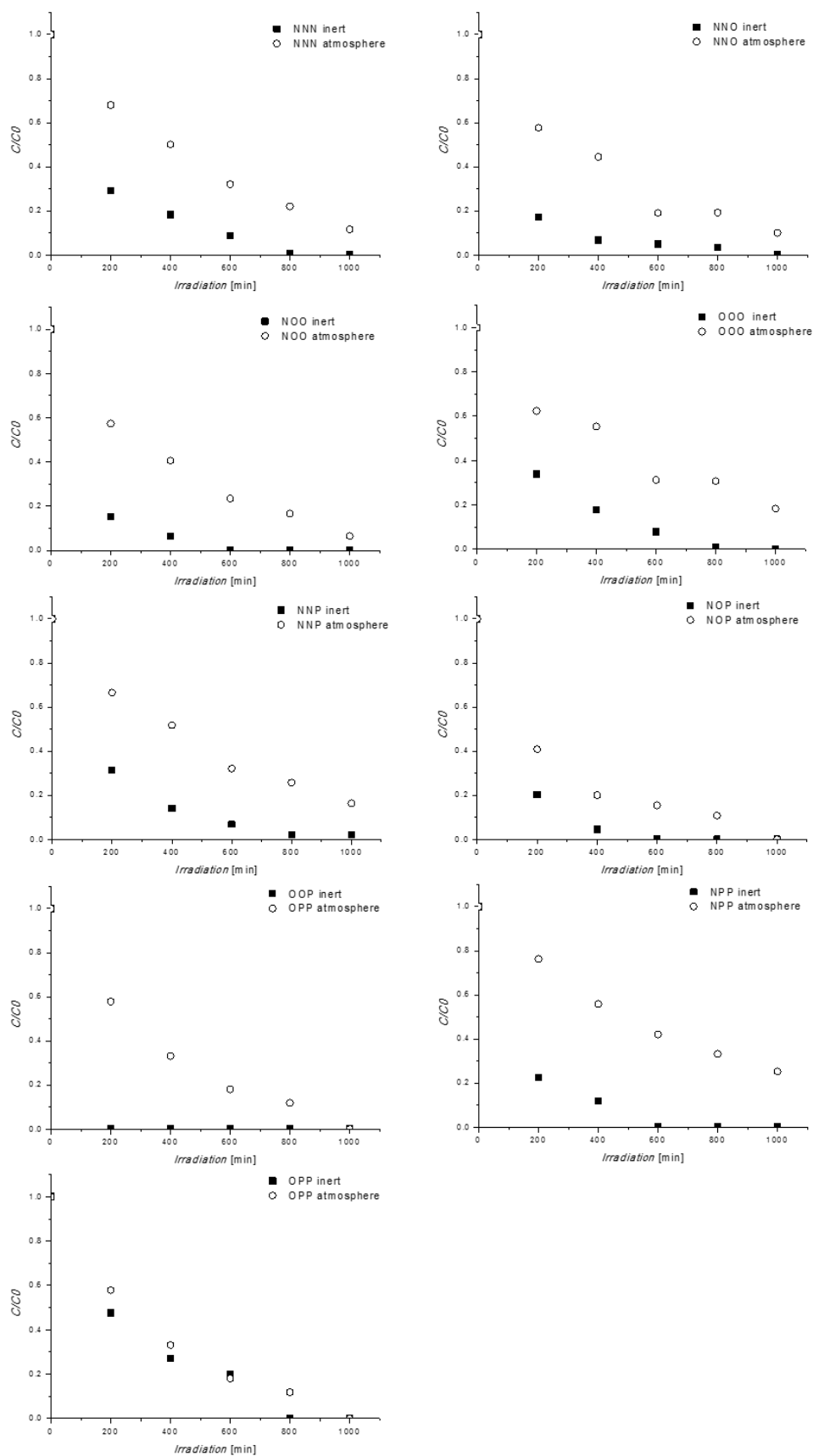


## PHOTODEGRADATION PLOTS OF COMPLEX LIBRARY 3

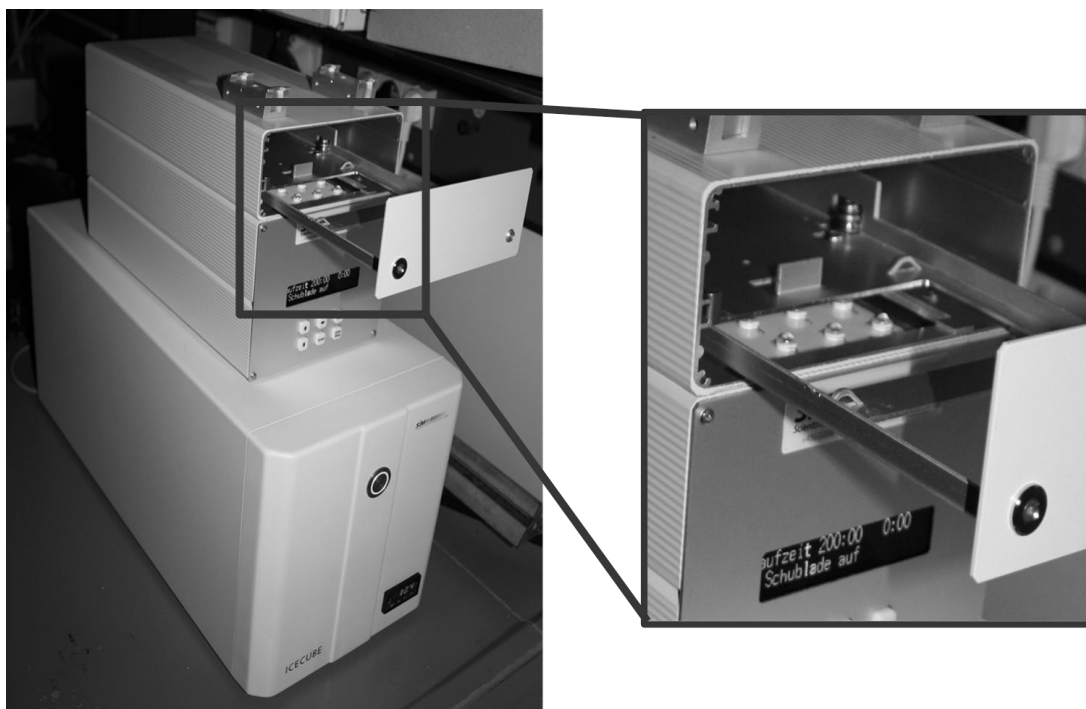


# APPENDIX

## PHOTODEGRADATION PLOTS OF COMPLEX LIBRARY 4



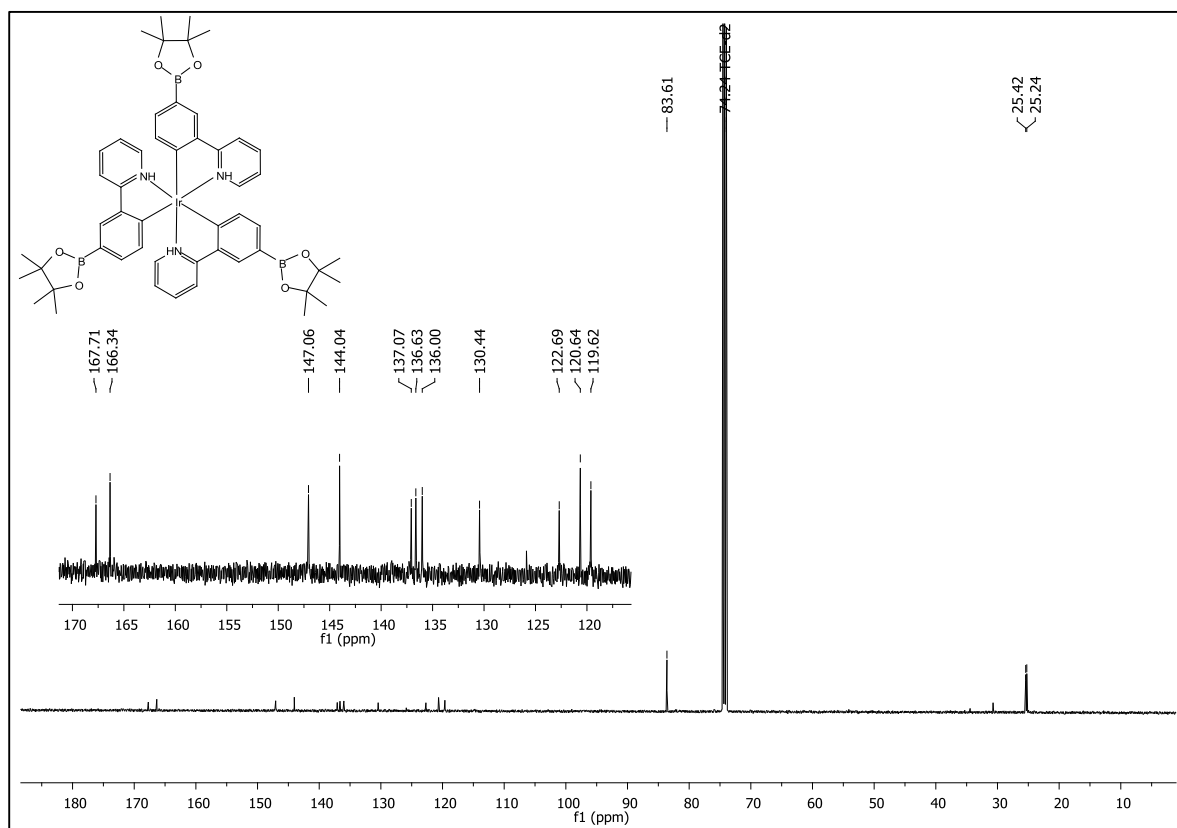
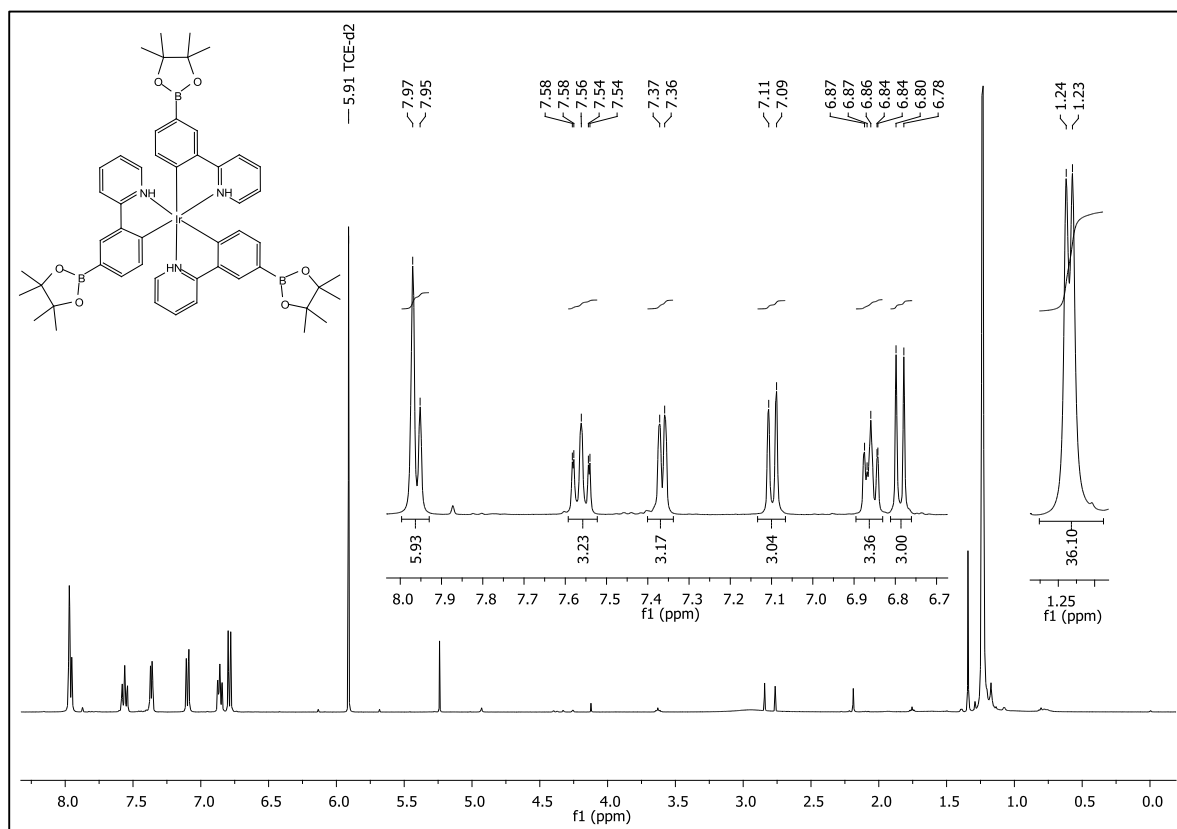
#### 1.4 Picture of the Irradiation Unit



## APPENDIX

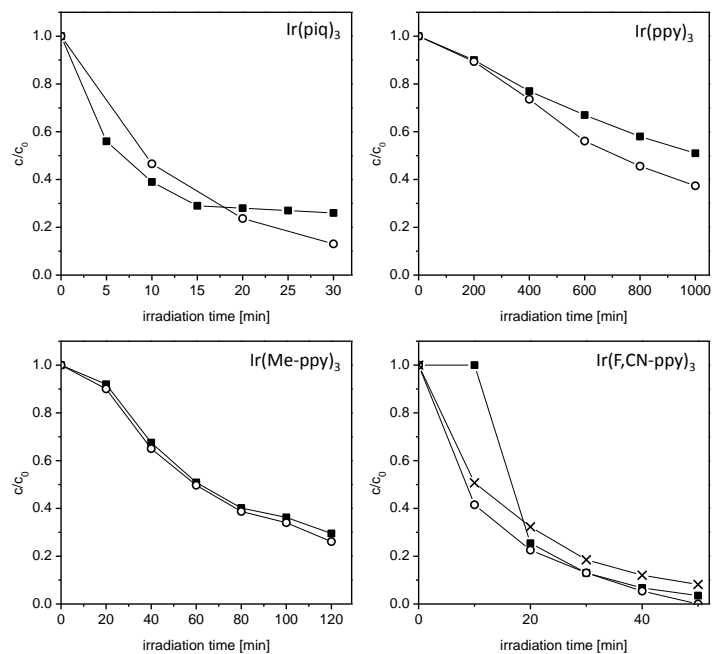
### 2. SUPPORTING INFORMATION OF CHAPTER 3

$^1\text{H}$  spectrum and  $^{13}\text{C}$  spectra of *tris*(5'-pinacolatoboron-2-phenylpyridine)iridium(III) **3** in TCD- $\text{d}_2$ .

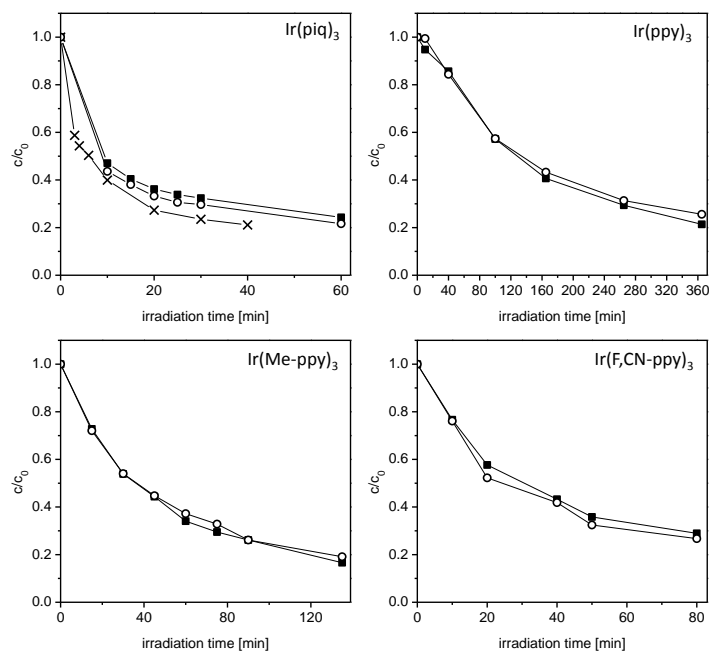


### 3. SUPPORTING INFORMATION OF CHAPTER 4

#### 3.1 Reproducibility of the degradation studies in toluene under ambient conditions

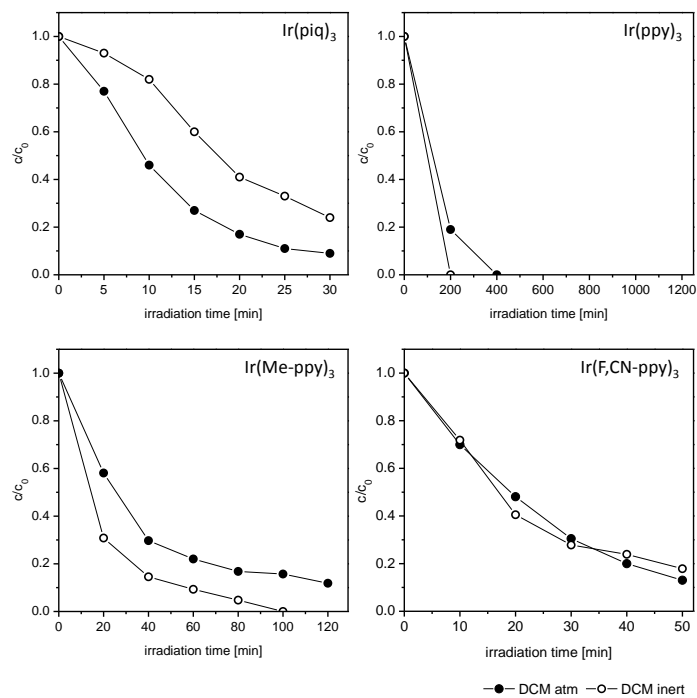


#### 3.2 Reproducibility of the degradation studies in a PMMA matrix under ambient conditions

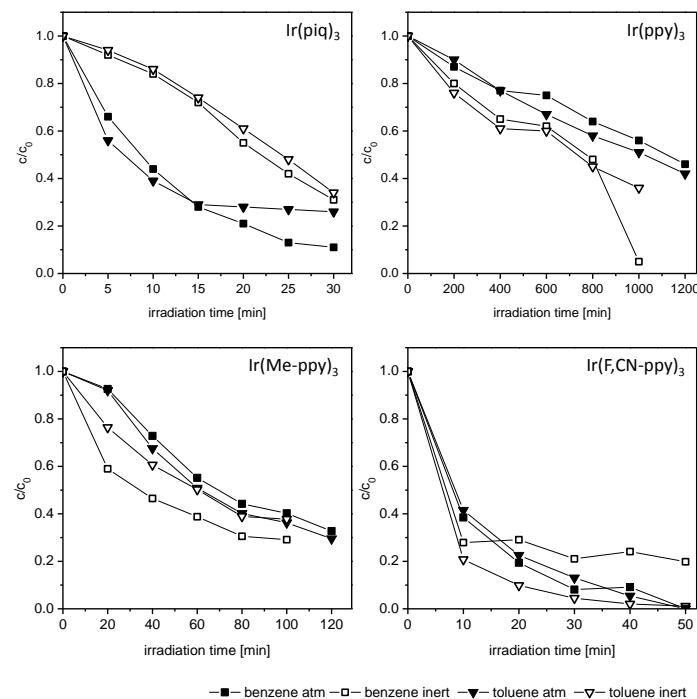


## APPENDIX

### 3.3 Degradation curves of $\text{Ir}(\text{piq})_3$ , $\text{Ir}(\text{ppy})_3$ , $\text{Ir}(\text{Me-ppy})_3$ and $\text{Ir}(\text{F,CN-ppy})_3$ in $\text{CH}_2\text{Cl}_2$ under ambient and inert conditions



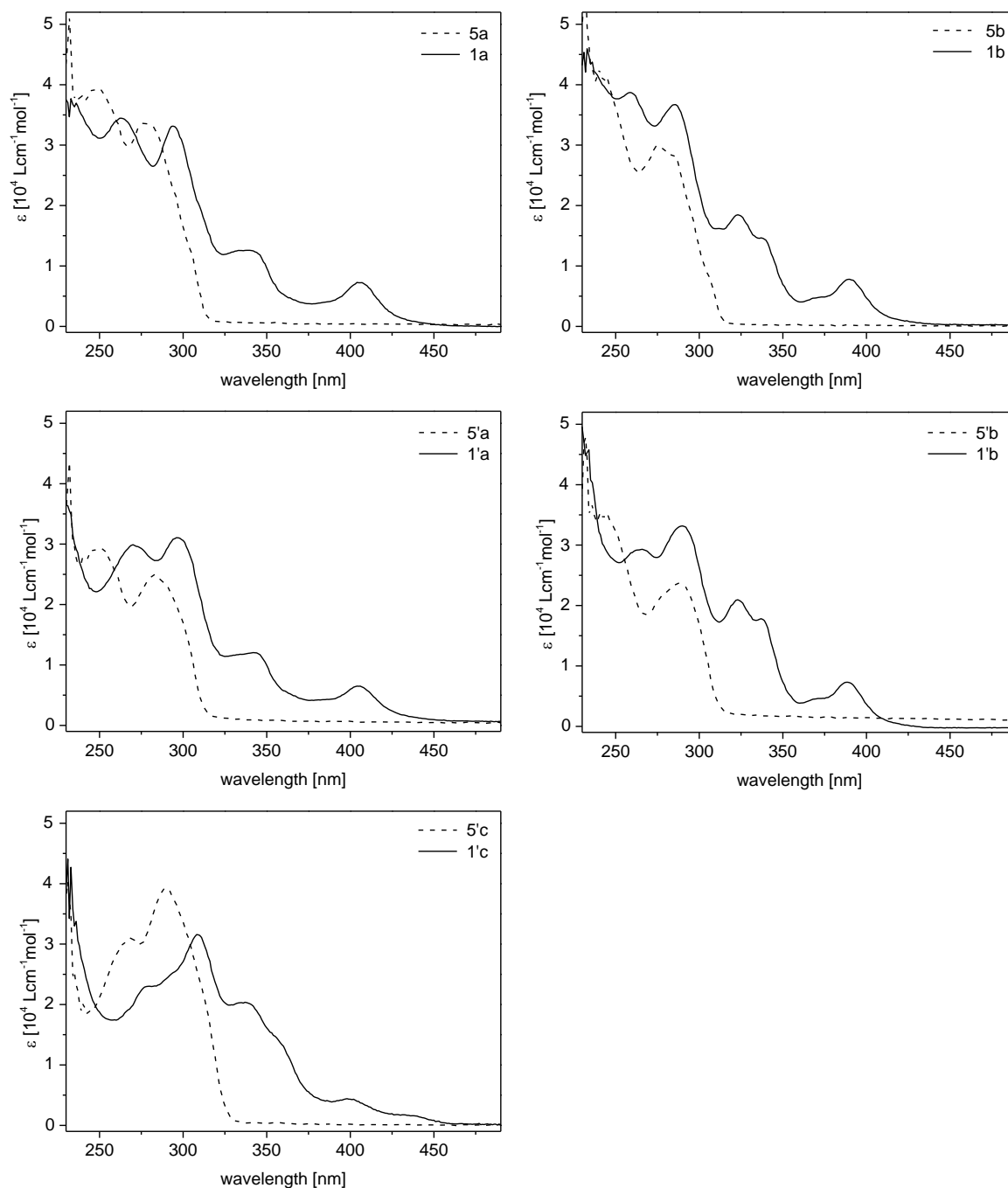
### 3.4 Degradation curves of $\text{Ir}(\text{piq})_3$ , $\text{Ir}(\text{ppy})_3$ , $\text{Ir}(\text{Me-ppy})_3$ and $\text{Ir}(\text{F,CN-ppy})_3$ in benzene and toluene under ambient and inert conditions





## 4. SUPPORTING INFORMATION OF CHAPTER 5

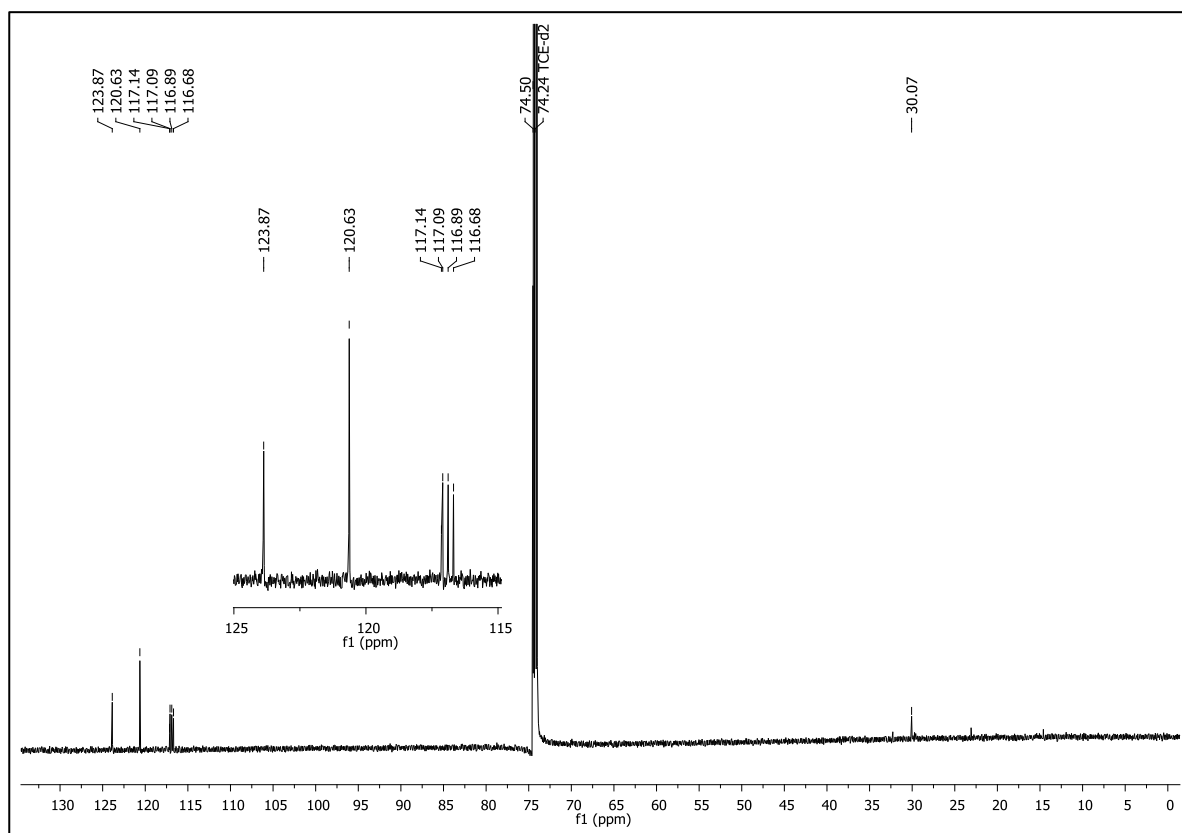
## 4.1 Absorption Spectra of the Ligands 5a,b and 5'a-c in Comparison with the Corresponding Complex Spectra 1a,b and 1'a-c



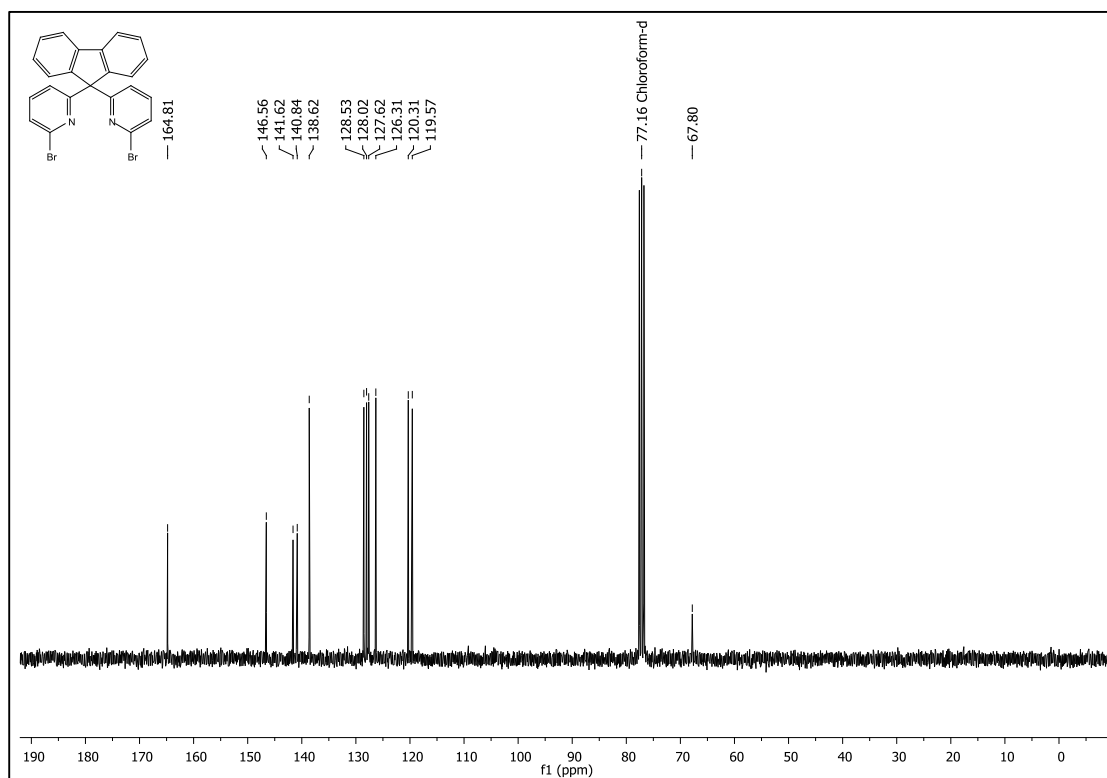
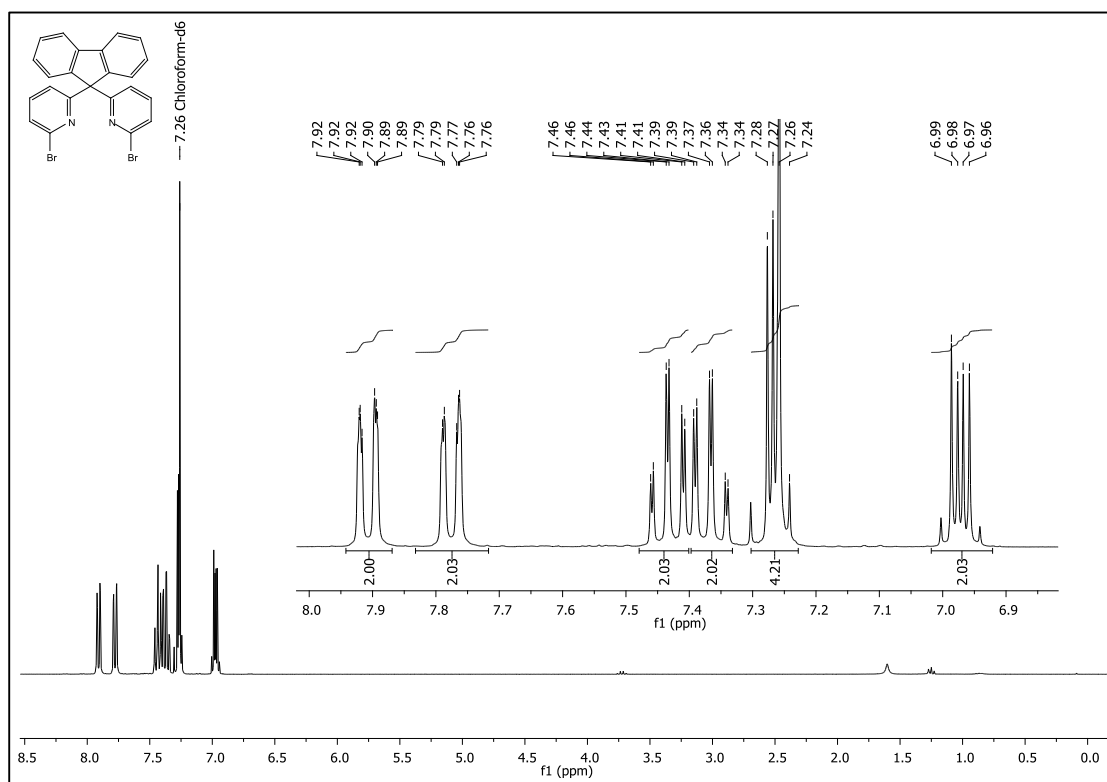
## APPENDIX

### 4.2 $^1\text{H}$ - and $^{13}\text{C}$ -NMR Spectra

For each compound occurring here, the  $^1\text{H}$  spectrum is depicted followed by the appropriate  $^{13}\text{C}$  spectrum. The solvent peaks are standardized and labeled. The spectra of the purely organic molecules were measured in  $\text{CDCl}_3$ . All complex-spectra were recorded in  $\text{TCE-d}_2$  under the addition of hydrazine hydrate, which suppresses oxidation processes of the complexes. Due to side reactions of  $\text{TCE-d}_2$ , induced through hydrazine hydrate (elimination reactions could be assumed) some additional peaks can be found in the  $^{13}\text{C}$ -spectra, which are crossed out. The spectrum below shows a blank sample only containing hydrazine hydrate in  $\text{TCE-d}_2$ , showing these deterioration products.

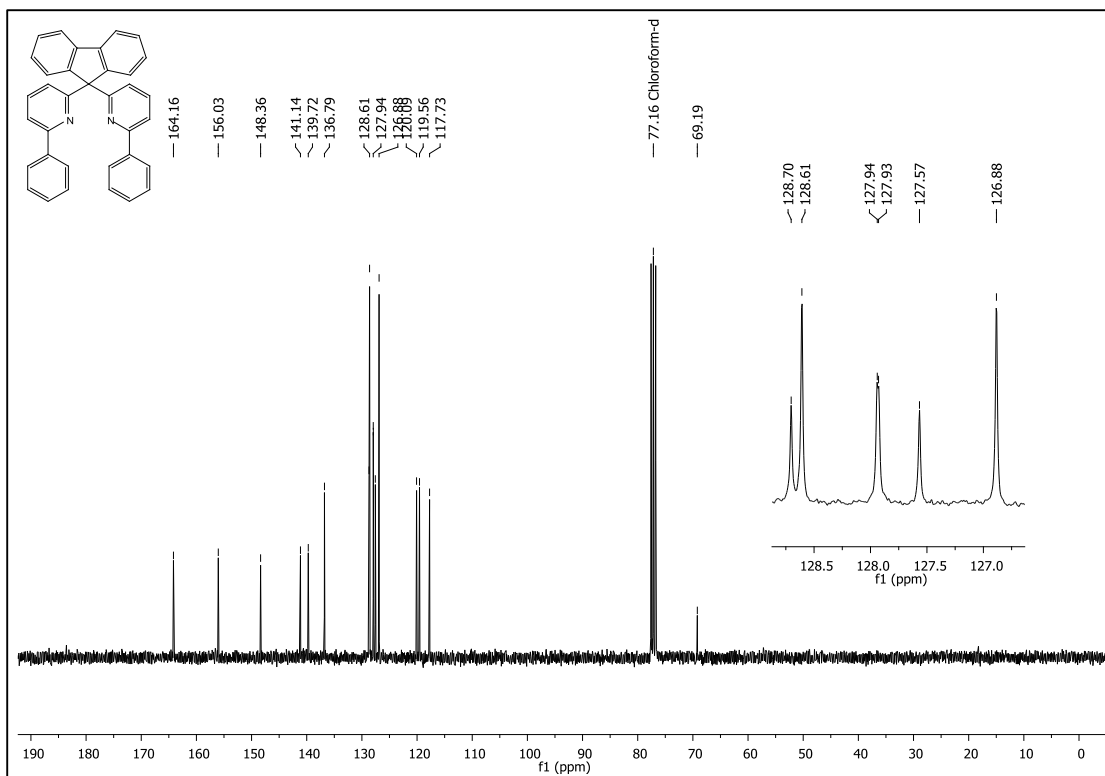
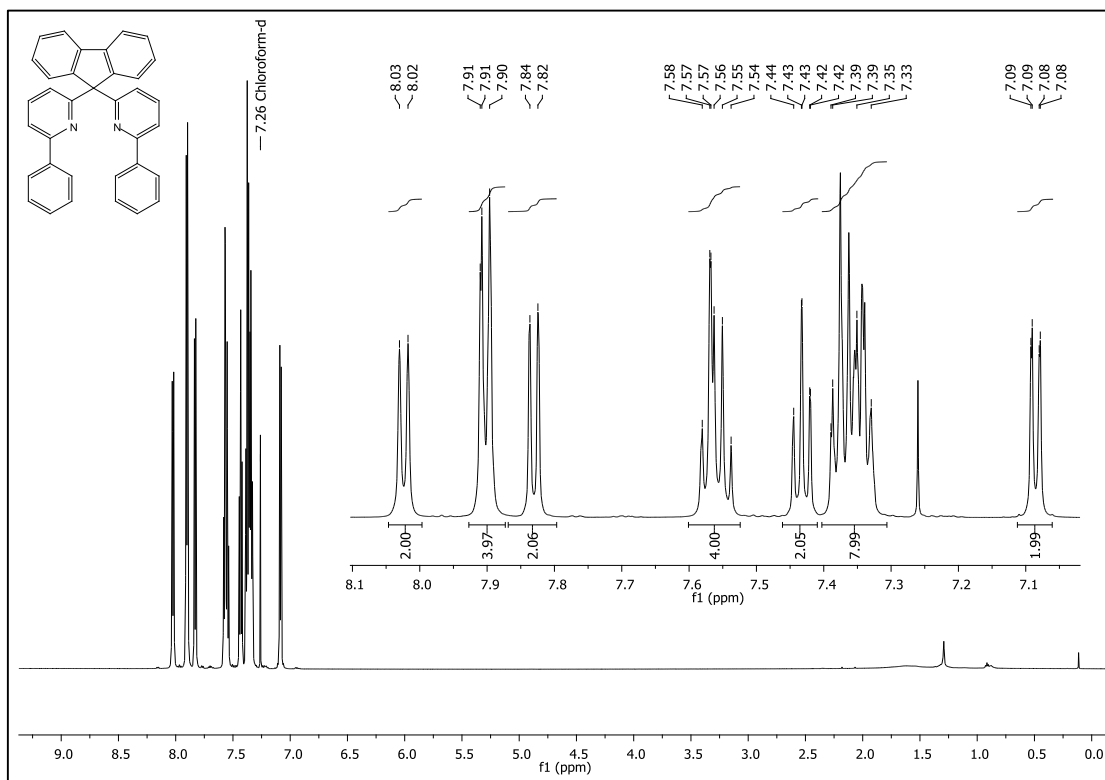


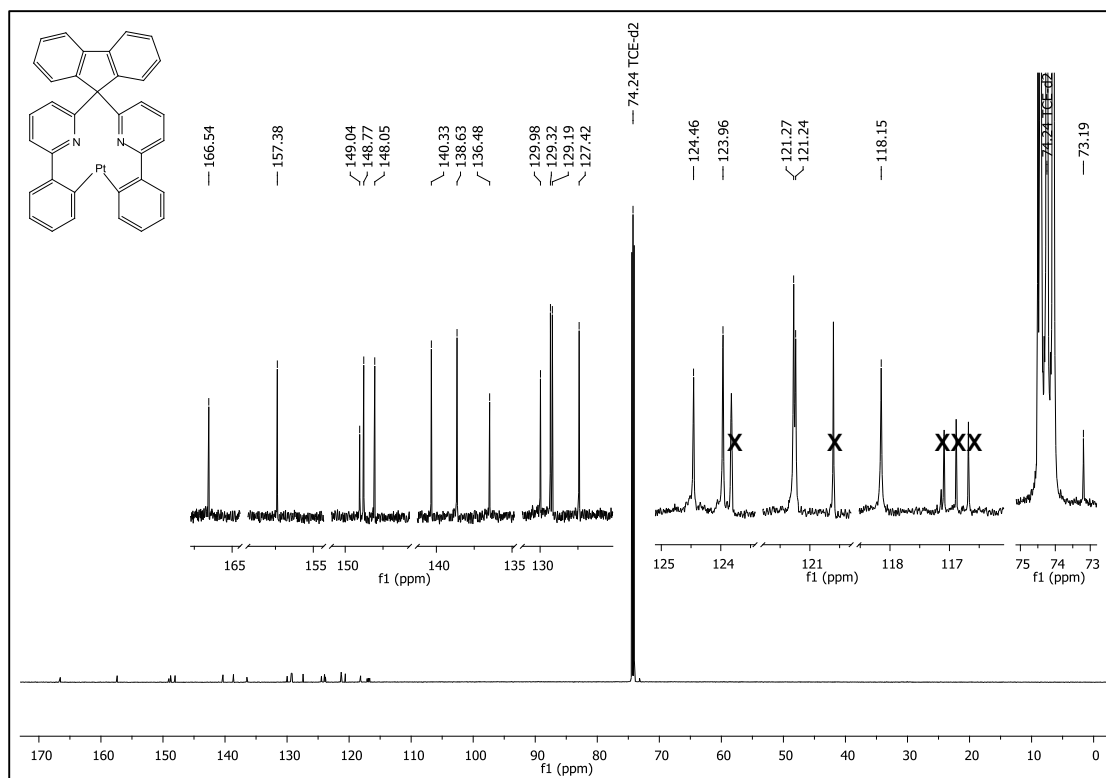
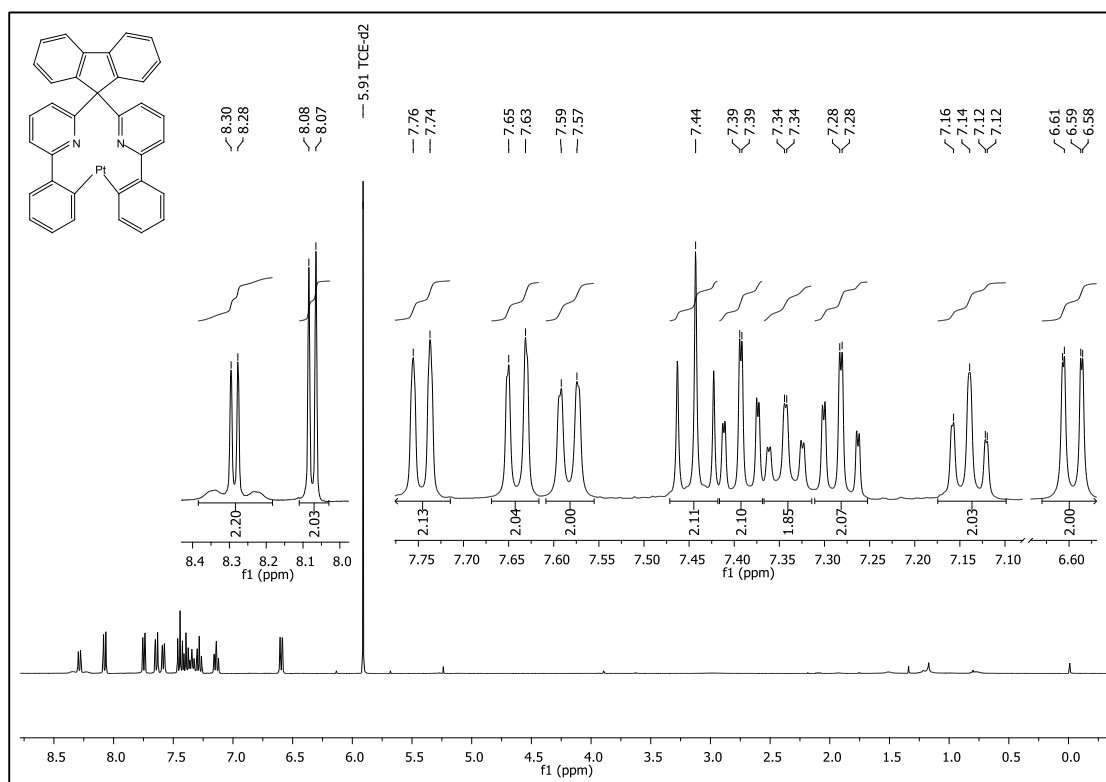
## COMPOUND 4



# APPENDIX

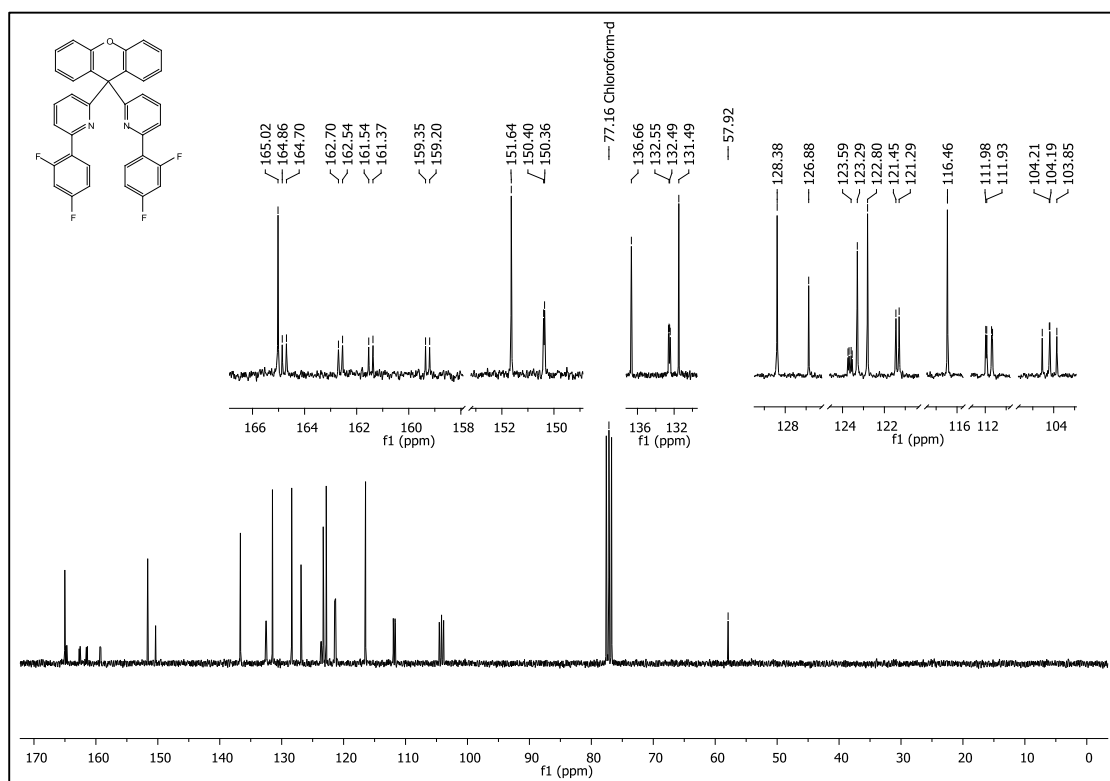
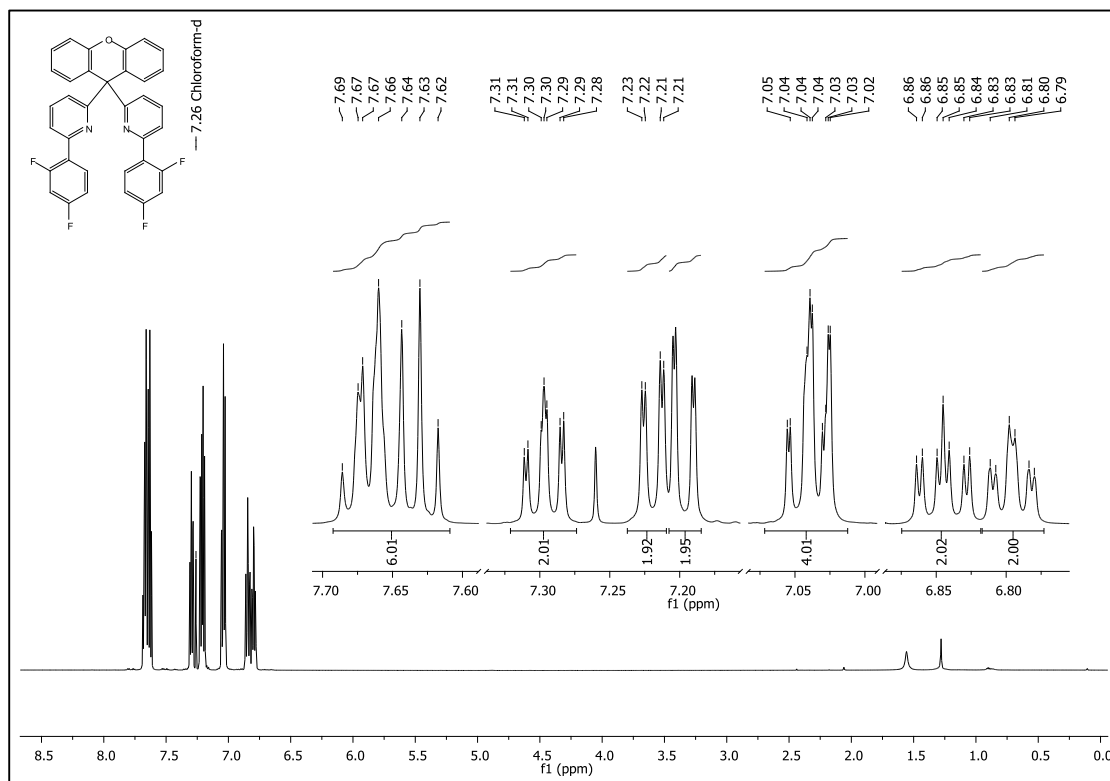
## COMPOUND 5a

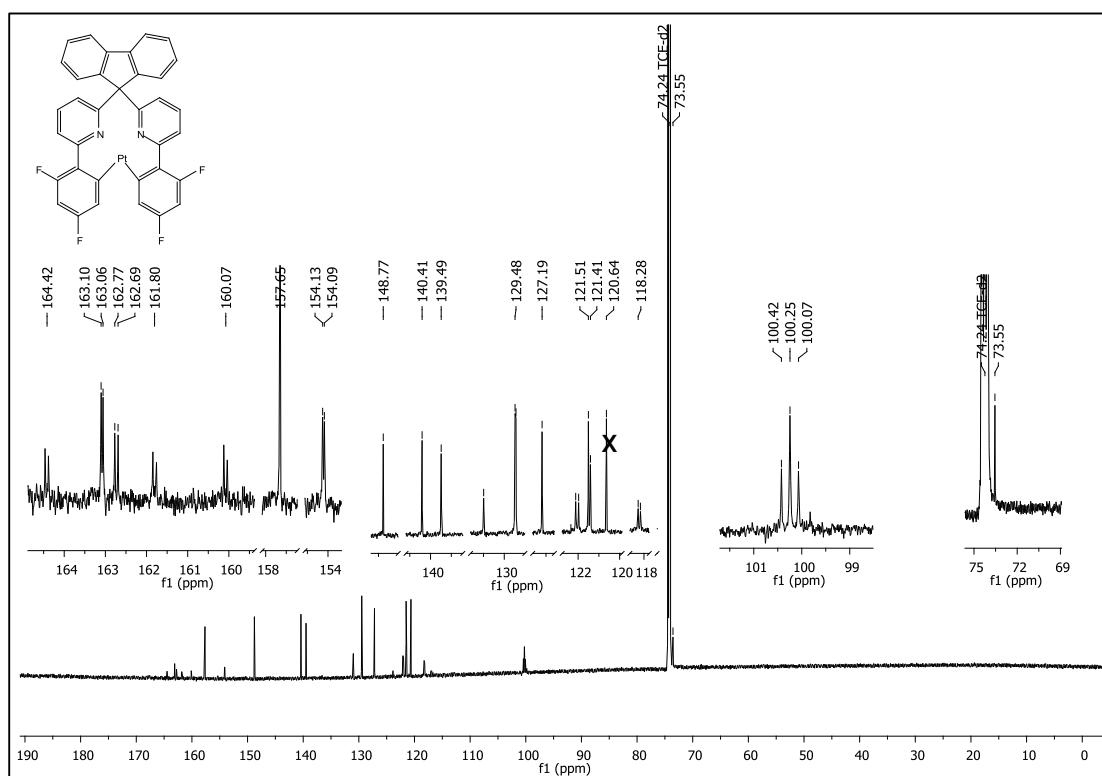
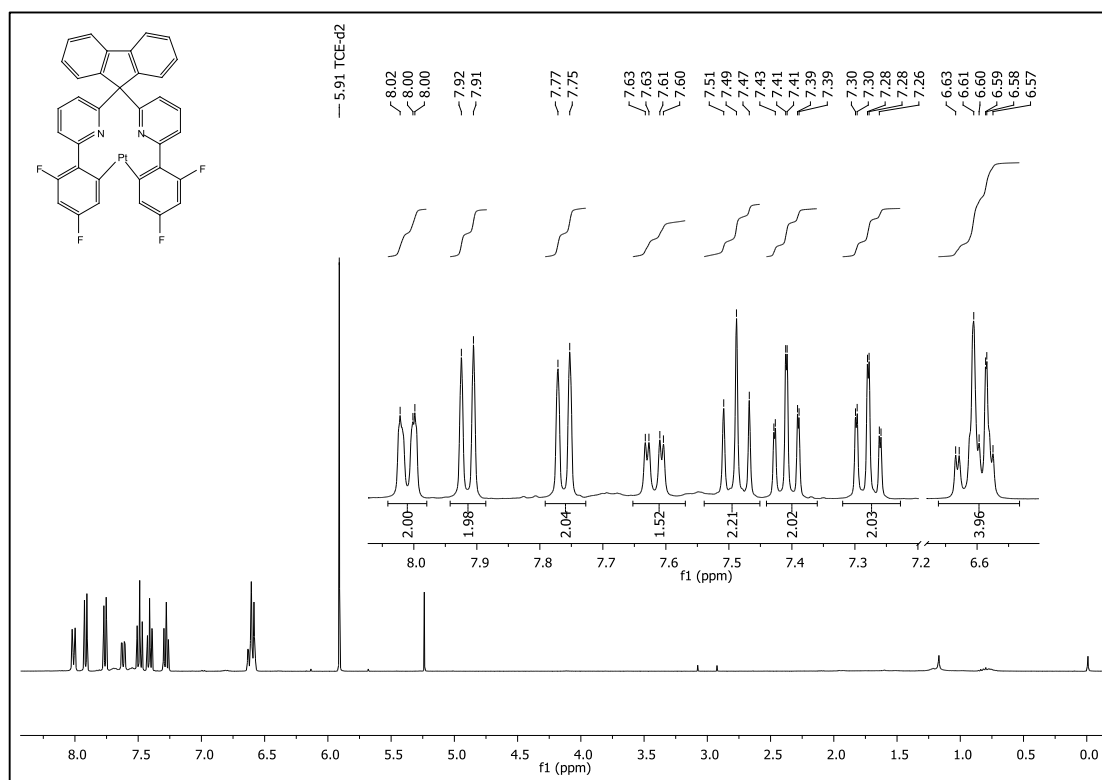


COMPOUND **1a**

# APPENDIX

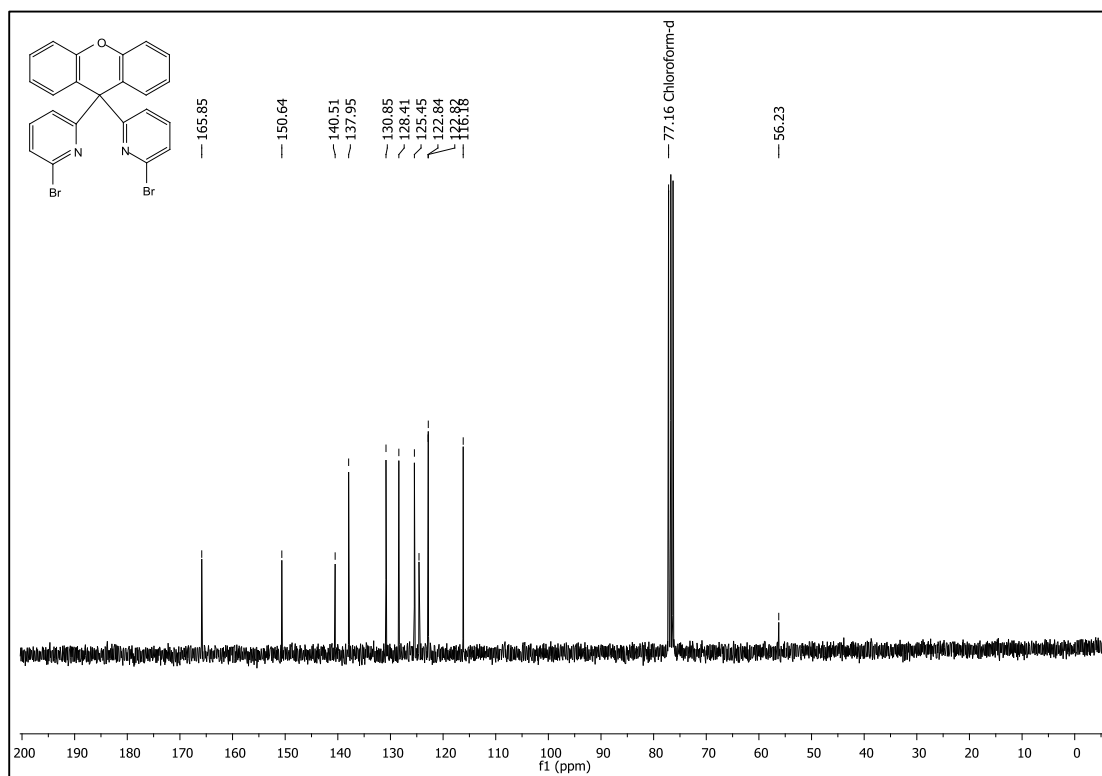
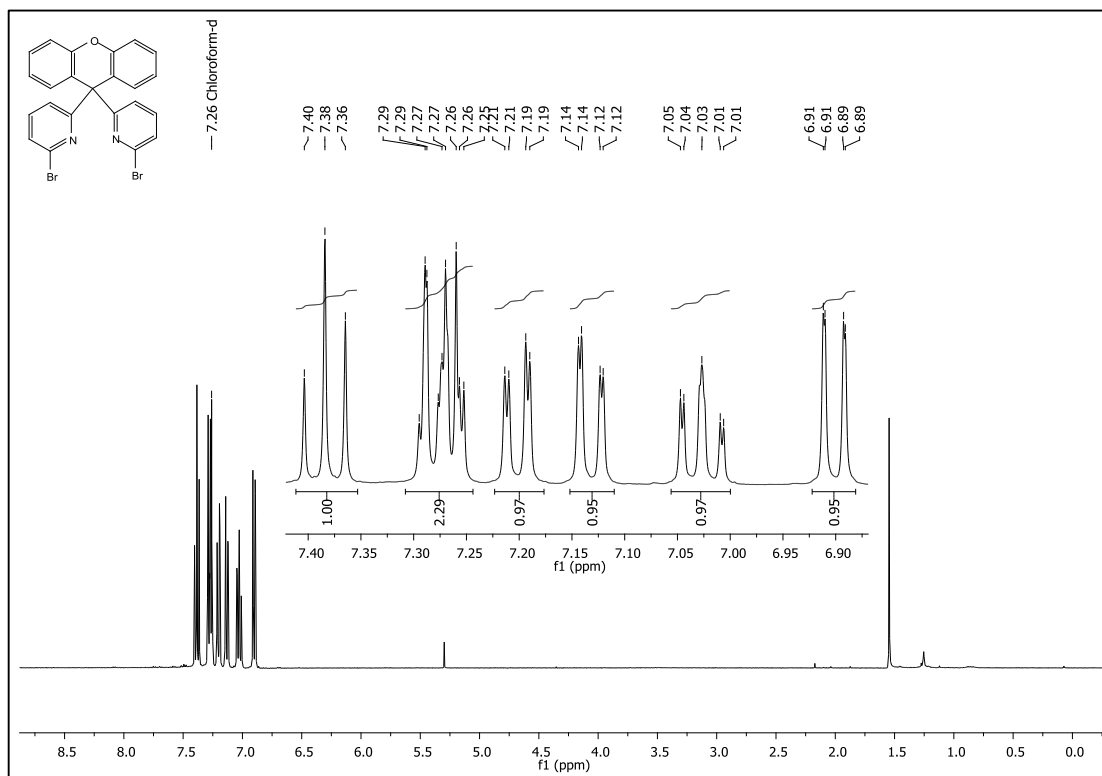
## COMPOUND 5b



COMPOUND **1b**

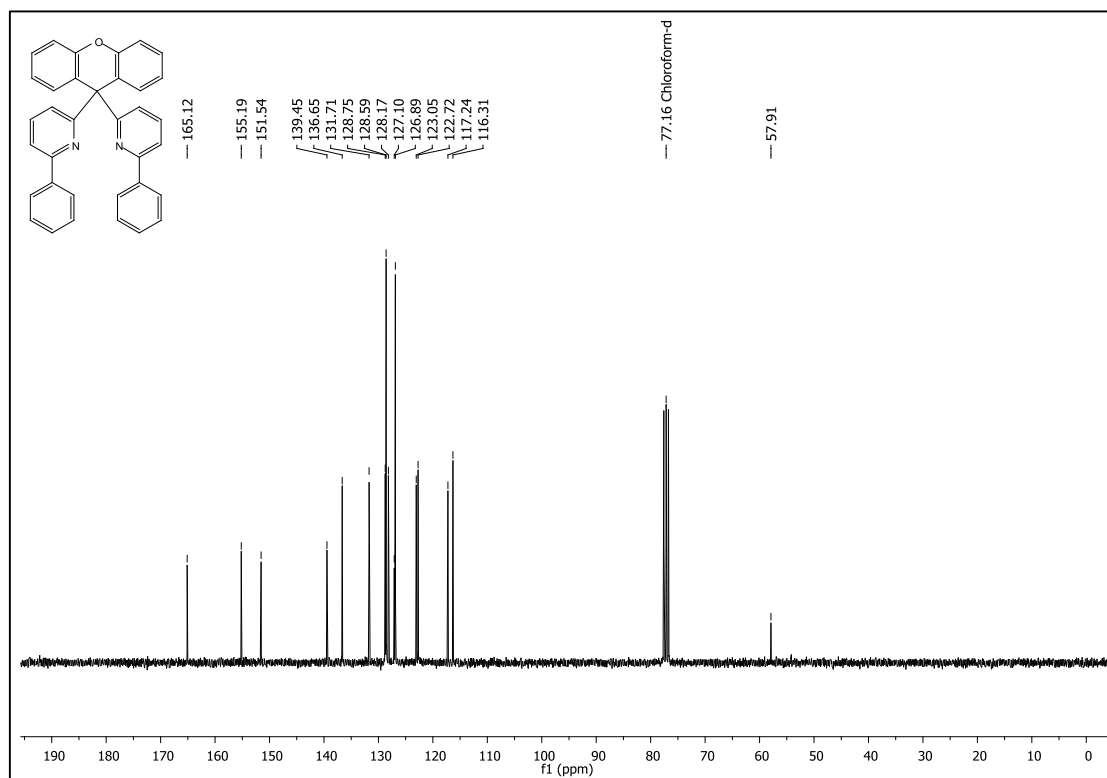
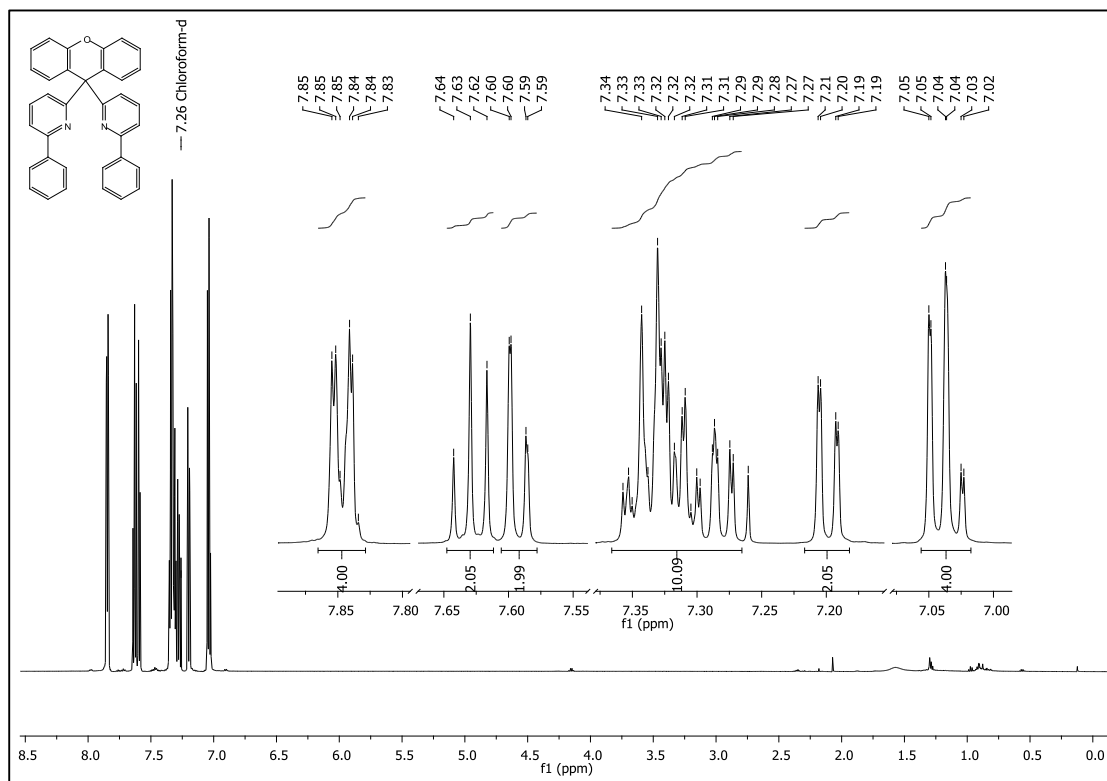
# APPENDIX

## COMPOUND 4'

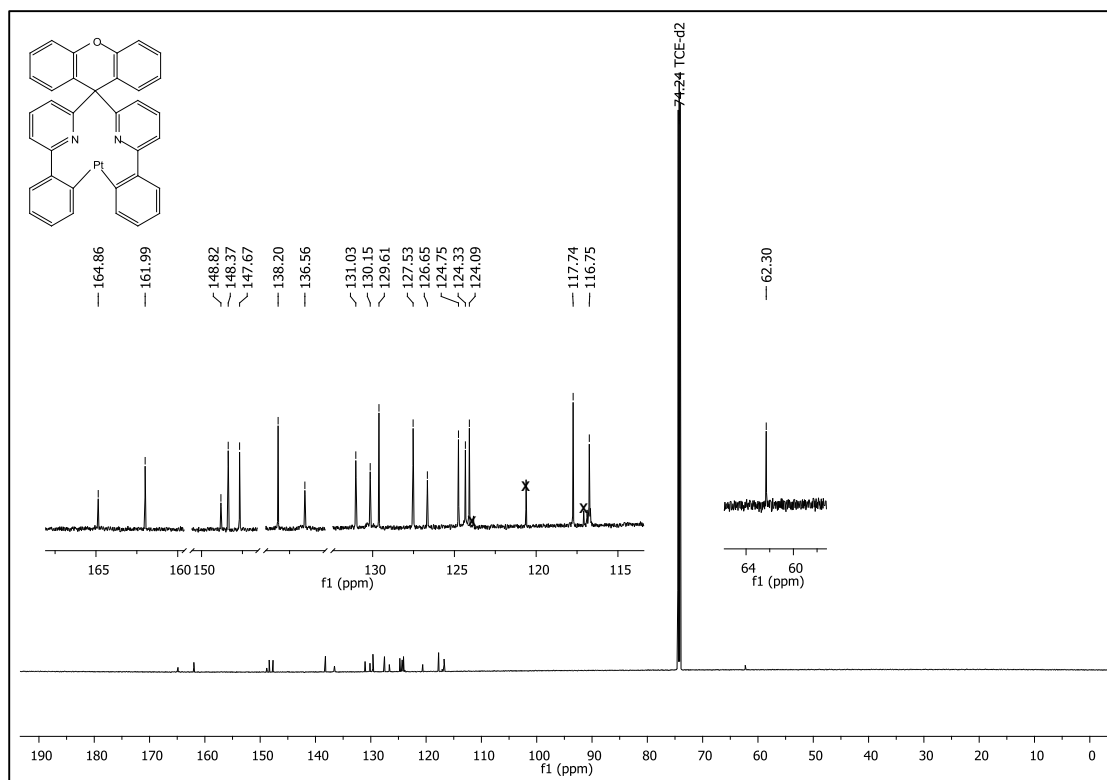




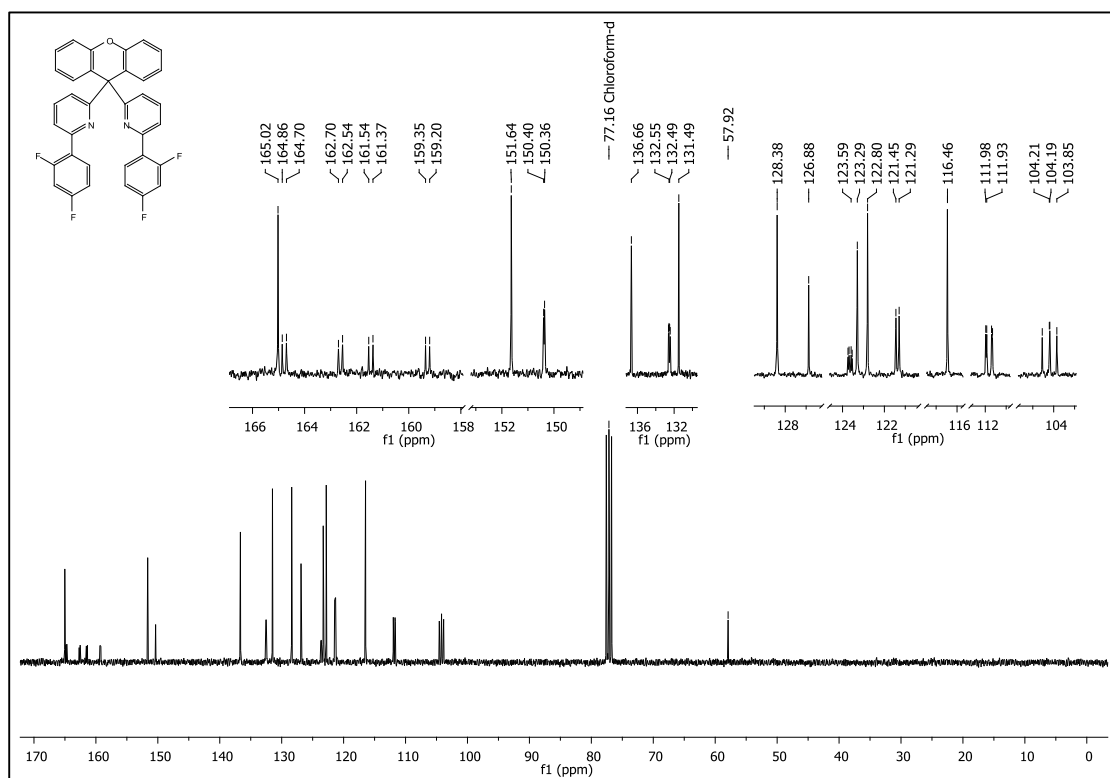
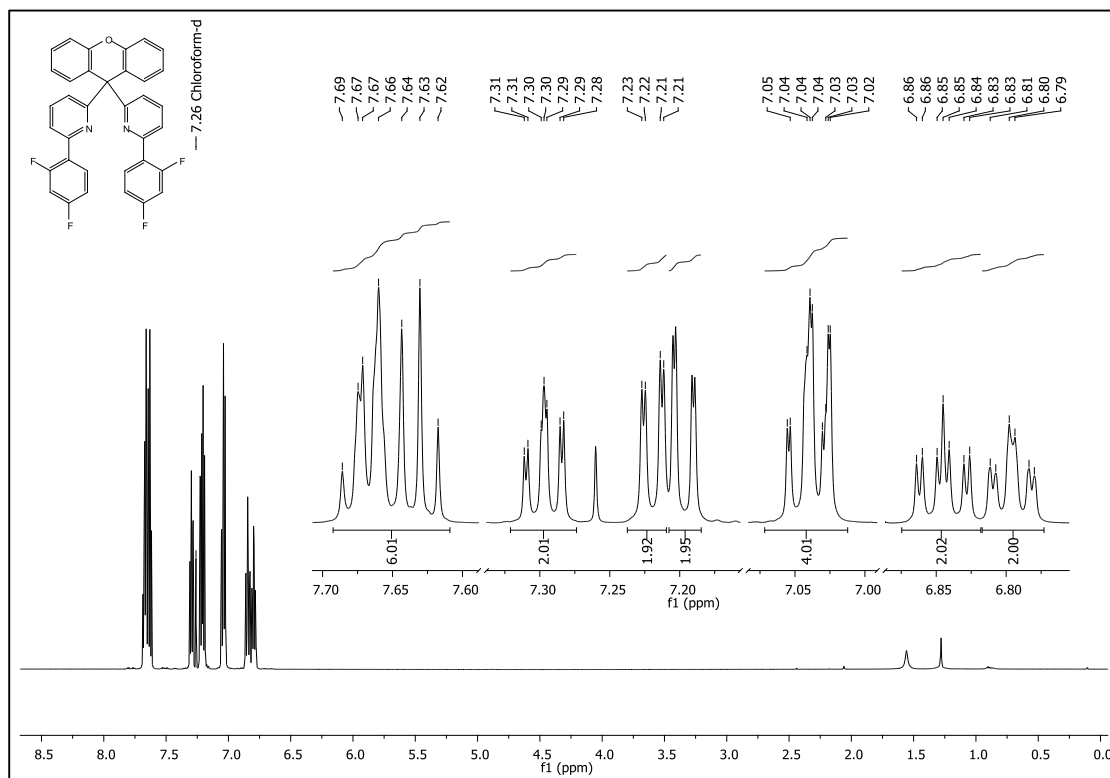
## COMPOUND 5'a



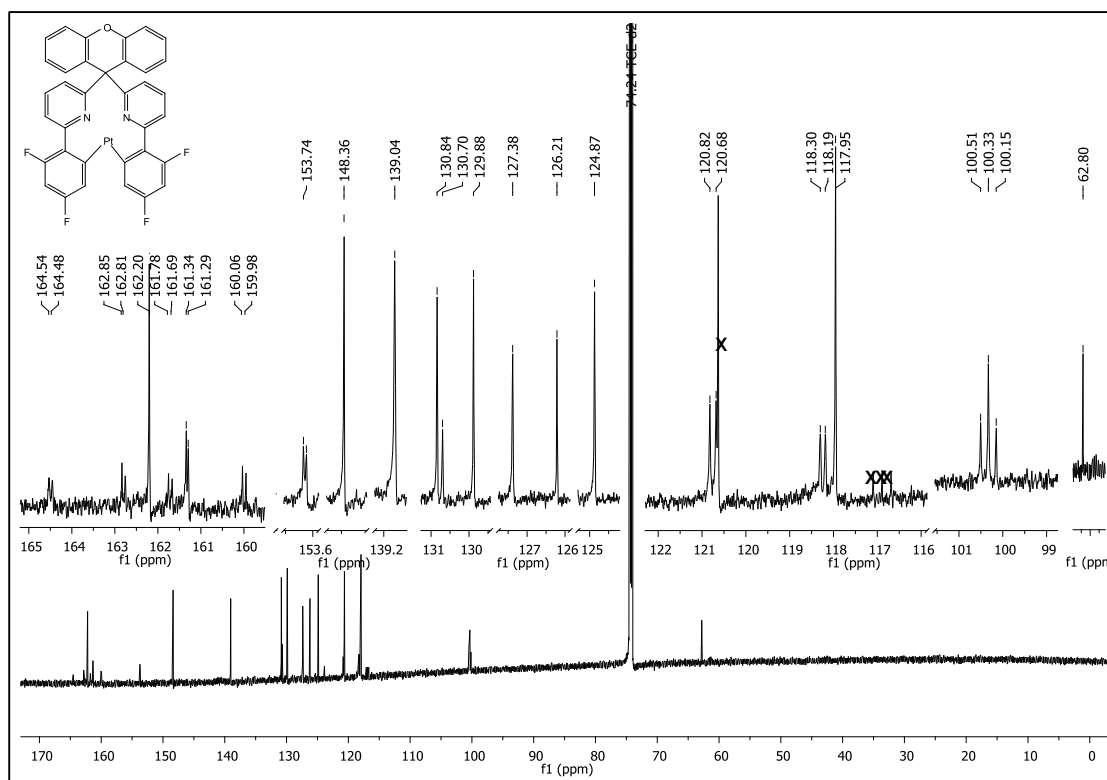
COMPOUND 1'a

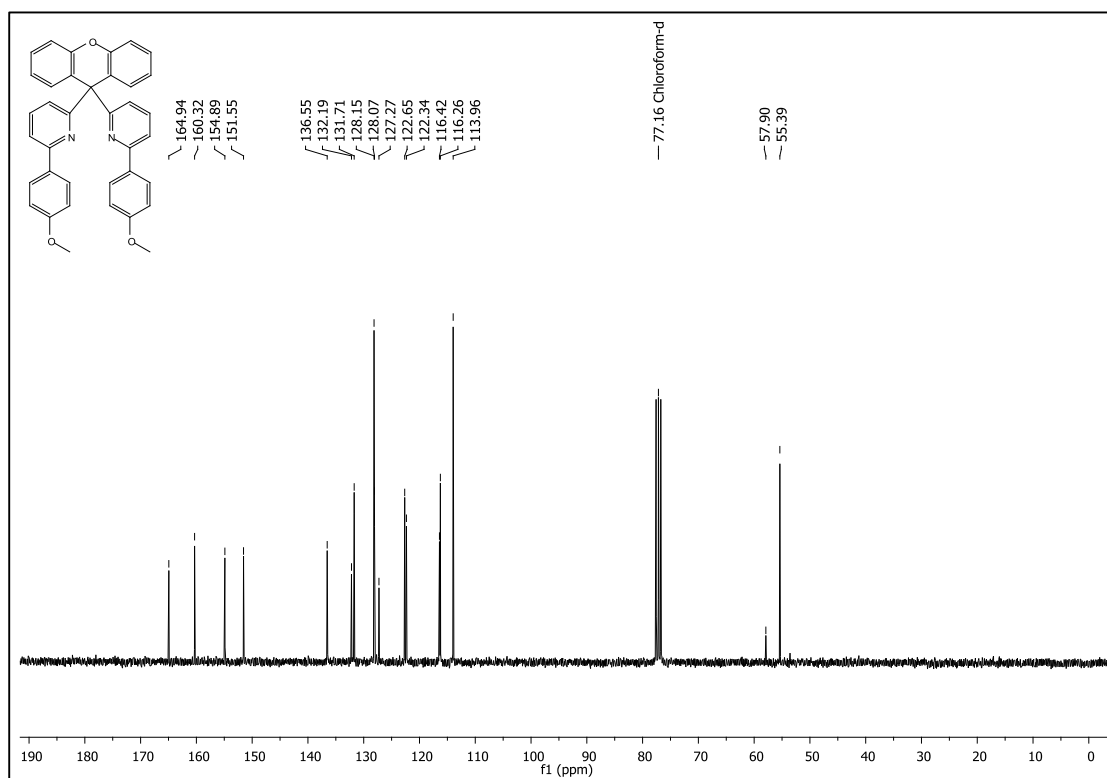
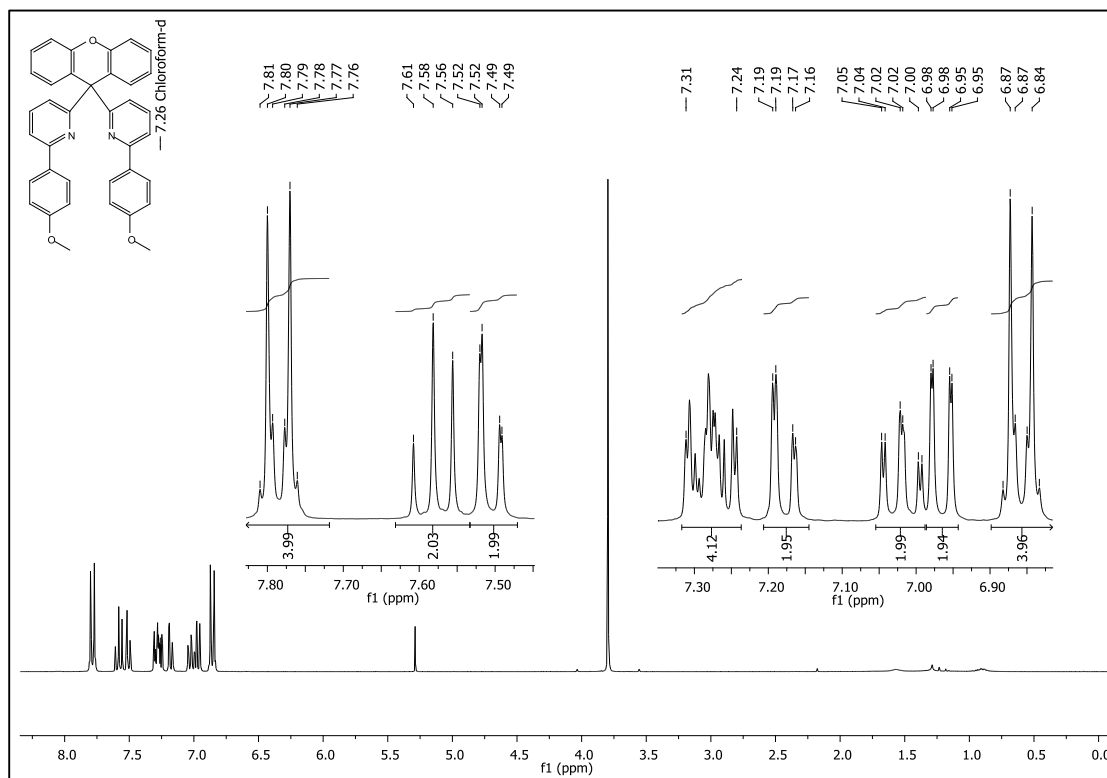


## COMPOUND 5'b



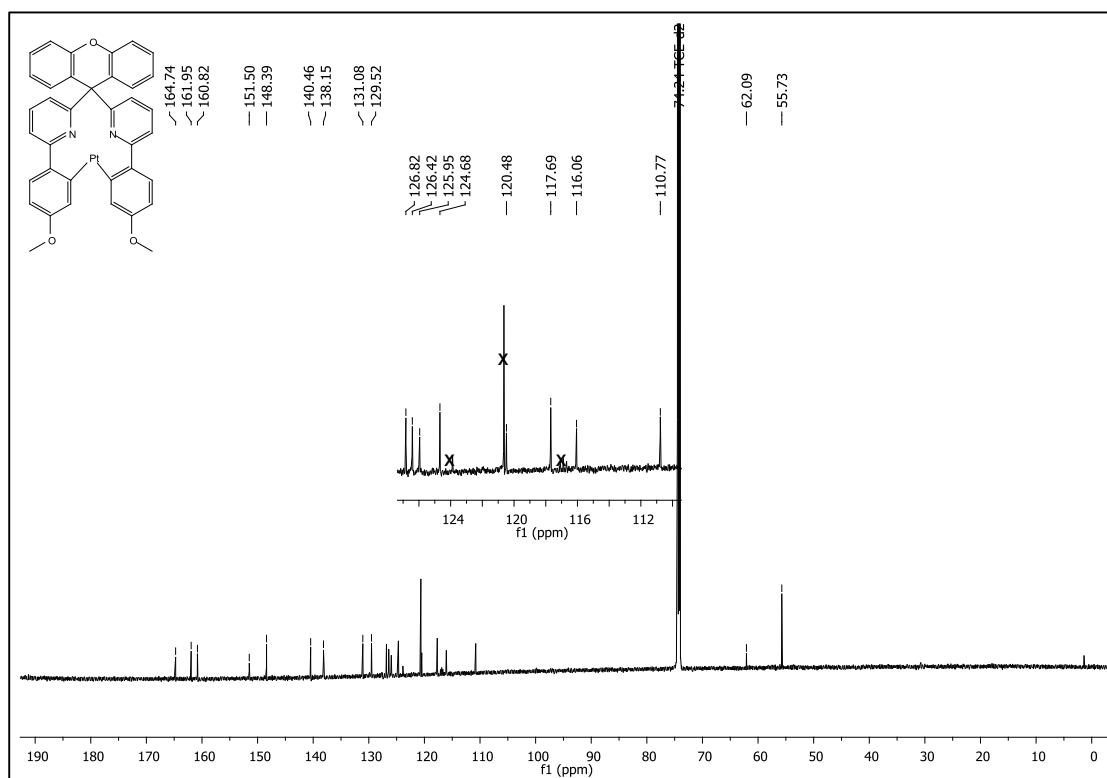
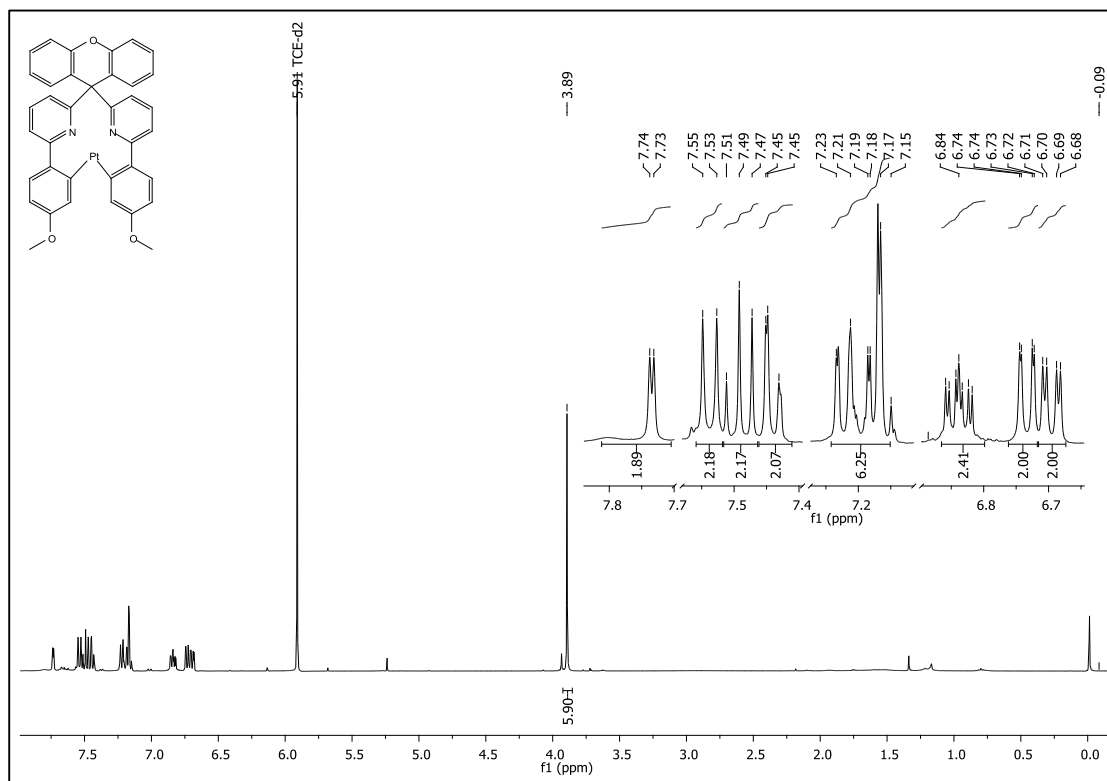
COMPOUND 1'b



COMPOUND 5'**c**

# APPENDIX

## COMPOUND 1'**c**



## 5. ABBREVIATIONS

3D	three dimensional
$^3\text{MC}$	triplet metal-centered state
acac	acetylacetonate
ADN	9,10-di(naphth-2-yl)anthracene
$\text{AlQ}_3$	<i>tris</i> (8-hydroxy-quinolato)aluminium
amu	atomic mass unit
APCI	atmospheric-pressure chemical ionization
atm	atmospheric
$\text{BAIQ}_2$	<i>bis</i> (2-methyl-8-quinolinolate)-4-phenylphenolato)aluminium
BCP	2,9-dimethyl-4,7-diphenyl-1,10-phenanthroline
BPC	4-(carbazol-9-yl)biphenyl
BPhen	4,7-diphenyl-1,10-phenanthroline
bzq	7,8-benzoquinoline
CBP	4,4'- <i>bis</i> (carbazol-9-yl)biphenyl
CDBP	4,4'- <i>bis</i> (carbazol-9-yl)-2,2'-dimethyl-biphenyl
CIE	commission internationale de l'éclairage
CV	cyclic voltammetry
d	diameter
d	doublet
DAD	diode array detector
dba	dibenzylideneacetone
dd	doublet of doublets
DFT	density functional theory
DMF	dimethylformamide
DMFL-CBP	2,7- <i>bis</i> (carbazol-9-yl)-9,9-dimethylfluorene
dppf	1,1'- <i>bis</i> (diphenylphosphino)ferrocene
dpyb	1,3-di(pyridin-2-yl)benzene
dpydFb	1,3-di(pyridin-2-yl)-4,6-difluorobenzene
DSSC	dye-sensitized solar cell
DTA	di-p-tolylamine
DTPA	di(p-tolyl)phenylamine
EBL	electron blocking layer
EL	electroluminescence
EML	emissive layer
EPR	electron paramagnetic resonance
EQE	external quantum efficiency
etc.	et cetera
ETL	electron transport layer
exc	excitation
<i>fac</i>	facial
Fc	ferrocene
Flrpic	<i>bis</i> (3,5-difluoro-2-(2-pyridyl)phenyl-(2-carboxypyridyl)iridium(III)
FLD	fluorescence detector
FWHM	full width at half maximum
GPC	gel permeation chromatography

## APPENDIX

h	hour
HBL	hole blocking layer
HIL	hole injection layer
HOMO	highest occupied molecular orbital
HPLC	high performance liquid chromatography
HR	high resolution
HTL	hole transport material
IC	internal conversion
i.e.	that is
IR	infrared
ISC	inter-system crossing
ITO	indium-tin oxide
<i>J</i>	coupling constant
Johnphos	(2-biphenyl)di- <i>t</i> -butylphosphine
K	Kelvin
LC	ligand-centered
LC	liquid chromatography
LDI	laser desorption/ionization
LED	light-emitting diode
LiQ	8-hydroxyquinolinolato-lithium
LT <sub>50</sub>	lifetime at half the initial luminance
LUMO	lowest unoccupied molecular orbital
m	multiplet
m/z	mass to charge
MALDI	matrix-assisted laser desorption/ionization
MC	metal-centered
MDQ	2-methyldibenzo-[f,h]quinoxaline
Me	methyl
MeOH	methanol
<i>mer</i>	meridional
MLCT	metal-to-ligand charge transfer
MO	molecular orbital
MS	mass spectrometry
N	normal
NMR	nuclear magnetic resonance
NPB	<i>N,N'</i> -bis(naphthalen-1-yl)- <i>N,N'</i> -bis(phenyl)-benzidine
OAc	acetate
OLED	organic light-emitting diode
ORTEP	oak ridge thermal ellipsoid plot
o-tolyl	ortho-tolyl
PC	phenylcarbazole
PEDOT:PSS	poly(3,4-ethylenedioxythiophene) poly(styrenesulfonate)
phbpy	6-phenyl-2,2'-bipyridine
PhOLED	phosphorescent organic light-emitting diode
pim	phenylimidazole
piq	1-phenylisochinolin
PL	phospholuminescence
pmb	1-phenyl-3-methylbenzimidazolin-2-ylidene
PMMA	poly(methyl metacrylate)
ppm	parts per million



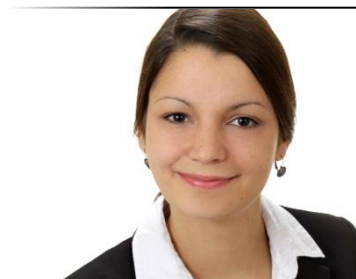
ppy	2-phenylpyridine
PTFE	polytetrafluoroethylene
Q-TOF	quadrupole time-of-flight
QY	quantum yield
Red	reduction
s	singlet
SPhos	2-dicyclohexylphosphino-2',6'-dimethoxybiphenyl
TAD	2,2',7,7'- <i>tetrakis</i> (N,N-diphenylamino)-9,9-bifluorene
TAPC	di-[4-(N,N-ditolyl-amino)-phenyl]cyclohexane
TBADN	2- <i>tert</i> -butyl-9,10-di(naphth-2-yl)anthracene
<i>t</i> Bu	<i>tert</i> -butyl
<i>t</i> BuXphos	2-di- <i>t</i> butylphosphino-2',4',6'-triisopropylbiphenyl
TCE	1,1,2,2-tetrachloroethane
TCTA	4,4',4''- <i>tris</i> (carbazol-9-yl)triphenylamine
TDAB	1,3,5- <i>tris</i> (diphenylamino)benzene
T <sub>g</sub>	glass transition temperature
THF	tetrahydrofuran
TLC	thin layer chromatography
TPBi	2,2',2''-(1,3,5-benzinetriyl)- <i>tris</i> (1-phenyl-1-Hbenzimidazole)
TPD	N,N'- <i>bis</i> (3-methylphenyl)-N,N'- <i>bis</i> (phenyl)-benzidine
tpy	terpyridyl
TTB	2,2',7,7'-tetra(N,N-ditolyl)amino-9,9-bifluorene
UDC	Universal Display Corporation
UV	ultraviolet
Vis	visible
Xantphos	4,5- <i>bis</i> (diphenylphosphino)-9,9-dimethyl-xanthene

## APPENDIX

### 6. CURRICULUM VITAE

#### PERSONAL DETAILS

Name: Susanna Schmidbauer  
Date of Birth: 24/09/1984  
Place of Birth: Landshut  
Nationality: German  
Email: susanna.schmidbauer@gmail.com



#### EDUCATION

- 11/2009 - 01/2013      **DISSERTATION**  
„Phosphorescent Emitters for OLED Applications – from Synthesis to Photodegradation”  
Chair: Prof. Burkhard König, Institut für Organische Chemie, Universität Regensburg
- 01/2009 - 09/2009      **DIPLOMA-THESIS**  
„Towards Dithienylethene-based Photoresponsive Gels”  
Chair: Prof. Burkhard König, Institut für Organische Chemie, Universität Regensburg
- 10/2004 - 12/2008      **CHEMISTRY STUDIES** at the University of Regensburg  
With in-depth studies in Medicinal Chemistry
- 06/2004      **GERMAN ABITUR** at the Von-Müller-Gymnasium, Regensburg  
With majors in Mathematics and French

#### TEACHING AND WORK EXPERIENCE

- 11/2009 – 12/2012      Self-reliant planning and processing of a sub-project within the consortium proposal „Neue Materialien für OLEDs aus Lösung” (NEMO), funded by the German Federal Ministry of Education and Research

#### FOREIGN EXPERIENCE

- 03/2009 - 07/2009      Research stay during Diploma Thesis at the Indian Institute of Science (IISc) in Bangalore, India

#### FUNDING

- 11/2009 – 07/2012      German Federal Ministry of Education and Research (BMBF)  
(Project funding)
- 03/2009 - 07/2009      German Academic Exchange Service (DAAD)  
(Research scholarship)

## 7. LIST OF PRESENTATIONS AND PUBLICATIONS

## POSTER PRESENTATIONS

**Susanna Schmidbauer**, Andreas Hohenleutner, Burkhard König. „Combinatorial Synthesis and Screening of Phosphorescent Iridium Complexes for Solution Processing“. Merck Student's Day 2012 (Darmstadt, Germany).

**Susanna Schmidbauer**, Andreas Hohenleutner, Burkhard König. "Chromatographic Investigations on the Photodegradation Behavior of Iridium Based Triplet Emitters". ORCHEM Chemistry Congress 2012 (Weimar, Germany). 4<sup>th</sup> EuCheMS Chemistry Congress 2012 (Prague, Czech Republic). Gordon Research Conference & Seminar „Electronic Processes in Organic Materials" (Barga, Italy).

**Susanna Schmidbauer**, Andreas Hohenleutner, Burkhard König. "Establishment of an Automated Screening Method for new OLED Emitters Prepared via Combinatorial Synthesis". 3<sup>rd</sup> EuCheMS Chemistry Congress 2010 (Nürnberg, Germany).

**Susanna Schmidbauer**, Andreas Hohenleutner, Burkhard König. "Establishment of an Automated Screening Method for new OLED Emitters Prepared via Combinatorial Synthesis". VII International Krutyn Summer School 2010 "Organic Optoelectronics on the Move" (Krutyn, Poland).

## ORAL PRESENTATIONS

**Susanna Schmidbauer**. "NEMO & the phosphorescent milestone". 12. Regensburger Weihnachtsskolloquium des Instituts für Organische Chemie 2012 (Regensburg, Germany).

**Susanna Schmidbauer**. "Molecular Switching and Photocatalysis in Gels". 2<sup>nd</sup> INDIGO Conference 2010 (Donaustauf, Germany).

**Susanna Schmidbauer**. "Towards Dithienylethene-based Photoresponsive Gels". 1<sup>st</sup> INDIGO Conference 2009 (Hyderabad, India)

## PUBLICATIONS

Andreas Hohenleutner, **Susanna Schmidbauer**, Rudolf Vasold, Dominik Joosten, Philipp Stoessel, Herwig Buchholz, Burkhard König. "Rapid Combinatorial Synthesis and Chromatography Based Screening of Phosphorescent Iridium Complexes for Solution Processing". *Advanced Functional Materials* 2012, 22, 3406-3413.  
DOI: 10.1002/adfm.201200397.

**Susanna Schmidbauer**, Andreas Hohenleutner, Burkhard König. "Chemical Degradation in Organic Light-emitting Devices: Mechanisms and Implications for the Design of New Materials". *Advanced Materials*. Accepted.  
DOI: 10.1002/adma.201205022.

**Susanna Schmidbauer**, Andreas Hohenleutner, Burkhard König. "Studies on the Photodegradation of Red, Green and Blue Phosphorescent OLED Emitters". Submitted.